ACKNOWLEDGEMENT

From the bottom of my heart I wish to dedicate this book to the people who rendered me a helping hand at various junctures in my life. It is no exaggeration to state that without the help of these people my life could have been quite different. I may not have been able to pursue my life as a scientist and this book could not have been written. These people are:

Dorothy Douglas
Isabel Taylor
Joan Strong
Catherine Gooch
Aden J. King
Frank A. Kanda

Dorothy and Isabel were instrumental in bringing me to the United States from Taiwan to enter Southwestern at Memphis (now known as Rhodes College) in 1950. During my undergraduate years, Joan made an arrangement with the bank so I could borrow money when I needed. Ms. Gooch through the Gooch Foundation of Memphis gave me a one-year full scholarship to finish my master's degree at University of Illinois.

Aden and Frank were my advisers at Syracuse University. They were the best advisers any graduate students can possibly dream to have. In particular, Aden contributed substantially to my financial needs through his King's Laboratory in Syracuse. Aden also arranged for me to continue my education as a post-doctoral research fellow at Harvard University under William N. Lipscomb who is a Nobel laureate for his contribution in boron-chemistry.

Unfortunately all the people listed above are no longer with us today. But, my personal relationship with these people is indeed privileged and shall remain in my heart forever.

August 13, 2002

Frederick E. Wang

Preface

The universe as a whole is made up of material with three distinct states, namely the solid state, the liquid state and the gaseous state. In 1662, Robert Boyle showed for the first time the relationship between volume and pressure of a gas under constant temperature to be inverse proportional to one another. In 1802 Gay-Lussac reported his discovery on the relationship between the volume of gas and temperature under constant pressure to be proportional to one another. These two relationships laid the foundation for the equation of state for gaseous state namely,

$$\mathbf{PV = nRT}$$

where P, the pressure, V, the volume and T is the temperature in absolute scale. In sharp contrast, an equation of state for liquid and solid state is still forthcoming to this date. While there has been some progress made in understanding the solid state with the arrival of X-ray and X-ray diffraction technique in identifying the atomic arrangements inside crystalline material, we are far from arriving at an equation of state for solids. This is particularly true in metallic solid in which sea of electrons roam about freely and a block of metal can only be considered as a gigantic molecule.

Investigation of this metallic solid is carried out:

* By physicists in terms of their conductivity, magnetic property and work functions. And they came up with a theory that deals with Fermi electrons, Brillouin zone and band structure.

* By chemists in terms of its chemical corrosion, crystal structure and the nature of bonding among atoms and their interatomic distances. And they came up with a theory that deals with multi-centered covalent bonding or resonating л-bond conjugated molecular chain and electro-potentials.

* By metallurgists in terms of the mechanical properties, such as modulus, fracture toughness, ultimate tensile strength. And they came up with a theory that deals with dislocation, fracture mechanic and continuum mechanics.

The problem was that a theory is formed in each discipline, based on their limited experimentation and interpretation. This method is analogous to a group of blind men who are allowed to feel and touch different body parts of an elephant and each comes up with a description of how an elephant as a whole should look like. This is to say that the description offered by each blind man may not be completely untrue but it cannot be used to describe an elephant as a whole. Inasmuch as the experimental observation made by each discipline comes from the same material no theory will be complete unless it can explain at least qualitatively all the experimental facts. These shortcomings led physicists to talk only about the quasi-free electrons and completely ignore the possible existence of covalent

bonded electrons. In sharp contrast chemist insists on resonating covalent bond with multicenter as the basis for electron conduction and thus ignore the possible existence of the quasi-free electrons. Metallurgists on the other hand ignore the existence of electrons (quasi-free or covalent bonded) and concentrate on atoms only. They provide metallographic evidence in support of their theme and offer their explanation in terms of dislocation that is capable of explaining a lot of observations but predicts nothing. In this book I intend to show that a theory based on a coexistence of covalent bond and quasi-free electrons in metals and alloys can satisfy many observations simultaneously either qualitatively or quantitatively.

Introduction

All the things we see and feel, even the air we breathe are altogether known as 'material.' Through centuries of scientific investigation we have come to know and understand that all material is composed of atoms and atoms are in turn made up of nucleus and electrons. The number of electrons surrounding the nucleus defined as atomic number dictates the characteristic of that atom. There are more than 100 different types of atoms on earth and they are systematically arranged in Mendeleeve's chart, or known as the 'PERIODIC CHART OF THE ATOMS.'

We also know that atoms are held together through electrons in forming material. Our experience convinces us that there are two types of electron bonding: a) strong bonding and b) weak bonding. The weak bonding does not involve direct electron-electron interaction but rather utilizes Van der Waals' forces or dipole-dipole interaction in forming bonding. The strong bonding, on the other hand, involves direct electron-electron interaction and can be differentiated into three groups: **Covalent bonding, Ionic bonding** and **Metallic bonding**.

COVALENT BONDING; involves a pair of electrons with opposite electron spin. The bond (or electron charge distribution) is essentially localized between nearest neighbor atoms that contribute electrons for the bonding. Since these electron pairs follow 'Bose-Einstein' statistics, therefore they are known as 'boson.' In this case the paired particles do not obey the Pauli Exclusion Principle and many electron pairs in the system may occupy the same energy level.

IONIC BONDING; also involves a pair of electrons with opposite electron spin. However, the bond (or electron charge distribution) is lopsided on one atom. And results in negatively charged atom on one and leaving the other atom positively charged. This creates a negative-positive charge attractive force that binds atoms together. Statistically, these particles are also 'Boson.'

METALLIC BONDING; in this bonding, electrons are not paired and are quasi-free to roam throughout the system. Because of unpaired electron spin, they follow the 'Fermi-Dirac' statistics and consequently obeying the Pauli Exclusion Principle. Therefore they are known as 'fermions' where no two electrons can occupy the same energy level and results in an energy band. The three distinct type of bonding as described above is too abstract and

difficult to follow without a Quantum-Mechanical upbringing. The understanding of these bonding may be enhanced by an illustration through an imaginary 'dog show' as follows.

Let us imagine that there is a dog-show to be held and people coming to the show are all exactly identical to one another in all respect. These persons are to be known as nucleus (or nuclei as you prefer). Each person is allowed to bring three dogs, which are to be called 'electron'. Naturally, the dogs (electrons) are all identical to one another and will be on a leash. The leash will be known as 'atomic orbital' and be held firmly by each nucleus. As long as the nucleus holds tightly on the leash the dogs (electrons) will not run away. This unit, namely the nucleus (person) and electrons (dogs) will be known as an atom. Now, as the atoms with their nuclei and their dogs (electrons) come close to one another heading to the dog-show, the dogs (electrons) from different nuclei will be barking (interact) at one another – the closer they are, the more vigorous will be the barking (interaction). Ultimately the atoms are hurdled into the space where the dog-show is to take place and the atoms come so close to one another that the dogs (electrons) not only would bark at one another but also would actually chase one another. With this picture in mind we can now illustrate the three distinct types of bonding in the following way:

Covalent Bond: a pair of dogs (electron), each comes from two adjacent nuclei (person), chase one another in a round-and-round way so that their leashes are twisted together (Fig. 1). As long as the person (nucleus) continues to hold onto their leash the two adjacent nuclei are tied (bonded) to one another through the twisted leash and the pair of dogs (electron). This is the picture of covalent bond and otherwise known as linear-combination-of-atomic-orbital (LCAO).

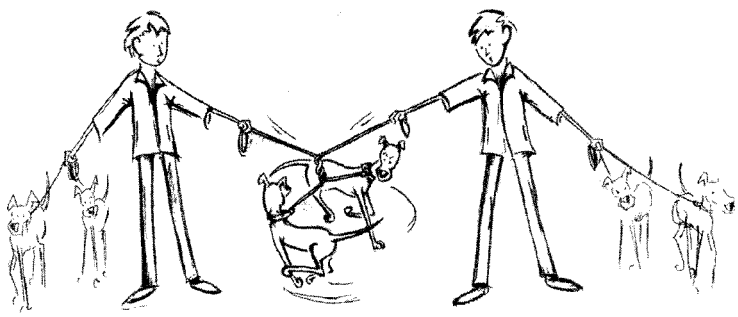

Fig. 1. Conceptual illustration of 'covalent bond' by picturing atoms to consist of boys as nuclei and dogs as electrons. Two dogs (electrons) forming a pair-bond between two atoms (boys).

Ionic Bond: it involves also a pair of dogs (electron) from two adjacent nuclei (persons) and having their leashes twisted together in the same way. The one big difference is that there are two distinct nuclei (persons) instead of identical nuclei (people). For example, a man-nucleus and a woman-nucleus and assume the man-nucleus is stronger than the woman-nucleus. The formation of a twisted pair of electron (dog) between man-woman-pair of adjacent nuclei will take place much in the same manner as in all identical nuclei. However, in this case the weaker woman-nucleus may let go the leash and results in paired electron (dog) being pulled to the man-nucleus side (Fig. 2). This results in man-nucleus with an extra electron (dog) while woman-nucleus short of one electron (dog). Thus, there is no direct leash tie to hold man-woman-nuclei pair together. However, the woman-nucleus would not leave because she sees her dog (electron) being held by the man-nucleus and cannot leave. Thus, the formation of positive-negative charged ionic bonded pair. It should be stressed therefore the ionic bond formation requires two distinct types of nuclei.

Metallic Bond: here we assume that each nucleus (person) is already leash-tied (covalent-bonded) to its two neighbors through leash-twisted pair of dogs (electrons) and therefore is hands-full. Under this circumstance the nucleus may not be able to hold onto the leash holding the remaining electron (dog) such that the electron (dog) may pull away from the nucleus (person) and become free to roam within the building confine. These dogs (electrons) running free are the so-called quasi-free electrons. The total number of dogs (electrons) vs. total number of people (nuclei) within the building remains the same with free-roaming dogs (electrons) providing cohesive attractive force to hold the dog-show attendants together.

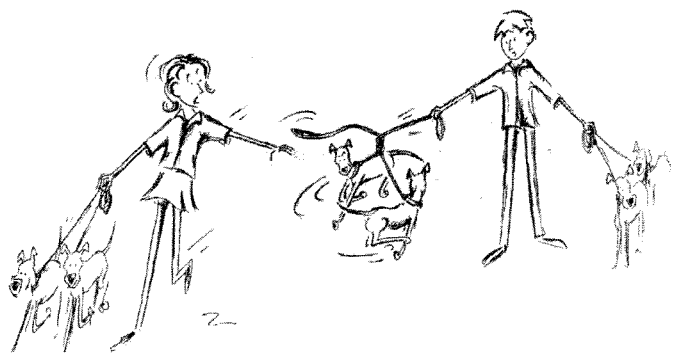

Fig. 2. Similar conceptual illustration as in Fig. 1 except this time nuclei are dissimilar (a boy and a girl) such that the weaker nucleus (in this case, a girl) cannot hold the lease and results in an 'ionic bond.'

Within these understanding, some specific feature of each bonding can be described. **Covalent bond** involves two and only two electrons. The nuclei that contribute electrons in forming the bond may or may not be the same type of atoms. Inasmuch as the bond is directly tied to the leash held by the nucleus the bond is necessarily directional and very strong and confined to the space between the two nuclei forming the bond. Since the bond requires a tight grip of the leash by the nucleus, the number of bonds can be formed by a given nucleus is therefore limited according to the strength or available atomic orbital of the nucleus.

Similarly, **Ionic bond** also involves electron pair but because the weaker nucleus gives up the leash entirely the bonding is not as strongly directional as well as in strength as in Covalent bond. Because the bonding is electrostatic in nature the bonding forces may involve not only the nearest neighbors but also the second, third, fourth and even higher order of neighboring attractive and repulsive forces and known as Madelung energy. **Metallic bond** involves all quasi-free electrons that are running free among nuclei and within the confine of the space. Therefore the bonding is totally non-directional and de-localized. They are considered as weak bonds. Due to the dynamic nature of these electrons they are treated as waves traveling in a space of periodically placed positively charged nuclei. These waves are known as Bloch-wave function. The periodic nature of nuclei distribution creates Brillouin zone boundary, which interact with the traveling Bloch waves. The bond created in this manner is found mostly in metallic elements and contributes to the conduction of electricity.

With the characteristic of each bonding type identified, we shall now show how all the material in this universe can be assigned to a particular type of bonding or a combination of bonding type as summarized in Fig. 3.

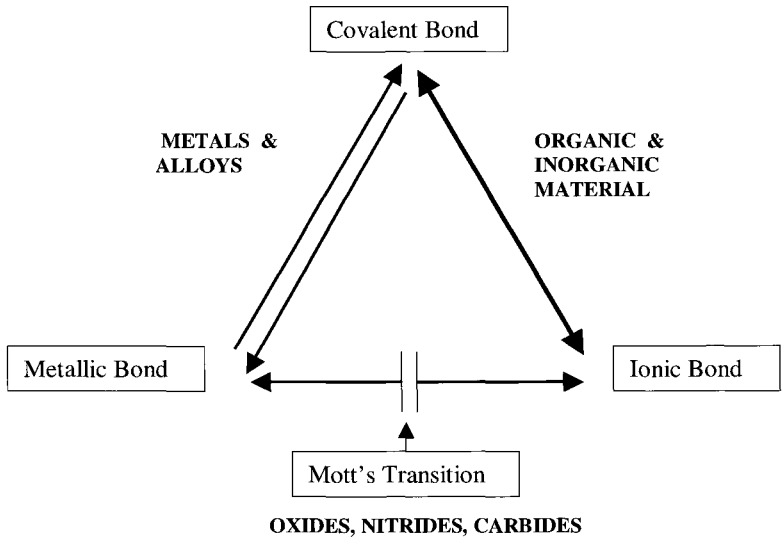

Fig. 3. Schematic representation of the relationship among the three bonding type.

In Fig. 3, a solid line ties covalent bond and ionic bond to another. This is to show that both the covalently bonded and the ionic bonded electrons are both 'bosons.' And quantum-mechanically they are equivalent to one another. At two extremity, i.e., 100% of covalent bond can be represented by a material known as diamond, whereas 100% of ionic bond can be represented by a material known as table-salt, Na(+)Cl(-). All the organic and inorganic material in this universe can be assigned between these two extremities. The difference, from one material to another, lies only in terms of the percentage of covalency or ionicity.

It is clear that ionic bonded material is an insulator and metallic bonded material is a conductor. Therefore, they cannot coexist in a material. For, by having sea of free electrons roaming freely will obliterate the stationary positive and negative charges forming ionic bond. Mott recognized this fact in 1974 in terms of Metal-Insulator transition. The material formed between Ionic Bond and Metallic Bond consists of special class of inorganic materials; carbides, oxides, nitrides, sulfides, and minerals. Experimentally, this class of material is often observed to undergo transformation from conductor to semiconductor to insulator either as a function of temperature, pressure or composition. The remaining material, metals and alloys, therefore reside between Metallic bond and covalent bond. Although these two bond types are incompatible in quantum-mechanic language, i.e., one is Boson and the other, Fermion; they can coexist in metals and their alloys. This recognition will be shown later to have a great impact in our understanding of metals and alloys.

In this manner, all materials in the universe can be assigned to one of these categories. It should be stressed that the three bonding types identified as the basic building blocks for binding atoms together in forming material, came from our painstaking experimental observation in the past centuries. They did not come from our theoretical calculations. Neither is our theory from first principle good enough to predict even an elementary fact, which element will be 'metallic' or which one will be 'non-metallic.'

A theory is an assumption that must first be compared against experimental facts. Further, a theory that is capable of explaining quantitatively to nth degree only about a single experimental fact is much less value than another theory that is capable of explaining a dozen of experimental facts simultaneously although only qualitatively. Only if the theory agrees well with the experimental facts, the theory can be put to the task of prediction. Should the theory fail in prediction, it cannot be considered a good theory no matter how many experimental facts it happens to agree or capable of explaining.

Within this understanding, I am proposing an assumption, an electron bonding theory, based on a coexistence of covalent and metallic bonds in the metals and alloys. This is rooted on the fundamental belief that electrons are the 'glue' that holds atoms together in material. But, because the glue comes in different forms even though the glue (electron) may have come from the same type of atoms the material they ultimately form may have totally different characteristics. A good example is found in carbon, which comes as diamond, graphite, charcoal, and more recently as fullerenes. Although they all formed from the same carbon atom they are glued together differently in their electron bonding and results in totally different material characteristics from one another. It is my opinion that physicists' theory based on quasi-free electron has some validity. However this theory is not complete because it ignores the possible coexistence of covalent bonding. As a result this theory fails to accurately predict whether an element should be a conductor, semiconductor or insulator. Nevertheless, the assumption eventually led to the proposal of the BCS superconductivity theory for which Nobel Prize was awarded in 1958.

Unfortunately, the BCS theory has had no consequence in predicting which element should be a good superconductor or which should be a poor one. Similarly, despite the success of dislocation theory proposed by metallurgists in explaining some mechanical properties observed in metals and alloys, it is totally useless in predicting mechanical properties. To this date a mechanical engineer in designing a structure would rely solely on the data obtained from measured material strength instead of the theoretical strength obtained from dislocation theory or calculations made from Continuum mechanics. This is a testimony of how little faith we have in the theory of dislocation or continuum mechanics.

Bonding Theory for Metals & Alloys

First, we shall lay down the fundamental rules assumed in the formulation of the theory. Although we do not have a rigorous proof at this point for each assumption made, they will be tested rigorously against an extensive array of experimental facts in the later chapters.

1. BASIC ASSUMPTION

a) Covalent (boson) bond and Metallic (fermion) band coexist in metals and alloys i.e., no metal or alloy can be 100% Metallic band or 100% Covalent bond.

b) The percentage of Covalent bond and percentage of Metallic band in a given metal or alloy ads up to 100%. All together they are known as valence electrons to differentiate from inner electrons that do not participate in bonding.

c) The quasi-free electrons from Metallic bond therefore not only had to move among positively charged ionic cores (as is assumed by physicists in Bloch wave function) but also had to dodge the region of negatively charged Covalent bonded electrons.

d) The percentage ratio between Covalent bond and Metallic band is a fixed constant value for a given metal or alloy. This constant shall remain fixed in a given metal or alloy within a given crystal structure.

R = % Covalent Bond / % Metallic Band = Constant.

e) The percentage ratio, between Covalent bond and Metallic band in a given metal or alloy, may be upset momentarily due to external influence. However, this upset-ratio will be restored to the original ratio either by breaking up some Covalent bond to increase Metallic bond or by transforming quasi-free electrons in the Metallic band to form more Covalent bond. This is to say that valence electrons may transform out of Covalent bond (boson) into quasi-free electrons (fermion) band or conversely transfer from Metallic band to Covalent Bond.

f) The relative energy level of Covalent bond *vs.* Metallic bond is not *a priori* but rather dependent on the type of Covalent bond existing in a given metal or alloy. At times Covalent bond energy level may be higher or lower than the Metallic band depending on the type of covalency in the Covalent bond.

g) The difference in the relative energy level between Covalent bond and Metallic band shall be known as the Energy Gap (EG). Generally speaking, the wider is the quasi-free Electron Band (EB) the smaller will be the EG.

h) Since the electrons in the EB are fermion, a wider EB means a larger number of quasi-free electrons and subsequently a stronger chemical reactivity and higher electron conductivity.

Unfortunately, the BCS theory has had no consequence in predicting which element should be a good superconductor or which should be a poor one. Similarly, despite the success of dislocation theory proposed by metallurgists in explaining some mechanical properties observed in metals and alloys, it is totally useless in predicting mechanical properties. To this date a mechanical engineer in designing a structure would rely solely on the data obtained from measured material strength instead of the theoretical strength obtained from dislocation theory or calculations made from Continuum mechanics. This is a testimony of how little faith we have in the theory of dislocation or continuum mechanics.

Bonding Theory for Metals & Alloys

First, we shall lay down the fundamental rules assumed in the formulation of the theory. Although we do not have a rigorous proof at this point for each assumption made, they will be tested rigorously against an extensive array of experimental facts in the later chapters.

1. BASIC ASSUMPTION

a) Covalent (boson) bond and Metallic (fermion) band coexist in metals and alloys i.e., no metal or alloy can be 100% Metallic band or 100% Covalent bond.

b) The percentage of Covalent bond and percentage of Metallic band in a given metal or alloy ads up to 100%. All together they are known as valence electrons to differentiate from inner electrons that do not participate in bonding.

c) The quasi-free electrons from Metallic bond therefore not only had to move among positively charged ionic cores (as is assumed by physicists in Bloch wave function) but also had to dodge the region of negatively charged Covalent bonded electrons.

d) The percentage ratio between Covalent bond and Metallic band is a fixed constant value for a given metal or alloy. This constant shall remain fixed in a given metal or alloy within a given crystal structure.

R = % Covalent Bond / % Metallic Band = Constant.

e) The percentage ratio, between Covalent bond and Metallic band in a given metal or alloy, may be upset momentarily due to external influence. However, this upset-ratio will be restored to the original ratio either by breaking up some Covalent bond to increase Metallic bond or by transforming quasi-free electrons in the Metallic band to form more Covalent bond. This is to say that valence electrons may transform out of Covalent bond (boson) into quasi-free electrons (fermion) band or conversely transfer from Metallic band to Covalent Bond.

f) The relative energy level of Covalent bond *vs.* Metallic bond is not *a priori* but rather dependent on the type of Covalent bond existing in a given metal or alloy. At times Covalent bond energy level may be higher or lower than the Metallic band depending on the type of covalency in the Covalent bond.

g) The difference in the relative energy level between Covalent bond and Metallic band shall be known as the Energy Gap (EG). Generally speaking, the wider is the quasi-free Electron Band (EB) the smaller will be the EG.

h) Since the electrons in the EB are fermion, a wider EB means a larger number of quasi-free electrons and subsequently a stronger chemical reactivity and higher electron conductivity.

i) The atomic arrangement of nearest neighbors in a given metal or alloy is singularly dictated by the Covalent bond which in turn determine the crystal structure for that metal or alloy.
j) The strength of Covalent bond in a given metal or alloy ultimately dictates the melting temperature for that metal or alloy.
k) Covalent bond is much more susceptible than Metallic band to temperature changes; therefore, one type of Covalent bond may transform into another type of more stable Covalent bond as a function of temperature. This is the reason metals and alloys often undergo structure change as a function of temperature. Thus, a given metal or alloy with different crystal structures will likely to have a different Covalent to Metallic bond percentage ratio.

These assumptions constitute the backbone of the theory being proposed.

2. ADDITIONAL POINTS TO CONSIDER CONCERNING THE THEORY

It is important to point out that the covalent bond has many faces. They can range from simple s, p, d, bonds to sp- or spd- hybridization bonds which may result in "σ" and "π" bonds that form the building block for single, double, and triple bonds. In more complex cases they can be resonance bonds or multi-centered bonds that are often observed in metals and alloys.

It should be stressed also that on many occasions, physicists who believe only in quasi-free electrons, have used the term, "covalent-like" or "narrow band" to justify some of their experimental observations. However, these terms do not change the fact that these electrons are still part of band structure and therefore, are fermions. Since Covalent bond electrons are boson, the statement, "covalent-like" is equivalent to saying "boson-like." In the language of statistical quantum mechanic the particle can either be fermion or boson but no in-between such as "boson-like." In my opinion such equivocation brought about the unfortunate consequence and hinders our fundamental understanding of bonding in metals and alloys. Within these understanding, the assumptions have been made as described above in forming the backbone of the theory.

"Theory is something we made up to make us feel as though we know more than we actually do" —— **Albert Einstein**

The theory being proposed shall now be tested against each experimental observation as detailed below.

I. Miscibility Gap (MG) Between Two Liquid Metals

1. EXPERIMENTAL FACTS AND CONVENTIONAL THEORY

For a collection of atoms, whether monatomic or not, to come together to form an alloy, the first step is to heat the metals to a temperature where the metals turn into their liquid state. However experimentally it is often observed as shown in Table I, that the metals are not always miscible in their liquid states to one another. That is, two metals in their liquid state do not form a homogeneous solution but rather separate out in two distinct regions (phases) – much like water and oil. Despite the abundance of these cases in metallic systems, physicists, chemists, and metallurgists alike choose to ignore this prevailing phenomenon. The miscibility gap (MG) between oil and water is understood readily in terms of their electronic bonding differences; water being ionic whereas oil being exclusively covalent bond. However, in the intermetallic system based on the "free" electron theory, the miscibility gap (MG) is totally unexpected and defies a conventional theoretical explanation. This is because the "free" electron theory is based on a 'sea' of free-electrons that are roaming about among the positively charged nuclei. Thus, there is no reason for two metals in their liquid state to exist in MG state. It is even more perturbing when chemists find lithium (Li) and sodium (Na) both of which are I-A elements and therefore chemically identical to form a MG. In fact, a MG also exists between potassium (K) and sodium (Na).

As is well known to all material scientists, the phase Diagram is the "road map" to the understanding and the ultimate usage of binary or ternary system of alloys. In fact, they are so important that many Ph.D. degrees have been awarded (including my own) to those who are willing to spend a couple of years of their lives in determining phase diagrams experimentally. Approximately 3000 binary alloy systems have been obtained in this manner. For more than thirty years, a group of scientists devoted their time to find a way to calculate phase diagrams from a small amount of data. This effort led to the scientific journal, CALPHAD, which is devoted to the possible calculation of phase diagrams.

If two metals do not mix in their liquid state, there would be no phase diagram to draw and thus no understanding of how to utilize the alloy. A good example of how a phase diagram can help us in utilizing an alloy is amply demonstrated in the formation of stainless steel. Without phase diagram, we would not know at what temperature the alloy should be annealed or to what temperature it should be quenched. Without this knowledge, we would not have created 'hard-steel' vs. 'soft-steel' etc. to make special steel to suit specific application. In summary, existence of MG is not a trivial matter and should be understood before we can embark on trying to understand other observations.

Table 1

List of binary metallic systems found to have Miscibility Gap (MG). Each system is symbolized by atomic notation (the range of MG in at. % referring to the second element is indicated numerically).

Ag – Cr	(10-100)	Ca – U	(1-98)	K – Na	(4-96)
Ag – Mn	(50-100)	Cd – Ga	(20-95)	K – Pb	(25-63)
Ag – Ni	(0-100)	Cd – Pu	(40-99)	K – Zn	(0-100)
Ag – Rh	(5-80)	Ce – Mn	(1-99)	La – Mn	(14-40)
Ag – Se	(10-100)	Co – Pb	(0-100)	La – Pu	(22-90)
Ag – Te	(10-30)	Co – Se	(3-30)	La – V	(2-88)
Ag – U	(0-100)	Cr – Cu	(6-56)	Li – Mn	(0-100)
Al – Bi	(0-100)	Cr – Cd	(2-62)	Li – Na	(3-92)
Al – Cd	(0-100)	Cr – Pb	(10-60)	Mg – Na	(0-100)
Al – In	(5-90)	Cr – Sn	(2-100)	Mg – U	(0-100)
Al – K	(0-100)	Cu – Pb	(15-67)	Mg – Pu	(15-90)
Al – Na	(0-100)	Cu – Se	(3-30)	Mn – Pb	(3-63)
Al – Pb	(0-100)	Cu – Te	(4-30)	Mn – Sr	(0-100)
As – Tl	(30-60)	Cu – Tl	(14-80)	Mn – Tl	(3-92)
Au – Re	(17-70)	Cu – U	(23-95)	Na – Zn	(2-93)
Ba – Mn	(6-99)	Cu – V	(27-98)	Nb – Y	(1-54)
Be – Ga	(2-85)	Er – V	(27-98)	Ni – Pb	(2-98)
Bi – Co	(1-85)	Ga – Hg	(2-96)	Ni – Tl	(3-92)
Bi – Cr	(1-80)	Ga – K	(38-95)	Pb – U	(38-95)
Bi – Ga	(1-75)	Ga – Pb	(3-94)	Sb – Se	(16-47)
Bi – Mn	(52-90)	Ga – Ta	(1-33)	Se – Sn	(53-85)
Bi – Si	(1-98)	Ga – Tl	(0-100)	Te – Tl	(69-98)
Bi – U	(50-98)	Hg – Se	(71-85)	Th – U	(27-92)
Ca – Cd	(20-70)	Fe – Sn	(31-70)	Tl – Zn	(10-98)

2. UNDERSTANDING THE MG BASED ON THE THEORY PROPOSED

The theory being proposed states that metals and alloys are consisted of covalent bond as well as metallic (quasi-free electron) band. Also, it has been pointed out that covalent bond has many faces. Therefore, it can be said that while the 'free'-electron part from both lithium metal and sodium metal are indistinguishable and may mix freely, the covalent bond part may be distinct from one another to the extent that they are prevented from mixing and forming a homogeneous solution. As stated in the proposed theory, the covalent bond is far more susceptible to the temperature change than the 'free'- electrons. Therefore at higher temperature, the covalent bond may loose its covalency completely and no longer prevent

the intermixing of two metals. At this point MG is expected to disappear – this is indeed the case is exemplified in the Li-Na phase diagram as shown in Fig. 4.

The reason that covalent bond is sensitive to temperature change is the fact that electrons can be moved (excited) from one atomic orbital to another with the temperature change. Readers who are not familiar with covalent bond should read *VALENCE BOND* by C.A.Coulson (Oxford University Press, 1979) [1] or *CHEMICAL BONDS* by H. B Gray (Benjamin/Cummings, Pub.Co.1973) [2].

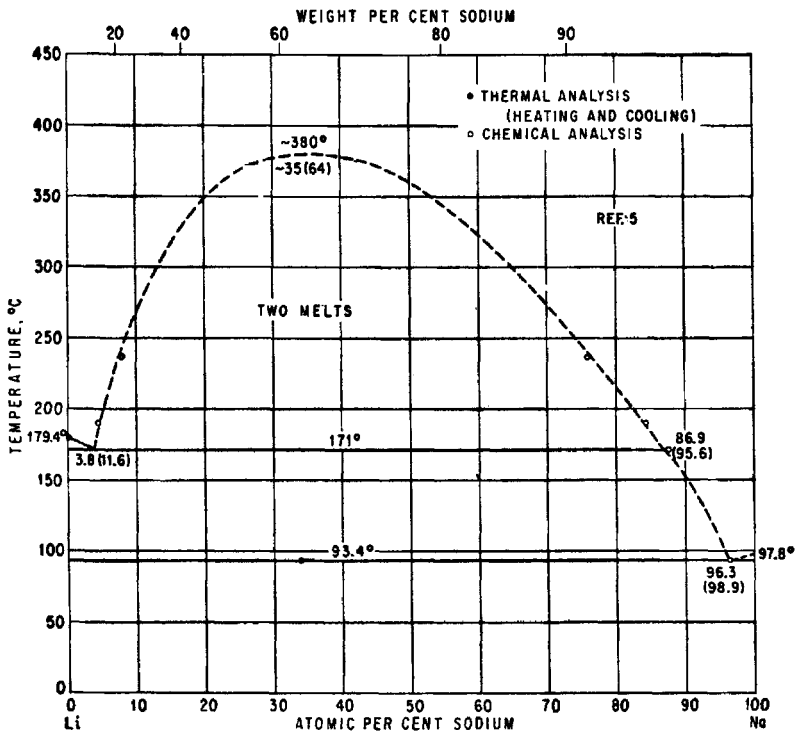

Fig. 4. The phase diagram of Li-Na system showing the MG disappearing at about 380°C.

II Phase Equilibrium Diagrams

As we emphasized in the previous chapter, the phase equilibrium diagrams (or commonly known as phase diagrams) between two elements (binary system) or among three elements (ternary system) are the 'road map' to the practical use of an alloy. Because phase diagrams are so vital to industry, compilation of the phase diagrams has been very active and extensive. To date, all the phase diagrams that have been compiled (Hansen, Elliot, and Shunk) [4, 5, 6] were obtained experimentally. The calculation of phase diagrams from some basic principles has not been successful. The reason for this is that any calculation has to begin in their liquid state. But, most liquids do not follow the ideal solution law, e.g., Raoult's and Henry's law. To make matters worse, we do not have an equation of state for the liquid state. Although we have a mean of investigating and determining liquid structure through low-angle X-ray diffraction studies, we do not know how the dynamic arrangement of structure comes about. That is whether the cluster of dynamic atomic arrangement is the result of the atomic potential or the atomic arrangement itself creates the potential. As a result, we cannot set up a mathematical model for the dynamic atomic arrangement or eventually an equation of state for the liquid state.

It is important to have a common understanding of the terminology used to describe a phase diagram as shown in Fig. 5 (a fictitious phase diagram between A and B). Generally, the temperature is set along the y-axis and the composition is set along the x-axis. The line (a) is known as the liquidus line. Above the line, the material is a homogeneous liquid whereas below the line the material is liquid plus solid. The A_xB_y is known as a *congruent-melting* compound where at its apex (melting point) the composition of liquid is the same as that of the compound. On the other hand, the compound, A_mB_n is known as an *incongruent-melting* compound (peritectic compound) where the composition of liquid is different from that of the compound. The melting temperature line for this compound is known as the peritectic line. The point (b) where the two liquidus lines intersect discontinuously is known as *eutectic point* and the horizontal line along that point is known as the *eutectic line.* The region close to pure elements designated as α and β are known as the *primary solid solution* showing the solubility range in each other.

It should be pointed out that an intermetallic compound, whether it is congruent-melting or incongruent-melting, is chemically and physically different from the elements it is made of. Thus, compounds are distinct from alloys. For example, compound alloy TiNi is totally nonmagnetic despite the fact it contains 50 atomic % of nickel [3]. It also resists chemical reaction despite the 50 atomic % of titanium. On the other hand, an alloy of an equi-atomic mixture of nickel and titanium will show the chemical and physical characteristics according to the individual characteristics of nickel and titanium. As was pointed out before, all the phase diagrams we have compiled are the result of experimental work rather than from calculations. Thus, the assumption is that the pressure is constant while it varied with temperature and composition. According to Gibb's phase rule, $F = C - P + 1$ (where F is the degree of freedom, C is the number of components and P,

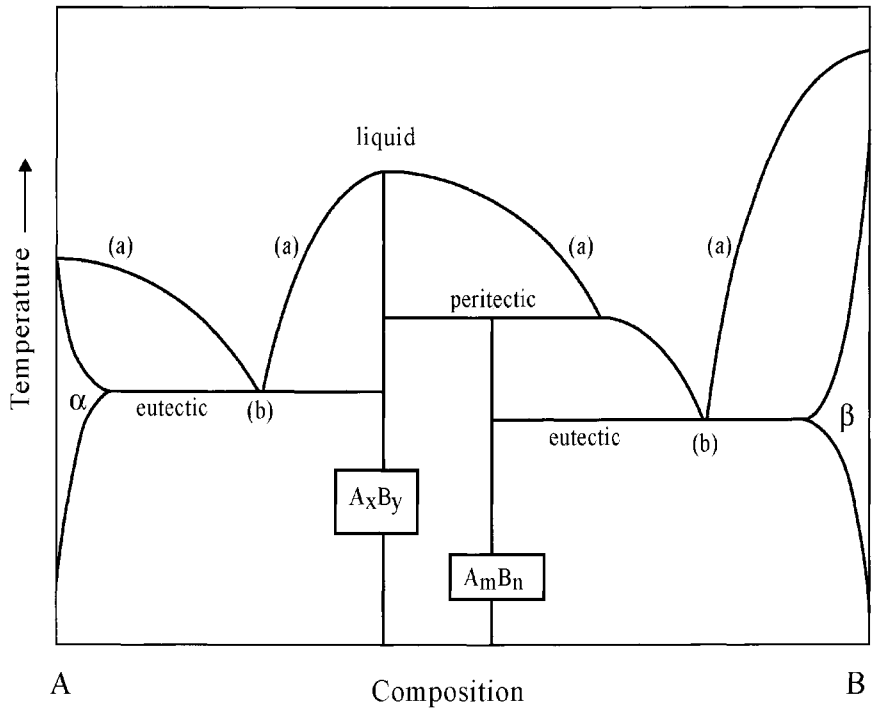

Fig. 5. An imaginary phase diagram between two elements, A and B showing critical region in a phase diagram

the number of phases). Thus, points (b) as shown in Fig. 5 will have no degree of freedom. In contrast along the liquidus line (a) the degree of freedom shall be limited to 1. And in the liquid state above liquidus line the degree of freedom shall be 2. According to the phase rule, in a given phase diagram the degree of freedom or the number of phases present can be predicted. However the rule is totally helpless in predicting the exact curve of the liquidus line or how many compounds it can form and for that matter whether the compound formed should either be congruently or incongruently melting type.

1. CORRELATIONS AMONG CONGRUENT-MELTING AB COMPOUNDS

Some years ago in a continuing effort to understand phase diagrams, I had discovered [3] the following empirical rules among more than 300 binary phase diagrams reported in the literature (Hansen, Elliot & Shunk) [4,5,6]. The metallic radii, R_A , R_B, used are from *INTERATOMIC DISTANCES* (The Chemical Society, London, 1958) [7] and the structural notation follows that described in *Handbook of Lattice Spacing and Structure of Metals* (Pearson, 1958) [8])..

a) For systems in which $R_A \approx R_B$, the liquidus curves are roughly symmetric on both sides of the compound composition.
b) For systems in which $R_A \neq R_B$ and the radius ratio, R_A / R_B (or R_B / R_A) falls in the range, 1.1 ~ 1.5, the liquidus curves are asymmetrical with the larger area (encompassed by the liquidus line and the compound line) lying on the side of the element with larger atomic radius.
c) For systems in which the radius ratio falls in the range of 1.6 – 2.0, the liquidus-curve-maximum actually shifts away from stoichiometric composition in the direction toward the side of the element with larger atomic radius.
d) The crystal structures of congruent-melting compounds all belong to the B1, B2, B3, B8, or B32-type in which A atoms are enveloped (the first coordination) by B atoms. And conversely, B atoms are enveloped (the first coordination) by A atoms. Crystallographically, all atoms in these structures occupy special positions that do not involve x, y, or z parameters.
e) The incongruent-melting (peritectic) compounds, on the other hand, have a crystal structure that falls into the B20, B26, B37, B_f or $L1_0$ type in which A atoms are not enveloped by B atoms. And conversely, B atoms are not enveloped by A atoms. In these cases, some of the atoms always occupy general positions involving x, y, and z parameters.

In essence, correlations a) through c) are related with the shape of the liquidus curves of AB congruent-melting compounds and subsequently to the size of atomic radius. On the other hand, d) and e) correlate the atomic arrangement or the crystal structures of the compound to their mode of formation, i.e., congruent- *vs.* incongruent-melting. As an example, we show three phase diagrams in Fig. 6 – (a), (b) and (c). Fig. 6-(a) is the Au-Sn system in which the atomic radius ratio is 1.44/1.40 = 1.03 representing the case a). Fig. 6-(b) is the Ca-Tl system having an atomic radius ratio of 1.96/1.70 = 1.15 representing the case b). In Fig. 6-(c) we see the extreme case of the Cr-B system in which the atomic radius ratio is 1.25/0.79 = 1.58 representing case c).

It should be pointed out that the correlations a) through e) share an underlying common factor. All correlations are attributable to an equilibrium condition existing between the solid and liquid states. This therefore suggests that an understanding of the liquid state is essential to the establishment of a theoretical reason for the correlation.

2. THEORETICAL CONSIDERATION

2.1 Atomic Configuration in the Binary Liquid System

If elements A and B are completely miscible in all compositions in their liquid state, it is reasonable to assume nearly equal interactions among the three possible cases; A-A, B-B and A-B in their liquid state. Let us assume the atomic radii of A and B are about equal to one another (i.e., $R_A \approx R_B$). With this assumption, the system is essentially a 'hard sphere' or a Bernal model [9]. In the absence of gravitational or other external effects, the liquid solution will reach a dynamic equilibrium where the system is random-dense-packed and homogeneous throughout. Under these conditions we ask the following question pertaining to the atomic configuration.

What is the probability of a given A (atom) being surrounded (i.e., immediate neighbors with distance $d_{AB} = R_A + R_B$) by n number of B (atom)'s as a function of composition?

If the immediate neighbor atoms (coordination number) m is known such as in a crystalline solid, the question can be answered readily by invoking the binomial theorem. Since in the liquid state the coordination number m varies dynamically throughout the system, the answer to this question requires more thought. We know that for a given β (the atomic composition of B), there exists an average number of B's surrounding A and that the number $\tilde{n}(\beta)$ can be written as:

$$\tilde{n}(\beta) = \sum_{n=1}^{m} W_n(\beta) \qquad (1)$$

where $W_n(\beta)$ is the fractional probability of having n number of B's surrounding A such that

$$W_n(\beta) = P_A^{nB}(\beta) / \sum_{n=1}^{m} P_A^{nB}(\beta) \qquad (2)$$

where $P_A^{nB}(\beta)$ is the probability of having *n and only n* B's surrounding A at a given β.

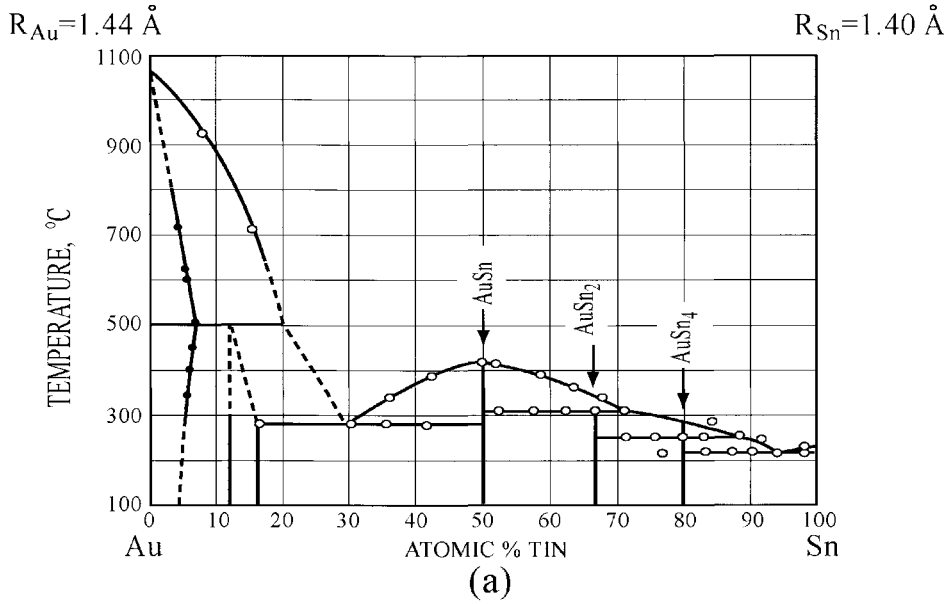
R_{Au}=1.44 Å
R_{Sn}=1.40 Å
TEMPERATURE, °C
1100
900
700
500
300
100
AuSn
$AuSn_2$
$AuSn_4$
0 10 20 30 40 50 60 70 80 90 100
Au
ATOMIC % TIN
Sn

(a)

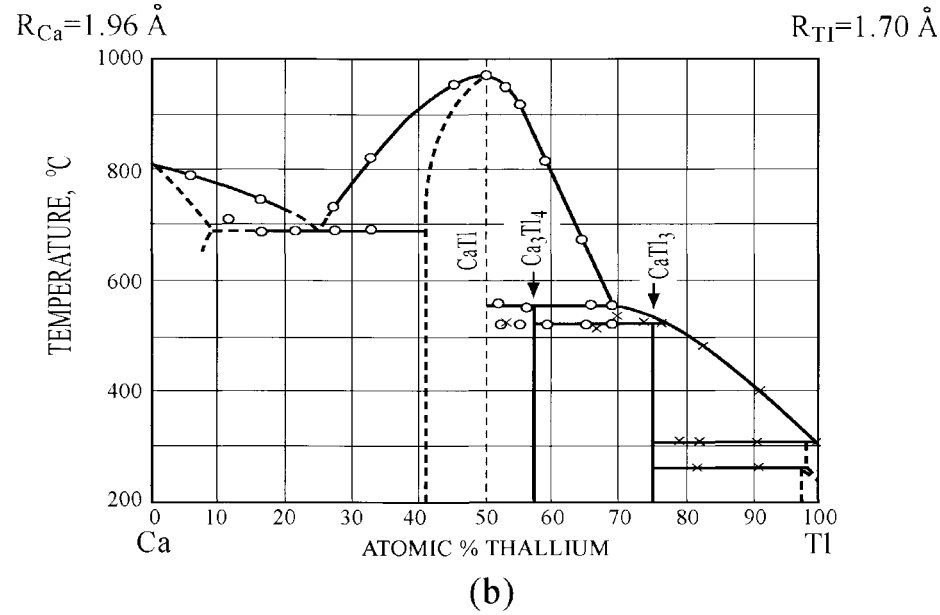
R_{Ca}=1.96 Å
R_{Tl}=1.70 Å
TEMPERATURE, °C
1000
800
600
400
200
CaTl
Ca_3Tl_4
$CaTl_3$
0 10 20 30 40 50 60 70 80 90 100
Ca
ATOMIC % THALLIUM
Tl

(b)

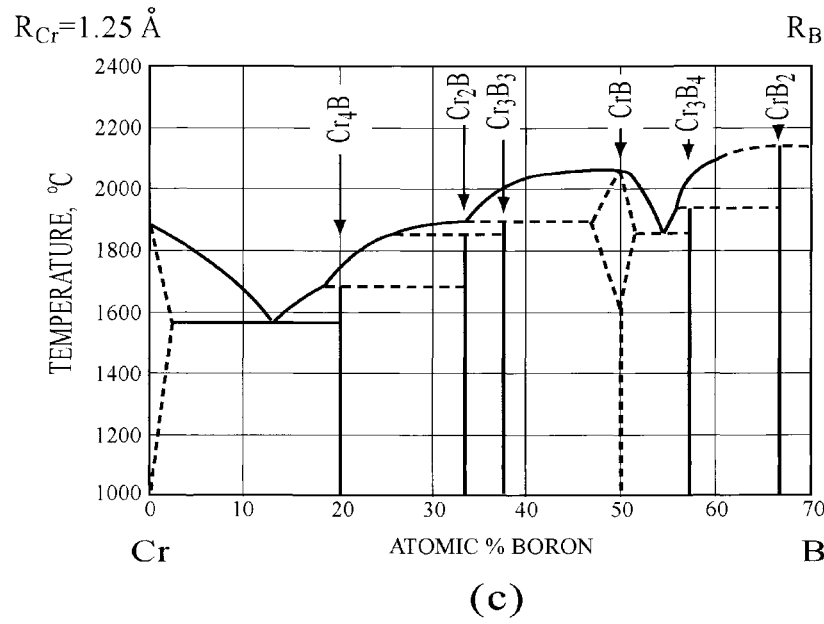

Fig. 6. (a) atomic radii of Au and Sn are nearly the same resulting in a symmetric liquidus curves, (b) atomic radii of Cu and Tl are somewhat different resulting in a asymmetric liquidus cuves with flatter side on Cu, (c) atomic radius of Cr considerably larger than the radius of B resulting in a very lopsided liquidus curves.

Number m is the maximum, spatially allowable, number of B's in a coordination sphere surrounding A. Therefore, the answer to the above question is equivalent to a characterization of $W_n(\beta)$ which we shall show to be equal **to** $\beta^{n-1}.\alpha$ where α is the fractional atomic composition of A.

Since the system under consideration can be regarded as a canonical ensemble [10], the probability of a specific atomic configuration around a given A can be equated to the fractional number of A's with that particular configuration. The probability of a given A being surrounded by n number of B's at composition β is equal to $(\beta)^n$ — assuming n is exceedingly small compared to the total number of B atoms in the system. Thus, a series of $(\beta)^n$ with various n values can be represented by a fractional number of A's as illustrated below.

In the case, $\beta = ½$, with the total number of atoms in the system equal to N, we have

n = 1; $(A_1, A_2, \underline{A_3, \bullet\bullet\bullet\bullet\bullet\bullet\bullet\bullet\bullet, A_{N/4} \bullet\bullet\bullet\bullet\bullet\bullet A_{N/2}})$

n = 2; $(A_1, A_2, \underline{A_3, \bullet\bullet\bullet\bullet\bullet A_{N/8} \bullet\bullet\bullet\bullet\bullet A_{N/4}})$

n = 3; $(A_1, A_2, \underline{A_3, \bullet\bullet\bullet A_{N/16} \bullet\bullet\bullet A_{N/8}})$

$\bullet\bullet\bullet\bullet\bullet\bullet\bullet\bullet\bullet\bullet\bullet\bullet\bullet\bullet\bullet$

$\bullet\bullet\bullet\bullet\bullet\bullet\bullet\bullet\bullet\bullet\bullet$

$\bullet\bullet\bullet\bullet\bullet\bullet\bullet\bullet$

n = m $(A_1, A_2, \bullet\bullet\bullet A_{N(1/2)m})$.

It is clear that any given A cannot attain (n + 1)B neighbors without first attaining nB neighbors. Thus, the A's within the bracket represent those with nB atoms, whereas the underlined A's represent those which also belong to the (n + 1)th level. Consequently, the number of A's with n =2 are a subset of those with n = 1. Analogously, the number of A's with n=3 are a subset of those with n=2 and so forth. It can be generalized that the number of A's with (n+1)B neighbors are a subset of the A's with (n)B neighbors. Consequently, the number of A's having n and only n B neighbors (excluding the n+1 subset) must be equal to $(\beta)^n - (\beta)^{n+1}$. Therefore, the probability of A being surrounded by n and only n_B atoms as a function of β is,

$$p_A^{nB}(\beta) = (\beta)^n - (\beta)^{n+1}. \quad \text{and}$$

$$W_n(\beta) = P_A^{nB}(\beta) / \sum_{n=1}^{m} P_A^{nB}(\beta) = (\beta)^n - (\beta)^{n+1} / \sum_{n=1}^{m} (\beta)^n - (\beta)^{n+1}$$

The total sum of the n and only n probabilities for all levels is,

$$\sum_{n=1}^{m} (\beta)^n - (\beta)^{n+1} = (\beta - \beta^2) + (\beta^2 - \beta^3) + \cdots\cdots\cdots + (\beta^{m-1} - \beta^m) + \beta^m$$

$$= \beta \qquad \text{thus}$$

$$W_n(\beta) = (\beta)^n - (\beta)^{n+1} / \beta = \beta^{n-1} \cdot \alpha \qquad (3)$$

In order to appreciate the physical meaning of the probability distribution, let us set n = 1; then, $W_1(\beta) = \alpha$, the curve of which is shown in Fig. 7. This curve shows that the probability of A being surrounded by one and only one B is highest for $\alpha \approx 1$ ($\beta \approx 0$) and is lowest for $\alpha \approx 0$ ($\beta \approx 1$). Physically, this must be correct because at $\beta \approx 0$ there are not enough B's for A to have more than one B neighbors. Thus, the probability for having one and only one B neighbors must be close to 1(one). Conversely, at $\beta \approx 1$, there are so many B's in the solution that the probability for A's to have one and only one B neighbor is nearly nil. The other probability curves given in Fig. 7 for different values of n can be interpreted in a similar manner.

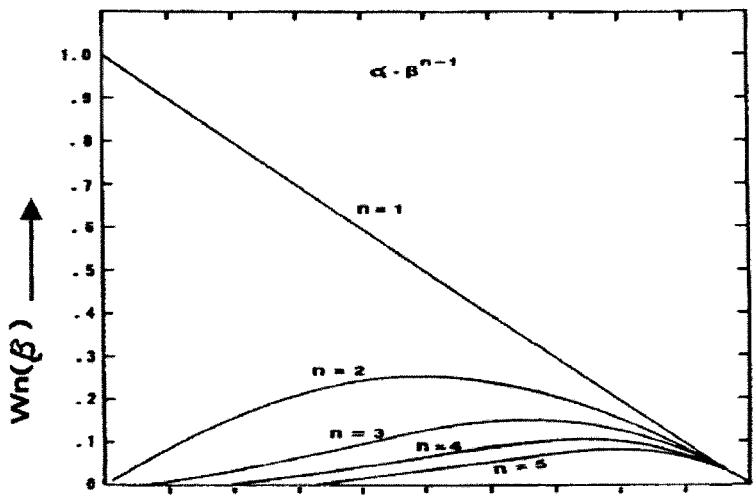

Fig. 7. Curves of $\alpha \cdot \beta^{n-1}$ as a function of β corresponding to different values of n.

Following the same line of logic, the probability of B being surrounded by n' and only n' A's can be written as a function of composition:

$$W_n(\alpha) = (\alpha)^{n'-1} \cdot \beta \qquad (4)$$

where n' may or may not be the same as n.

Now, we shall ask the following question which is pertinent to the total atomic configuration (i.e., the entropy of mixing) in a binary liquid system;

What is the probability of an atomic configuration in which A's are surrounded by n number of B's which are in turn surrounded by n' number of A's as a function of composition?

Inasmuch as the probabilities $W_n(\beta)$ and $W_{n'}(\alpha)$ as shown in equations (3) and (4) are derived independently, the question posed above can be answered by forming a joint function between the two probabilities as follows:

$$P_{A\ B}^{n\ n'}(\beta) = W_n(\beta) \cdot W_{n'}(\alpha) \Big/ \sum_{n=1}^{m} \sum_{n'=1}^{m} W_n(\beta) \cdot W_{n'} = (\beta^{n-1} \cdot \alpha)(\alpha^{n'-1} \cdot \beta) / \Gamma$$

$$= (\beta^n \cdot \alpha^{n'}) / \Gamma = [\beta^n (1-\beta)^{n'}] / \Gamma \qquad (5)$$

where $$\Gamma = (\tfrac{1}{2}) \sum_{n=1}^{m} \sum_{n'=1}^{m} W_n(\beta) \cdot W_{n'}(\alpha)$$

Since Γ is a simple gentle curve, zero (0) at $\alpha = 1$ or $\beta = 1$ with a maximum at $\beta = \tfrac{1}{2}$ (as shown in Fig. 8), the characteristics of $P_{AB}^{nn'}(\beta)$ can be obtained by considering only the numerator, --- $\beta^n (1-\beta)^{n'}$. By differentiating $\beta^n (1-\beta)^{n'}$ with respect to β and setting the derivative equal to zero,

$$\frac{d}{d\beta}[\beta^n (1-\beta)^{n'}] = \beta^{n-1} (1-\beta)^{n'-1} [n - \beta(n+n')] = 0$$

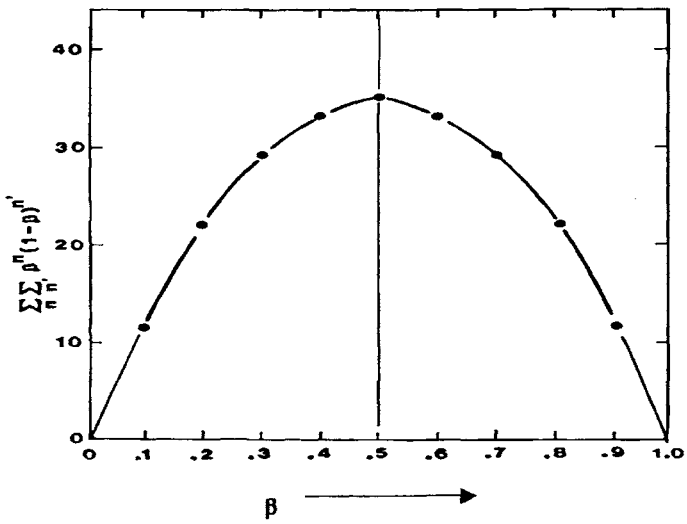

Fig. 8. Distribution function of 'A' surrounded by 'B' and 'B' in turn surrounded by 'A' as the function of B composition (β).

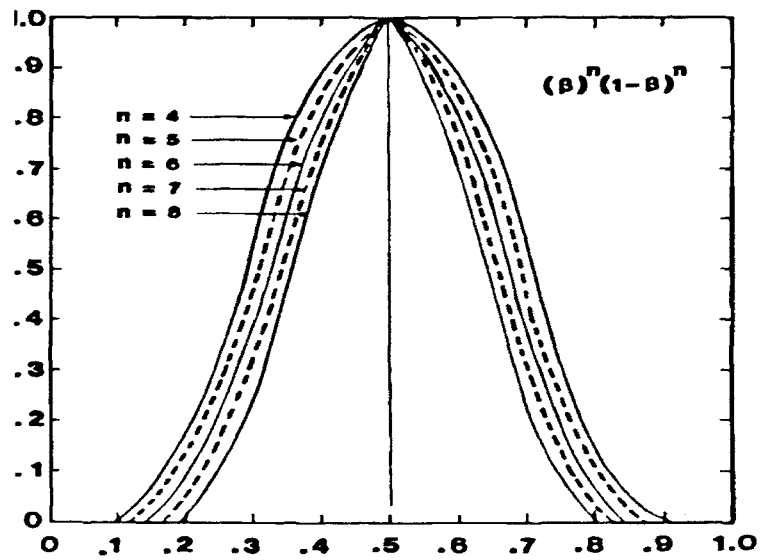

Fig. 9. Curves of β^n (1-β) corresponding to n = 4,5,6,7 and 8.

We find two minima at $\alpha = 0$ and $\beta = 0$ and a maximum at $\beta_m = n/(n + n')$. Curves representing $\beta_n (1 - \beta)^{n'}$ for different values of n and n' are shown in Fig. 9.

Each curve is normalized to 1 at its maximum. These curves, essentially, represent the entropy of mixing for different n and n' values. It is evident that the maximum always occurs at $\beta_m = n/(n + n')$ independent of the actual magnitude of n and n'. However, it is important to note (for a later comparison with the experimental results) that:

While the curve maximum is dependent only on the n /n' ratio (and not on their magnitude), the slope of the curve will be more gentle (or sharper) the smaller (or larger) are the magnitude of n and n'.

This is quite evident in the curve shown in Fig. 9.

2.2. Effect Due to Differences in Atomic Radius

We shall now examine the effect of atomic size difference between A and B on the $P_{AB}^{nn'}(\beta)$ curves. This effect can best be seen by comparing the $\rho(r)$'s --- the radial distribution functions ---- in the range $0 < r < d_{AB}$ (where $d_{AB} = R_A + R_B$), for both $R_A / R_B = 1$ and $R_A / R_B \neq 1$. For these discussions refer to Fig. 10- a, b, c. It is clear that when $R_A / R_B = 1$, the $\rho(r)$ for having A or B at the origin are essentially the same (Fig. 10- a). On the other hand, when $R_A / R_B \neq 1$, the $\rho(r)$ will be different (Fig. 10- b, c) [11,12]. This difference in the $\rho(r)$ can be related to the configuration probability by the following reasoning. Inasmuch as d_{AA} is shorter than d_{AB} the integrated area up to d_{AB} in the case of having A at the origin will contain more area due to peak, d_{AA} than due to peak, d_{AB}. This is to say that A will 'see' fewer B's than are actually present in the system of composition β. Therefore, $W_n(\beta)$, describing the probability of A being surrounded by n B's requires modification. As a first approximation, we shall correct the probability of finding one B in a melt of composition β by setting $\beta' = \beta (d_{AA} / d_{AB})$ and $\alpha' = 1 - \beta'$. With this correction, the probability of A being surrounded by n B's is modified to read $W_n^*(\beta') = (\beta')^{n-1} \cdot \alpha'$. Since the first peak in the $\rho(r)$ of having B (atom with larger radius) at the origin occurs at d_{AB} (which is the limit of our interest) no such complication exists and no modification is required of $\mathbf{W_{n'}(\alpha)}$. Therefore, the joint probability due to the size difference, $R_B > R_A$, is modified to read (again, for convenience, deleting Γ, the denominator):

$$P_{AB}^{nn'}(\beta) = W_n^*(\beta') \cdot W_{n'}(\alpha)$$
$$= [(\beta')^{n-1} \cdot \alpha'][(\alpha)^{n'-1} \cdot \beta] \qquad (6)$$

For the $R_A > R_B$ case, the modification is conversely applied only to the probability of B being surrounded by A's and leads to $W_n^*(\alpha') = (\alpha')^{n'-1} \cdot \beta'$. The modified probability curves of equation (6) corresponding to three different radius ratios, $R_B / R_A = 1.25$,

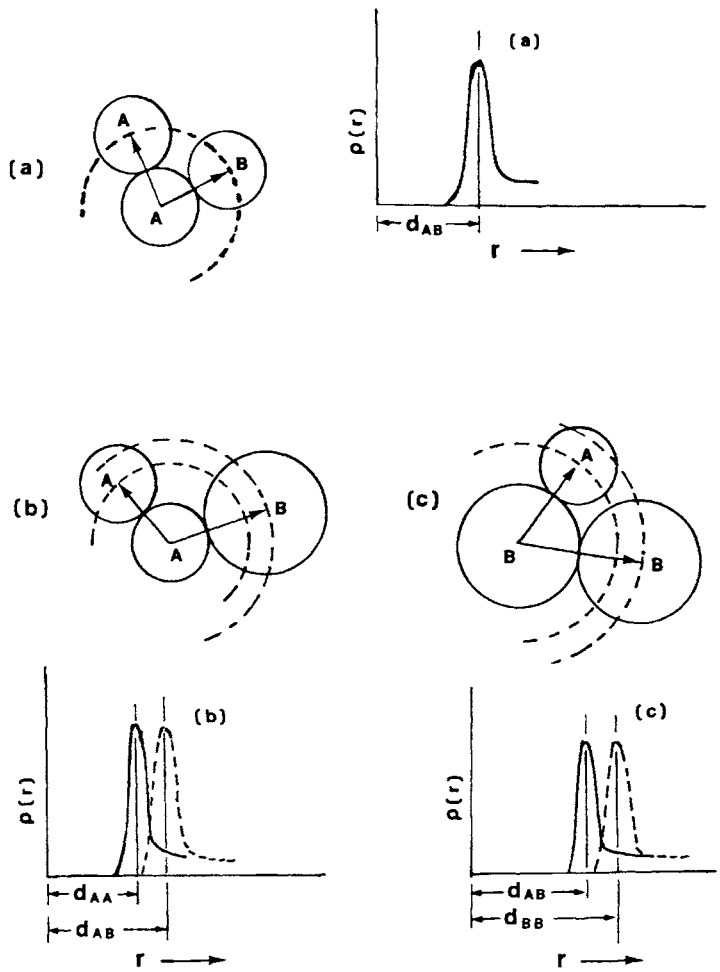

Fig. 10. Pictorial representation of atomic configuration in the immediate neighborhood and the corresponding radial distribution function for (a) $R_A = R_B$ with A at origin, (b) $R_A < R_B$ with A at the origin and (c) with B at origin.

1.5, and 2.0 for n = n' = 4 are shown in Fig. 11-a. Note that the curve maxima, β_m, shifts progressively toward the B-rich (larger atomic radius) side from the stoichiometric composition as the R_B / R_A ratio is increased. That similar shifts also occur for n/n'= 2 with R_A/R_B = 1.35 is shown in Fig.11-b. Thus, it can be summarized that:

The effect of atomic size on $P_{AB}^{mn'}(\beta)$ is to shift β_m toward the side with the larger atomic radius and the magnitude of shift is proportional to the atomic radius.

Prior to a discussion on the correlations, d) and e) relating crystal structure and its mode of formation – whether congruently or incongruently melting, we must examine the following facts. We have shown that certain atomic configurations are more probable than others for a given composition through the configuration probability, $P_{AB}^{mn'}(\beta)$. However, the configuration probability thus derived, is based solely on the Gibbs' canonical ensemble concept [13] in which the 'system average' is equated to the 'time average.' Therefore,

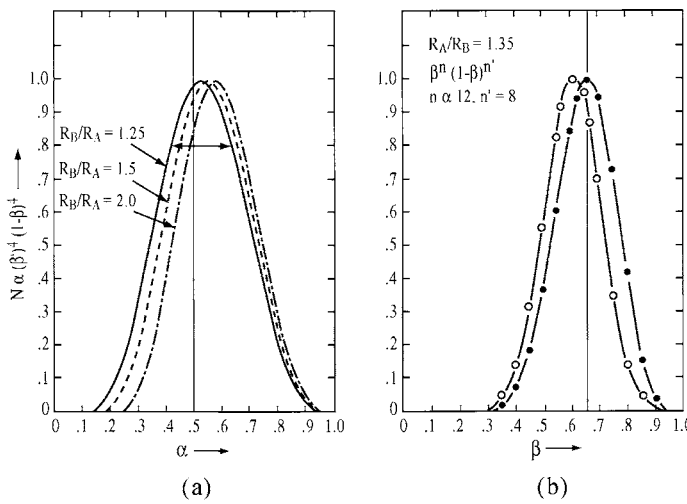

Fig. 11. Demonstrating the probability curve shift due to the R_A/R_B ratio change.

strictly speaking the configuration probability we have derived does not truly represent the liquid state in terms of local atomic configuration probability as given in Eq. (5) represents a static state and gives us only the statistical distribution of configuration as a function of composition. In order to describe the liquid state properly, we must also consider local configuration fluctuations as a function of time.

2.3 Fluctuation of Atomic Configurations as a Function of Time

Let us take a given configuration, in a micro-region of liquid space, denoted by C_{ℓ}^{n}, where n indicates an equal coordination number for A and B; ℓ represents the continually fluctuating nature of the configuration. Due to the continual movements of atoms, the local configuration, C_{ℓ}^{n} may be termed 'configuration in passing,' i.e., the configuration that exists momentarily while the atoms are passing one another. For this reason, C_{ℓ}^{n} will have a 'life-time', $\Delta \mathbf{t}$, the time interval between the formation and dissipation of the configuration in the specific micro-region of liquid space. It is clear that $\Delta \mathbf{t}$ should be about the same for all local configurations with different n. If this were not so, the equilibrium state, and subsequently the Gibbs' canonical ensemble [13] would not hold and would lead to a non-equilibrium state.

Logic would suggest that $\Delta \mathbf{t}$ must be inversely proportional to the average velocity, $\overline{V}$, of the atoms in the system. Following the Boltzman distribution function [14] the number of atoms dN_v, with velocity, V (independent of direction and expressed in polar coordinates) can be written as:

$$dN_v = N[m/2\pi kT]^{3/2} \cdot \exp[-mv^2/2kT]4\pi V^2 \, dV$$

Thus, the average (direction-independent) velocity, $\overline{V}$, is

$$\overline{V} = 1/N \oint V dN_V = [m/2\pi kT]^{3/2} \oint \exp[-mv^2/2kT]4\pi v^3 \, dv$$

$$= [8kT/m]^{1/2}$$

Since $\overline{V} = \Delta d / \Delta t$, by setting $\Delta d = d_{AB}$, we have

$$\Delta t = d_{AB} [m/8kT] \qquad (7)$$

Now, consider another 'life-time', Δt_C, which is due to the potential energy. By taking a certain isotropic potential Φ (r) – say Lennard-Jones type [15] and assuming the potential to be symmetric [16], there will be a characteristic frequency, υ_C, associated with the harmonic potential. Thus, Δt_C, can be written as:

$$\Delta t_C = 1/\upsilon_C = 2\pi[m/\kappa]^{1/2} \qquad (8)$$

where κ is the force constant and m, the atomic mass.

Let C_S^n represent the static configuration that resides within the potential in the micro-region of liquid –space i.e., the counterpart to the configuration, C_ℓ^n. We know that the relationship exists between the static, C_S^n, and the dynamic, C_ℓ^n configurations should somehow be related to the two 'life-time's, Δ t andΔ t_C. This relationship we write as:

$$P(C_\ell^n \cup C_S^n) = \exp[\Delta t / \Delta t_C] \qquad (9)$$

such that

$P(C_\ell^n)$ when $\Delta t < \Delta t_C$

$P(C_\ell^n \cap C_S^n)$ when $\Delta t = \Delta t_C$

$P(C_S^n)$ when $\Delta t > \Delta t_C$

These mathematical relationships are based on a physical argument (as detailed below) rather than on a mathematical derivation and may be regarded as questionable, *a priori,* at this point. The ultimate justification for Eq. (9) is, therefore, based on physical intuition and rests on agreement of the final results with experimental evidence. As an example, the relationship will be utilized in the next chapter to calculate the melting temperature of metallic elements. In the meantime we shall show that the static configuration probability derived in Eq. (5) as a function of composition **β** must be weighted by Eq. (9). This leads to a new function (setting n = n' and dropping A and B subscripts):

$$L^n(\beta, T) = P^n(\beta) \cdot P(C_\ell^n \cup C_S^n)$$

$$= P^n(\beta) \cdot \exp[\Delta t / \Delta t_C] \qquad (10)$$

which is a function of both the composition and temperature. We now show that this function can be directly related to the liquidus curve associated with an AB stoichiometric composition (n = n') having a local configuration, C_S^n.

2.4 Liquidus Curve in Terms of $L^n(\beta, T)$

Based on this modified, weighted relationship, conditions for the physical states are now stated as follows:

Condition	Physical State
$P^n(\beta) \cdot \exp[\Delta t / \Delta t_C - 1] < 1$	liquid
" " $= 1$	melting point
" " > 1	solid

For the following discussion see Fig. 12. In order to fully appreciate these physical correlations, let us assume a given configuration probability, $P^n(\beta)$ in which $\beta_m = ½$ and $P^n(1/2) = 1$. Setting $T = T_m$ leads to $\Delta t = \Delta t_C$ and $\exp[(\Delta t / \Delta t_C) - 1] = 1$. Under these conditions and according to the criterion, $P^n(\beta) \exp[\Delta t / \Delta t_C - 1] = 1$, there can be only one point in the composition-temperature phase diagram at which a solid-liquid equilibrium state exists - namely at $\beta = ½$ and at $T = T_m$. If the $P^n(\beta)$ curve was symmetric (with $R_A = R_B$) and assumed a value of 0.8 at $\beta = 1/3$ and at 2/3, in order for the $P^n(\beta) \cdot \exp[\Delta t / \Delta t_C] = 1$ to hold requires $\exp[(\Delta t / \Delta t_C) - 1] = 1.25$ and subsequently $\Delta t / \Delta t_C = 1.22$. From Eq. (7) it can be seen that the solid-liquid equilibrium temperature, T_2, for $\beta = 1/3, 2/3$, should be less than T_m ($\beta = ½$) by the ratio, $T_m/T_2 = (1.22)^2 = 1.48$. This demonstrates that at $T_2 = 0.675(T_m)$, there are two points in the composition-temperature phase diagram at which the solid-liquid equilibrium can exist. It is equally clear that since $P^n(\beta)$ can only equal to one (at its maximum) or less than one for when $T_1 > T_m$ (and $\Delta t / \Delta t_C < 1$) there can be no points throughout the whole composition-range at which liquid can coexist with solid in equilibrium.

In this manner, the criterion, $P^n(\beta) \cdot \exp[\Delta t / \Delta t_C - 1] = 1$, represents the liquidus curve in the composition-temperature phase equilibrium diagram. Clearly, the shape of the $L^n(\beta, T) = 1$ curve must be parallel with the configuration probability, $P^n(\beta)$. The correspondence between these physical arguments and an actual phase equilibrium diagram (the Li-Hg system) for T_1, Tm, and T_2 is illustrated in Fig. 12.

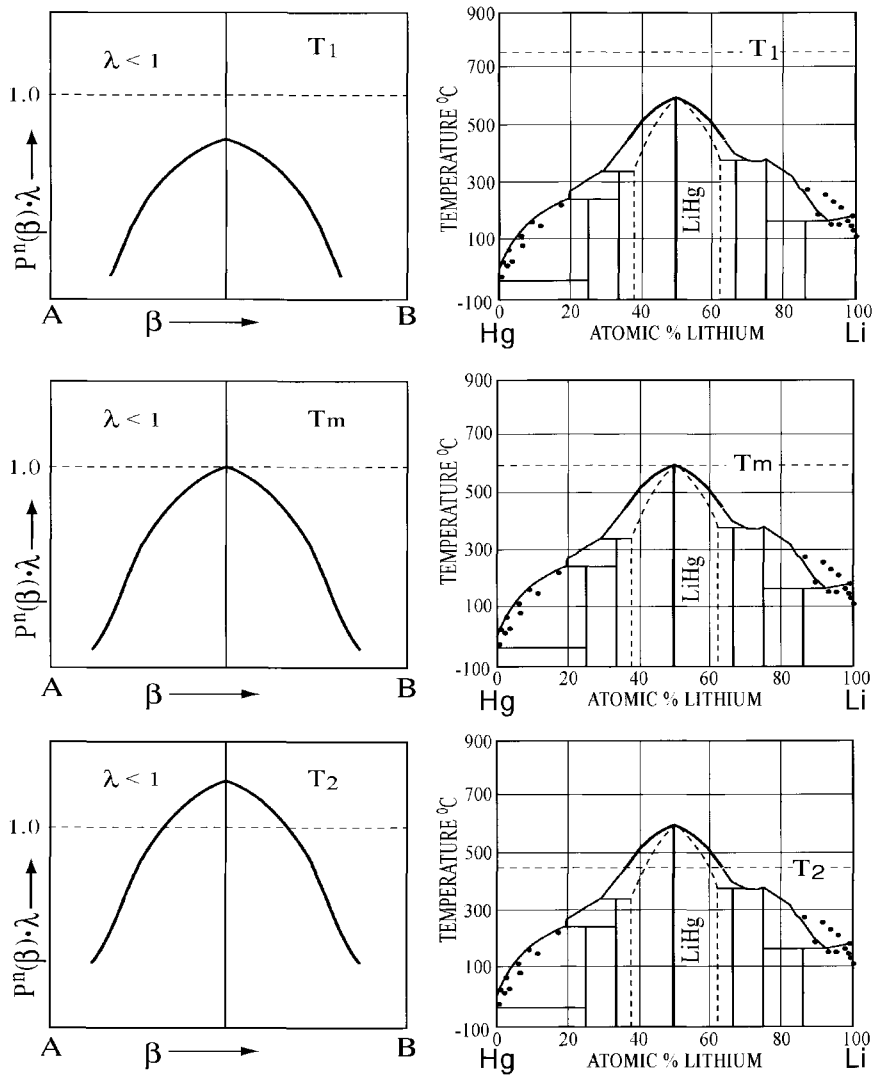

Fig. 12. Theoretical liquidus curves vs. the liquidus curve for HgLi at temperatures: T_1. T_m amd T_2. where $\lambda = \exp[(\Delta t/\Delta t_c) - 1]$.

2.5 Congruent vs. Incongruent Melting in Terms of Local Configuration

Thus far, we have utilized only the L-J (Lennard-Jones) type potential in demonstrating the (liquidus-curve) – (atomic-configuration) relationship. In many cases, however, there will exist additional potentials due to even stronger short-range interactions such as covalent or ionic bonds that are responsible for compound formation. Let us assume a binary A-B system in which a strong short-range interaction, f_{AB} , exists in a tetrahedral-geometry (such that A interacts with 4B's and B in turn interacts with 4A's in a tetrahedral configuration). We shall denote this potential by $\Phi^4(r)$. Associated with this potential will be κ_4, ν_4 and Δt_4 analogous to those defined above in the L-J potential. Since the $\Phi^4(r)$ potential will yield tetrahedral geometry in both the static, C_S^4 *and liquid* C_ℓ^4 , the criterion of equation (12) will apply only if $P^n(\beta) = P^4(\beta)$, where $P^4(\beta)$ is the configuration probability that dictates the presence of absence of C_ℓ^4. This is to say that other probability curves, $P^5(\beta), P^6(\beta), \cdots\cdots$ etc. will be ignored by the $\Phi^4(\beta)$ potential even though they may be present in the liquid state. With this understanding, the criterion for compound formation is,

$$L^4(\beta,T) = P^4(\beta)\cdot \mathrm{P}\left(C_S^4 \cup C_\ell^4\right) = P^4(\beta)\cdot \exp\left[\left(\Delta t/\Delta t_C\right)-1\right]$$

In other words, the criterion requires that the configuration in passing, C_ℓ^4, conform to the static configuration, C_S^4, and vice versa. This implies that at its melting point, T_m^4, the conditions, $\Delta t = \Delta t_4$ and $C_S^4 = C_\ell^4$ are the required condition for congruent-melting. Needless to say, the liquidus curve associated with this compound will follow exclusively that of $P^4(\beta)$. Therefore, this qualitatively explains the experimental correlation, d). Thus, for a stoichiometric AB compound in a binary system to be congruently melting, the crystal structure of the compound must be one of those that are describable in terms of "A surrounded by B's and B in turn surrounded by A's."

On the other hand, if the atomic arrangement in an AB compound cannot be described in terms of "A surrounded by B's and B surrounded by A's" because some d_{AA} or d_{BB} are shorter than d_{AB}, the static configuration, C_S^n, will never match the local dynamic configuration, C_ℓ^n based on the $P^n(\beta) = \beta^n(1-\beta)^n$ curve. Thus, $C_S^n \neq C_\ell^n$, unequal liquid and solid composition, defines incongruent-melting compounds. This is the essence of correlation e). It is logical to conclude that in congruent-melting compounds, f_{AB} dominates over f_{AA} and f_{BB} whereas in incongruent-melting compounds, either the f_{AA} or f_{BB} dominates over f_{AB}.

3. EXPERIMENTAL EVIDENCE IN SUPPORT OF THE THEORY

3.1 AB Compounds with Coordination Number of n = 4

As illustrated in the Fig. 13 among the crystal structures of congruently-melting AB compounds, the B1 and B8 types have a coordination number of n = 6; and B2, a coordination number of n = 8. The B3 and B32 structure type has a coordination number of only n = 4. The theoretical prediction is that the liquidus curves, $L^4(\beta,T)=1$ associated with the compound structure of n = 4 coordination should be patterned after their respective configuration probability, $P^4(\beta)$. Inasmuch as the $P^4(\beta)$ curve is the most gentle compared with $P^6(\beta)$ or $P^8(\beta)$, the liquidus curves for compounds of the B3 or B32 types (with n=4) are expected to be gentle in their slope compared with those associated with compounds with higher coordination number; e.g. B1, B2 or B8. Experimentally, the AB compounds, AlSb, AsGa, AsIn, CdSe, CdTe, InSb, GaSb, HgTe, InSb, and TeZn all have an n = 4 atomic coordination number. It should be pointed out that these compounds are all "II-VI" or "III-V" valence compounds such that the n = 4 tetrahedral coordination is not unexpected. What is not known and understood up to now is that the slope of their liquidus curve should be gentle as shown in Fig. 14. Readers can also find similar gentle liquidus curves for AlLi and InLi which have B32-type crystal structure with atomic arrangement of n = 4.

3.2 AB_2 Compounds

The experimental correlations, a) through e), obtained for the stoichiometric compounds and their theoretical justifications can now be extended to non-stoichiometric compounds. We shall start by examining AB_2 compounds based on available data [4, 5,6,17].

Correlation a); we found no systems having an AB_2 compound with $R_A = R_B$. Therefore, no confirmation (or refutation) can be made.

Correlation b); there are a number of systems in which an AB_2 compound exists with $R_A \neq R_B$. The fact that the liquidus curves associated with these compounds indeed follow the correlation is demonstrated in Fig. 15. The sole exception, $CaAl_2$, is probably due to experimental error. The Au-Na system, in which the originally reported phase diagram [18] shows a contradiction to the correlation whereas the revised phase diagram [19] conforms to the correlation, is an example of such an error (Fig. 16).

Correlation c); there are no extreme cases where $R_A >> R_B$ or $R_A << R_B$, among the AB_2 compounds on which to judge this correlation.

Correlations d) and e); there are 46 known systems in which both the phase diagram and the crystal structure of AB_2 compound have been reported. This is summarized in Table II, where there are 33 congruent-melting and 13 incongruent-melting compounds. Congruent-melting compounds assume three structure-types: C1, C15, and C16, all of which can be described in terms of "A surrounded by nB's and B in turn surrounded by nA's as illustrated in Fig. 17. Following the β_m = n/(n +n') rule, the maximum for the liquidus curves of these compounds should occur at β_m = 8/(8+4) = 12/(12+6) = 2/3, or 4/(4+8) = 6/(6+12) = 1/3, as observed experimentally. The incongruent-melting

compounds, the equation, $\beta^n(1-\beta)^{n'}$, does not apply to the atomic arrangement in these structures and finally some of the atomic positions involve x, y, z, parameters. It is clear, that d_{AA} or d_{BB} in these structure-types are shorter than d_{AB}.

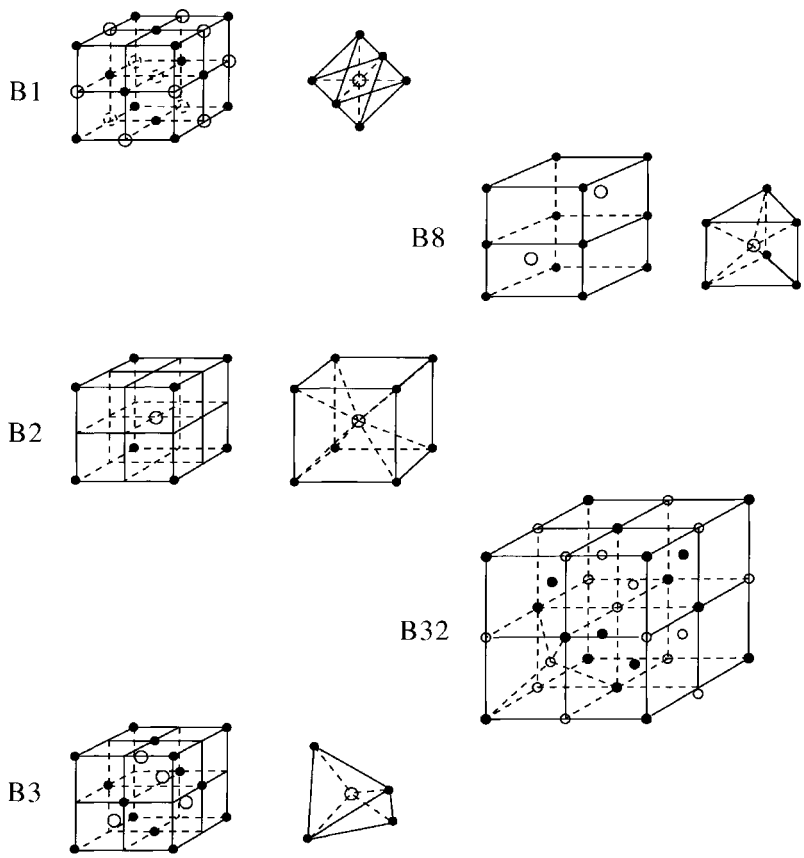

Fig. 13. Pictorial representation of B1, B2, B3, B8, and B32-type structure that are assumed by congruent-melting AB compounds. The A surrounded by B's and B surrounded by A's feature is shown.

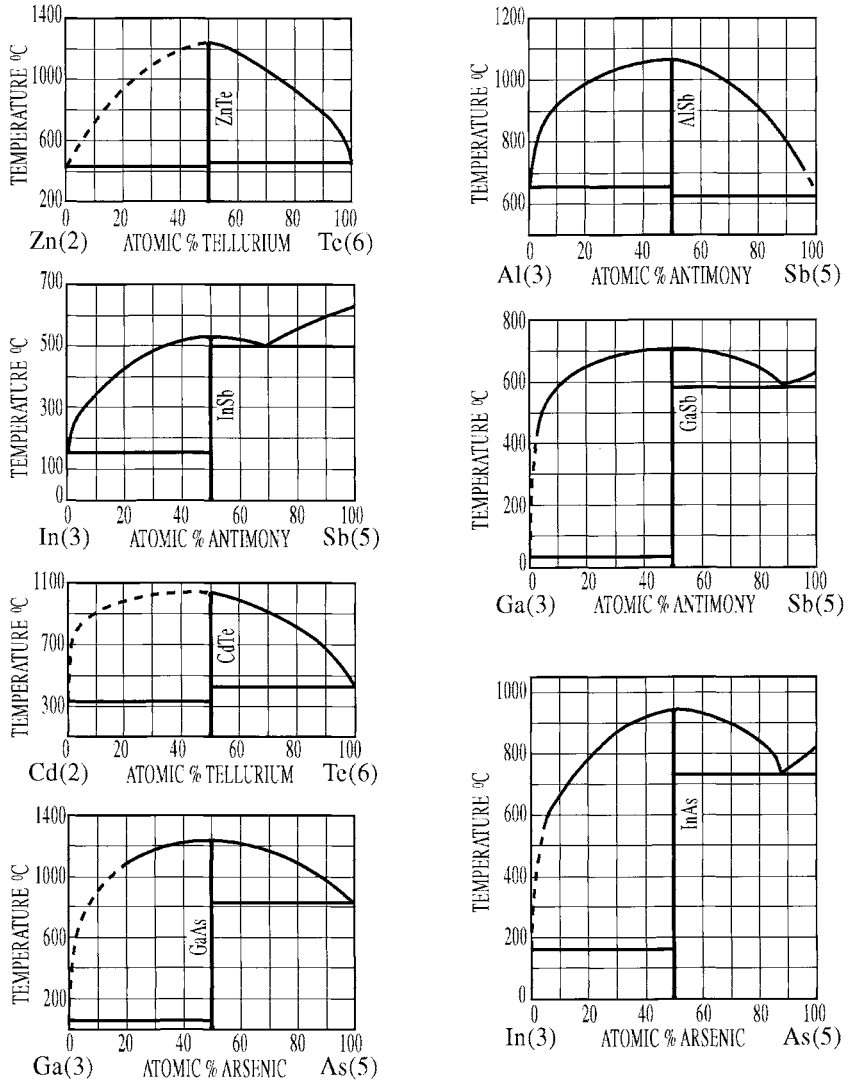

Fig. 14. Phase diagrams containing 'II-VI' or 'III-V' compounds which assume the B-3 type structure. Consistently gentle liquidus curves associated with these compounds are observed.

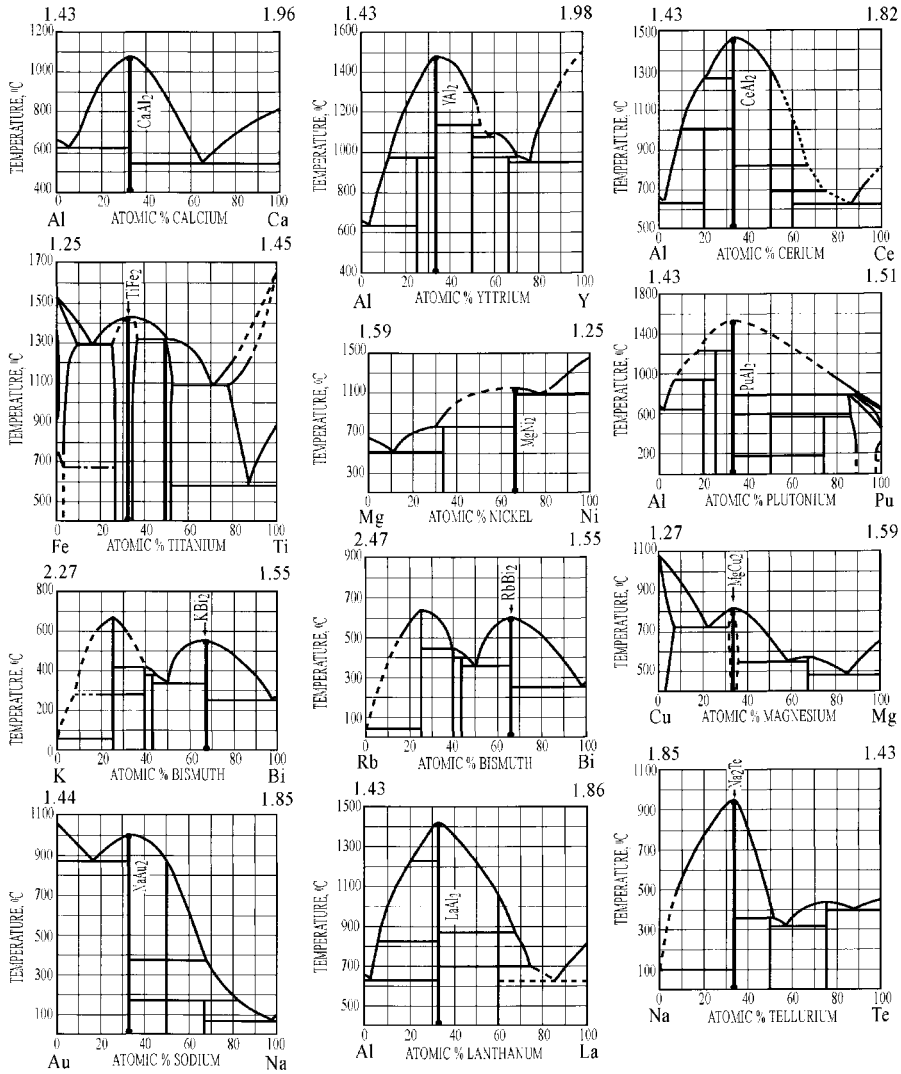

Fig. 15. Phase diagrams containing AB_2 compounds (where $R_A \neq R_B$). Liquidus curves leaning toward the element with the larger atomic radius is observed.

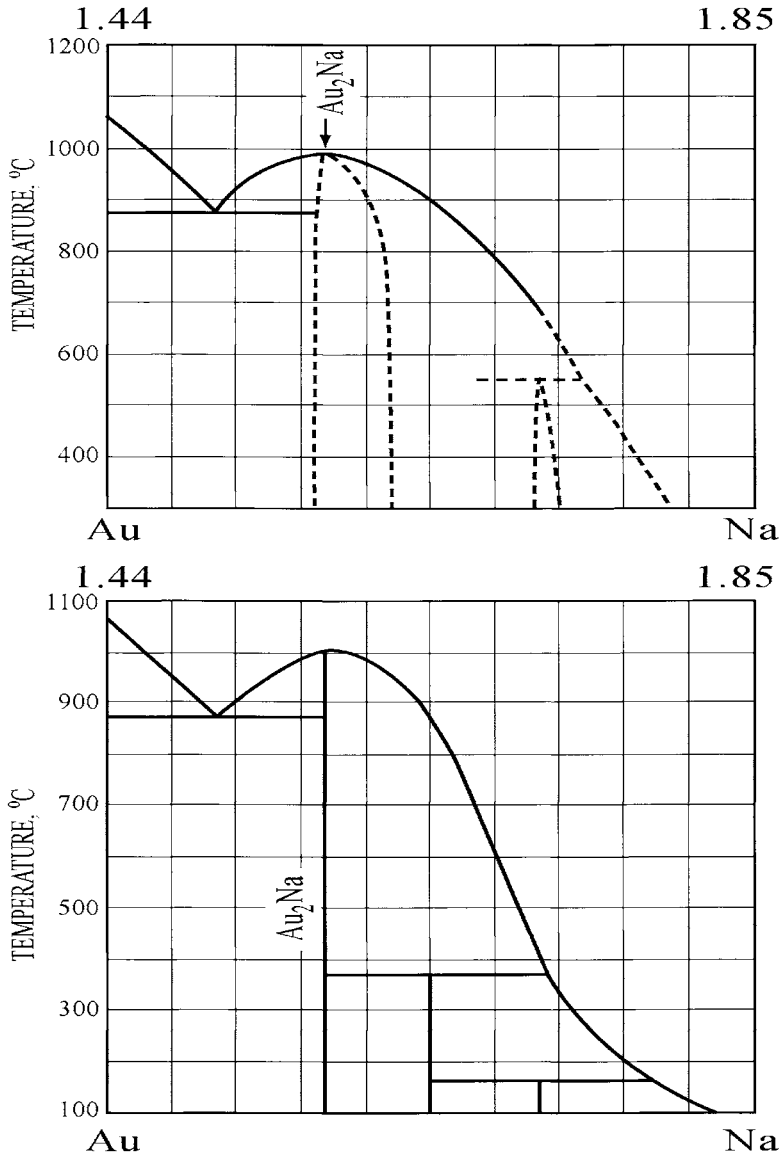

Fig. 16. Comparison of original (above) [4] and revised (revised) [5] phase diagrams of the Au-Na system.

Table 1

Observed correlation between compound formation mode (congruent vs. incongruent melting) against crystal structure type of AB_2 compounds. The underlined compounds are suspect either with the liquidus curve determination or the crystal structure type.

Congruent-melting

C1(CaF_2)-type	C15($MgCu_2$)-type		C16($CuAl_2$)
$SeAg_2$	$CaAl_2$	$PuCo_2$	BNi_2
$AuAl_2$	$CeAl_2$	$ZrCo_2$	$FeGe_2$
$AuIn_2LaAl_2$	$TiCo_2(\alpha)$		
$CoSi_2$	UAl_2	$ZrCr_2$(H)	$PdPb_2$
$SiMg_2$	$NaAu_2$	$PuAl_2$	$SiPt_2$
$SnMg_2$	KBi_2	UMn_2	$RhSn_2$
$TeNa_2$	UCo_2	$NdAl_2$	$SiTa_2$
$PbMg_2$	$MgCu_2$	YAl_2	
	$HfCo_2$		

Incongruent-melting

$CoSn_2$(C16)	$CrSb_2$(C18)	$CaTi_2$(complex)	$CoSb_2$(C18)
$CaLi_2$(C14)	Ca_2Cu(C23)	$MnSi_2$(complex)	
$CeFe_2$(C15)	$CaSi_2$(C12)	Ca_2Si(C23)	$NiTi_2$(complex)
$AuSn_2$(complex)	$NiMg_2$(C16?)		
$SbCu_2$(C38)			

The incongruent-melting formation modes reported for $CoSn_2$ (C16) and for $CeFe_2$ (C15), we believe are again due to experimental error, either in the phase diagram determination or in the structure identification. In support of this belief, we show in Fig. 18, the original [20] and the revised [21] phase diagrams for the Ce-Fe system. There is no doubt the revised phase diagram (bottom) shows the $CeFe_2$ formation to be extremely close to congruent-melting mode.

The similarity in atomic arrangement among the three Laves phases [22], i.e., C14, C15, and C36, is well known. Despite this similarity, C15 is the only structure type in which atoms assume only special positions and their arrangement conforms to the "A surrounded by 12 B's and B surrounded by 6 A's" pattern (see Fig. 17). This fact is in complete agreement with the preceding theoretical arguments that only Laves phases of the C15 structure type should be formed congruent-melting. Two systems, Ti-Co and Zr-Cr,

as shown in Fig. 19 provide indirect support for this supposition. $TiCo_2$ exists side by side in two modifications [23]; $\alpha - TiCo_2$ of the C15 type and $\beta - TiCo_2$ of the C14 type.

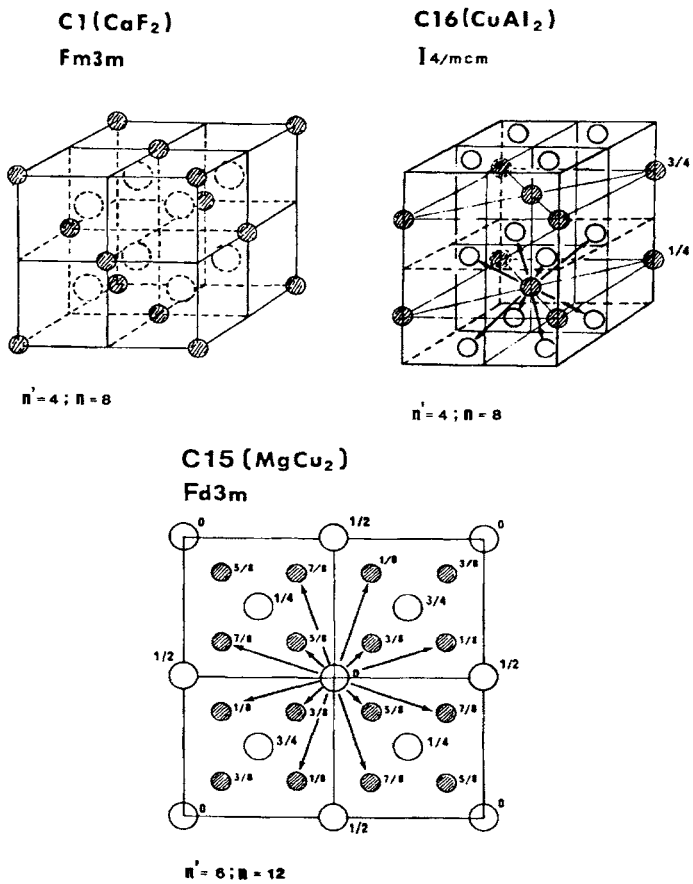

Fig. 17. Pictorial representation of the C1, C15 and C16 structure type which are assumed by congruent-melting compounds. The coordination number of A and B are n' and n respectively.

Inasmuch as the liquidus line from TiCo is slanted downward from α-$TiCo_2$ to β – $TiCo_2$ (right to left in the diagram shown), if any congruent-melting exists, it is associated with (C15 type). Therefore, the prediction is in agreement with experimental observation. $ZrCr_2$ is formed congruently and has an internal structure modification from a C15 type at high temperature to a C14 type at low temperature [24]. This is exactly what would be predicted from the theory in that a C14 type cannot be congruent-melting and thus cannot be the high temperature form.

3.3. AB_3 Compounds

More than 60 AB_3 compounds are known to exist [4,5,6] in binary systems in which both the crystal structure and the phase diagram have been investigated. With the sole exception of $TiNi_3$, all congruent-melting AB_3 compounds have been found to assume one of the three structure types: $L1_2$ ($AuCu_3$), DO_3 ($BiFe_3$), or DO_{18} ($AsNa_3$) as shown in Table 2. In the DO_{18} and DO_3 structure types there are two distinct A atomic sites with different coordination number of B atoms (see Fig.20). However, by taking the average coordination number, n' = [(2x3) + (4x1)] /6 = 5/3 for DO_{18} and n' = [(8x4) + (4x6)]/12 = 14/3 for DO_3, the maximum for all three structure types are again found to occur at β_m = n/(n+n') = ¾ conforming to the "A surrounded by B and B surrounded by A" rule. Incongruent-melting compounds, on the other hand, assume structures (e.g.,DO_3, DO_{19}, A15) that do not have the characteristic feature of "A surrounded by B and B surrounded by A." Obviously, some of the d_{AA} or d_{BB} distances in these structures are shorter than d_{AB} as typified by the short d_{BB} distances in A15 compounds. Therefore, the inter-atomic forces, f_{BB} , are expected to be stronger than f_{AA} or f_{AB}. This expectation has been verified [25] in an investigation of the electron density distribution in V_3Si. With this understanding, the underlying justification of the correlation between the superconducting temperature, T_C, and the compound formation mode for the A15-type will become more obvious as will be discussed in the later section of "*SUPERCONDUCTIVITY.*"

It is of interest to note that there are 5 systems (Ce-In, Hg-Li, In-Pr, Ir-Ti, and Pd-Sn) in which both AB_3 and A_3B compounds are found to exist. The correlation between the mode of formation and the structure type is again found to be obeyed in these cases as shown below.

System	AB_3 (mode) - Structure	A_3B (mode) - Structure
Ce-In	$CeIn_3$ (cong.) - $L1_2$	Ce_3In (cong.) – $L1_2$
Hg-Li	$HgLi_3$ (cong.) – DO_3	Hg_3Li (incong.) – DO_{19}
Ir-Ti	$IrTi_3$ (incong.) – A15	Ir_3Ti (incong.) – $L1_2$
In-Pr	$InPr_3$ (incong.) – fcc	In_3Pr (cong.) – $L1_2$
Pd-Sn	$PdSn_3$ (incong.) – complex	Pd_3Sn (cong.) – DO_3
Pb-Pt	$PbPt_3$ (incong.) – Ll_2	

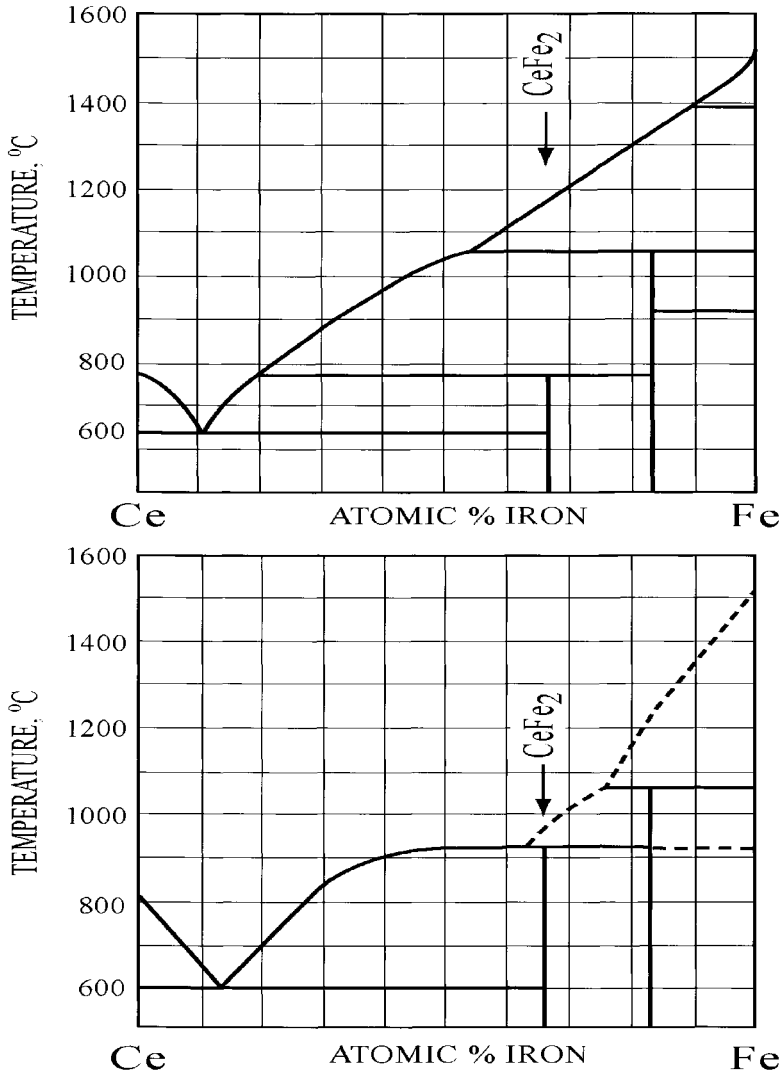

Fig. 18. Comparison of the original (above) [4] and the revised (below) [5] phase diagrams of the Ce-Fe system. The change in the formation mode of $CeFe_2$. from unequivocally incongruent-melting to nearly congruent-melting is to be noted.

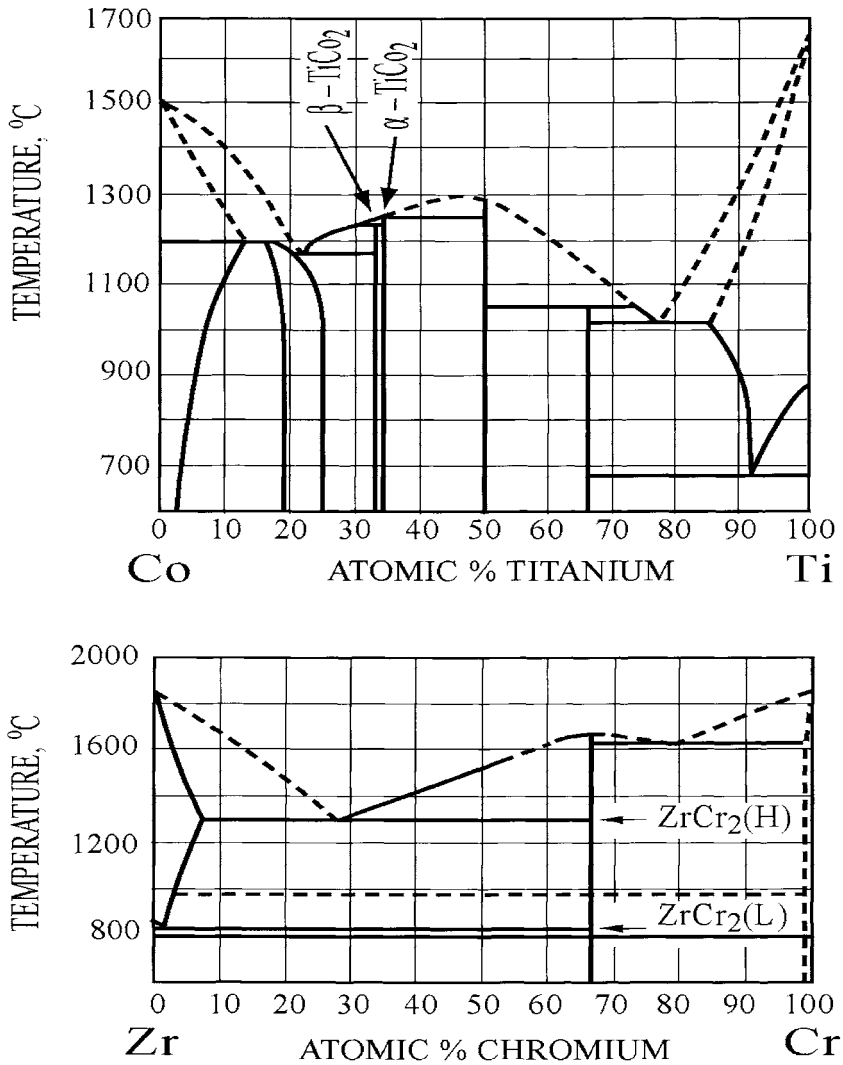

Fig. 19. Phase diagrams of the Co-Ti and Cr-Zr systems. α–$TiCo_2$ (C15 type) with higher melting-temperature and β–$TiCo_2$ (C16 type) with lower melting-temperature is noted. ZrCr (H) high temperature form again has C15 type structure whereas ZrCr(L) low temperature form has a C16 type structure.

Table 2

AB_3 congruent-melting compounds according to their structure-type.

CONGRUENT-MELTING						
$L1_2$ - type				DO_3 – type	DO_{18} - type	
$AlCe_3$	$InCe_3$	$PrTl_3$	$CoPt_3$	$BiLi_3$	$AuMg_3$	
$AlNi_3$	$LaPb_3$	$PrAg_3$	$PrIn_3$	$CeMg_3$	$BiNa_3$	
$CaSn_3$	$LaSn_3$	$PuPb_3$	UGe_3	$HgLi_3$	KBi_3	
$CaPb_3$	$LaTl_3$	$SnPt_3$	$GaPr_3$	$InCa_3$	SbK_3	
$CaTl_3$	$NbIr_3$	$SrBi_3$	$PrPb_3$	$LaMg_3$	$SbNa_3$	
$CeIn_3$	$PbPd_3$	$TaIr_3$	$PbPu_3$	$PrMg_3$	$SbRb_3$	
$CePb_3$	$TaRh_3$	$PrSn_3$	$SnNi_3$			
$CeSn_3$	$PdCu_3$	$TiIr_3$				

In view of this agreement, Ir_3Ti and $PbPt_3$ are either wrong in their phase diagram or wrong in the crystal st ructure reported. In fact, the crystal structure of two congruent-melting compounds, $LaTl_3$ and $SnNi_3$ originally reported [26,27] to be A3 and DO_{19} respectively, have been revised to be $L1_2$ and DO_3 type [28,29] in agreement with the predicted correlation.

Insofar as the effect of the atomic size difference on the shape of the liquidus line is concerned, there are not enough suitable phase diagrams (containing congruent-melting AB_3 compounds) to establish a statistical conclusion in support or nonsupport of the theoretical prediction. Nevertheless, the two related systems, Bi-Li (nearly equal atomic size) and Bi-Na (unequal atomic size) appear to be in support of the theoretical prediction.

3.4. AB_4 Compounds

Only eight (8) AB_4 compounds have been reported [4,5.6] to form congruently. However, with the exception of $BaAl_4$ and $CsHg_4$, these compounds were later found to have been erroneously identified with respect to their compound composition as detailed below:

$CaAu_4$ – Crystal structure work [30] showed the compound to be $CaAu_5$.
$SnLi_4$ – Structure work [31] showed the compound to be Sn_5Li_{22}.
$RbAu_4$ – Crystal structure work [32] showed the compound to be $RbAu_5$.
$GdCo_4$ – The revised phase diagram [33] shows the compound to form incongruently.
YCu_4 – A crystal structure study [34] showed the compound to be Ycu_5 .
YFe_4 – A crystal structure study [35] showed the compound to be YFe_5

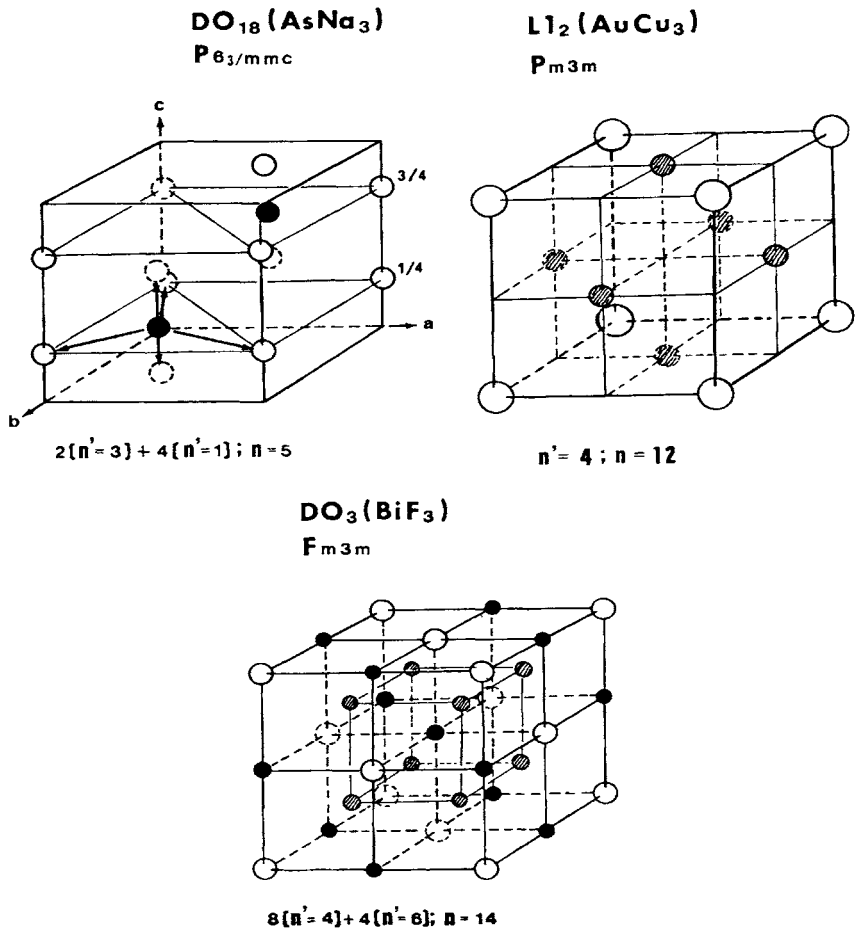

Fig. 20. Pictorial representation of the DO_{18}, $L1_2$, and DO_3 type structures which are assumed by congruent-melting AB_3 compounds. The special feature of "A surrounded by B's and B surrounded by A's" associated with congruent- melting compounds is to be noted.

With the six compounds that have been shown to be in error, a reinvestigation of the remaining two compounds, namely $BaAl_4$ and $CsHg_4$ are in order. Phase diagram studies [36, 37, 38] on the Ba-Al system show serious disagreements among the investigators. Additionally, similar compounds (e.g., $BaLi_4$, $BaMg_4$ - shown later to be Ba_6Mg_{23}) are all shown later to be incongruent-melting. The only phase diagram work on the Cs-Hg system, in which $CsHg_4$ was identified was carried out [39] in 1907 and has not been verified.

The phase diagram investigations appear to indicate that there are no AB_4 compounds that form in a congruent-melting manner. According to the theory given here, this meant that there are no AB_4 compounds whose atomic arrangement can be described as 'A surrounded by B and in turn B surrounded by A'. This arrangement is impossible for an AB_4 stoichiometric compound can be argued theoretically by considering the following boundary conditions:

a) Because B is four times of A, the structure must be cubic (with 4-fold symmetry).

b) For one A placed in the center of a cubic unit cell, the B's (must be 4 or 8) occupying special positions (no general positions involving x,y,z).

Under these restrictions, B can be placed at eight corners of a cube (0,0,0) or at the center of six faces; (1/2, 1/2, 0), etc. or along the center of cube edge; (0,0,1/2) etc. or even at the center of eight small cubes; (1/8,1/8,1/8) etc. or a combination of the available positions. Thus, it is possible to have an A surrounded by B only but it is not possible at the same time for B to be surrounded by A only. Consequently, the atomic arrangement for AB_4 compounds cannot have a situation where 'A surrounded by B and B in turn surrounded by A'. This, therefore, is the reason we do not have congruent melting AB_4 compounds. This fact is also supported by the single crystal structure study [40] of Sr_6Mg_{23}, $SrMg_4$, Ba_6Mg_{23} and $BaLi_4$ in which Sr and Ba atoms are found to be triangularly and octahedrally clustered as shown in the following figure (Fig. 21).

3.5 AB_5 Compounds.

A series of AB_5 congruent-melting compounds (e.g., $SnMg_5$, $CaZn_5$, $CeCo_5$, $LaCu_5$, $SrAu_5$) are found at this stoichiometry. These compounds assume exclusively the $D2_d$ – type structure. This structure has two distinct B atomic sites with coordination numbers of 3 and 4 as shown in Fig. 22. Thus, the average coordination number for B is n' = [(2x3) + (3x4)] = 18/5. Thus, the maximum of the liquidus line occurs at $\beta_m = n/(n + n') = 5/6$ confirming the $\beta^n (1-\beta)^{n'}$ rule once again.

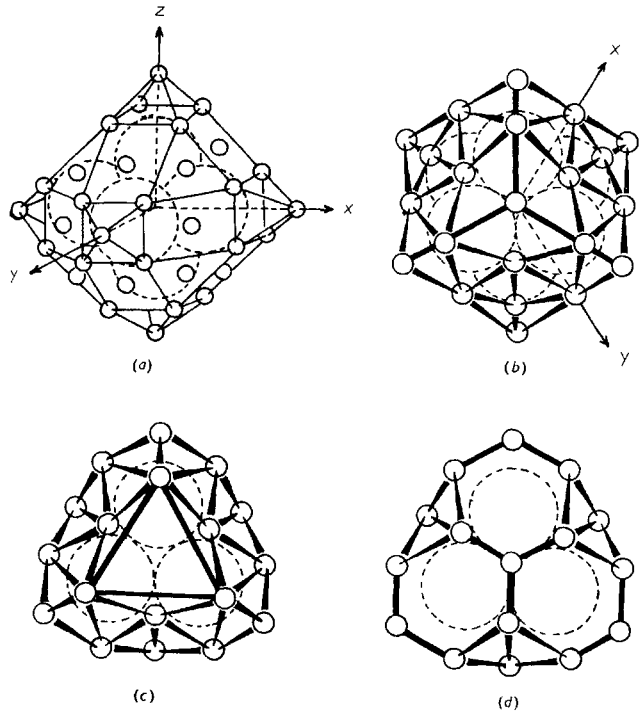

Fig. 21. (a), (b) Octahedral cluster of 6 Sr atoms surrounded by 50 Mg atoms in Sr_6Mg_{23} (fcc) and $SrMg_4$ (hexagonal), (c) triangular cluster of 3 Sr atoms surrounded by 33 Mg atoms in $SrMg_4$ and (d) triangular cluster of 3 Ba atoms surrounded by 29 Li atoms in $BaLi_4$.

3.6 AB_6, AB_9, AB_{13} Compounds

Although phase diagrams show the existence of AB_6 , AB_9 , and AB_{13} compounds, congruent-melting type compounds belonging to these stoichiometries are relatively few in number and their crystal structures are poorly characterized. Thus, no correlation can be made between them.

3.7. A_2B_3 Non-Stoichiometric Compounds

There are a number of A_2B_3 compounds (e.g., As_2Te_3, As_2Se_3, As_2Zn_3, Bi_2Se_3, Bi_2Te_3) that are congruent-melting. A complete structure study has been made [41,42] on Bi_2Te_3 and Bi_2Se_3 . Through this study, the structure has been established as rhombohedral

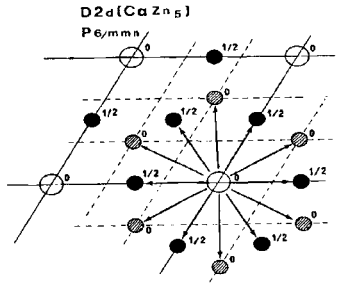

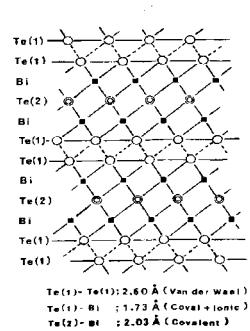

Fig. 22. (On left) Pictorial representation of the $D2_d$ –type structure assumed by congruent-melting AB_5 compounds. Where n and n' are the coordination numbers surrounding A and B respectively in the structure.
Fig. 23. (On right) Pictorial representation of the crystal structure of Bi_2Te_3 according to [63] showing the layered structure demarcated by Van der Waal's distances.

($R\bar{3}m$) with the layered atomic arrangement shown in Fig. 23. Based on the interatomic distances found, a bonding-model (which distinguishes Van der Waals, covalent, and covalent-ionic bonding in different layers) was proposed [43] and verified [44] for the structure. This crystal structure and bonding model shows that within the layer structure demarcated by Van der Waals distances (Fig. 23), the "A surrounded by B's and B surrounded by A's " rule governing congruent-melting compound is faithfully followed.

4. SUMMARY AND DISCUSSION

Two new empirical correlations among binary phase equilibrium diagrams have been established:

(1) The shape of the liquidus curve vs. the atomic sizes of the elements forming the compound.
(2) The formation mode vs. the crystal structure of the compound.

Since these two correlations share a common factor – the liquid state – a theoretical explanation of the correlation is given based on a description of the liquid state. This theoretical approach has not only accounted for the empirical correlations observed but also predicted additional correlations, which are collaborated experimentally.

One of the predicted correlations concerns the gentleness (or sharpness) of the liquidus curve vs. small (or large) values of n, the coordination number, as exemplified by the "II – VI" and "III – V" AB compounds of the B3 structure type as shown in Fig. 14.

Another predicted correlation led to the calculation of melting temperatures for a number of metallic elements based on the $(\Delta t/\Delta t_C) = 1$ relationship as described fully in the following chapter. From the theory presented here a possible way for calculating phase diagrams from the first principles becomes apparent. Such calculations may involve the following steps.

(a) Calculation of a series of $\beta^n (1-\beta)^{n'}/\Gamma$ curves for different n and n' values (restricted to whole numbers) and for different R_A/R_B ratios as a function of composition.

(b) Calculation of the static potential, $\phi(r)^{n\,n'}$ for the immediate neighbors associated with the static configuration, $C_S^{n\,n'}$ at various ratios of n/n'.

These calculations may be accomplished by invoking methods such as the Hartree-Fock-Roothaan LCAO-MO-SCE type [45], the Xα scattered wave type [46,47] or the psuedopotential [48]. Through such calculations, the information with regard to the following possible formation of compounds will become available: (1) compound composition in terms of (n/n'), and (2) relationships among f_{AA}, f_{BB}, and f_{AB}, the interatomic forces within the compound, which can be used to determine the compound formation mode (congruent vs. incongruent) and (3) T_m, the melting temperature associated with the compound based on the $\Delta t_C^{n\,n'} = \Delta t(T)$ relationship. Once the existence of compounds from (b) and their liquidus curves from (a) are established, eutectic compositions (where two liquidus curves intersect) and eutectic temperatures can be characterized.

In this manner, the whole outline including compounds, their mode of formation and the shape of their liquidus curves of an A-B phase equilibrium diagram can be drawn. It must be clearly understood that in these calculations, the local interatomic potentials will not (unlike the Lennard-Jones type) be isotropic. This is because the potentials to be calculated are for the static configuration, $C_S^{n\,n'}$, and not for the dynamic configuration, $C_l^{n\,n'}$. However, this fact will not alter the bases for obtaining the characteristic frequency, υ_C, related to a potential-well and the time interval for a single vibration, $\Delta t_C^{n\,n'} = \upsilon_C^{-1}$. That is, the second part of the description of liquidus curve is unaffected by the spatial anisotropy. Concomitantly, the first part involving the configuration probability, $P_{AB}^{n\,n'}(\beta)$, can also be shown to be unaltered by the anisotropy as follows. As shown above, $P_{AB}^{n\,n'}(\beta)$ has a maximum at $\beta_m = n/(n+n')$, such that for n = n', regardless of the magnitude of n, $\beta_m = 1/2$ will be the maximum composition. Similarly, it can be reasoned that as long as n = n', regardless of the type of anisotropy involved, the maximum will still occur at $\beta_m = 1/2$. For example, between the B1 and B8 structure types (see Fig. 6), where n = n' = 6 but with different spatial configuration, no difference in the liquidus curves maxima will be expected – and is so observed experimentally. This reasoning is in complete agreement with the theoretical assertion that the static configuration, $C_S^{n\,n'}$, in the solid will

interact (i.e., exists in equilibrium) only with a liquid configuration, $C_{\ell}^{n\,n'}$, that is identical in spatial configuration as well as in its coordination numbers, n and n'. A trial calculation following the scheme described above should be carried out.

Conventionally, the equilibrium existing between solid and liquid (such as existing at the melting point of a congruent-melting compound) is simply regarded as L ⇆ S. This however, implies erroneously that the liquid as a whole is in equilibrium with the solid. The fact is that the liquid state, in its equilibrium, is composed of a collection of dynamically fluctuating configurations, $C_{\ell}^{n\,n'}$ (with different n and n'), that are in equilibrium with one another. Inasmuch as a compound with a configuration, let us say, C_S^4 with n = n' = 4, can only be in equilibrium with that portion of liquid state with C_{ℓ}^4 configuration, the true equilibrium should be written more correctly as

$$C_S^4 \leftrightarrows C_{\ell}^4 \leftrightarrows L^4$$

where L^4 represents the whole liquid composed of all other configurations excepting C_{ℓ}^4.

The theoretical model proposed herein for describing the liquid state has two parts, $P_{AB}^{n\,n'}(\beta)$ and $\exp\left[\left(\Delta t/\Delta t_C\right)-1\right]$. The first part is based on the 'hard-sphere' or Bernal's [9] model in which defined atomic radii are assumed. This assumption is overwhelmingly justified by the agreement between the calculated and observed shapes of liquidus curves. Bernal's hard-sphere model has also been used with a high degree of success in describing certain aspects of amorphous metallic alloys [49,12,50] and liquid metals [51]. In view of these facts, it is reasonable to conclude that the description of the liquid state, (at least in metallic alloys) using the hard-sphere model is a good approximation. Whether a description of the liquid state in two separate terms as shown above is rigorously correct requires more evidence. Such a study might include prediction of density and viscosity changes in liquid state as a function of composition.

One of the methods for describing the liquid state is based on the Radial Distribution Function (RDF). Because the RDF is obtainable from low angle X-ray diffraction study, this method is attractive to both the theorists and experimentalists. Theoretically, the basic step of the method involves calculation of the potential energy, Φ_P, by combining $\rho(r)$ with $\phi(r)$ gives the interatomic potential,

$$\Phi_P = N/2\int\phi(r)\rho(r)4\pi r^2 dr$$

However, in this expression, both $\phi(r)$ and $\rho(r)$ are average values of individually distinct interatomic potentials and atomic configurations, e.g., $\phi(r)^{n\,n'}$ and $\rho_{AB}^{n\,n'}(\beta)$ as discussed in this chapter. As a result, a calculation based on average values such as that done in RDF cannot lead to a meaningful interpretation. For example, the RDF in an A-B binary system (assuming $R_A = R_B$) will be monotonic across the whole composition range both theoretically and experimentally (providing the atomic scattering factors of A and B are

about the same). Since the average potential, $\phi(r)$, is a single function of interatomic distances, r, with $R_A = R_B$ and with $f_{AA} \approx f_{BB} \approx f_{AB}$ (which is to be expected in a completely miscible liquid), the Φ_P will also be monotonic across a composition range. On the other hand, by recognizing the individual configurations, $P_{AB}^{n\,n'}(\beta)$, and individual interatomic potential, $\phi(r)^{n\,n'}$, the potential energy for the A-B system (under the same condition) can be written as:

$$\Phi_P = \sum_{mn'} \phi(r)^{nn'} \rho_{AB}^{nn'}(\beta)$$

In this expression, it is seen that significant changes in the potential energy can be expected as a function of composition. Therefore, the liquid state can be more accurately described by not taking the averages, but by breaking up the averages into individual effects.

REFERENCES

[1] C.A. Coulson, Valence Bond, Oxford Univ. Press (1979)
[2] H.B. Gray, Chemical Bonds, Benjamin Cummings, Pub. Co. (1973)
[3] F.E. Wang, CALPHAD VII, Max Planck Meeting (1978).
[4] M. Hansen and K. Anderko, Constitution of Binary Alloys, McGraw-Hill Book Co., New York (1958).
[5] R.P. Elliott, Constitution of Binary Alloys – 1st Supplement, McGraw-Hill Book Co., New York (1965)
[6] F.A. Shunk, Constitution of Binary Alloys – 2nd Supplement, McGraw-Hill Book Co., New York (1969).
[7] Interatomic Distances, The Chemical Society, Burington House, London (1958).
[8] W.B. Pearson, Handbook of Lattice Spacings and Structure of Metals, Pergamon Press, New York (1958).
[9] J.D. Bernal, Nature, 183(1959)141.
[10] J.O. Hirschfelder, C.F. Curtiss and R.B. Bird, Molecular Theory of Gases and Liquids, John Wiley, New York, Chapman and Hall, London (1954).
[11] D.E. Polk, J.Non-Cryst. Sol. 11(1973)381.
[12] J.F. Sadoc, J. Dixmier and A. Guinier, J.Non-Cryst. Sol., 12(1973)46.
[13] R.H. Fowler and E.A. Guggenheim, Statistical Thermodynamics, Cambridge Univ. Press Chapter VI (1949).
[14] L. Pauling and E.B. Wilson, Inrod. To Quantummechanics, McGraw-Hill Book Co., New York (1935).

[15] J.E. Lennard-Jones and A.F. Devonshire, Proc. Roy. Soc. (A) 163(1937)53, ibid. 165(1938)1.
[16] The assumption of a symmetric potential-well may not be too far off from the physical reality in that in a random-close-packed liquid state, atoms would tend to slid-by one another tangentially, instead of colliding head-on.
[17] E.M. Savitski, Yu. V. Devingtral and V.B. Gribulya, Doklady Akademii Nauk, SSSR, 183(1968)1110.
[18] C.H. Mathewson, Intern. Z. Metallog. 1(1911)81.
[19] G. Kienast and J. Verma, Z. Anorg. Allgem. Chem., 310(1961)143.
[20] R. Vogel, Z. Anorg. Chem., 99(1917)25.
[21] L.J. Witternberg and G.R. Grove, US Atom.Energ.Comm., MLM-1199(1964).
[22] F. Laves, Theory of Alloy Phases, Amer.Soc.Metals, Cleveland OH (1956).
[23] R.W. Fountain and W.D. Forgeng, Trans. ASM, 50(1958)617.
[24] W. Rostoker, Trans.AIME, 197(1953)304.
[25] J.L. Staudenmann, P. Coppens and J. Muller, Sol.Stat.Comm., 19(1976)29.
[26] A. Rossi, Gazz.Chim.Ital., 64(1934)955.
[27] P. Rahlfs, Metallwirtschaft, 16(1937)343.
[28] A. Iandelli, Accad.Nazl.Lincei, Rend.Classe.Sci.Fis.Mat., 29(1960)62.
[29] K. Schubert, K. Anderko and M. Kluge, Naturwissenschften, 43(1956)248.
[30] C.J. Raub and D.C. Hamilton, J.Less-Common Metals, 6(1964)486.
[31] E/I. Gladyshevskii, G.I. Oleksiv and P.I. Kripyakevich, Kristallographia, 9(1964)338; Soliet Physics, 9(1964)269.
[32] C.J. Raub and V.B. Compton, Z.Anorg.Allgem.Chem., 5(1964)332.
[33] E.M. Savitskii, V.F. Terekhova and I.V. Burov, Zh.Neorgan.Khim., 7(1962)2572.
[34] W.H. Wernick and S. Geller, Act.Cryst., 12(1959)662.
[35] K.A. Geschneider Jr.,, Rare Earth Alloys, D.Van Nostrand Co., Princeton, NJ (1961).
[36] E. Alberti, Z.metallkunde, 6(1934)26.
[37] I. Motosada, Nippon Kinzoku Gakkaishi, 17(1953)632.\
[38] F.A. Kanda and D.V. Keller, US At.Energy Comm., TID (1964)p.20849.
[39] N.S. Kurnakov and G.J. Zukovsky, Z.Anorg.Chem., 52(1907)416.
[40] F.E. Wang, F.A. Kanda, C.F. Miskell and A.J. King, Act.Cryst., 18(1965)24.
[41] E.. Donges, Z.Anorg.Chem., 265(1951)56.
[42] K. Schubert, K. Anderko, M. Kluge, H. Buskow, M. Ilschner, E. Dorre and P. Esslinger, Naturwissenchaften, 40(1951)269.
[43] J.R. Drabble and C.H.L. Goodman, J.Phys.Chem.Sol., 5(1958)142.
[44] J.R. Wiese and L. Muldawer, J.Phys.Chem.Sol.,15(1960)13.
[45] C.C.J. Roothaan, Rev.Mod.Phys., 23(1951)9.
[46] K.H. Johnson and F.C. Smith Jr., Phys.Rev. B5(1972)831.
[47] J.C. Slater, The Self-Consistent Field for Molecules & Solids, McGraw-Hill Book Co., New York (1974).
[48] W.A. Harrison, Psuedopotentials in the Theory of Metals, Benjamin, New York (1966).
[49] J.L. Finney, Proc.Roy.Soc., A-319(1970)495.
[50] J.Dixmier, J.de Phys. 35(1974)C4-11.
[51] R. Evans and D.A. Greenwood (Eds.), Liquid Metals, Conf. Ser. No 30, The Inst. Of Phys.(Bristol and London) (1976).

III Phenomenon of Melting

1. BACKGROUND

The understanding of melting temperature of an element has always been a challenge to material scientists. Through years of investigation, we know that there are more than one hundred elements known to exist in this universe. The differentiation of one element (atom) to another is based on the number of electrons surrounding an atom. We know the size of these atoms vary from about 1 Å to a maximum of 3.5 Å. And their atomic ionization potential varies from about 5 volts to 25 volts. On the other hand, the electro-negativity varies from 0.7 (eV) for Fr (francium) to 4.0 (eV) for F (fluorine). It is observed that these physical differences among atoms are no greater than an order of magnitude. In sharp contrast, the melting points of elements can vary by as much as a thousand–fold. For example, W (tungsten) has a melting point of 3,400°C, whereas, the melting point of Hg (mercury) is a mere –38.86° C. Indeed, there are no other physical parameters among atoms (elements) that vary by this magnitude.

Melting points can be defined as the point (temperature) at which the solid and the liquid states coexist in equilibrium. This understanding implies that a solid can be heated from a low temperature to a temperature at which the structure of the solid collapses and turns into liquid. Conversely, a liquid at a high temperature (above its melting) can be cooled to its freezing point at which the liquid will then turn into a solid. In spite of this observation, our attempts to understand the phenomenon of melting have always ignored the liquid state. This is because we know very little about the liquid state and more about the solid state. Therefore, starting with Lindemann's Formula [1], the physical description of the phenomenon has been based exclusively on the properties of the solid state, e.g., theorized in terms of its lattice instability [2-6], its free energy of dislocation motions [7~9], or equating to a simple order-disorder transition [10]. Although the phenomenological descriptions of melting based on solid phase alone (disregarding liquid state) was shown to be partially successful in calculating melting temperatures, they fall short in providing insight into the physical mechanism [11,12] for the phenomenon of melting.

As shown in the previous chapter, a better understanding of phase diagrams was made possible by invoking a description of the liquid phase [13] proposed earlier. We shall now show that by utilizing the same liquid phase description together with the experimentally observed force constants and inter-atomic distances, a mathematical formula for calculating melting temperatures can be derived. More importantly, it will be shown that the formula thus derived also shows how the melting temperature can be altered due to the presence of impurity or due to pressure changes.

2. MONATOMIC MELTING IN TERMS OF MICROSCOPIC ATOMIC CONFIGURATION

Physically, melting point implies the coexistence of the solid and the liquid phase. Microscopically, the situation can be represented by considering the coexistence of C_d^n and C_s^n; the dynamic and static microscopic atomic configurations. Here, *n*, denotes the number of nearest neighbor atoms in the configuration under consideration. Since C_d^n signifies a configuration in motion, it will have a lifetime, Δt_d, - the time interval between the formation and dissipation of the configuration. It is recognized that in the liquid state, there exists a series of distinct micro-configurations having different *n's*. However, under equilibrium condition, Δt_d should be the same for all distinct micro-atomic-configurations with different *n's*. For if they were different, the equilibrium state and subsequently the Gibbs' canonical ensemble would not hold and the system would be in a non-equilibrium state [15]. Logically, the Δt_d must be inversely proportional to the average velocity, $\overline{V}$ of the moving atoms. In the molten state, (liquid state) there is no energy barrier against atomic migration, so configurations change freely as a function of time. Following the Boltzman distribution law and by taking translation energy as (1/2) mV^2, the number of atoms, dN_V, with velocity, V, (expressed in coordinates) can be written as:

$$dN_V = N[m/2\pi kT]^{3/2} \exp[-mV^2 / 2kT]\, 4\pi V^2\, dV .$$

Thus, the average direction independent velocity, $\overline{V}$ is

$$\overline{V} = (1/N) \int V dN_V = [m/2\pi kT]^{3/2} \int \exp[-mV^2/2kT] 4\pi V^3\, dV$$

$$= [8kT/m]^{1/2}.$$

Since $\overline{V} = \Delta d/\Delta t$, and by setting $\Delta d = \chi$ (the shortest inter-atomic distance in solid phase and $\Delta t = \Delta t_d$, we have

$$\Delta t_d = \chi[m/8kT]^{1/2} \qquad (1)$$

This equation shows that the life-time of a dynamic configuration, Δt_d, is solely a function of temperature for a given atomic mass, m, and interatomic distance, χ. Now, we

consider another time-interval, Δt_S, corresponding to a static configuration. C_s^n, in the solid state. Due to interatomic potential, $\Phi(r)$, between atoms there exists a characteristic vibration frequency, υ, associated with the potential. Thus, Δt_S, can be written as:

$$\Delta t_S = 1/\upsilon = 2\pi [m/\kappa_x]^{1/2} \qquad (2)$$

where κ_x is the force constant between atoms separated by distance, χ. Because Δt_S is a constant (assuming a harmonic potential) whereas Δt_d is a variable as a function of temperature, three conditions are possible as follows:

$$\Delta t_d < \Delta t_S ; \quad \Delta t_d = \Delta t_S ; \quad \Delta t_d > \Delta t_S .$$

Physical interpretation of these three conditions is:

1. $\mathbf{\Delta t_d < \Delta t_S}$; the time atoms take to move through the distance, χ, is so short that they cannot be 'trapped' by the potential, $\Phi(\chi)$, and the configuration, C_d^n ,is essentially in 'passing' i.e., liquid phase.

2. $\mathbf{\Delta t_d = \Delta t_S}$; atoms move at velocity just slow enough to be 'trapped' by and/or fast enough to escape from the potential, $\Phi(\chi)$. The static and dynamic configuration therefore coexist in equilibrium i.e., $C_d^n = C_s^n$. Thus, freezing and melting occur simultaneously at this point. The temperature corresponds to this point is essentially the melting temperature, T_m.

3. $\mathbf{\Delta t_d > \Delta t_S}$; the time atoms take to move through distance, χ , is longer than the characteristic vibration time , Δt_d . Thus, they can be 'trapped' by or unable to escape from the potential, $\Phi(\chi)$ and the configuration is in static (solid) state.

3. EQUATION FOR CALCULATING MELTING TEMPERATURE

Taking the case of $\Delta t_d = \Delta t_S$ and equating Eqs. (1) and (2), and also substituting T_m for T, we have

$\chi[m/8kT_m]^{1/2} = 2\pi [m / \kappa_x]^{1/2}$ or

$T_m = 1/4\pi^2 [\kappa_x \chi^2 /8k] = 1/32\pi^2[\kappa_x x^2/k]$ (3)

which is overtly similar to Lindemann's formula,

$T_m = (1/9)[\kappa_D . U_m/ k]$ (4)

where κ_D is the Debye force constant and U_m, an undefined fraction of interatomic distance. Despite this similarity, a fundamental difference exists between Eq. (3) and Lindemann's formula Eq. (4). Eq. (3) implies that the melting point, T_m , of an element can be calculated from its known interatomic force constant, κ_x, and interatomic separation, χ. The interatomic distance, χ , is readily available from crystal structure study [14,17]. On the other hand, the known force constant, κ_x, is available indirectly from the longitudinal acoustic vibration frequencies taken from inelastic scattering of neutrons at zone boundaries. These vibration frequencies are then converted to force constants between planes, $k_0(hkl)$, through the relationship [18],

$$\omega^2(q) = 4k_0(hkl)/m.$$

Using the vectorial relationship, $k_0(hkl)$ is then converted to the force constant between atoms, k_x. For (110) in bcc, (111) in fcc, and (0001) in hexagonal structure systems, the conversion factor is equal to $(3/2)^{1/2}$.

4. CALCULATED vs. OBSERVED MELTING TEMPERATURE

The melting temperatures for the thirty-one elements, whose inelastic neutron scattering data are available, were calculated and compared against the observed melting temperatures as shown in Table 1. In this calculation, the thirty-one elements are sorted into three groups according to their crystal structure type. Different correction factor, A,

Table 1.

Summary of the calculated vs. observed melting temperature for various metallic elements.

Element Symbol	ω^2 (AL) (rad/sec)	k_x (x10^5) (dy/cm)	χ (x10^8) (cm)	T_m (°K) calculated	observed
Face-centered-cubic(111)		A factor = 1.04			
He	0.084	0.00017	.292	.31	1
Ne	1.016	0.0104	3.15	24.0	24.0
Ar	1.580	0.0321	3.77	108	84
Kr	.832	0.0354	3.99	134	116
Al	33.64	0.460	2.86	910	932
Ni	31.98	0.954	2.50	1538	1726
Cu	22.59	0.730	2.54	1214	1356
Pd	17.35	0.938	2.74	1817	1825
Ag.	9.86	0.541	2.90	1174	1235
Pb	1.88	0.198	3.40	590	608
Pt	12.96	1.284	2.78	2561	2045
Au	8.72	0.873	2.88	1868	1337
Body-centered-cubic(110)		A factor = 1.5			
Li	32.0	0.113	3.04	358	454
Na	5.70	0.066	3.70	309	370
K	2.24	0.044	4.54	310	335
Rb	0.84	0.036	4.94	300	312
Cr	37.14	0.982	2.50	2111	2130
Fe	37.91	1.075	2.48	2274	1808
Mo	25.58	1.247	2.72	3174	2893
W	17.98	1.690	2.74	4339	3682
Nb	13.05	0.616	2.86	1733	2520
Ta	7.47	0.687	2.86	1936	3269
Hexagonal (0001)		A factor = 3.3			
Be	97.30	0.443	2.22	1652	1551
Mg	9.87	0.121	3.18	925	922
Zn	3.55	0.117	2.66	626	682
Y	4.04	0.182	3.54	1726	1795
Zr	6.52	0.301	3.18	2304	2125
Cd	1.50	0.086	2.98	578	594
Tb	2.37	0.191	3.42	1691	1629
Ho	2.58	0.215	3.48	1971	1747
Tl	.96	0.099	3.40	866	576

is then applied to each group in the manner consistent with the symmetry of the crystal structure as described below and given in more detail in the *DISCUSSION*. Since the derivation of the average velocity in the liquid state is assumed to be completely isotropic and whereas in the solid state they are anisotropic with the degree of anisotropy being dependent on the structure type, a different correction factor, A, is required for each crystallographic group. The magnitude of A-factor assigned for each group is based on the best-fit between the calculated and observed, T_m, for that group.

It is of interest to note that the A-factor derived in this manner shows: A = 1.04 for the fcc group, A = 1.5 for the bcc group and A = 3.3 for the hexagonal group. The value of which follows the degree of anisotropy. With the exception of Pt, Au, Nb, Ta, and Tl, the differences between the calculated and observed are all less than 25%. This degree of difference is small considering the possible experimental error in both the measurement of phonon frequency and the melting temperature [19].

5. MELTING TEMPERATURE DEPENDENCE ON PRESSURE

The dependence of melting temperature on pressure is well known. For example, ice may melt below 0 °C under pressure. This phenomenon can be understood in our model by changes in the average velocity, $\overline{V}$, in the liquid state. Assume a substance under pressure, P_0 , at its melting temperature, $(T_m)_0$, i.e., with the liquid and solid states in equilibrium at pressure, P_0. Under this condition, we have an average velocity, $\overline{V}_0$, in liquid state and $(\Delta t_d)_0 = \Delta t_s$. However, if the pressure is increased to $P_1 > P_0$ at constant temperature, $\overline{V}_0$ will decrease to a lower average velocity, $\overline{V}_1$ which is less than $\overline{V}_0$ and leads to $(\Delta t_d)_1 > \Delta t_s$, the condition for solid state. Thus, at higher pressure, P_1, with everything else remaining the same, the substance will be in solid state. The condition for melting, i.e., $(\Delta t_d)_0 = \Delta t_s$, can only be restored by increasing temperature to

$$(T_m)_1 > (T_m)_0$$

such as to regain $(\Delta t_d)_0 = (\Delta t_d)_1 = \Delta t_s$ condition. That is, the substance has a new higher melting temperature, $(T_m)_1$ at pressure P_1 . The same logic dictates that if P_1 is further increased to $P_2 > P_1$, the temperature must be increased also to a new $(T_m)_2 > (T_m)_1$ in order to restore the melting condition. Thus, melting temperature rises proportionately with pressure. It is clear that the P-T relationship for any substance can be obtained once the dependence of average velocity, V , on pressure near its melting temperature is known. Inasmuch as the P-V and P-η (viscosity) relationship are closely related and η is in turn related to compressibility, κ, $dT/dP \propto \kappa$ relationship is also describable by use of the

Clausius-Clapeyron equation. Because the magnitude of changes in χ and k_χ in solid state are negligible compared to the changes in viscosity, η, or average velocity, $\bar{V}$, in the liquid state due to pressure changes, it is justified to ignore the effect of χ and k_χ changes in these consideration.

6. MELTING TEMPERATURE DEPENDENCE ON IMPURITY

Another important aspect of experimental as well as theoretical consideration of the phenomenon of melting lies in the melting temperature dependence of the presence of soluble impurities. Here, a serious deficiency exists in the 'one-phase'-theory of melting which considers only the stability of solid phase in one form or another. This deficiency stems from its inability to treat Debye temperature or the vibration amplitude changes due to the presence of foreign atoms. As was pointed out in my earlier paper [13], bringing the liquid state into the microphysical picture of melting allows treatment of the dT/dC relationship in the present model in the following manner.

The three possible conditions, which distinguish the liquid, solid, and melting states according to our model, are: $\Delta t_d < \Delta t_S$, $\Delta t_d > \Delta t_S$ and $\Delta t_d = \Delta t_S$. These conditions now can be expressed in terms of the probability field for C_d^n and C_S^n [13] the microscopic local atomic configurations as follows:

$$P\left(C_d^n \cup C_S^n\right) = \exp\left[\Delta t_d / \Delta t_S - 1\right] = 1$$

from which three conditions become possible as

$P\left(C_d^n\right) = 1$ - liquid state, when $\Delta t_d < \Delta t_S$

$P\left(C_d^n \cap C_S^n\right) = 1$ - melting, when $\Delta t_d = \Delta t_S$

$P\left(C_S^n\right) = 1$ - solid state, when $\Delta t_d > \Delta t_S$

These probability field expressions relate the probability for the existence of C_d^n and/or C_S^n in the liquid as one or zero depending solely on the Δt_d to Δt_S relationships. However, this relationship is not valid in a binary liquid solution of B in A (let us say 10% of B in A). This is because the probability of configuration, C_d^n, where n is the coordination number with 10% B will not be as high as when the liquid contains only A.

For this reason, the probability, $P_{AB}^{mn'}(\beta)$ where β is the fraction of B – due to composition differences, will always be less than one for $\beta \neq 0$. Therefore, the melting criterion, $\Delta t_d = \Delta t_S$ or $\exp[\Delta t_d / \Delta t_S - 1] = 1$, set forth earlier must be modified by another probability, $P_{AB}^{mn'}(\beta)$, leading to a new criterion for the melting condition.

$$P_{AB}^{mn'}(\beta) P\left(C_d^n \cup C_S^n\right) = P_{AB}^{mn'}(\beta) \exp[\Delta t_d / \Delta t_S - 1] = 1$$

It is clear that if $P_{AB}^{mn'}(\beta) = 1$ such as in pure A ($\beta = 0$), the condition for melting is simply reduced to $\exp[\Delta t_d / \Delta t_S - 1] = 1$ or $\Delta t_d = \Delta t_S$, as described before. However, if the probability, $P_{AB}^{mn'}(\beta)$ was less than one – let us say 0.8, the condition for melting according to the new criterion will require $\exp\left[\left(\Delta t_d / \Delta t_S\right) - 1\right] = 1.25$ and leads to a new $(\Delta t_d)' = 1.22(\Delta t_S)$. And subsequently, the new melting temperature, T_m' with $P_{AB}^{mn'}(\beta) = 0.8$ would be related to the T_m with $P_{AB}^{mn'}(\beta) = 1$ by the ratio, $T_m / T_m' = (1.22)^2 = 1.48$. Consequently, T_m' will be lower than T_m. Since $P_{AB}^{mn'}(\beta)$ changes continually with composition change, T_m will decrease accordingly. In short, the liquidus curve in the composition-temperature phase equilibrium diagram at constant pressure reflects the change in the probability, $P_{AB}^{mn'}(\beta)$.

7. SUMMARY AND DISCUSSION

In this section, we have shown that by relating physical parameters from both the liquid and solid states, a formula for calculating the melting temperature of a monatomic solid can be derived. The reasonable agreement between the calculated and observed T_m's for the 31 elements examined, attest to the validity of the formula derived and subsequently the physical model invoked. The strength of the physical model is further enhanced by the logical manner in which the melting temperature dependence on pressure and impurity can be shown.

One of the shortcomings in the present model is the assumption of isotropy in the liquid state, whereas, in the solid state, a definite symmetry exists from the crystal structure. This discrepancy results in the necessity to differentiate the 31 elements examined into three groups according to their crystal symmetry, i.e., fcc, bcc, and hexagonal. It is of interest to note that the 'A-factor' chosen based on the best-fit for each group turns out to be: fcc (A=1.04), bcc (A=1.50) and hexagonal (A=3.30). The magnitude of 'A-factor' is correlated exactly with the crystal symmetry; i.e., the less isotropic the crystal symmetry, the bigger is the 'A-factor.' This is to say that if the local configuration, C_d^n, includes only those symmetry alignment that happen to be identical to the crystal sym-

metry, the 'A-factor' would not be necessary. One can consider those configurations that have the same coordination number, n, but do not conform to the crystal symmetry as impurity. As a result, they can be treated in the similar manner as in impurity case by invoking the probability, $P_{AB}^{nn'}(\beta)$. Consequently, the more the crystal symmetry deviates from isotropy the greater is the 'impurity' and thus the theoretically calculated $(T_m)_c$ would be smaller than the observed T_m. This is indeed the case as observed in the 'A-factor' assigned to three distinct crystal structure groups.

Another observation from Table 1 show the disagreement between the calculated and the observed melting temperatures that exceed 25%, all are in 'heavy' atoms. For example, Pt (at. wt. = 197), Nb (at. wt. = 92.9), Ta (at.wt. = 181), and Tl (at.wt. = 204). It is my view that they may be related to the 'effective' mass. In our derivation of Eq. (3), the atomic mass, m was simply considered as equal on both sides of the equation and thus was cancelled out. However, this may not be true in the microscopic configuration being considered here. While it is beyond the scope of our present discussion, I thought it is necessary to point that out here.

7.1 More Detailed Accounts of Nb, Ta, vs. Mo, W.

It is of extreme interest to note that the calculated T_m for Nb and Ta are lower than the observed and conversely, the calculated T_m for Mo and W are higher than the observed. This fact is rather puzzling in view of the fact that all four elements have a common crystal structure of bcc. Furthermore, the four elements, Nb (sometime called Cb) Mo, Ta and W all have 4d, 5d atomic orbital and they all form continuous solid solutions with one another. Therefore, metallurgically, the four elements are totally compatible with one another which contradicts the sharp differences in their observed vs. calculated melting temperatures. To understand these differences we first look at the differences (or similarities) in their phonon dispersion curves (Fig. 1) along the three principal axes. A distinct difference is observed between the dispersion curves for Mo and W, on one hand, and those for Nb and Ta on the other in the $[\xi\xi 0]$ and $[\xi 00]$ directions.

(a) In the $[\xi\xi 0]$ direction, at the zone boundary, $\Sigma_4 > \Sigma_3$ for Mo and W, whereas $\Sigma_4 < \Sigma_3$ for Nb and Ta.

(b) In the $[\xi 00]$ direction, Δ_1 has a pronounced maximum at about $\xi = 0.6$ for Mo and W; whereas the similar maximum is small for Nb and practically zero for Ta. In the region close to the zone boundary, Δ_1 (longitudinal) and Δ_5 (transverse) are practically the same for Nb and Ta.

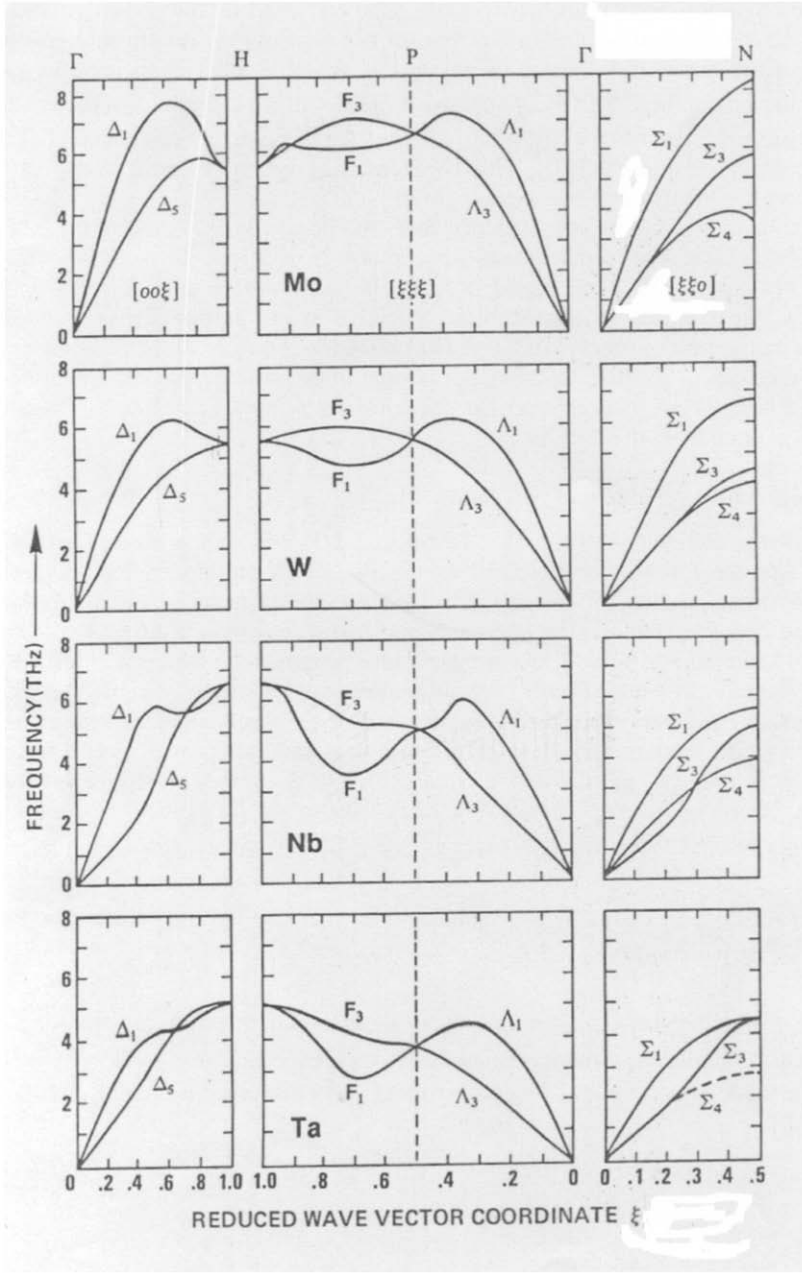

Fig. 1. The phonon dispersion curves along the three principle axes for Mo, W, Nb and Ta.

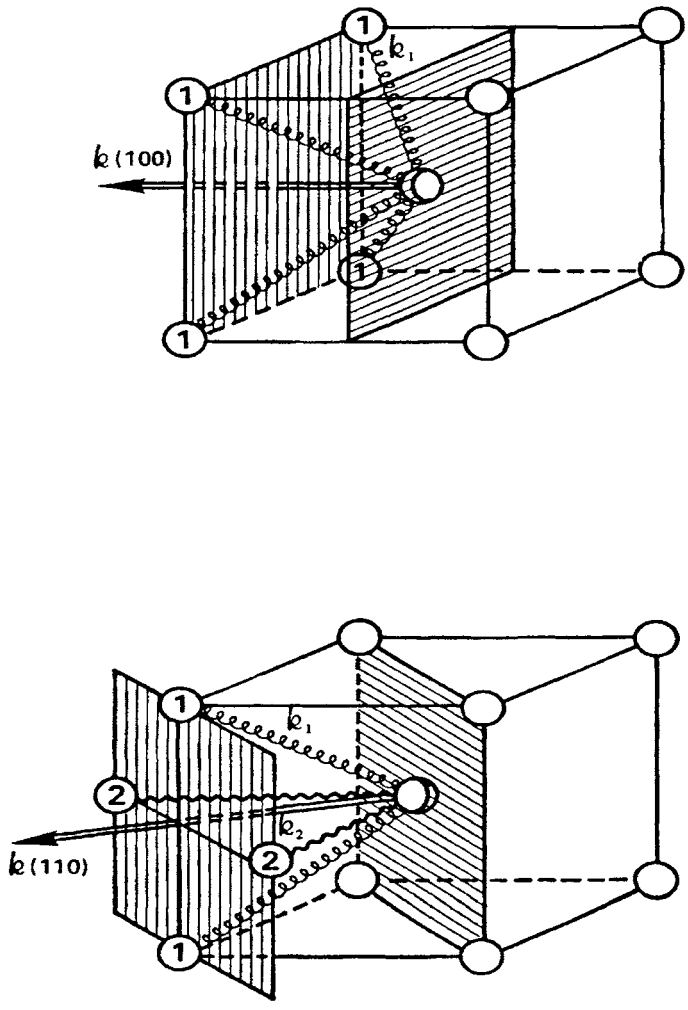

Fig. 2. Pictorially showing the force constant relationship in a bcc structure in ‹100› and ‹110› directions.

We now show that these differences are due to the distinction between the first and the second nearest neighbor force constants of the four elements. Let k_1 and k_2 be the first and second nearest neighbor force constants. And $k_1(hkl)$ and $k_2(hkl)$ be their respective force constants in the <hkl> direction, and $k(hkl)$, the interplanar force constants for (hkl) planes. Then, the following force constant relationships can be derived for a bcc structure as illustrated in Figs. 2, & 3.

$$k(100) = 4k_1\,(100) = (4/\sqrt{3})\,k_1$$
$$k\,(110) = 2\,k_1(110) + 2\,k_2(110) = 2 + \left(2/\sqrt{2}\right) k_2\sqrt{(2/3)}\; k_1$$

Thus, k_1 and k_2 can be obtained from known $k\,(100)$ and $k\,(110)$. Experimentally, it is known that for Mo and W, k_2 is larger than k_1 whereas for Nb, k_2 is only 13% of k_1 and for Ta, k_2 is near zero. Values of k_1 and k_2 can now be compared to the transverse waves, Σ_3 and Σ_4 in the $[\xi\xi 0]$ direction. As is shown in Fig. 3, the contribution to the Σ_4 branch is polarized in the $< 1\bar{1}0 >$ direction and is dominated by k_2 whereas the contribution to the Σ_3 branch that is polarized in the <001> direction is dominated by k_1. These facts dictates that $\Delta k(\Sigma) = k(\Sigma_3) - k(\Sigma_4)$ should be roughly the same in sign and magnitude as $\Delta k = k_1 - k_2$. Indeed, this holds true for all the four elements as summarized in Table II (also see Fig. 1). The fact that k_2 is calculated to be zero for Ta, predicts that $k(\Sigma_3)$ is the same as $k(\Sigma_1)$ at the zone boundary. This is shown experimentally in Fig. 1.

Table 2

Summary of the magnitude of phonon vibration frequencies as well as force constants in certain directions for Mo, W, Nb, and Ta. The distinction between two groups, namely Mo, W, vs. Nb, Ta is clear.

	$\Omega^2(\Sigma_3)$	$\omega^2(\Sigma_4)$	$k(\Sigma_3)$	$k(\Sigma_4)$	$\Delta k(\Sigma_3 - \Sigma_4)$	$\Delta k(\Sigma_1 - \Sigma_2)$
	<100>	$<1\bar{1}0>$				
	$X10^{26}(rad/sec)^2$		$x10^5$ (dy/cm)			
Mo	5.40	13.28	0.215	0.529	−.314	−.368
W	6.31	7.99	0.481	0.609	−128	−.180
Nb	9.87	6.31	0.380	0.243	+.137	+.243
Ta	7.99	3.09	0.600	0.232	+.368	+.346

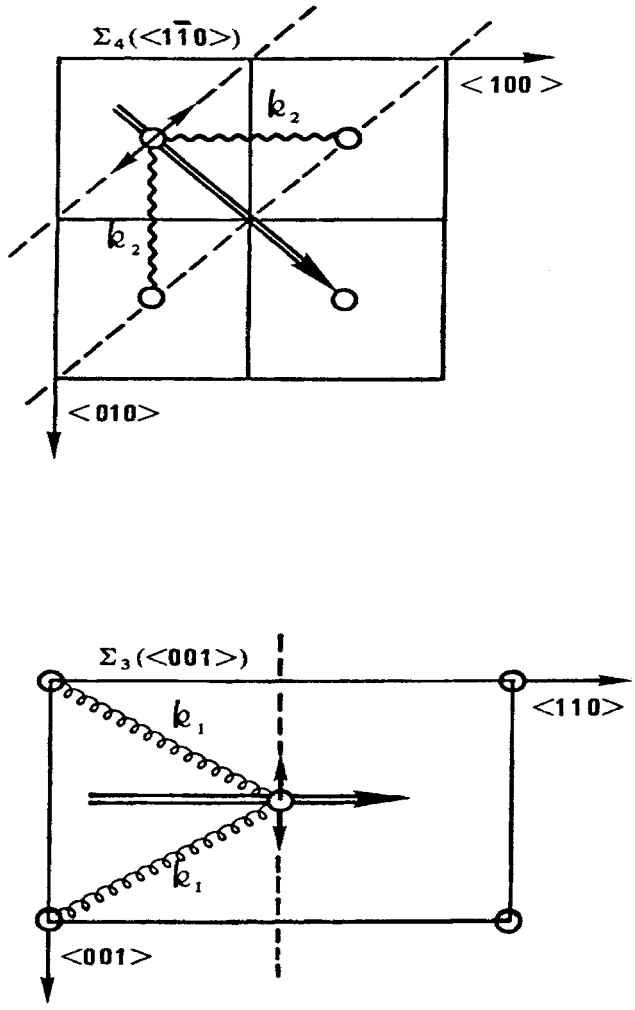

Fig. 3. Similar to Fig. 2, force constants relationship is illustrated pictorially for a bcc structure.

The differences in the phonon dispersion curves for Mo, W, Nb and Ta in the $[\xi 00]$ direction can be understood in the following way. The normalized phonon frequencies for $[\xi 00]$ propagation are given [21] by

$$\omega_L^2 = 1 - \mathrm{Cos}(\pi\xi) + (3\,k_2 / 2\,k_1)\,\mathrm{Sin}^2(\pi\xi)$$

for longitudinal polarization , and for transverse waves,

$\omega_T^2 = 1 - \mathrm{Cos}(\pi\xi)$.

From the first expression, longitudinal phonons are predicted to have a maximum frequency at a value of ξ given by $\mathrm{Cos}(\pi\xi) = -(\alpha_1/\alpha_2)$. Therefore, the critical value of (α_1/α_2) at which the longitudinal mode has a maximum at $\xi < 1$ is 1/3. From Table 2. we see that Nb and Ta fail to meet this criterion, but W and Mo are expected to have a maximum. The Δ curves of Fig. 1 show that this prediction is substantially in accord with the experimental observation. These analyses definitely indicate that α_2 is comparable in magnitude to α_1 in Mo and W, but in Nb and Ta, α_2 is very small and α_1 is the dominant binding force. Inasmuch as the 'Covalent'-bond is a short range force and whereas 'Metallic'–bond is a long range force, it is logical to conclude from the evidence that 'Covalent'–bond dominates in Nb and Ta, whereas 'Metallic'–bond dominates in Mo and W. Within this context, it is important to point out that in recent years, the discovery of 'Covalent'-bond electrons being responsible for superconducting has been proposed from both the chemical-physics approach in terms of 'COVALON'-conduction [21,22] as well as the band-structure point of view in terms of 'quasi-orbital' electrons [23]. The calculated melting temperature, T_m, and the superconductivity characteristics for the four elements are summarized in Table 3. It is to be noted that the calculated T_m for Nb and Ta are lower than the observed and conversely the calculated T_m for Mo and W are higher than the observed. Parallel to this observation is their superconduting characteristics; a) the superconducting temperature, T_c, for Nb and Ta are considerably higher than those of Mo and W as shown in the Table 3. And b) Nb and Ta are type-II superconductors whereas Mo and W are type-I superconductors [20]. These correlations will be discussed in more detail in the section of *'SUPERCONDUCTIVITY.'* Additional insight into the microscopic physical phenomenon of melting is provided in the present model as follows: Experimentally, it is well known that liquids may be supercooled by tens or even hundreds of degrees below its melting temperature, T_m , without freezing into solid [24]; see Table 4 for the list of observed maximum supercooling for various metals. On the other hand, solids have not been observed, in equilibrated state, to superheat above its T_m without melting into liquid state. This observation can also be understood qualitatively in the present model by considering the average velocity, $\overline{V}$, of atoms in the liquid state and the characteristic vibration frequency, υ_S, in the solid – the criteria invoked in the formulation of this physical model. The formation of microscopic configuration, C_d^n, requires a group of n atoms within the same microscopic region to simultaneously assume velocities that are equal or less than $\overline{V_\ell}$. The freezing of liquid into solid, therefore, is a matter of probability and leads to a super-cooled liquid. On the other hand, the criterion for heating solid into melting does not depend on the probability but solely a function of the characteristic vibration frequency, υ_S, and thus, a solid cannot be overheated. Following a similar line of logic, one can also understand the reason for nucleation or the term commonly known as 'seeding', which can bring about a spontaneous solidification of a super-cooled liquid. This is because an introduction of nuclei is microscopically

Table 3

Showing the relationship between the superconductivity characteristics and the temperature deviation between the observed and calculated for the two groups.

Element	Superconductivity			T_m(obs.)	T_m(obs.) – T_m(cal.)
	T_c	Type	isotope		
Nb	9.25° K	II	1	2520° K	- 787° K
Ta	4.47° K	II	1	3269° K	-1333°K
Mo	0.91° K	I	7	2893° K	+ 281° K
W	0.01° K	I	5	3682° K	+ 657° K

Table 4.

Summary of the super-cooling temperatures experimentally obtained for various metals.

Metal	T_m(C)	Max. S-Cool (C)	Metal	T_m(C)	Max. S-Cool(C)
Sn	232	76	Au	1064	230
Bi	271	90	Cu	1083	236
Pb	327	80	Mn	1244	308
Al	660	130	Ni	1453	319
Ag	962	227	Co	1495	330

equivalent to a creation of C_d^n / C_S^n interfaces. Inasmuch as the formation of C_S^n is determined by the probability of having a group of n atoms in one locale to have the velocities equal to or less than $\overline{V}$, creation of interfaces effectively reduce the number of atoms required in forming C_S^n. As a result, the probability for the formation of C_S^n is increased dramatically and leads to the formation of more solids. These new solids create more interfaces that in turn bring-in more solids and so forth and ultimately lead to a 'spontaneous crystallization.'

REFERENCES

[1] F.A. Lindemann, Z.Physik, 11(1910)609.
[2] L. Cartz, Proc.Phys.Soc.,London , B68(1955)951.
[3] J.J. Gilvarry, Phys.Rev. 102(1956)308, ibid. 103(1956)1700.
[4] J.H.C. Thompson, Phil.Mag., 44(1953)131.
[5] Y. Ida, Phys.Rev., 187(1969)951; B-a(1970)2488.
[6] R. Furth, Proc.Roy.Soc.,London, A183(1944)87.
[7] N.F. Mott, Proc.Roy.Soc., London, A215(1952)1.
[8] D. Kuhlmann-Wilsdorf, Phys.Rev., A140(1965)1599.
[9] F.D. Stacey and R.D. Irvine, Aust.J.Phys., 30(1977)641.
[10] J.E. Lennard-Jones and A.F. Devonshire, Proc.Roy.Soc., London, A170(1939)464.
[11] T. Yoshida, Y. Kuramoto and H. Okamoto, Bussi, 15(1974)3.
[12] K. Ishizaki, P. Bolsaaitis and I.L. Spain, Phys.Rev. B7(1973)5412.
[13] F.E. Wang, CALPHAD, 2(1978)239.
[14] Hansen, (1958), Elliott, (1965), Shunk (1969); Const.Binary Alloys, McGraw-Hill Book Co. New York.
[15] J.A. Pryde, The Liquid State, Hutchinson Univ.Library, London (1966).
[16] K. Ishizaki, P. Bolsitis and I.L. Spain, Sol.Stat.Comm., 15(1974)1591.
[17] INTERATOMIC DISTANCES, The Chemical Soc., London, Burlington House W.1.(1958).
[18] G.L. Pollack, Rev.Mod.Phys., 36(1964)748.
[19] R. Hultgren et al., Selected Values of Thermodynamic Properties of Elements, Metals Park, Ohio, Amer.Soc.Metal.
[20] B.W. Roberts, Survey of Superconductive Materials and Critical Evaluation Selected Properties, J.Phys.Chem, Reference Data (1976).
[21] F.E. Wang and Y.N. Chiu, Chem.Phys., 12(1976)225.
[22] Y.N. Chiu and F.E. Wang, Chem.Phys., 18(1976)301.
[23] E. Kruger, Phys.Stat.Sol., b-85(1978)261; b-90(1978)719.
[24] A.R. Ubbelohde, The Molten State of Matter; Melting and Crystal Structure, Wiley-Interscience, New York (1978).

IV Superconductivity

1. BACKGROUND

Superconductivity is a phenomenon in which the resistance of the material to the electric current flow is zero. Kamerlingh Onnes made the first discovery [1] of the phenomenon in 1911 in mercury (Hg) as shown in Fig.1. Since that time, superconductivity has been found to occur in many metallic elements and intermetallic compounds. And more recently has been found even in organo-metallic compounds, semiconductors and ceramics. However, it is to be noted that superconductivity has not been found in all metals. For example, Li, Na, and K, have been investigated for superconductivity down to 0.08°K, 0.09°K and 0.08°K respectively and the results indicated no sign of superconductivity. The uniqueness of superconductivity compared to all other physical phenomena is that the phenomenon is not relatable to periodic table, such as atomic number, atomic weight, electro-negativity, ionization potential etc. In fact, superconductivity does not even correlate with normal conductivity. In some cases, a superconducting compound may be formed from non-superconducting elements.

Associated with the superconductive state is a perfect diamagnetism in which the magnetic flux is expelled from the material. This is known as the Meissner effect [2]. This magnetic property associated with superconductors cannot be accounted for by the assumption that the superconducting state is equivalent to zero electrical resistance. By assuming a superconductor to be a perfect conductor in which there is nothing to scatter the moving electrons, we cannot account for the Meissner effect. For a perfect conductor placed in a magnetic field does not produce permanent eddy current to screen off the magnetic flux. Furthermore, experimentally, no magnetic material has been found to be a superconductor thus far. There are many other physical characteristics observed along with superconductivity. They will be listed later.

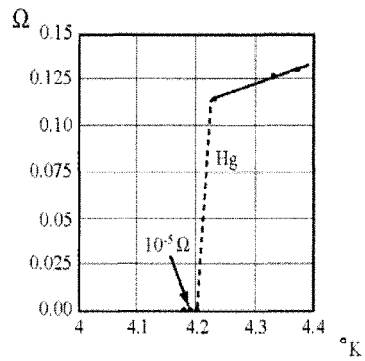

Fig. 1. Showing near zero electrical resistance at about 4.2°K for mercury (Hg); as discovered by Kamerlingh Onnes.

1.1 The BCS Theory of Superconductivity

In 1957, Bardeen, Cooper and Schrieffer proposed [3] a quantum theory of superconductivity, known as the BCS theory, for which they received a Nobel Prize. Their theory in non-mathematical terms can be summarized as follows:

a. An attractive interaction between electrons through electron-lattice-electron interaction can lead to a ground state separated from excited states by an energy gap.
b. The magnetic flux penetration depth and coherence length emerge as a consequence of the theory.
c. It predicts a relationship between superconductivity temperature, T_C, the lattice vibration, θ_{Debye}, and average atomic mass, M , as $T_C \propto \theta_{Debye} \propto M^{1/2}$ such that $M^{\alpha}.T_C$ = constant. Since M is an average atomic mass, it is also known as the 'Isotope' effect.
d. The criterion for the transition temperature, T_C, of an element is related to the electron density of orbital $D(\varepsilon_F)$ at the Fermi surface and the electron-lattice interaction U, which can be estimated from the electrical resistivity. For $UD(\varepsilon_F) << 1$, the BCS theory predicts $T_C = 1.14\ \theta \exp[-1/UD(\varepsilon_F)]$.
e. Magnetic flux through a superconducting ring is quantized and the effective unit of charge is 2e. The BCS ground state predicts paired electrons, which are derived from quasi-free electrons (Fig. 2).

Some forty-eight years from the time the BCS theory was proposed, a large number of experimental evidence on superconductivity has accumulated. But, they do not seem to support the theory. Some obvious paradox is: experimentally, the higher the resistivity at room temperature, the more likely that metal will be a superconductor when cooled. This directly contradicts the BCS's idea that paired electrons originate from fermi electrons. Further, if paired electrons (boson) indeed come from fermi electrons

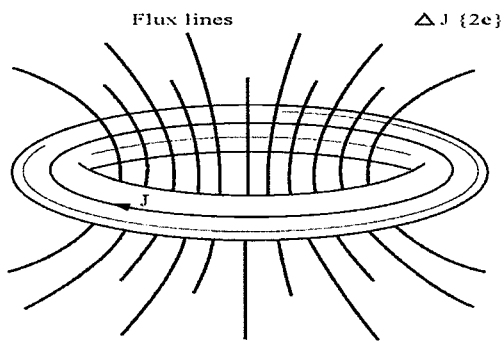

Fig. 2. The electrical current induced by magnetic field is quantized in 2e units.

(fermion) it would be a 'boson condensation.' The boson condensation temperature calculated for metallic electron concentration is of the order of the Fermi temperature of 10^4 ~ 10^5 ° K. Since the superconducting transition temperatures are much lower, any electron pair is expected to break up into fermion, not forming one. The proposal of the Cooper electron pair is justified solely on the mathematical argument that although the kinetic energy may be high their potential energy is lowered to the extent that they become stable. And requiring the momentum vector for two electrons to be opposite to one another, i.e., $+k\uparrow$ and $-k\downarrow$. The physical interpretation is that the two electrons in the pair should be running away from one another in the sea of other free-electrons. In the 'isotope' effect, the α parameter was predicted to be around ½. However, in experiments this value not only varies widely, ($\alpha = 0$ for Zr and $\alpha = 0.61$ for Tl) but in some cases the parameter is found to be negative.

In summary, any theory must be judged not by how it explains the experimental observation but rather by how it predicts the outcome of experiments yet to be performed. On this score, the BCS theory fails miserably. It has neither predicted nor shown the way of obtaining a single high temperature superconductor. This still holds true at this writing.

1.2. Experimental Facts on Superconductivity

We shall now summarize the major experimental observations made related to the superconductivity.

1) Occurrence of superconductivity and the T_C associated with the superconducting elements have not been correlated with other physical attributes, such as atomic number, ionization potential, atomic orbital, crystal structure, etc.
2) Superconductivity is related to normal conductivity to the extent that in general, good conductors at room temperature are either non-superconductors or poor superconductors.
3) Magnetic materials are not superconductors; Magnetism and superconductivity appear to be mutually exclusive. In fact, doping of magnetic impurity usually destroys superconductivity.
4) Superconductivity with zero electrical resistivity does not mean it can carry an unlimited amount of current. Every superconductor has its own current limit.
5) Superconducting current is quantized in 2e charges instead of one e.
6) Superconducting current is self-sustaining in the absence of outside disturbance or interference.
7) Based on their difference in reacting to magnetic flux, superconducting material can be differentiated into Type-I and Type-II. The Type-II superconductors are usually associated with intermetallic compounds instead of elements and their superconductivity is not easily affected even with a high magnetic field.
8) Under high pressure, superconducting temperature of a superconductor can become higher or lower. Again, no factor has been identified for the difference.

9) Superconductivity has been found in metallic elements and intermetallic compounds and within their solid-solution-range. But, superconductivity has not been found in an alloy with an arbitrary composition.
10) Pure organic and inorganic material that does not exhibit any normal electrical conduction is not a superconductor.
11) Superconductivity occurs as a low temperature phenomenon. So far no superconductivity phenomenon has been found above 100° K.
12) Transition from normal conductivity to superconductivity is a virtual perfect second-order phase transition; that is, there is no latent heat or a sharp finite discontinuity in the specific heat; therefore, it is a cooperative phenomenon.

These facts are extremely important in the sense that any theory proposed must agree at least qualitatively with, not one or two observations, but with all observations. The theory for superconductivity proposed herein must meet this criterion. Now, it can be recalled that the fundamental assertion laid out as the basis for the *Bonding Theory for Metals and Alloys* on page 7 was that all metals and alloys contain both covalent-bond and free-electrons. Prior to a full description of the theory for superconductivity based on this assertion, the following question is in order. Can covalent-bond electrons play the role of conducting electric current? And if they can, under what circumstance and what limitations? The answers to these questions are very important to me because I have always believed that the paired electron conduction found in superconducting state was not created from free-electrons but rather existed all along in metals and alloys. Philosophically, it is very difficult for one to accept the Cooper pair concept that a new type of bonding (that is totally different from 'covalent-bond') is created at low temperature and supposedly exists only at low temperature and nowhere else. Our understanding of 'covalent-bond', 'ionic bond' as well as 'metallic bond' is based on a wide range of experimental observations and found in many compounds and alloys. For these reasons, the paired electrons found in the superconducting state may actually be the covalent-bonds. And these covalent bonded electrons reveal its existence only at low temperature for a reason. We shall then investigate this particular reason through the theoretical investigation of 'covalent-bond' conduction as described below which resulted in the 'COVALON' conduction theory.

2. 'COVALON' CONDUCTION THEORY

The covalent bond as described in detail on pages 11-14, involves an electron pair and therefore is a boson. In chemical language, a molecular chain is known as a 'saturated' bond if all the bonds within the molecule chain are of 'σ' bond (or single bond). It is not possible to bring about an electron charge transfer of any kind to this type of molecular chain. However, if the bonding involves 'double' or 'triple' bonding , i.e., involves 'π' and 'δ' bonds (known as unsaturated bonding), it is possible to create a charge transfer. A molecular chain with alternate bonding of —[-(single)-(double)-]$_n$— type known as a 'conjugated' molecular chain can bring about a very interesting type of

charge transfer as described by Wang & Chiu [4]. The essential feature of a conjugated molecular chain is that a valence bond structure may be drawn to consist of 'double' ('σ' plus 'π') and 'single' ('σ') alternating bonds. It is well known that in such molecules, the 'σ' and 'π' bonds can be treated more or less independently [5, 6] and that the 'π' electrons are primarily responsible for the electric conduction. It has also been shown that in conjugated compounds, electrical conduction takes place in bulk [7]. Heretofore, π-electrons have been treated in terms of a quasi-free unpaired state and their conductivity in terms of band structure [7]. However, this approach ignores entirely the possibility of the π-electrons transfer along the chain in paired states consistent with their covalent nature. The first thought that came to mind on paired-electron conduction is that the chemist found that the 'double'-bond is always shorter in length than the 'single'-bond as illustrated in Fig. 3-(a). The shortening and lengthening of the bond length along the chain will correspond to an antisymmetric normal mode of vibration with a frequency, υ. Let us assume the π-bonds can move from left to right through some mechanism as shown in Fig. 3-(b) with a frequency, ω. The question is — can we theoretically find the magnitude of υ and ω? And if we can, then would the two values be compatible to one another. Because unless the values of υ and ω are reasonably close to one another, the idea of paired electron conduction along a conjugated chain, i.e., COVALON conduction would not be possible, no matter how attractive it may seem. Such a theoretical investigation for the values of υ and ω, is described below.

It is postulated that a cooperative effect arises when the paired electron transfer out of (or into) a bond coincides with the simultaneous lengthening (or shortening) of this bond due to antisymmetric normal mode of vibration (Fig. 3-a). In this figure, r_1. k_1. and r_2. k_2 represent the interatomic distance and force constant for single and double respectively. The atomic positions in the two states, a and b (before and after the pair wise charge transfer) shows how the antisymmetric mode of vibration can bring about the proposed COVALON conduction. In Fig.3-(b) the bond-pair electron can move from left to right in a synchronized manner. It will be shown that the antisymmetric vibration frequency, ν, and paired charge transfer frequency, ω, are comparable to one another. Thus it is possible to achieve COVALON conduction. We shall show that this corresponds to a double harmonic oscillator (DHO) model for the two neighboring — double-single — bonds. As a result, the potential barrier separates three temperature zones for conductivity emerges as shown in Fig. 4. In Fig. 3-(a), the two states before and after charge transfer are achieved with an antisymmetric normal mode of molecular vibration, which coincides with the charge transfer. Since in any normal mode of vibration, the center of the mass must be preserved, all of the atoms will be displaced. In an infinite chain of odd number atoms, C_{2n+1}, the displacement for neighboring atoms are $-\ n(r_1 - r_2)/(2n+1)$ for odd numbered atoms and $+\ (n+1)(r_1 - r_2)/(2n+1)$ for even numbered atoms regardless of position. For a large n, the displacement reduces to $(r_1 - r_2)/2$ with opposite signs between neighboring atoms.

By assuming electronic vibrational motions to be separable, as in the Born-Oppenheimer approximation (this assumption for tight-bond electrons such as covalent bonds is inaccurate and will be corrected later) we can find the electronic interaction between the two harmonic oscillators as a function of vibrational coordinates. First, we shall consider the vibration of the center atom only and take the force constant to be

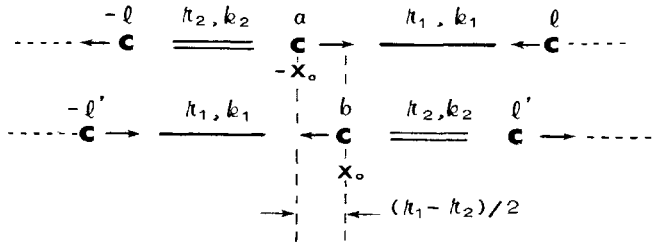

(a)

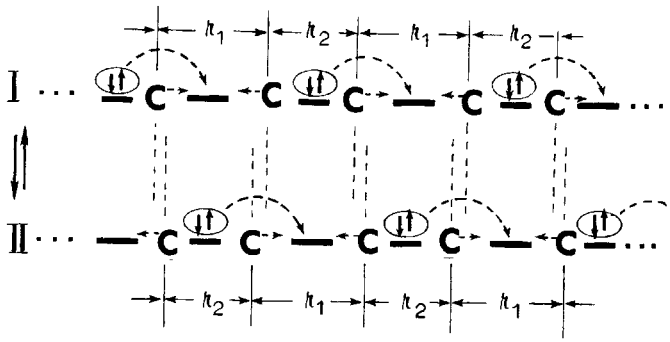

(b)

Fig. 3; (a) Atomic positions in the two states before and after the pair wise charge transfer. (b) Synchronized motion between the antisymmetric vibration ν and pair wise charge transfer frequency, ω, leading to COVALON conduction.

$k = k_1 + k_2$. Inasmuch as 'σ' and 'π' bonds can be treated more or less independently [5,6], the non-stationary electronic states before and after electron transfer can be expressed in terms of two Heitler-London covalently bonded π-electrons

$$\Psi_A = \left(1/\sqrt{2}\right)\left[\Phi_{-\ell}(i)\Phi_a(j) + \Phi_{-\ell}(j)\Phi_a(i)\right] x \left(1/\sqrt{2}\right)\left(\alpha_i\beta_j - \beta_i\alpha j\right) \qquad (1a)$$

$$\Psi_B = \left(1/\sqrt{2}\right)\left[\Phi_b(i)\Phi_{\ell'}(j) + \Phi_b(j)\Phi_{\ell'}(i)\right] x \left(1/\sqrt{2}\right)\left(\alpha_i\beta_j - \beta_i\alpha_j\right) \qquad (1b)$$

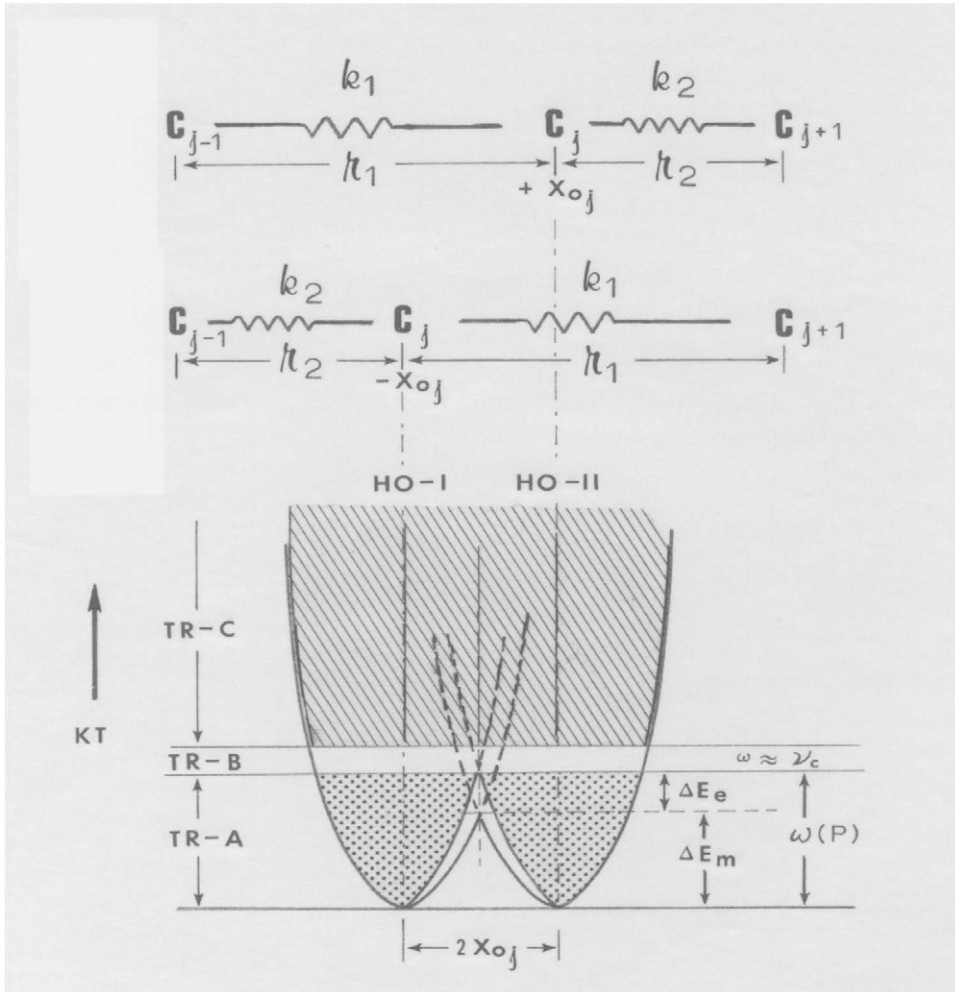

Fig. 4. Schematic representation of a 3-atom Double Harmonic Oscillator (DHO) with r_1,, r_2 interatomic distances and k_1, k_2 force constants, and of TR-A, TR-B, TR-C temperature ranges corresponding to the DHO model.

The corresponding electronic energies, in terms of vibrations coordinates and harmonic approximation are:

$$W_A = E_e^0 + (k/2)(\chi + \chi_0)^2 \qquad (2a)$$

$$W_B = E_e^0 + (k/2)(\chi - \chi_0)^2 \qquad (2b)$$

If the electrons at left see the potential at right (or vice versa), the two wave functions will mix. Letting the mixed stationary state wave function be

$\Psi = C_A\Psi_A + C_B\Psi_B$ and $H\Psi = E\Psi$,

we obtain the secular determinant,

$$\begin{pmatrix} H_{AA} - E & H_{AB} - ES_{AB} \\ H_{AB} - ES_{AB} & H_{BB} - E \end{pmatrix} = 0 \qquad (3)$$

If we let $H_{AB} - ES_{AB} = U$ as in one electron Huckel molecular orbital treatments, the stationary solution can be obtained for negative U, as

$$\Psi_+ = \sin(\alpha)\Psi_A + \cos(\alpha)\Psi_B \qquad (4a)$$

$$\Psi_- = \cos(\alpha)\Psi_A - \sin(\alpha)\Psi_B \qquad (4b)$$

where α is defined through

$$\mathrm{Tan}(2\alpha) = (2|U|)/\hbar\chi\chi_0 \qquad (4c)$$

The corresponding stationary state energies are:

$$W_\pm = E_e^0 + (\hbar/2)(\chi^2 + \chi_0^2) \mp \sqrt{\hbar^2\chi^2\chi_0^2 + |U} \qquad (5)$$

with

$$dW_\pm/d\chi = \hbar\chi\left(1 \mp \hbar\chi_0^2/|U|\sqrt{1 + \hbar^2\chi^2\chi_0^2/|U|^2}\right) \qquad (6a)$$

$$d^2W_\pm/d\chi^2 = \hbar(1 \mp \hbar\chi^2/|U|) \qquad (6b)$$

For a strong coupling case, $|U| > \hbar\chi_0^2$, there is only one minimum at $\chi = 0$ for both W_+ and W-, viz.,

$$W_{\pm}(s) = E_0^2 + (\hbar / 2)\chi_0^2 \mp |U| \qquad (7a)$$

For a weak coupling case, $|U| < \hbar \chi_0^2$, the upper curve W_- still has one minimum at $\chi = 0$,

$$W_-(w) = E_e^0 + (\hbar / 2)\chi_e^0 + |U| \qquad (7b)$$

But the lower curve W_+ has three extremes: one maximum at $\chi = 0$.

$$W_+^{max}(w) = E_e^0 + (\hbar / 2)\chi_0^2 - ||U| \qquad (7c)$$

and two minima having the same value at $\chi_{L,R} = \pm \sqrt{\chi^2 - |U|^2 / \hbar^2 \chi_0^2}$ as shown in Fig. 5, thus,

$$W_+^{min}(w) = E_e^0 -- |U|^2 / 2\hbar \chi_0^2 \qquad (7d)$$

The energy barrier between the two minima is

$$\Delta E = W_+^{max}(w) - W_+^{min}(w) = (\hbar / 2)\chi_0^2 - |U| + |U|^2 / 2\hbar \chi_0^2 \qquad (8)$$

Overtly, these results refer thermodynamically to the adiabatic states with the electronic energy, W, expressed as a function of the χ coordinates as shown in Fig. 5. However, since for each $|U|$, the interacting integral given, there is a new energy curve, $W(\chi)$, and since the interaction integral, $|U|$ must be corrected by multiplication of Franck-Condon factors in an exact treatment, it can only be increased or decreased by the thermal energy, kT, which affects the Franck-Condon overlap of the populated vibrational levels.

	Non-interacting	Interacting
TR-A	$kT < \Delta E$	$\|U\| < k\chi_0^2$
TR-B	$kT \approx \Delta E$	$\|\|U\| \approx k\chi_0^2$
TR-C	$kT > \Delta E$	$\|U\| > k\chi_0^2$

The validity of this correspondence can be tested, for example, by considering the case, $|U| \approx k\chi_0^2$ Under this situation, $W_+^{max}(w) = W_+^{min}(w)$, such that the energy barrier, ΔE, no longer exists between the two states in agreement with the $kT = \Delta E$ case (or the vibrational energy level at the top of the barrier is populated by kT). The probability of the transfer, P, on the other hand, may be related to the coefficients of Ψ_A and Ψ_B in the stationary wave function. For example, $P = |\cos(\alpha)|^2 / |\sin(\alpha)|^2$. If kT reaches the height of the barrier, ΔE, the vibrational amplitude reaches the maximum point, $\chi = 0$. At this point, $\tan(2\alpha) = \infty, \alpha = \pi/4$ and $P = \left[\cos(\pi/4)/\sin(\pi/4)\right]^2 = 1$. In order to evaluate the magnitude of E, we use the following parameters. For typical "double" and "single" bond length and force constants, we take those given for propylene [8].

$R_1 =$ 1.488 Å, and $(r_1 - r_2)/4 = 0.0337$ Å with

$k_1 = 4.5 \times 10^5$ dyn cm^{-1} ; $k_2 = 9.7 \times 10^5$ dyn cm^{-1} .

Although the 'resonance' interaction integral is a two-electron integral, for an approximation, we write

$$U = H_{AB} - ES_{AB} = 1/2(2H_{-\ell b}S_{a\ell'} + 2H_{a\ell}S_{\ell b} + 2H_{-\ell\ell'}S_{AB} + 2H_{AB}S_{-\ell\ell'} - ES_{-\ell b}S_{a\ell'} - ES_{-\ell\ell'}S_{AB} - ES_{AB}S_{-\ell\ell'}) \quad (9)$$

The overlap integrals, S, are evaluated approximately using integral tables [9], whereas the integral H is approximated [10] by

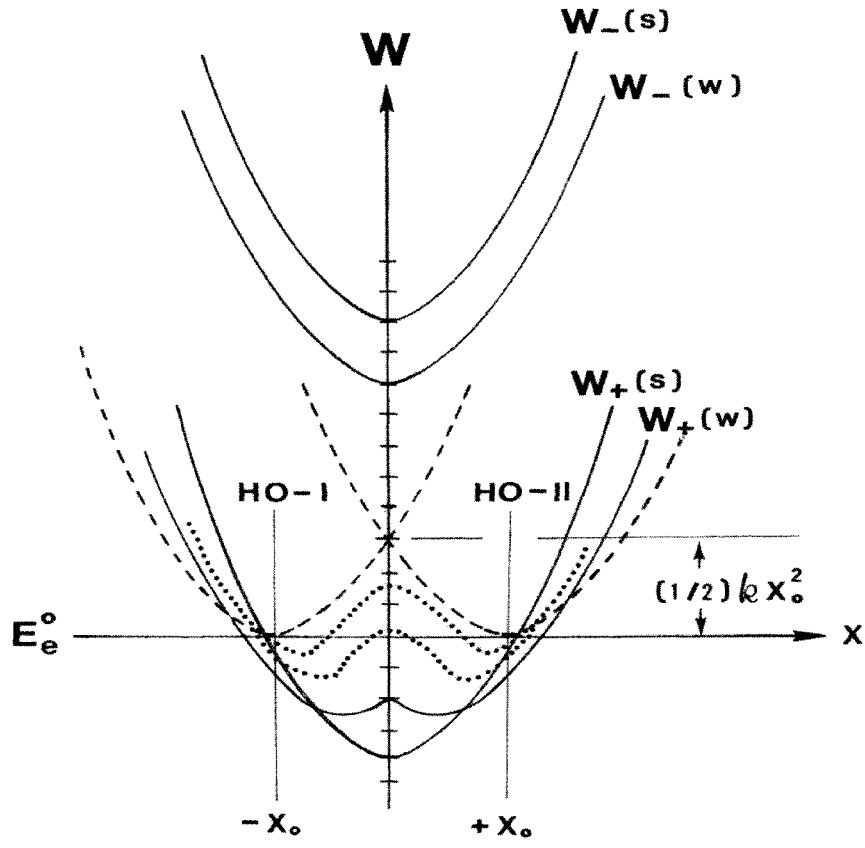

Fig. 5. Schematic representation of various energy curves due to weak (w) and strong (s) interactions between two harmonic oscillators. Energy in arbitrary units with the following values: $(k/2)\chi_0^2 = 3$, $E_e^0 = 0$; for strong coupling, $|U| = 7$, for weak coupling, $|U| = 5$. The dotted curves indicate the intermediate states for weak coupling case, [W.(w)].

$$H_{-\ell b} = (S_-), \qquad H_{-\ell b} = (S_{-\ell b}/S_{12})H_{12} \tag{10}$$

in which H_{12} is the corresponding integral in benzene between two neighboring carbon atoms and is set to be -14.0 eV [11,12] and E is set to be –108 eV and is the average H_{AA} value for the two electrons in question here. It is assumed to be more than two times the one-electron value of –50 eV [11,12] to allow for larger values due to second

"double" bond is not really a full double bond with two π-electrons, from the bond-length-bond order relationship [13] we obtain the π-bond order for the 'single' and 'double' bonds as $P_1 = 0.156$ and $P_2 = 0.905$ respectively. The difference, $P_2 - P_1 = 0.749$, then represents the net fraction of π-electrons, which should be multiplied into U as a correction. This gives a corrected $U' = -3.39\times10^{-13}$ erg. Similarly, although $\hbar\chi_0^2 = 1.61\times10^{-13}$ erg for the center atom, actually all three atoms vibrate during the electron transfer, so the value should be multiplied by three to give a rough estimate. The resulting $\hbar(\chi_0')^2 = 3\hbar\chi_0^2 = 4.83\times10^{-13}$ erg is larger than $|U'|$ indicating that the case corresponds to TR-C, the weak coupling.

The energy barrier, ΔE, in the TR-C range is therefore computed to be

$$\Delta E = (\hbar/2)(\chi_0') - |U| + |U|^2/2\hbar(\chi_0')^2 = 0.20\times10^{-13}\ \text{erg} \approx 145°K$$

Following the theory of exciton charge transfer between molecular dimmers [14] we now write the frequency of transfer between the two states as

$$\omega = \left(4|U|/h\right)\sin(2\alpha) \quad \text{and}$$

$$\omega = 4|U|/h \qquad \text{at} \quad |U| \approx \hbar\chi_0^2,\ \alpha = \pi/4$$

This is consistent with $\omega = \nu$ or $4|U| = h\nu$, if we take $h\nu$ to be the total classical energy of the harmonic oscillators, $h\nu = 2(\hbar/2)(2\chi_0)^2$. However, this ` agnitude is related only to the electronic potential curve (i.e., Born-Oppenheimer approximation) and does not include vibronic interaction. That is to say, the Franck-Condon effect must be considered. This effect can best be visualized by considering a fast transfer frequency in which the π-electrons on the left have already transferred to the right (viz.,the electronic potential has changed to that for a 'single' bond), but, the nuclear position for the shorter bond is not yet changed. Therefore, the Franck-Condon factor, R_{00}, involved here is that of a displaced oscillator and is calculated using available tables [15]. Again, because the vibration involves all three atoms, the factor, $R_{00} = 0.527$ should be raised to the third power as an approximation. The frequency of electron transfer, ω, and the velocity of charge movement, V_e, are estimated as follows:

$$\omega = \left[4|U'|R_{00}^3\right]/h = 0.299\times10^{14}\,s^{-1} \qquad (11)$$

$$V_e = \omega\left[(r_1 + r_2)/2\right] = 0.424\times10^{6}\,\text{cm}\,s^{-1}$$

The phonon vibration frequency on the other hand is obtained using $\hbar = \hbar_1 + \hbar_2$ and the reduced mass, m, for a one-center atom. We obtain

$$\upsilon = \pi/2\sqrt{\hbar/m} = 0.4\times10^{14}\,S^{-1} \qquad (12)$$

By comparing the resonance frequency Eq.(11) and the phonon vibration frequency Eq.(12), we see that they are almost the same, $0.3 \sim 0.4 \times 10^{14}$ s^{-1}. This affirms the possibility of a spin-paired covalent-bonded electronic charge transfer. For vibrations in a linear crystal there are certainly low frequency acoustic vibrations in addition to the high frequency anti-symmetric vibrations which correspond to optical modes. Thus, there are other possibilities for refinement. In spite of the crudeness of the model, this sample calculation also gives a reasonable transition temperature, TR-B of 145 °K, as well as a reasonable cooperative electronic resonance and phonon vibration effect, $\omega \approx \nu$. Consequently, it is shown that the possible existence of a "COVALON" conduction as suggested here is reasonable and lays a foundation for completing the story of superconductivity as described in the following.

In reducing the problem to a two-state model involving two neighboring 'double'-'single' bonds we are exploring a special attribute based on the chemical insight of covalent bond as a principal factor in superconductivity. It is interesting to note the overt similarity that exists between 'Covalon' and the one–dimensional superconductivity considered by Frohlich [16] and others [17]. As pointed out by Bardeen [18], following Frohlich's model, the combined electron-phonon gas was assumed to be drifting with the same total momentum. Accordingly, electrons are trapped between atoms that are drawn closely together and are repelled by a region where atoms are further apart. If the pairing pattern in which atoms 1 and 2 are together, 3 and 4 are together, and so on, is moved so that now 2 and 3 are together, 4 and 5 are together, and so on, then the electrons simply move right along with that lattice distortion wave.

However, beyond this overt similarity, there are differences. For example, 'Covalon' by the nature of covalency would have to operate under a much more stringent correlation than that existing in the Frohlich's model between one paired π-electron and all other such pairs along the chain. This is a natural consequence of distortion in the alternating 'single'–'double' bonds. This treatment also differs from that of self-consistent field treatment [19] of a linear chain and that of Little [20] in our inclusion of bond vibration. 'Covalon' also differs from polaron treatments [21] in the consideration of the movement of spin-paired correlated electrons in a covalent bond, instead of movement of spin-uncorrelated electrons in the zeroth order.

In essence, what is advocated here is that the paired electron charge observed in the phenomenon of superconductivity has always existed in metal and alloys. And this was not observed at high temperature because phonon vibrations. But at low temperature, phonon vibrations of higher harmonic are calmed down to the extent the existence of paired charge can be seen. This is fundamentally different from the Cooper pair conception that the paired electrons (boson) are created at low temperature from quasi-free electrons (fermion). As to the question of whether the 'covalon' described here by itself can lead to superconductivity. The answer is no, not by itself. For the Covalon conduction we considered here has to do only with one single conjugated molecular chain. There is no mechanism within the covalon conduction to sustain the conduction indefinitely. At this point, all we have shown is that a covalent bonded pair of electrons can, under certain conditions, conduct electric current in pairs. It is important to note that such conduction will be possible only at low temperatures where a higher mode of vibration must be suppressed so that the anti-symmetric normal mode of vibration, υ, can be seen. When this fibration frequency matchs the paired electrons

tunnel frequency, ω, the phonon vibration not only does not hinder the flow of covalon conduction but indeed will assist its flow ($\nu \cong \omega$).

Based on a Double Harmonic Oscillator Model, it is shown how the 'Covalon' conduction concept, in which a pair-wise charge transfer of covalent bonded electrons, can be coupled with anti-symmetric normal mode of vibration in a conjugated molecular chain. The potential barrier for this double oscillator separates the charge transfer into three distinct temperature regions: (i) below, (ii) near and (iii) above the barrier (see Fig. 5). For aromatic hydrocarbons, this barrier is estimated to correspond to 145 °K. In the narrow region near the top of the barrier, if ω (resonance frequency) matches υ (phonon vibration frequency), it is shown that a cooperative charge transfer takes place that could lead to para-conductivity. From the transfer frequency per second for an aromatic hydrocarbon chain, the velocity of intra-chain charge movement, $V_c \approx 0.424 \times 10^6$ cm s^{-1}, is obtained.This compares favorably to the group velocity, V_g(free electron) $\approx 10^7$cm s^{-1} for quasi-free conduction electrons in metals. The numeric values obtained here alone cannot serve to prove or disprove the correctness of the Covalon conduction theory proposed. They can, however, serve to encourage further investigations that will be shown in the following sections including a number of predictions made based on the theory.

2.1. Physical Characteristics of Covalon Conduction

1) Covalon conduction is a spin-paired two-electron charge transfer that can take place when, the anti-symmetric normal mode of vibration, υ, matches ω, the electron pair tunneling frequency.

2) Because the phonon vibration frequency, υ, is 'visible' only when all other higher order of phonon vibration (whether be acoustic or optical) are harnessed, Covalon conduction must be a low temperature phenomenon.

3) By the nature of the conjugation along the chain, there is no preference as to which direction Covalon should travel. Covalon would travel in either direction along the chain dictated by the electro-potential applied.

4) Inasmuch as Covalon involves the spin-paired covalent bond along the chain, physically it can travel only along the chain.

5) While the matching of $\nu \approx \omega$ will lead to zero resistance to the Covalon flow, the current carried along the chain will be limited by the phonon frequency, υ, of the anti-symmetric normal mode of vibration and the chain density. For in a single vibration, a spin-paired Covalon will conduct two electron charges.

6) Since the frequency of vibration, υ, may vary from one type of chain to another (because of different force constant, k, and different atomic mass, m), the current limitation will vary from one type of chain to another.

7) Since Covalon is a spin-paired boson (not fermion) conventional electromagnetic effect from electron-current flow will not be expected and must be studied and explored separately.

8) It should be understood clearly that Covalon conduction as described here is limited to a particular type of chain, i.e., *conjugated chain.* Therefore, an existence of covalent bonded chain without conjugation will not lead to the production of Covalon conduction.

9) It is true that Covalon conduction is not hindered but rather assisted by the phonon vibration of an anti-symmetric normal mode of vibration and can lead to a high conductivity. But there is no inherent mechanism within the Covalon conduction to sustain the current flow once the electro potential is removed.

It is clear that no organic compound with a polymer chain of conjugation has been found to be superconducting. It is equally clear that all known superconductors are metal, compound alloy, or metal-oxide of some kind (including 'ceramics'). This fact suggests that the quasi-free electrons do play an important role in superconductivity. Thus, the key to the superconductivity mechanism should lie in a combination of Covalon-conduction and quasi-free electrons.

2.2. Superconducting Mechanism Incoporating Covalon Conduction and 'free' Electrons

Let us assume a metal or an alloy having both the quasi-free electrons and a conjugated covalent-bonded chain. We shall call the electrical conduction carried by quasi-free electron as 'normal' and the conduction carried by covalent-bonded chain as 'covalon.' These two mechanisms can be illustrated as follows:

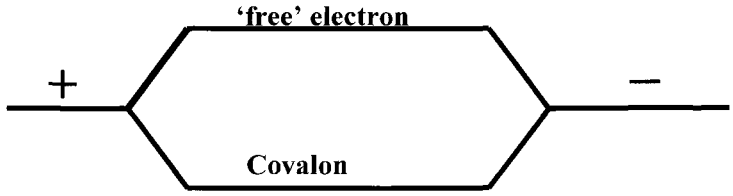

Fig. 6. Pictorial representation of a coexistence of COVALON and 'free' electron conduction.

The electrical resistivity of the two conduction mechanisms can be analyzed as a function of temperature.

At high temperature: (above superconducting state) the electrical resistance due to the two mechanism are as follows:

$$\rho_{free} = \rho_0 + \rho_T \quad ; \quad \rho_{covalon} = \infty$$

where ρ_0 is residual resistivity and temperature independent; ρ_T, on the other hand, is the resistivity due to phonon scattering and is temperature dependent. Therefore, at high temperature all the conduction is through the free-electron mode and no current is carried through Covalon conduction. But, as the temperature is decreased, at some point, all the phonon vibration along the chain is suppressed except the anti-symmetric normal mode of vibration. This leads to the condition, $\nu = \omega$, and induces the Covalon conduction to set in with

$$\rho_{free} = \rho_0 \quad \text{and} \quad \rho_{covalon} = 0$$

At this point, all the current will be carried by the Covalon conduction mode. This is because no matter how small the residual resistivity, ρ_0, may be, as long as it is a finite value, the current will flow exclusively through Covalon mode. At this point, the quasi-free electrons are considered 'frozen' i.e., they are not affected by electro potential being applied to the metal or alloy. Since Covalons are boson and quasi-free electrons are fermion, Covalon conduction along the chain will cause perturbation in the sea of free-electrons. This perturbation creates plasmon waves much the same as when a stone is dropped in the middle of an otherwise calm pond of water and produces a ripple effect as illustrated in Fig. 7 in two-dimension. As seen in the figure the amplitude of ripple wave will become smaller and smaller as distance, d, is increased and ultimately will die down. In a crystalline state, a conjugated chain will have a number of similar chains parallel to it such that the ripple will affect or induce the flow of Covalon conduction in another chain as illustrated in Fig. 7. Let us assume Covalon is induced in the A-chain and as the result, a plasmon wave is caused to propagate to A'-chain. Since the plasmon wave changes its potential from positive at t_1 to negative at t_2 dynamically, Covalon at

position, p_1 at time t_1 in A' chain may experience an attractive force from the plasmon wave and move toward P_2, and reach that position at t_2. However, at t_2, the plasmon wave has changed its positive to negative and results in pushing Covalon to move further toward position, P_3 at time t_3 and so on. The Covalon conduction thus induced in chain A' as the result of the Covalon conduction in chain A, will now generate its own plasmon wave to induce many other chains (including chain A) throughout the crystal

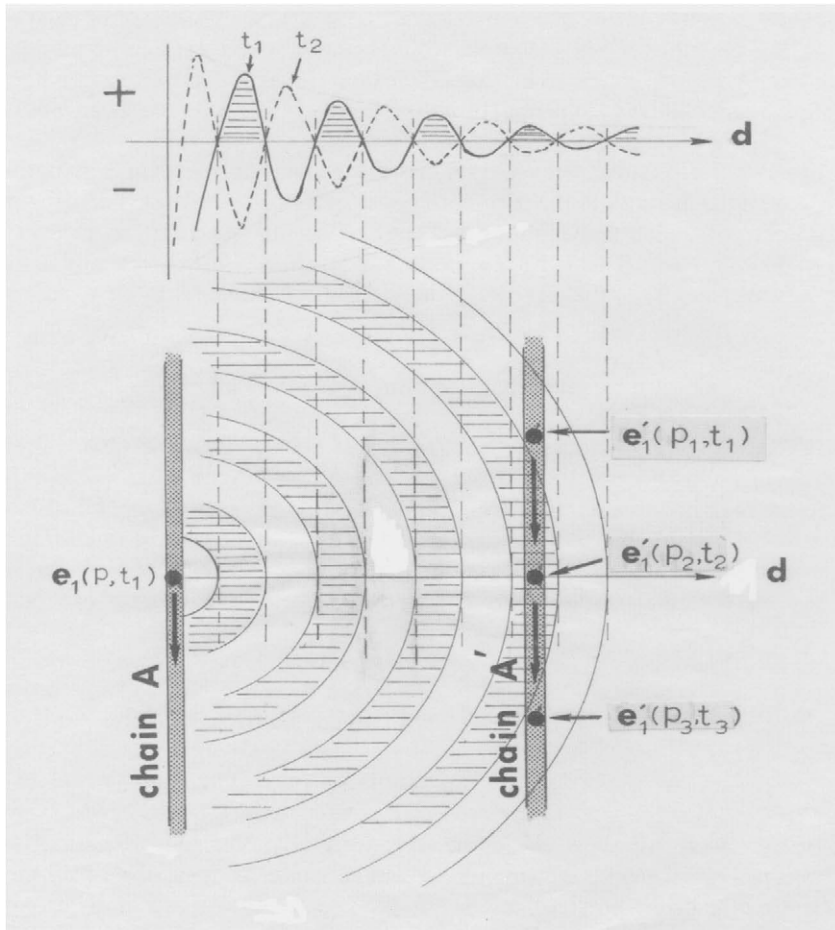

Fig. 7. Pictorial representation of a 'Covalon' $e_1(p_1, t_1)$ traveling in chain A creating plasmon wave that affects another 'Covalon' $e_1'(p_1', t_1)$ in chain A' to move toward (p_2,t_2). Since at t_2 the plasmon wave changes its sign, the 'Covalon' continues to move toward (p_3, t_3) and so on. It is not shown in the drawing but chain A' now emits its own plasmon wave back to chain A thus creating a cooperative effect.

toward Covalon conduction. This type of phenomenon is known as cooperative effect as found in superconductivity. This particular effect can be regarded as self-enhancing such that the covalon conduction and subsequently a superconducting current (even in the absence of electro-potential) will continue to flow forever!

With this physical picture, we can begin to analyze other attributes due to this type of superconductivity mechanism. Let us assign the quasi-free electron concentration as N(e) and we shall see how it affects the superconductivity. For this discussion, refer to Fig. 8- (b) where the plasmon wave intensity is plotted against N(e) in arbitrary units.

a) It is clear that if N(e) = 0, there would be no plasmon and thus no plasmon wave to reach other similar chains to enhance or induce Covalon conduction in other chains. Therefore, there will be no superconductivity.

b) For a given distance, d, between the chains the plasmon wave effect will increase with the increase in the density of quasi-free electrons, N(e). Then, the plasmon wave effect will reach a maximum and start to decline with further increase in the electron density, N(e). This is because further increase in N(e) will actually dampen the plasmon wave, similar to the increase in the viscosity of the water in the pond leading to a decrease in ripple propagation.

c) Artificially, we can alter the N(e) by applying ultra high pressure to the crystals. Under ultra high pressure we do not expect covalent-bonding to be affected but we would expect the N(e) to increase. Whether this would lead to an increase or decrease in the plasmon wave effect between the chains will depend on the initial position of $N(e)_0$ prior to the high pressure application.. That is, if $N(e)_0$ –L was on the left of maximum the plasmon wave intensity it will increase and if $N(e)_0$ –R was on the right of maximum the plasmon wave intensity it will decrease under pressure (see Fig. 8 (b)). We shall see later how this theoretical argument is in agreement with the experimental observation.

d) Ideally, for plasma (sea of free-electrons) to propagate a plasmon wave, it must be 'frozen' i.e., be perfectly still and not perturbed by other effect. Thus, if the nuclei throughout the crystal were magnetic, they would interfere with the propagation of plasmon waves.

In Fig. 8-(a) we show the curve experimentally obtained [57] for T_C vs. e/a (electrons per atom) among the structurally similar elements in support of the prediction derived from the theory proposed.

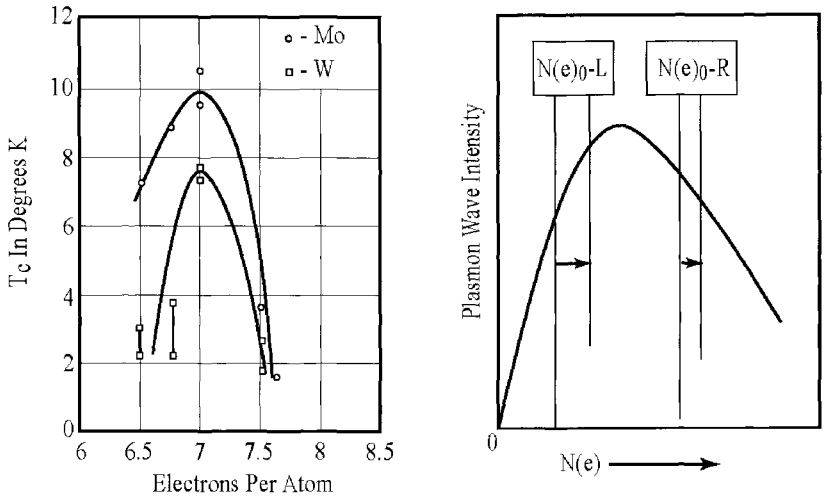

Fig. 8. (a) Experimentally obtained [57] plot of T_C vs. electron concentration in forms of (e/a) electron to atom ratio. (b) Theoretical model of plot of 'plasmon wave intensity' vs. N(e) electron concentration.

2.3. Prediction Based on the Covalon Conduction Theory

Within the theory presented here, the onset of superconductivity, T_C, is when the condition, $\nu = \omega$, takes place. At this point, the normal conduction through free-electrons becomes zero and therefore is 'frozen'. As stated before, the phonon (anti-symmetric normal mode) vibration is written as:

$$\nu = 1/2\pi\sqrt{k/m}$$

where k is the force constant and m is the atomic mass. For a given metallic element, the atomic orbital associated with that element is a fixed quantity and does not vary from one atom to another. In contradistinction, the atomic mass may vary from one atom to another depending on the number of stable isotopes found for that element. It is clear that under this situation, a unique phonon vibration, ν, will be more difficult to obtain if there are more isotopes that exist for the element. This simple but elegant reasoning led to the prediction that if one was to plot T_C vs. N (number of naturally occurring isotopes) there should be recognizable curve. The result of such a plot was published in *Solid State Communication* [22] and reproduced in Fig. 9. Unfortunately, I could not describe in the paper how I came about to assemble this plot. For to do so, I must give my own theory that contradicts outright the Nobel Prize winning BCS theory and that I have to denounce the 'Cooper pair' theory. And the chances are that I could not even have the

paper accepted for publication and would be summarily rejected by an anonymous referee. In fact, as the story went, within a week of the publication of this T_C vs. N plot, in which no mention of how I came to look for this correlation, I received a number of telephone calls telling me that they could explain this interesting correlation based on the BCS theory! Following the principle of "Never mind of predicting – but, only to explain." One of those 'explanations' indeed appeared in *Solid State Comm.*[23].

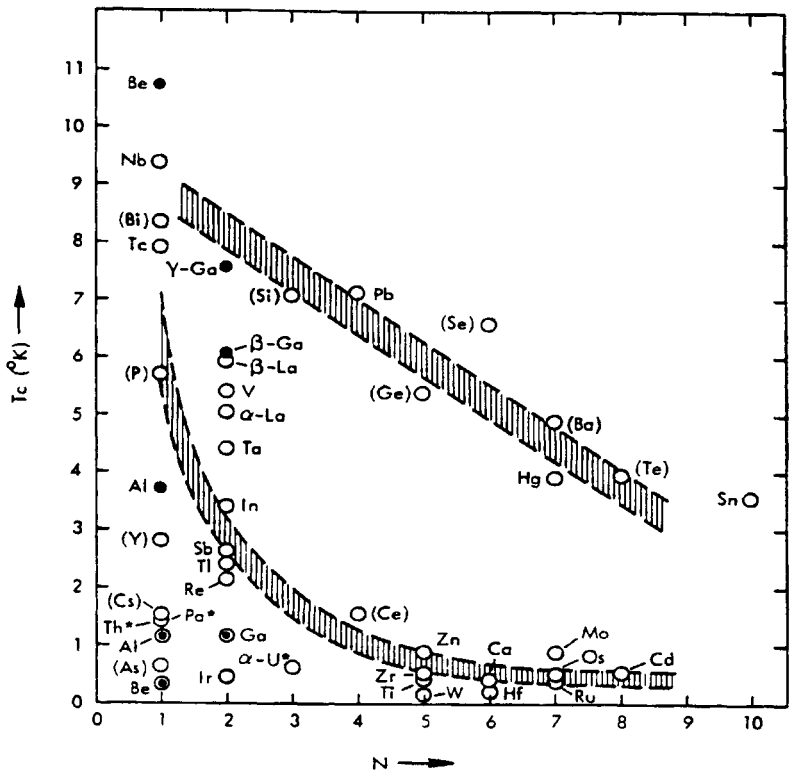

Fig. 9. Correlation of superconducting critical temperature, T_C , vs. N, the number of naturally occurring stable isotopes. The shaded curves should be considered only as showing the trend and the possibility of separating into two groups. The T_C data are obtained from *Properties of Selected Superconductive Materials* ;Natl. Bureau of Stand. Technical Note (1972). The number, N, is obtained from *American Institute of Physics Handbook* (McGraw-Hill Book Company, 1972. ( ) – superconducting only under high pressure, * - radioactive, ⊙ and • - represents more than one T_C for the same element under different physical environment.

I shall not elaborate on the triviality of this 'explanation' but only to ask one question to the author who wrote this article (since the referee forgot to ask). If the BCS theory was correct, why then Sc, and Y, metallic elements which all have only one isotope and also have a high $N(e)_f$ (electron density of states at the Fermi level), the requirement imposed for a high T_C by the BCS theory, are not superconductors? Of course, they can explain somehow. But, in the Covalon conduction theory there is no need for an explanation or no elaborate mathematical equation necessary. It can be easily understood in terms of their atomic orbital. The answer in Covalon conduction theory is simply that both elements are III-A elements in the periodic chart and their atomic orbital are *not conducive* in forming conjugated covalent bonds, therefore there is no Covalon conduction to lead them to superconductivity.

The correlation as summarized in Fig.9 is remarkable in the sense that it supersedes the following factors that heretofore were invoked in one way or another to correlate to the phenomenon of superconductivity: (a) transition or non-transition elements, (b) crystal structure type, (c) atomic number, (d) valence electron concentration.

It may be suggested that the correlation obtained is purely fortuitous and that the agreement is simply coincidental. Nevertheless, there are other factors that tend to argue against such a suggestion as follows:

a) Considering the fact that the reported T_C data have a degree of uncertainty, the correlation is remarkably good. Out of 40 elements listed the T_C of only 9 elements (Cs, Al, As, Be, Ga, Ir, Th, Pa and α-U) appear to be somewhat lower than the correlation indicates. However, Pa, Th, and α-U are radioactive elements and their atomic mass is constantly changing with time. And in a strict sense, these elements should not be considered as N=1 or N=3 elements but should have higher N number. In fact, the lower T_C for these elements render support to the correlation.

b) Further, Al, Be, and Ga, are the elements whose reported T_C appears to vary widely from one investigator to another, reportedly due to various causes, e.g., whether the element is in granular form [24] for Al, or whether the element is pure [25] or in the presence of some chemicals [26] for Be, or even under certain pressure regime [27] for Ga. In contradistinction, the elements whose T_C appears to fit well with the curve do not seem to have these idiosyncrasies.

c) The number, N, as given in Fig. 9 is obtained by counting every stable isotope found to exist in the element in nature, irrespective of the percentage (abundance) of isotopes involved, i.e., *UNWEIGHTED*. Consequently, the average mass, $\overline{M}$, appear to have little effect on T_C and is not critical, contrary to the suggestion by the BCS theory. This conclusion is consistent with the experimental observation that the T_C shifts due to 'isotope effect' (based on average mass difference) is rather small – at most about 140 m °K for Sn and usually less than 10 m °K.

It is of interest to note that a definite trend exists in the correlation curve that elements with N=1 possess a higher T_C in general than elements with N=2, which in turn possess a higher T_C than elements with N=3 and so forth as is anticipated from the Covalon_conduction theory. Furthermore, through the virtue of such a correlation,

elements are divided into two groups. One group consists dominantly of B elements (upper curve) whose T_C drop vs. N curve is nearly a constant. The other group consists primarily of A elements whose T_C drop vs. N is rather sharp and remains fairly low beyond N= 4. For A and B element differentiation the reader should consult the *PERIODIC CHART OF THE ATOMS* where the grouping is made according to the number of valence electrons and therefore, have to do with their atomic orbital.

The correlation agreement obtained here renders further support to the proposed Covalon conduction theory and leads to a further prediction that for a given element with $N > 1$, the T_C for that element will become higher if the number N is reduced to $N = 1$ (isotopically pure) through an isotope separation process. Conversely, if Nb and La with $N = 1$ are doped with relatively long half-life isotopes, their T_C should go down. These experiments have not been carried out yet by anyone as of this writing.

It is important to point out once again that in general, intermetallic compounds (when they are found to be superconducting) have a higher T_C than the T_C found for the metallic elements. One of the well- known binary compounds is the A_3B (β-W type) represented by Nb_3Ga, Nb_3Ge. Nb_3Al, Nb_3Sn etc. with $T_C > 14^\circ K$. We shall analyze this intermetallic compound in terms of Covalon conduction.

3. Nb_3Al IN TERMS OF COVALON CONDUCTION THEORY

Nb_3Al crystallizes in cubic, Pm3n symmetry with a unit cell dimension of 5.18 Å as shown in Fig. 10. From the figure it is shown that Nb atoms, linked by solid line and essentially forming three straight 'chain's, are mutually perpendicular to one another. Although in pure metals, Nb and Al have the same metallic radii of 1.43 Å, in Nb_3Al, the intra-chain Nb-Nb distance of 2.59 Å is much shorter than the expected 2.86 Å from its metallic radius. The implication is that there is a strong interaction between Nb atoms along the chain. On the other hand, the Nb-Al distance of 2.89 Å is quite close to what is expected from metallic radii of the two elements. The inter Nb chain distance of 3.16 Å indicates the independence of each chain. From the Covalon conduction point one would expect the Nb chain to be formed not only through covalent bond but more importantly that it is formed through 'conjugation'. In order to confirm these possibilities, Chiu & Wang theoretically investigated, starting with the atomic orbital of Nb (sometimes known as Cb- columbian) and reported the results in two papers: *Charge-Overlap Study of Multiple Metal-Metal Bonding and Conjugation in Linear Chains of Transition-Metal Atom.* (Inorganic Chemistry, 21. pp.4264-4274, 1982); *Multiple Metal-Metal Bonding and A-chain Integrity in Superconducting A_3B (β-Tungsten) Alloy* (Sol. Stat. Chem. 45, pp.353-367, 1982). For the detail of this investigation, readers are encouraged to look into these two papers. The conclusion was that by computing the *s, p,* and *d* orbital overlaps across the transition elements series, a rational comparison of trend was established. And using these overlaps, molecular orbitals were calculated. These calculations established the strong *d* bond between the A

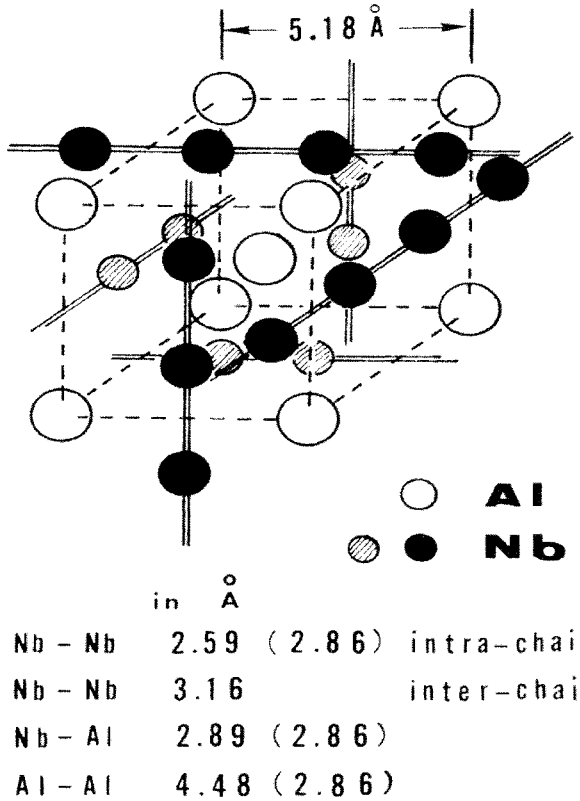

Fig. 10. The crystal structure of Nb_3Al and their interatomic distances.

atoms in A_3B intermetallic compounds. It was noted in this study, that the compounds with superconducting properties are precisely those especially rich in resonance structure (within the A-chain) possessing the possibility of 'long-short' bond alteration along the multiply bonded A-chain. The conjugated chains, hitherto not treated in the literature, in the intermetallic compound are calculated for each element and the average maximum bond orders and energies are estimated. The difference in the force constants between the 'long' and 'short' bonds is estimated. It was concluded that there is a strong correlation that exists between the propensity to multiple bond formation and the property of superconductivity in these A_3B compounds. It is reasonable, therefore, to conclude there is no solid solution that exists on the aluminum rich side. The Covalon conduction is operative in these compounds within the A-chain where the bonded electron pair moves along the 'long-short' bonds in harmony with the antisymmetric vibration and leads to superconductivity. The free electrons, which serve as a plasmon wave to interact between the Nb chains, are obviously contributed by Al atoms which do not participate in the formation of Nb chains. With this understanding, it is easy to see

the reason why the SSR (Solid Solution Range) of Nb_3Al as shown in Fig. 11 extends from 75 at.% (stoichiometry) of Nb up to 82 at.% of Nb. This means Al cannot and does not substitute for Nb but Nb can substitute for Al as much as seven atomic percent beyond the stoichiometry. In another words, Al does not have correct atomic orbital to substitute for Nb in the chain formation. On the other hand, Al serves only as 'filler' and the metallic radii of Al and Nb are nearly the same, therefore Nb can substitute freely for Al. It may be argued that since this is only one experimental fact, the result given here may be fortuitous. I agree with this argument, therefore I collected the data given for 28 A_3B compounds with respect to their phase equilibrium diagram (and subsequently their SSR) and their superconducting critical temperature T_C and found even more convincing proof as discussed below.

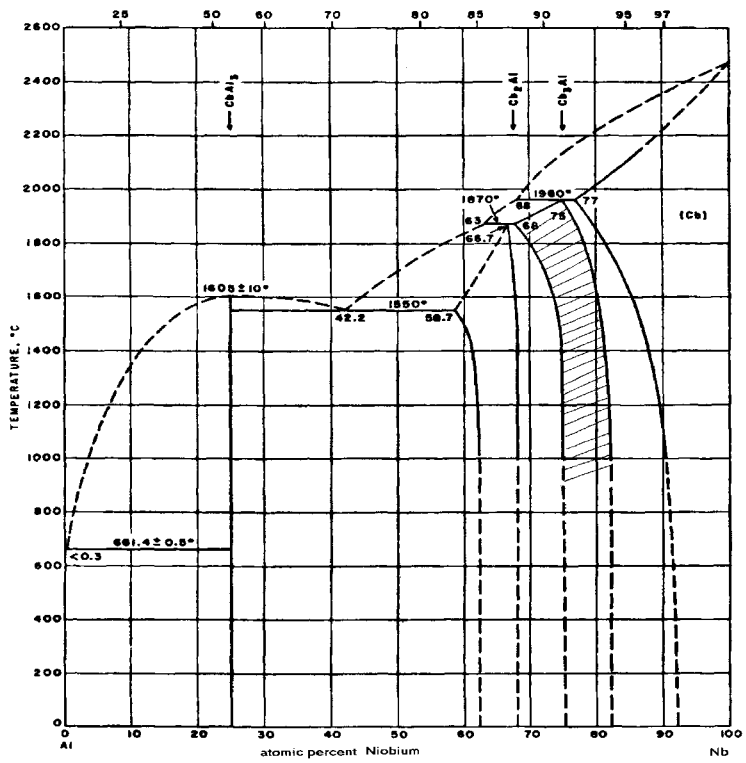

Fig. 11. The shaded area represent compound, Nb_3Al with the solid solution ranged from 75 to about 82 at.% of niobium. It should be noted that there is no solid solution that exists on the Al rich side.

For these discussions refer to the original papers: *Superconducting Critical Temperature, T_C,, and Phase Equilibrium Diagram of A_3B type Compounds,* (J.Phys.Chem.Solids, 35, pp.273-278, 1974), and *The T_C -SSR Correlation in A_3B Compounds,* (Solid Stat.Comm., 23, pp803-808, 1977). Among the 69 A_3B type compounds known to exist to this date [28], only 23 systems for which both the phase equilibrium diagram as well as the superconducting critical temperature, T_C, have been reported in the literature [29]. The SSR (Solid Solution Range) of these twenty-three A_3B compounds as shown in their phase equilibrium diagram can be categorized into four groups: (a) the SSR extends only on the A-rich side, (b) the SSR extends only on the B-rich side, (c) the SSR extends on both sides, and (d) shows no SSR whatsoever. These results are summarized and shown in Fig. 12 along with their superconducting temperature, T_C. Our contention is that the A-chain is critically important to the Covalon-conduction and therefore to the superconductivity. With this contention, one can predict that those compounds whose SSR extends on both sides or extends only on B-rich side must be either are not superconductors or are poor superconductors. This is because their A-chain is not strong and thus has a poor Covalon conduction and poor superconducting properties. Contrarily, the compounds whose SSR extends only to the A-rich side or without SSR on either side would be a good superconductors. With these predictions, Fig. 13 was plotted. All the good superconductors appear to have their T_C proportional to the SSR, whereas the group of poor superconductors appears not to have this trend.

In view of these observations, the conclusion that strong -A-A- chain integrity is indeed an important factor in the superconductivity of not only in A_3B compounds but also in all superconductors is inevitable. The fact that the A-atoms can come only from IV-A (Ti, Zr, Hf), V-A (V, Nb, Ta) and VI-A (Cr, Mo, W) transition elements tends to suggest chemical bonding involving special atomic orbital to be operative within the A-chain.

Next, a possibility of the A-chain being a conjugated atomic chain having – 'double'-'single'-alternate bonding along the chain must be considered and the evidence given in order to establish the Covalon conduction. A direct experimental evidence for the conjugation is not possible but there are a number of pieces of indirect evidence to be given here that collectively do make a good case. (1) A_3B compounds tend to be metastable. By having T_m , a martensitic transition [30] is attributable to the instability of a conjugated chain (saturated bonding involving only 'single' bonds are inherently stable)., (2) According to Axe and Shirane [31], at T_m (typified in Nb_3Sn) two of the three mutually perpendicular A-chains actually assume 'long' – 'short' alternating interatomic distances along the chain. This is reminiscent of 'single' – 'double' bond alternation in a conjugated chain, and (3) it has been shown in the theoretical treatments of conjugated atomic chains [4,32] invoking vibronic interactions, that a high electron conduction along the chain involving pair wise charge transfer is possible and likely.

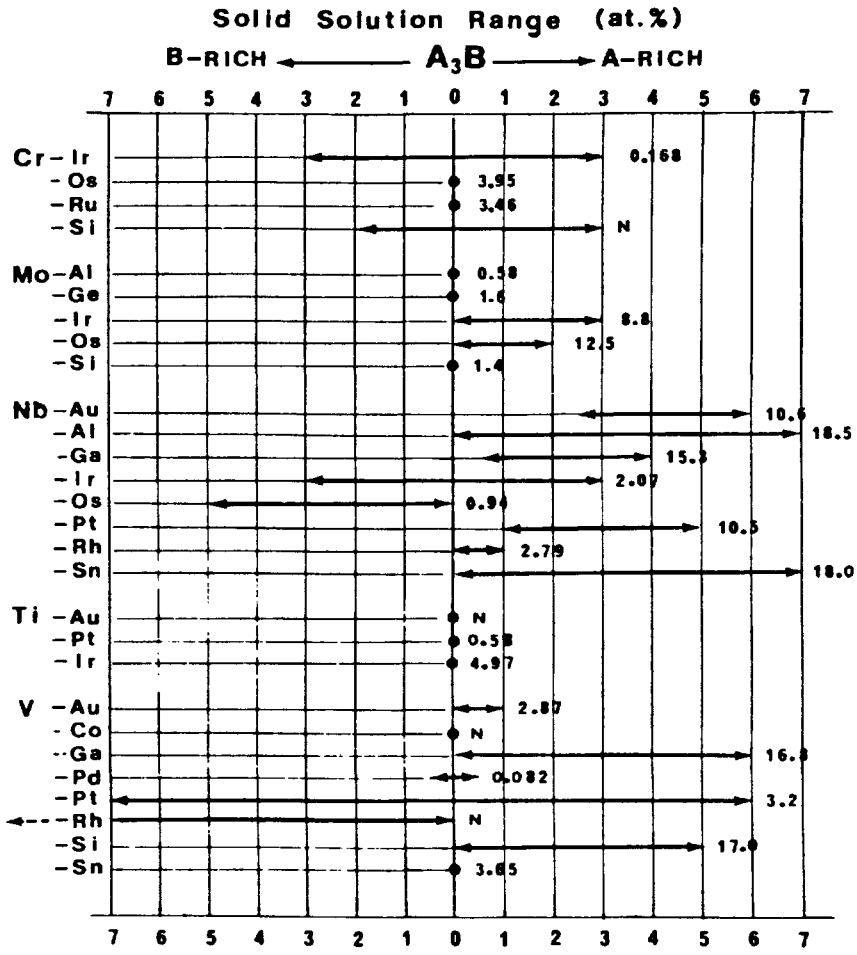

Fig. 12. The SSR (Solid Solution Range) for the 28 A_3B compounds are indicated by the solid line with arrows. Solid circles indicate no SSR. The numerical value of T_C for each compound is indicated. N indicates no superconductivity found down to 0.015 K.

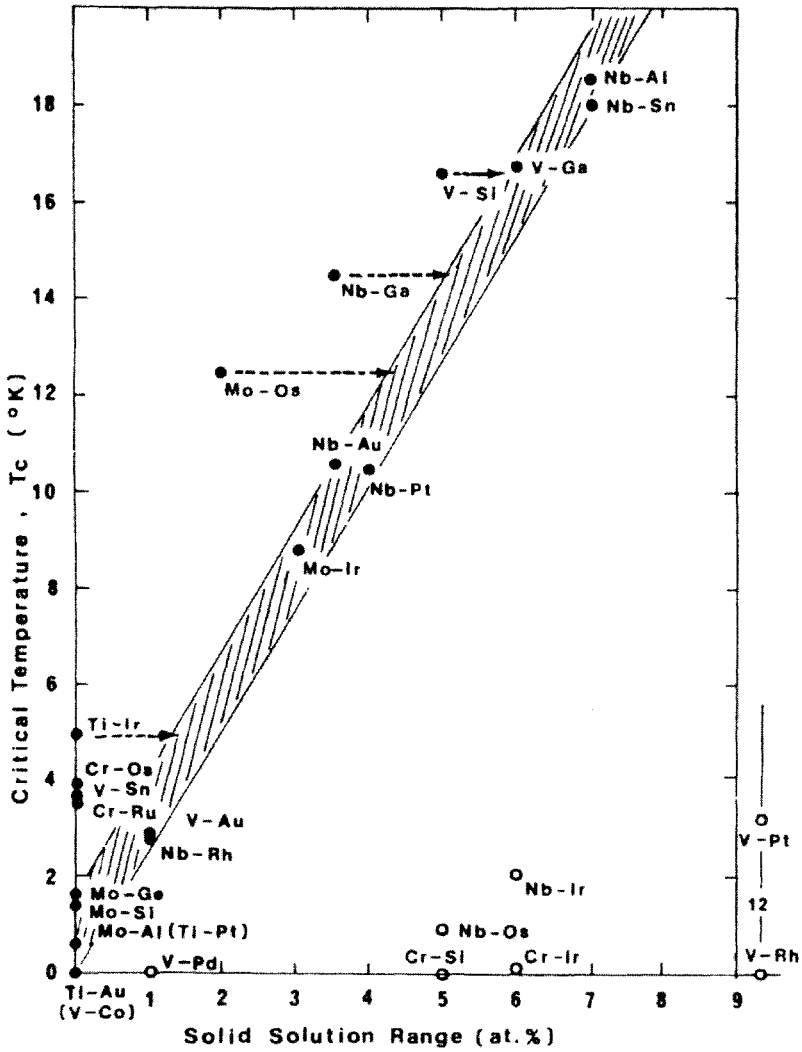

Fig. 13. T_C vs. SSR for the 28 A_3B compounds. ● - compounds whose SSR extend only on the A-rich side. ○- compounds whose SSR extend on both sides or only on the B-rich side . Arrow indicates possible error in the SSR determination.

There is one piece of evidence that comes from the phase diagram study described in the earlier chapter of *PHASE EQUILIBRIUM DIAGRAM*. To refresh the memory, it was concluded that a fundamental difference exists between the congruent-melting vs. incongruent-melting (peritectic) mode of compound formation. The atomic arrangement of a congruent-melting compound is such that the A (atom) is surrounded by the B (atom) and in turn, the B (atom) is surrounded by the A (atom). In sharp contrast, the atomic arrangement of incongruent-melting (peritectic) compounds have either the A (atom) or the B (atom) that form 'chains' or 'islands' among their own type atoms. Within this understanding, one can predict with confidence that any A_3B compounds which have its SSR only on the A-rich side or no SSR range whatsoever must be formed through the incongruent-melting mode. And these compounds are good superconductors. In fact the prediction can be extended to include all the intermetallic compounds (not limited to A_3B type) that are good superconductors. In this manner, it is extremely satisfying to be able to tie the phenomenon of superconductivity to the phase diagram which is a manifestation of all the thermodynamic properties, including information concerning electronic arrangements as well as atomic arrangements.

Conclusion: ***All superconducting intermetallic compounds are formed through incongruent (peritectic)-melting. But, not all incongruent-melting compounds are superconducting, because 'chain' or 'island' formation may involve covalent bonding but not necessarily involve 'conjugation'.***

4. COVALON CONDUCTION IN [TCNQ-TTF]

Earlier, I criticized the Cooper pair being philosophically unacceptable because the proposed pair is not seen elsewhere outside of the BCS superconductivity theory. The same measurement must be placed against the Covalon-Conduction theory proposed here. We shall show therefore, that a number of physical property changes observed in [TCNQ-TTF] (tetracyano-p-quinodimethane-tetrathiofulvalene), an organic compound, as a function of temperature can be interpreted and understood in terms of 'Covalon-conduction'.

Crystals of TCNQ salts have been shown to exhibit high electrical conductivity [33-36]. One of the highest conductivity has been found in the [TCNQ-TTF] complex [37-39]. Additionally, other interesting physical characteristics have also been found in this complex compound [37-42]. The experimental observations show the electrical conductivity of [TCNQ-TTF] to be divided into three distinct temperature ranges:

TR-A, below about 56 °K, is a semiconductor-like [40-42] region. The conductivity has a positive temperature coefficient.

TR-B, between about 56 °K and 60 °K is the semiconductor-conductor transition region. In a few cases where the crystallinity was extraordinarily good, anomalously high conductivity ($\approx 10^{14}\ \Omega\ \text{cm}^{-1}$) has been observed along the $\bar{b}$ axis [38,41].

TR-C, above 60 °K up to about 300 °K is a metal-like region. Following a sharp drop in anomalously high conductivity (when existing), the conductivity has a negative temperature coefficient.

From the molecular physics point of view, TCNQ is an organic molecule in which the carbon atoms are bonded to one another containing alternating 'double' and 'single' covalent bonds as shown in Fig. 14-(a), -(b). This is known as *conjugation.* It is well known that in such molecules, the 'σ' and 'π' bonds can be treated more or less independently [5, 6] and that the π-electrons are invariably treated in terms of quasi-free, spin unpaired state and their motion in the molecules in terms of band structure [33]. Dominance of such a view is in large part due to the fact that the Delocalized-Molecular-Orbital theory is a one-electron model that neglects the interaction of electrons with the vibration of the molecular skeleton, i.e., assumes equal bond length between all atoms. As was explained earlier in *3-COVALON CONDUCTION THEORY* section, these shortcomings were remedied by incorporating different bond lengths for 'single' and 'double' bonds respectively and by coupling the resonance movement of the paired-electrons with the simultaneous lengthening and shortening of the bond.

A correspondence between the 'Covalon' model and the electrical conductivity characteristics observed in TR-A, B, and C temperature ranges can be made as follows: According to the crystal structure investigation [43] the closest intermolecular distance in [TCNQ-TTF] crystals is between TCNQ and TTF, i.e., the distance between TCNQ or TTF molecules themselves are further apart. Thus, the physical path of electron conduction through the crystals is not through a stack of TCNQ or TTF but rather through -(TCNQ)- (TTF)- (TCNQ)- alternation. Therefore, stepwise charge transfer is [see Fig. 14(c)] as follows:

Step 1, **intramolecular** charge transfer within TCNQ

Step 2, **intermolecular** charge transfer from TCNQ to TTF.

Step 3, **intramolecular** charge transfer within TTF.

Step 4, **intermolecular** charge transfer from TTF to TCNQ,

and back to step 1.

Within such a physical path, the conduction mechanism can be differentiated into three parts; intramolecular charge transfer within TCNQ, within TTF, and intermolecular charge transfer between TCNQ and TTF. Because TTF is known [44] to be capable of electron conduction in its ground state, and is readily polarizable to the $(TTF)^{+2}$ state, intramolecular charge transfer within TTF is expected to take place readily by means of polarization charge transfer. On the other hand, due to spatial proximity between the nitrogen atoms on TCNQ and the hydrogen (or possibly sulfur) atom [45] on TTF, the intermolecular charge transfer between TCNQ and TTF may take place with ease through a 'hopping' mechanism. Although the exact nature of these two conduction

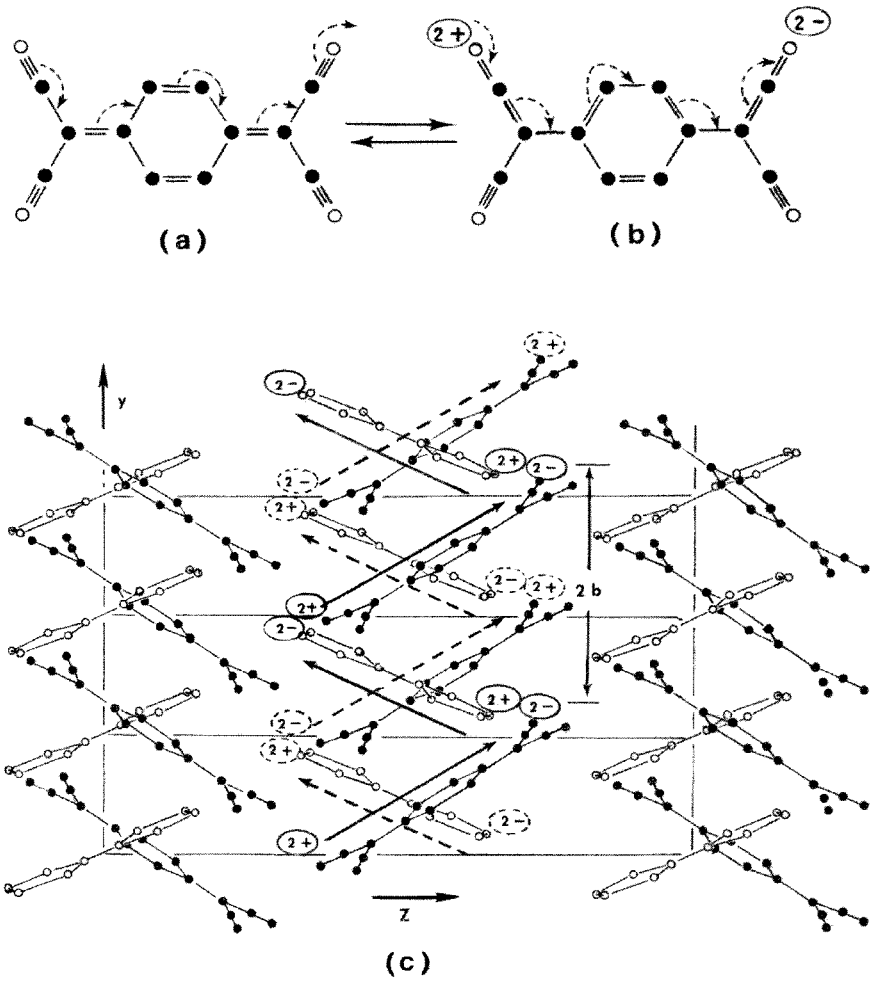

Fig. 14. (a), (b): the two possible states of TCNQ. Dotted lines with arrow indicate the direction and of movement of the five pairs of π-electron bond during the Covalon-conduction. (c) Projection of the [TCNQ-TTF] crystal structure onto the $\bar{b}-\bar{c}$ plane; solid and dotted lines indicate the helical paths of pairwise charge transfer in the <010> direction. The TTF (open circles) are behind the TCNQ (solid circles).

mechanisms is not known, it is clear that they are not semiconductor-like. In contrast, the remaining mechanism, the intramolecular charge transfer within TCNQ (a conjugated molecule), can become semiconductor-like at low temperatures. Unlike TTF, TCNQ is not a conductor in its ground state [34]. Thus, it is the poorest conductor

among the three conduction mechanisms. Since the three conduction mechanisms are interconnected in a series (in our model), the overall electron conduction characteristics in [TCNQ-TTF] crystals will be controlled by the poorest conductor, i.e., the intramolecular charge transfer within TCNQ which is dictated by Covalon-conduction.

With these understandings, the principal electrical conduction changes observed in [TCNQ-TTF] at each temperature range can now be compared against the Covalon model proposed in the following manner. (refer to Figs. 15 & 16).

TR-A (below about 56 °K)

Experiment: (1) Conductivity is semiconductor-like [37-42], and (2), Weakly paramagnetic down to 20 °K [45-47], (c) The EPR g-factor is temperature dependent [46]; increases from average $\bar{g}$ (at 60° K) = 2.0059 to $\bar{g}$ (at 20° K) = 2.0082 which is very close to the reported isotropic g value of 2.00838 for $(TTF)^+$.

Theory: (1) The effective energy barrier between the two harmonic oscillators, ΔE (∞ $1/\omega$), which determines the probability of electron transfer along the conjugated chain; decreases with increasing temperature; thus, conductivity is semiconductor-like. (2) The spin susceptibility is due only to the unpaired π-electrons from TTF (all the π-electrons on TCNQ are in the paired state). Thus, the susceptibility is weak. (3) The spin-paired π-electrons on TCNQ resonate between the two harmonic oscillator states at frequency, ω. Such oscillation can perturb the g-factor of $(TTF)^+$. As the ω increases with the temperature rise, the perturbation becomes greater, and the g-factor deviates more from that of the pure $(TTF)^+$.

TR-B (56 – 60 °K)

Experiment: (1) Although there is some disagreement as to the exact magnitude, it is generally agreed [37-42] that in this narrow temperature range, conductivity increases anomalously to $10^3 - 10^4$ $(\Omega\ cm)^{-1}$ in the b direction. (2) The spin susceptibility remains low despite the high conductivity [45-47]. (3) The EPR line-width increases dramatically [46] from about 1 gauss to 20 gauss. (4) No dramatic change occurs in the EPR g-factor [46]. (5) The thermoelectric power is essentially zero independent of small impurities [48]. (6) The anomalously high conductivity is strongly dependent upon the perfection of the crystals [41].

Theory; (1) Anomalously high conductivity arises because of the emergence of pairwise charge transfer (matching of ω and ν), the Covalon conduction as depicted in Figs. 14-(a), (b). The magnitude of conductivity expected from [TCNQ-TTF] crystal in the b direction is calculated in the following section and (2) Inasmuch as Covalon conduction is a spin paired charge transfer, it does not contribute to spin susceptibility and the observed susceptibility remains low despite the high conductivity. (3) No theoretical treatment of the EPR relaxation time in transforming from spin-paired to spin-unpaired

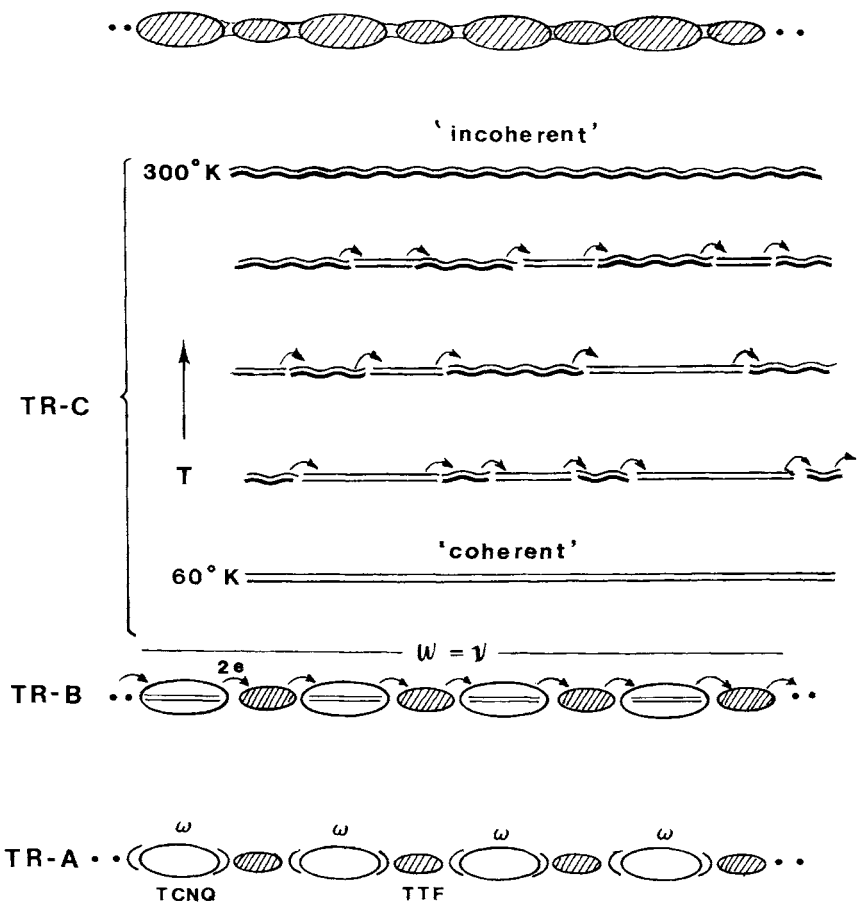

Fig. 15. Pictorial presentation of the physical concept of electron charge transfer in [TCNQ-TTF] as a function of temperature. TR-A ; each TCNQ resonates between the two harmonic oscillator states at a temperature dependent frequency, ω. Electrons on TTF are in an unpaired state (shaded)., TR-B; 'Covalon' conduction sets in under the condition, $\omega = \nu$ (represented by arrows within TCNQ. TR-C; this suggests the diminishing ratio of 'coherent'(straight lines) to 'incoherent'(wavy) parallel lines) with the temperature increase.

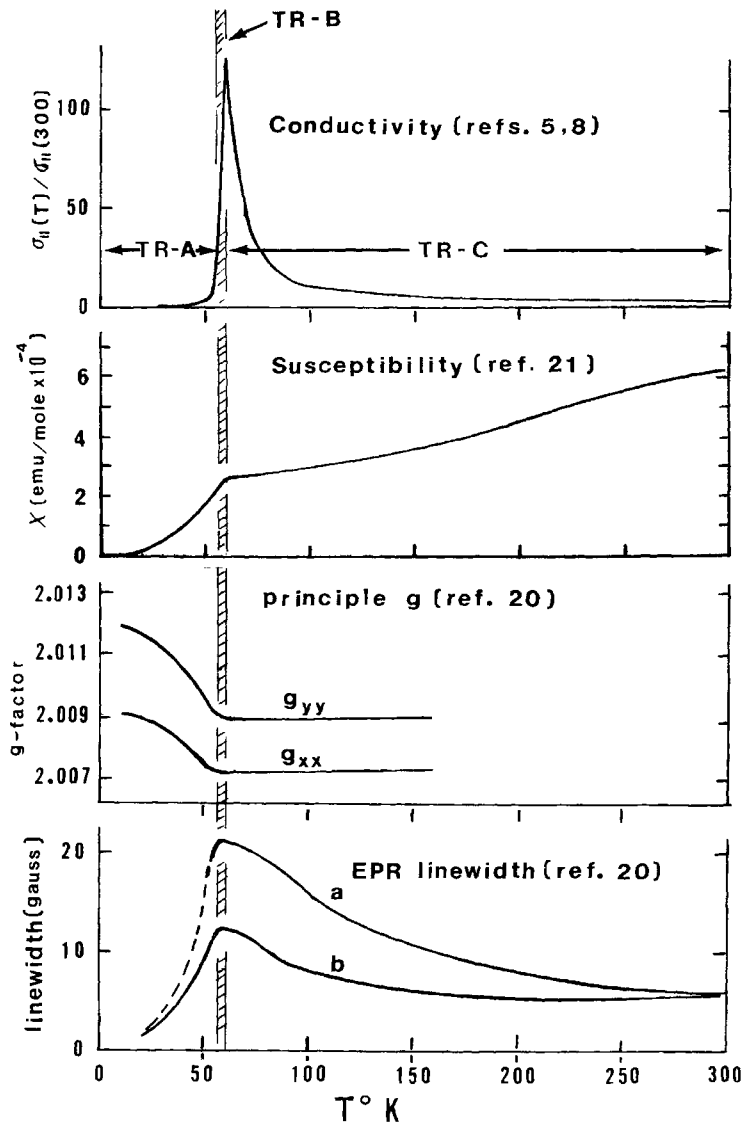

Fig. 16. A collection of the principal physical characteristics of [TCNQ-TTF] as reported in the literature is illustrated. For convenience, various aspect of the physical data, are divided into three temperature regions: TR-A, TR-B and TR-C.

states has been made. Nevertheless, a qualitative picture that is consistent with our understanding of EPR line width [49,50] can be presented. The physical path of electron flow as depicted in Fig. 15 at TR-B requires a continuous spin-state exchange between spin-paired to spin-unpaired π-electrons in TTF (indicated by small arrows in Fig. 14). Such a continuous exchange therefore affects the lifetime and energy of spin states of the π-electrons on TTF and causes the EPR line-width to broaden dramatically. (4) Since the π-electrons from TTF that are responsible for the g-factor in TR-B are the same electrons in TR-A (below 60 °K), no change in the g-factor is expected. (5) Inasmuch as the thermoelectric power is a measure of the entropy per carrier, and 'Covalon' conduction mechanism is one that takes place at the molecular level, the thermoelectric power will remain zero even in the presence of impurities. (6) For 'Covalon' conduction to be macroscopically observable all TCNQ must be interconnected by TTF spatially in proper sequence and orientation, a 'perfect' crystal is a prerequisite for an anomalously high conductivity.

TR-C (60 – 300 °K)

Experiment: (1) A sharp drop occurs in anomalously high conductivity just above ~ 60 °K [38-41], (2) Conductivity has a negative temperature coefficient [37-42], (3) Spin susceptibility, on the other hand, increases with the temperature rise [45,47], (4) The EPR line width decreases nearly in the same manner as conductivity with the temperature rise and becomes relatively constant at about 300 °K [46], (5) The single EPR g-factor remains essentially constant throughout the temperature range [46].

Theory; (1) When the temperature rises above 60 °K, due to the fragmentation of 'coherent' chain (i.e.,disruption of long range constructive cooperation between resonance electron movement and antisymmetric vibration), the anomalously high conductivity suffers sharp drop. (2) As the 'coherent' segments are interleaved with 'incoherent' segments, the overall conductivity becomes dependent on the conductivity of individual segments and the proportion thereof. Since the conductivity along an 'incoherent' segment is [33] only $\approx 10^{2}\ (\Omega\text{cm})^{-1}$ compared to $\approx 10^{4}\ (\Omega\text{cm})^{-1}$ for 'coherent' segments, and 'incoherent' segments increase in number and length with temperature rise, the overall conductivity should decrease with the temperature rise. In essence, the decrease in conductivity is due to two factors: (i) decrease in the proportion of 'coherent' segments and (ii) lowering of conductivity within 'incoherent' segments due to phonon scattering. (3) Due to the increase in the length and number of 'incoherent' segments, the number of unpaired π-electrons therefore increases with the temperature rise and results in an increase in spin susceptibility. At a certain high temperature, the whole chain becomes 'incoherent' and the magnetic susceptibility reaches a saturation point. The magnitude of this expected susceptibility is calculated below. (4) Since the electron spin-state exchange (which is responsible for line width broadening) takes place only within 'coherent' segments, the continual shortening of the 'coherent' segments implies a continual narrowing of line width in the EPR with increasing temperature, as observed. (5) Because the physical path in both the 'coherent' and 'incoherent' segments

involves direct interconnection between TCNQ and TTF and is essentially the same in both, the g-factor should be a singlet and remain constant in this region as observed experimentally.

To further support the theoretical model, we shall now show some quantitative agreements between theory and experiment

Spin Susceptibility at 60 °K and at 300 °K

The Pauli spin susceptibility is expressed [51,52] as

$$\chi_S = \mu^2 \, n(e) \qquad (1)$$

where μ is Bohr magneton and n(e) is the electron density of states. For one-dimensional 'Covalon' conduction such as that assumed in [TCNQ-TTF]. n(e), the electron density of states can be written as,

$$n(e) = (2L/h)(m^*/2E_f)^{1/2} \qquad (2)$$

$$E_f = (1/2m^*) (nh/4L)^2 , \qquad (3)$$

The Fermi Energy expressed in terms of, m^*, the effective electron mass, h, the Planck's constant, and n, the number of unpaired electrons residing in length, L. It is clear, the m^* is not easily assessed from the model, nor available from other calculations. But, for the calculation to be done here we shall assume $m^* = 10\ m_0$, the effective electron mass to be ten times that of electron rest mass. This assumption is not unreasonable in that while the electrons are 'delocalized' they are still tightly bound and the effective electron mass can be this high. For example, the effective electron mass for the d-orbital electrons in transition metals is known [53] to be greater than ten times the 'rest- mass.'

By substituting Eqs. (2) and (3) into Eq.(1) and dividing it by V_u, the unit molecular volume of [TCNQ-TTF], Pauli spin susceptibility is reduced to

$$\chi_s = \left[\mu^2 8 (L/h)^2 \left(m^*/n\right)\right] / V_u \qquad (4)$$

where L at 60 ° K and at 300 °K are obtained from the known structure of [TCNQ-TTF], whereas, n at both temperatures is deduced from the model presented here as follows: According to the model, there are only two unpaired electrons residing within TTF molecule having a molecular length of 8 Å; thus, n = 2 and L = 8 x 10^{-8} (cm) at 60 °K. On the other hand, at 300 °K, all the π-electrons are unpaired and yield 12 electrons (unpaired) per TCNQ-TTF molecule within the 'incoherent' chain. The length in which the 12 electrons reside therefore is 8 Å(TTF) + 11.8 Å(TCNQ) + 2x2.6 Å (space between TCNQ and TTF) = 25 Å; thus, n = 12 and L = 25 x 10^{-8} (cm) at 300 °K. Along with these numerical values, other parameters in the equation (4) are [38];

$\mu = 0.927 \times 10^{-20}$ (erg/gauss)

$h = 6.6 \times 10^{-27}$ (erg/sec)

$m^* = 10\ m_0 = 91.1 \times 10^{-28}$ (gm)

$V_u = 4.18 \times 10^{-22}$ (cm^{-3})

The volume susceptibility of [TCNQ-TTF], χ_S, thus calculated is then converted to its molar susceptibility, χ_m, by multiplying the molecular weight of 408 for [TCNQ-TTF] and dividing by the crystal density of 1.6 gm/cc. The results are in excellent agreement.

	Calculated (emu/mole)	**Observed (emu/mole)**
At 60 °K	**277×10^{-6}**	**266×10^{-6}**
At 300 °K	**500×10^{-6}**	**600×10^{-6}**

Conductivity at TR-B (56-60 °K)

It should be noted that because [TCNQ-TTF] crystallizes in monoclinic form and because conductivity is a tensor property, four independent pieces of conductivity data are required to completely define the conductivity in the principal directions. However, because the $\bar{b}$ axis, being perpendicular to both the $\bar{a}$ and the $\bar{c}$ axes, it is the only direction whose conductivity can be measured independently. Under the 'Covalon' conduction mechanism, a pair electron charge is transferred across the chain at each resonance between the two harmonic oscillation states as shown in Fig. 14-(a), (b). With the knowledge of ω, the resonance frequency and N, the density of paired electrons, conductivity can be calculated.

As shown in Fig. 14-(a), there are five pairs of covalent bonded π-electrons in TCNQ that can contribute to the 'Covalon' conduction. These five pairs are augmented by another pair from TTF (through double ionization to $(TTF)^{+2}$ state) making up a total of six pairs of π-electrons per TCNQ-TTF molecule. By combining this knowledge with the known unit molecular volume, V_u, of TCNQ-TTF, N may be calculated.

The theoretical conductivity in [TCNQ-TTF] crystals at TR-B in the $\bar{b}$ direction therefore is

$$\sigma_b = [N(2e)^2 \cdot \tau]/2m^* = 2.7 \times 10^4\ (\Omega\,Cm)^{-1}$$

where $N = 6 \times (1/V_u) = 1.44 \times 10^{28}$ (m^{-3})

$2e = 3.2 \times 10^{-19}$ (coulomb)	
$\tau = 1/\omega = 3.3 \times 10^{-14}$ (sec)	from [4]
$m^* = 10 \times m_0 = 91.1 \times 10^{-28}$ (gm)	as assumed in the susceptibility calculation

This is again in excellent agreement with the experimental value [37-42] for imperfect crystals of

$$\sigma_b \text{(observed)} = 10^3 \backsim 10^4 \ (\Omega \text{ cm})^{-1}$$

The fact that the experimental values are somewhat scattered, further renders credence to the model proposed. For, as stressed before, the 'perfection' or long range order in crystals is required for 'Covalon' conduction and results in a variation in the value of anomalously high conductivity at TR-B depending on the degree of perfection of the crystal used.

TR-B Temperature

The TR-B temperature, which separates the TR-A and the TR-C range, for cyclic conjugated chain has been calculated in a previous paper [4] in terms of ΔE, the energy barrier between the two harmonic oscillator,

$$\Delta E = (k/2)(\chi_0')^2 - |U'| + |U'|^2 / 2k(\chi_0')^2$$
$$= 0.20 \times 10^{-13} \text{ (erg)} \simeq 145 \ ^\circ\text{K}$$

where $|U|$ is a corrected (for Franck-Condon factor) resonance interaction integral and k and χ_0' are the force constant and distance between the two harmonic oscillators respectively. This value is higher compared to the 60 °K for [TCNQ-TTF] but within a reasonable agreement.

A number of other TCNQ-related complexes have been studied [33-36]. But, TCNQ-TTF has been found to be unique in having the anomalously high conductivity. What makes TTF unique from all the other 'cations' used in forming TCNQ complexes? The answer it turns out is found in the 'Covalon' conduction. For TTF is the only cation investigated thus far to have its first and second electron ionization potentials, not only small but also very close to one another [40] such as to facilitate its ability to exist as $(TTF)^{+2}$. From the 'Covalon' conduction point of view, this property of being able to exist in the $(TTF)^{+2}$ state by giving up two electrons at a time is of fundamental importance. For only then can 'Covalon' conduction, which requires two electrons to pass through TTF, be achieved. Thus, the proposed 'Covalon' conduction model predicts that a TCNQ-complex can and will exhibit an anomalously high conductivity, when and only when the cation used in forming the complex is readily polarizable to (+2) state.

5. SUMMARY & DISCUSSION

The 'Covalon' conduction mechanism as proposed here for superconductivity has the following characteristics:

a) Spin-paired electrons (boson) exist in all metals and alloys at all temperatures. However, they are not 'visible' at high temperature. They are not created at low temperature from free-electrons (fermion) as proposed in Cooper pair. Rather, their existence become 'visible' at low temperature under $\omega = \upsilon$ condition which leads to T_C. Indirect evidence in support of this thesis is the fact that (1) miscibility gap exists even for 'open' metals such as Na and K in their liquid state, and (2) for binary compounds, superconductors always form through the incongruent-melting mode.

b) The 'Covalon' conduction thus created can lead to an anomalously high conductivity such as shown in [TCNQ-TTF]. They can become superconducting only if these 'Covalon' (boson) can influence one another through a sea of free-electrons (fermion) that leads to a cooperative effect as observed experimentally. In the case of cuperate-oxides or ceramics, the sea of electrons are replaced by the oxygen bonding between chains to correlate between chains [54,55,56]. In fact, this should be a more reliable method of communicating between chains and leads to high-temperature superconductors.

c) The importance of the matching of $\omega = \upsilon$ for 'Covalon' conduction lead to the prediction of the correlation of T_C vs. N (number of isotopes) as shown in Fig. 9. The underlying logic is in the $\nu = 1/2\pi\sqrt{k/m}$ equation in which if the atomic mass, m, is not a constant but rather varied along the chain the phonon vibration frequency, υ, will not be a discrete value and be more difficult for resonance frequency, ω, to match and consequently harder to create 'Covalon' and subsequently lower T_C. Therefore, with everything else held constant, (such as between Nb and Mo) the greater is the number of isotopes the lower will be the T_C.

d) The fact that this 'Covalon' conduction can only lead to anomalously high conductivity but not superconductivity is demonstrated in [TCNQ-TTF]. In proposing superconductivity to come through 'Covalon'–'Covalon' interaction via the free-electron concentration, N(e) , a relationship between T_C and N(e) can be predicted as shown in Fig.8. This qualitative curve has the experimental support obtained by Matthias, Geballe and Compton [57] in terms of the T_C *vs.* e/a ratio for A_3B compounds i.e., the e/a ratio is directly related with the N(e). In particular, these authors observed that e/a ratio can only be affected through B atom substitution. A forced substitution of A atoms catastrophically degrade the superconductivity because the 'Covalon' conduction is disrupted.

e) If the material is magnetic, no superconductivity is observed for that material at the same temperature and state. Qualitatively, it can be understood again in term of 'Covalon' formation. For, magnetic material implies that there is an unpaired electron spin around the atom that in turn implies an incomplete covalent bonding (with or without conjugation) between atoms. Consequently there is no 'Covalon' formation and subsequently no superconductivity.

f) Since 'Covalon' conduction has its root in covalent bonding, the superconductivity found in the A_3B compounds must be very sensitive to their crystal

chemistry, particularly with respect to the A elements. A strong correlation between their crystal chemical factor and their T_C was shown in the paper of Wang [28].

g) At the onset of superconductivity, with $\omega = \upsilon$, all conduction will go through 'Covalon' conduction mode, which is a boson, therefore, the Meissner effect anomaly can be understood.

h) In 'Covalon' conduction according to this model, the current carried will have a limit that is directly relatable to the resonance frequency, ω, between the two harmonic oscillators. This allowed the calculation of conductivity for [TCNQ-TTF] as shown above. For superconductive material, the limiting current can be estimated with the knowledge of the resonance frequency, ω, and the density of 'chains.'

As far as the differentiation of Type-I and Type-II superconductors is concerned, no theoretical work has been done that supports or refutes the model being proposed. But, my own feeling is that the differentiation may lie in whether 'Covalon' conduction is based on single isolated straight chain such as in the A_3B compounds or based on a 2-dimensional 'chicken wire mesh' such as that found in graphite ('double' – 'single' bond alternation in 2-dimension). In fact, an intercalated compound based on |graphite |potassium | alternating layers as shown in Fig. 17, has been found to be a superconductor,(Geballe, *Scientific American,* 225, 1971) whereas graphite or potassium by themselves are not superconducting! Thus, superconductivity based on a 2- or 3-dimensional network of 'Covalon' conduction are, in my opinion, Type-I superconductors. And one-dimensional network of 'Covalon' conduction is of Type-II. The basis for the conjecture of Type-I superconductors being a 2- or 3-dimensional 'Covalon' conduction network is that it will be very easy for the applied magnetic field to destroy the 'Covalon' conduction. This is why Type-I superconductor has only one critical field, H_C. From a crystallographic point of view, multi-dimensional network of 'Covalon' conduction is more likely to be found in elements. This is because a given atom can only be surrounded by its own kind and the probability of forming a one-dimensional monatomic chain is most unlikely. This, therefore yields a conclusion that all superconducting elements must be Type-I. On the other hand, in a binary compound alloy, an A atom would be surrounded by both the A atoms as well as by the B atoms. Therefore, the chance is good for forming a one-dimensional chain and more likely to result in a Type-II superconductor. A good example is shown in Fig. 18 in which pure metal, Pb, is Type-I whereas Pb-In alloys at various compositions show Type-II superconductor characteristics.

All these agreements may be criticized as being too qualitative and required more rigorous mathematical treatment. And I fully agree, particularly in the area of 'Covalon'→ free-electron → 'Covalon' interaction. However, all these semi quantitative agreements come as a natural physical consequence of the model and the number of agreements is simply overwhelming. More importantly, a great amount of experimental support for 'Covalon' model comes not only from superconductivity itself but also from the field such as 'liquid metal miscibility gap' or 'phase diagram' and 'crystal chemistry' etc. which at first glance may seem not related with super-conductivity itself.

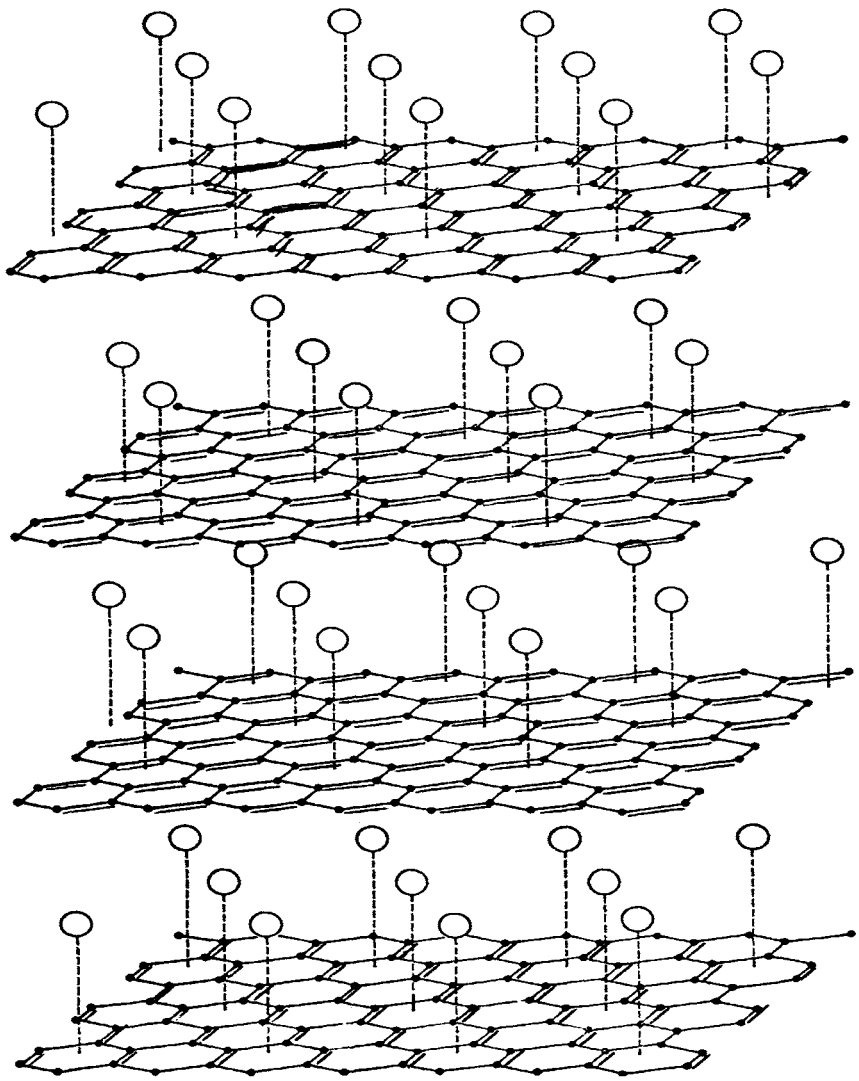

Fig. 17. Pictorial representation of intercalated superconducting compound of 2-dimensional graphite (carbon atoms interconnected with solid lines; each line represents a pair of covalent bond) interleaved with potassium (circles) which ionizes easily to K^{+} and provide 'free electrons'. According to the model, COVALON conduction takes place within the graphite plane and affects the COVALON on the adjacent graphite plane through plasmon waves provided by the free electrons from the potassium metal.

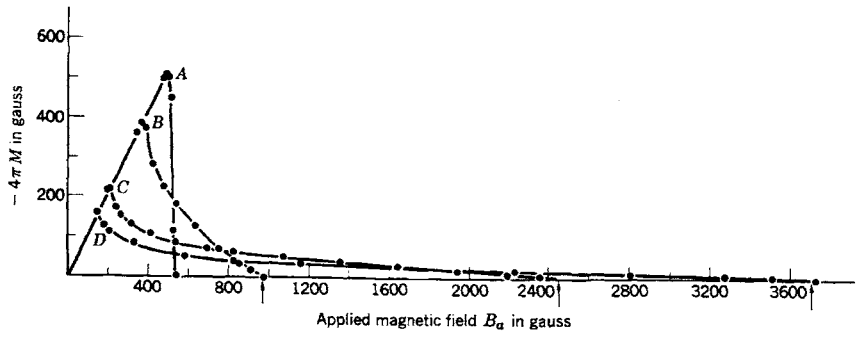

Fig. 18. Superconducting magnetization curves of (A) Pb and (B) Pb-In (2.08 wt. %) , (C) Pb-In (8.23 wt. %) and (D) Pb-In (20.4 wt. %). Showing pure Pb to be type-I and transforming into type-II with the addition of In.

Finally, there is the question of how accurately the theory thus proposed can predict. For without the ability to predict, a theory is only a theory. The theory has already predicted the correlation between T_C and N, the number of naturally occurring isotopes as shown in Fig. 9. Subsequent prediction to this correlation is that if and when the number of stable isotopes in an element such as Mo, were to be separated and isolated into only one isotope with the same atomic mass its T_C shall rise.

Generally speaking, the factors that constitute superconductivity shall be:

a) The existence of a network of conjugated covalent bonding which will provide 'Covalon' conduction. A one- dimensional chain is best and most preferred. Followed by two or three-dimensional network. Knowing the type of atom involved, the Linear Combination of Atomic Orbital (LCAO) method or other valence bond calculation can be invoked to determine whether the atom under consideration is suited for conjugation and what type. Once, the type of conjugation is known, the resonance frequency, ω, can be determined.

b) For a given type of atom that can form conjugation, the fewer the number of naturally occurring isotope, the better for superconductivity. A single isotope, such as found in Nb, is the best for the phonon vibration frequency, υ, a fixed number.

c) 'Covalon' conduction thus established must be 'interconnected' to one another through plasmon waves provided by 'free' electrons or in case of ceramic or oxides through the inter-chain linkage of oxygen, or nitrogen atoms that are rich in electrons so that 'Covalon' conduction will be self-enhancing and self-sustaining and lead to superconductivity. These 'free' electrons can be provided by interstitial atoms that can readily give up electrons such as K, Na (I-A or II-A elements from the periodic chart) or sulfur and nitrogen that can provide 'free' electrons. The 'free' electron concentration, N(e), along with the

inter-chain distance for a one-dimensional case or the inter-planar distance for the two-dimensional network, shall decide the ultimate T_C obtainable for the system. Application of high pressure to the high temperature T_C superconductors e.g., ceramic or oxides (that do not have free-electrons) will not lead to a change in free-electron concentration, and therefore will not alter their superconducting temperature, T_C.

d) All these considerations shall be compared with the pertinent phase equilibrium diagram to see if the compound is formed through incongruent-melting. If the compound is formed through congruent-melting, the chance is overwhelming that the compound will be a poor superconductor.

These, therefore, constitute the guidelines for finding superconductors or how to raise the superconducting temperature. Since 'Covalon' conduction is a nucleus to superconductivity and covalent bond is a poor conductor at room temperature, a good conductor at room temperature implies a poor covalent bond and therefore will not be a superconductor; or will be a poor superconductor at best at low temperature. Inasmuch as a good covalent bond can come from compound formation, good superconductors, particularly Type-II, shall be expected to come from intermetallic compounds or special type of ceramic oxides and nitrides.

REFERENCES

[1] H. Kamelingh Onnes, Leiden Comm. 120b (1911).
[2] W.Meissner and R.Ochanfeld, Naturwissenschaftern , 21(1933) 787.
[3] J.Bardeen, L.N.Cooper and J.R.Schrieffer, Phys.Rev, 108(1957)108.
[4] F.E.Wang and Y.N.Chiu, Chem.Phys, 12(1976)225.
[5] C.A.Coulson , Valence, Oxford Univ. Press (1953).
[6] L.Pauling and E.B.Wilson, Intro. Quantum Mechanics, McGraw-Hill, New York (1935)
[7] H. Kallmann, and M. Silver, SYMPOSIUM ON ELECTRICAL CONDUCTIVITY IN ORGANIC SOLIDS , Interscience, New York (1961).
[8] G.Herzberg, Electronic Spectra and Electronic Structure of Polyatomic Molecules, Van Nostrand, Princeton, New Jersey (1945).
[9] M.Kotani, A. Ameriya, E. Ishiguro and T.Kimura, Table of Molecular Integrals, Maruzen, Tokyo (1955).
[10] S.P. McGlynn, L.G. Vangguickenbone, M Kinoshita and D.G. Carroll, Introd. To Applied Quantum Chemistry, Holt, Rinehart and Winston, New York (1972).
[11] R.S.Mulliken, C.A. Rieke and W.G. Brown, J. Amer.Chem.Soc., 41(1941)63.
[12] F.A. Cotton, Chemical Application of Group Theory, Wiley-Interscience, New York, (1971).
[13] L. Salem, The Molecular Orbital Theory of Conjugated Systems, Benjamin, New York (1966).
[14] Th. Foster, Delocalized Excitation & Excitation Transfer, Bulletin No. 18, U.S. Atomic Energy Commission, Florida State Univ. (1965).
[15] J.R. Henderson, R.A. Willett, M.Muramoto and D.C. Richardson, Table of Hormonic Franck-Condon Overlap Integrals Including Displacement of Normal Coordinates, Douglas Aircraft Co. Report S.M. (1964)45807.
[16] H.Frohlich, Adv. Phys. 3(1954)325.
[17] P.A. Lee, T.M. Rice and P.W. Anderson, Phys.Rev.Letters, 31(1973)462.
[18] J.Bardeen, Sol.Stat.Comm., 13(1973)357.
[19] R.A. Hamis and L.M. Falicov, J.Chem.Phys., 51(1969)5034.
[20] W.A. Little, Phys.Rev., 134A(1964)1416.
[21] I.G. Austen and N.F. Mott, Adv. Phys., 18(1969)41.
[22] F.E. Wang and M.A. Mitchell, Sol. Stat. Comm., 15(1974)867.
[23] D.M. Gualtrieri, Sol.Stat.Comm., 16(1975)917.
[24] A. Leger and J. Klein, Phys. Letters, 28A(1969)751.
[25] R.L. Falge, Jr. Phs. Letters, 24A(1967)579.
[26] N.E. Alekseevskii, V.I. Tsebro and E.I. Flippovich, Zh. ETF, Pis, Red., 13(1971)247.
[27] W. Buckel and W. Gey, Z. Phys., 176(1963)336.
[28] F.E. Wang, J.Sol.Stat.Chem., 6(1973)365.
[29] Phase Equilibrium Diagrams – Constitution of Binary Alloys, M. Hansen (1958); R.P. Elliott (1965); and F.A. Shunk (1969), McGraw-Hill, New York; Superconducting Critical Temperature Properties of Selected Superonducting Materials, B.W. Roberts, NBS Technical Note 724 (1972).
[30] J.J. Hauser, Phys. Rev. Letters, 13(1964)470; B.W. Batterman and C.S. Barrett, Phys.Rev.Letters, 13(1964)390.
[31] G.Shirane and J.D. Axe, Phys.Rev. B4(1971)2957, ibid;, B8(1973)1965.
[32] Y.N. Chiu and F.E. Wang, Chem. Phys., 18(1976)301.
[33] Symposium on Electrical Conductivity in Organic Solids, J. Kallman and M. Silver, eds., Interscience, New York, (1961); Organic Semiconductors, J.J. Brophy and J.W. Buttery, eds., Macmilan, New York,(1962); Electronic Conduction in Organic Molecular Solids,

Adv. Chem. Phys.,Vol. VII, Interscience, New York, (1964); Organic Semiconductors, John Wiley, New York (1967).
[34] E. Meneffe and Pao-Yoh Han, J.Chem.Phys., 36(1962)3472.
[35] W.J. Siemons, P.E. Bierstedt and R.G. Kepler, J.Chem.Phys., 39(1963)3523.
[36] I.F. Shchesolve, Phys.Stat.Sol., 12(1972)9.
[37] J. Ferranis, D.O. Cowan, V. Wallatla Jr. and J.H. Perlstein, J.Amer.Chem.Soc., 95(1973)948.
[38] L.B. Coleman, M.J. Cohen, D.J. Sandman, F.G. Yamagishi, A.F. Ganito and A.J. Heeger, Sol.Stat.Comm., 12(1973)1125.
[39] R.P,.Groff, A. Suna and R.E. Memifield, Pys.Rev.Lett., 33(1974)418.
[40] D.B. Tanner, C.S. Jacobsen, A.F. Ganito and A.J. Heeger, Phys.Rev.Lett., 32(1974)1301.
[41] M.J. Cohen, L.B. Coleman, A.F. Ganito and A.J. Heeger, Phys.Rev. B10(1974)1298.
[42] A.J. Heeger and A.f. Ganito, Low Dimensional Cooperative Phenomena, (ed. H.Keller), Plenum Press, New York (1975).
[43] T.J. Kistenmacher, T.E. Phillips and D.O. Cowan, Acta. Cryst., B30(1974)763.
[44] F. Wudl, G.M. Smith and E.J. Hufnagel, Chem.Comm., 42(1970)1453.
[45] J.F. Perlstein, J.P. Fenaris, V.V. Walatka, D.O. Kowan and G.A. Candela, AIP Conference Proc. No. 10 part 2 (1973)1494.
[46] Y. Tomkiewiez, B.A. Scott, L.J. Tao and R.S. Title, Phys.Rev.Lett., B10-32(1974)1363.
[47] J.C. Scott, A.F. Ganito and A.J. Heeger, Phys.Rev., B10(1974)1363.
[48] P.M. Chaikin, J.F. Kwak, T.E. Jones, A.F. Garito and A.J. Heeger, Phys.Rev.Lett., 31(1973)601.
[49] A.M. Overhauser, Phys.Rev., 89(1953)689.
[50] R.J. Elliott, Phys.Rev., 96(1954)266.
[51] L.D. Landau and E.M. Lifshitz, Statistical Physics, Pergamon Press Ltd., London (1958); A.H. Morrish, The Physical Principle of Magnetism, John Wiley & Son, New York (1965).
[52] C. Kittel, Solid State Physics, John Wiley & Sons, New York (1956); J.M. Ziman, Principle of Theory of Solids, Cambridge Univ. Press (1964).
[53] J.G. Daunt, Progress in Low Temperature Physics, C.J. Gorter (ed.) North-Holland, Amsterdam (1955).
[54] Y.N. Chiu, S.H. Brown, N. Sondergaard and F.E. Wang, Theo.Chim.Acta, 90(1995)205.
[55] Y.N. Chiu, P. Palting, S-T. Lai, M.Z. Fu and F.E. Wang, J.Sol.Stat.Chem., 129(1997)174.
[56] Y.N. Chiu, J. Xiao, M. Fu, K. Liu, P. Palting, L-Y C. Chiu and F.E. Wang, J.Molecular Struc.(Theochem), 581(2002)239.
[57] B.T. Mattias, T.H. Geballe, L.D. Longinotti, E. Corenzwit, G.W. Hull, R.H. Willens and J.P. Maita, Science, 156(1967)645.
[58] Proc. of the Conference on Fluctuation in Superconductors, Stanford Research Inst., Menlo Park, California (1968).

V. NITINOL; A Metal-Alloy with Memory

1. BACKGROUND

It was in the late 1959 a peculiar property of Ti-Ni stoichiometric alloy was first discovered by W.J. Buehler and his coworkers at Naval Ordnance Laboratory (NOL). This peculiar property was in the sharp acoustic damping capacity change of the alloy i.e., exists a sharp transition temperature (near room temperature) above which the alloy 'rings' like a bell and below which makes a 'thud' sound upon being hit with a hammer or being dropped on the concrete floor. Later, this peculiar acoustic damping capacity change was found to be related to the phenomenon of 'shape-recovery'. Following the tradition at Naval Ordnance Laboratory, the alloy was named **NITINOL** (**Ni**)nickel – (**Ti**)titanium – (**NOL**). Since the transition temperature was near room temperature, the peculiar transition was not attributable to structural change that involves diffusion (Nitinol has a melting temperature of around 1300 °C). Therefore, the transition must be due to a diffusionless transformation. A group of alloys including steel, having a diffusionless transformation, is already well known before Nitinol. In honor of Martens [1] who first discovered the transformation, they are known as 'Martensitic transformation.' Traditionally, while there is no diffusion involved in the transformation, there is a definite crystal structure transformation with the structure above the transition is referred to as 'austenite' and the structure below the transition is known as 'martensite.' Other well-known systems that have martensitic transformation are: indium-thallium [2], copper-aluminum [3] and gold-cadmium [4] etc. The reason Nitinol attracted so much attention was (1) the transition lies near room temperature thus easy to see and (2) the large force associated with the shape recovery and its repeatability without a noticeable fatigue, and (3) the alloy was extremely malleable and can be rolled into sheet, drawn through dies into wire form. For, these properties are extremely desirable in industrial applications. In fact, the 'Cryofit', a tubing coupler made by Raychem (Fig. 1) exactly utilizes this property. A score of patents related to the use of Nitinol for converting 'thermal' energy into 'mechanical' energy are all based on this unique property.

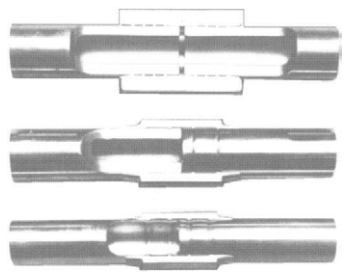

Fig. 1. Cut-away view of 'Cryofit' (Raychem Corp.); tube coupler.

Among them is my own patent of 'Thermobile' a simple energy conversion system, utilizing two wheels of different radius and a single strand of Nitinol wire inter-connecting the two wheels as shown in Fig.2. Just as important if not more so for industrial application is the fact that neither element, Ti nor Ni are 'exotic' material and therefore relatively inexpensive and readily available. Having all these superb characteristics, a score of industries were attracted to it and Nitinol was touted as the material of the century. However, all these enthusiasm did not last long, for once the engineers got involved in designing a device using Nitinol, they found it was very difficult to manipulate the alloy to alter or control the property to fit their application. Worse, the property including memory effect could not be reproduced faithfully and resulted in a very poor (or impossible) quality control.

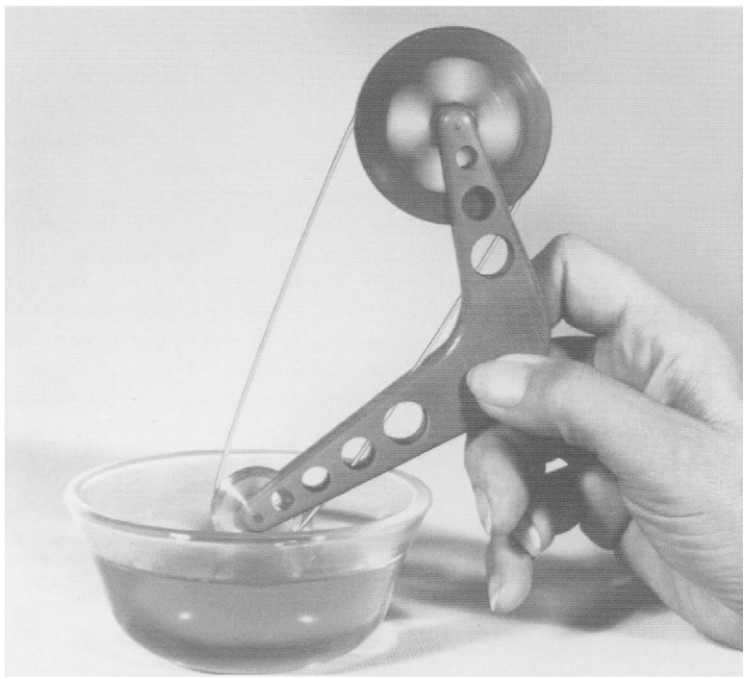

Fig. 2. The 'Thermobile' energy conversion device using two wheels and a strand of Nitinol wire loop; Converting directly the thermal into mechanical energy (Wang, US Patent 4,275,561).

The temperature for the acoustic damping capacity change from Nitinol was found to be different for alloys that were prepared at different laboratories (even though both alloys have 'identical' composition). Further, the shape memory response to temperature change, such as how fast and how much force, also varied a great deal from one alloy to another.

To make matters worse, Nitinol did not respond to the remedy applied based on the conventional metallurgical wisdom. Compounded with these problems is the fact that the alloy characteristics associated with the transition changed with a small change in the process of fabrication. It was around this time that I joined Buehler's group at NOL and began to study Nitinol problems. At the time I had a notion that Nitinol problems may in fact be solved or understood by incorporating the concept of covalent bond. And the first task was to investigate the crystal structure of Nitinol and see how the atoms may move during the transition. To do this correctly one must have a single crystal of Nitinol for X-ray diffraction study. But, to my disappointment I found that a single crystal of a size (within few tenth of a millimeter) could not be obtained from Nitinol alloy. I had to devise a way to obtain single crystal of the size [5] large enough for X-ray diffraction. Eventually with single crystals in hand I was able to follow the atomic movement as a function of temperature and gained some insight as to the mechanics of the transition [6].

This study led to an important conclusion that what is happening in Nitinol is unique from all other known alloy systems with martensitic transformation. These unique properties include the following:

1.1. Cooperative Atomic Shear

For Nitinol - at the transition M_S, atoms begins to shear uniformly throughout the crystal. As the temperature is lowered the atomic shear continues to increase. At temperature, M_f , the atoms shear to their maximum point and assume a new structure. Thus, between M_S and M_f temperature interval the crystal structure of Nitinol is undefined and belongs neither to 'austenite' nor to 'martensite'. Therefore, thermodynamically, it should be classified as the second–order transformation. This is illustrated in Fig. 3. Conventionally - above M_S temperature, the whole crystal assume a crystal structure identified as 'austenite'. At M_S temperature, a new crystal structure of 'martensite' begins to form through two-dimensional (planar) atomic shear. The two crystal structures of 'austenite' and 'martensite' therefore share an identical plane known as *Invariant Plane*. As the temperature is lowered, the two dimensional shear (or more correctly, 'shift') continue to take place one plane at a time such that the *Invariant Plane* moves in the direction as to increase the volume of 'martensite' at the expense of 'austenite'. Ultimately, at M_f temperature the whole crystal becomes 'martensite'. Since between M_S and M_f any given micro-volume of the crystal must belong to either the 'austenite' or the 'martensite', the transformation is of the first–order thermodynamically. This case is pictorially illustrated in Fig. 4.

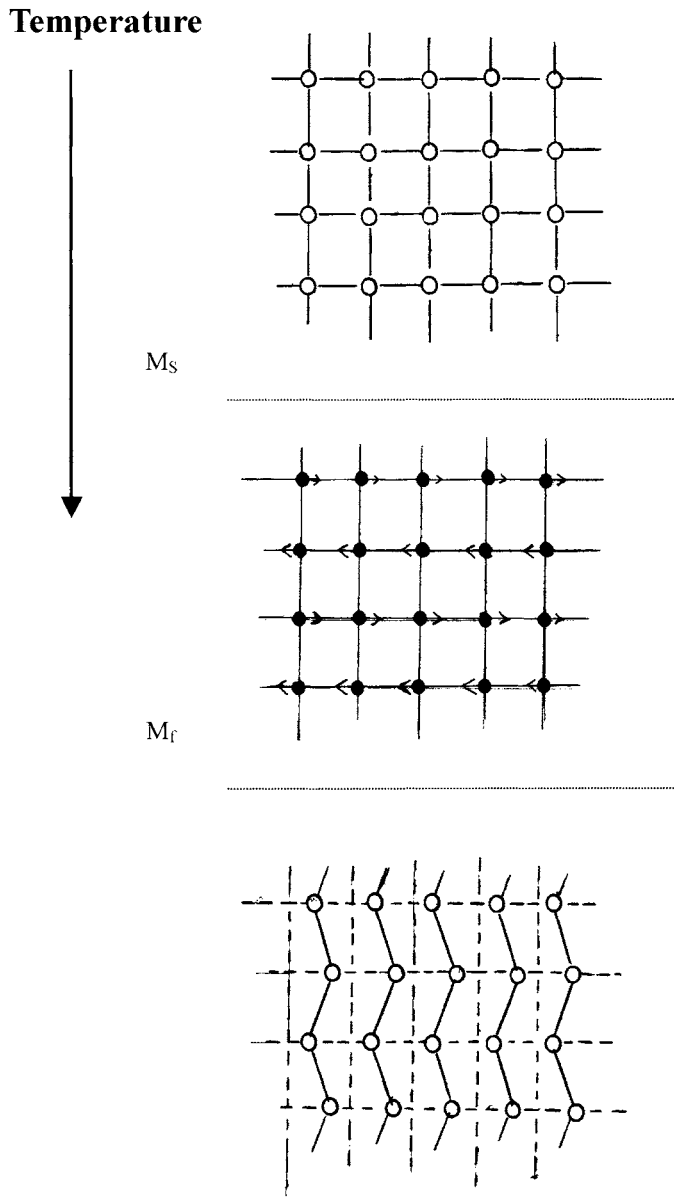

Fig. 3. 2-dimensional pictorial illustration of atomic movements in Nitinol during the transition; above M_S (○) , intermediate between M_S and M_f (•) with arrow indicating direction of atomic shear, and below M_f(○).

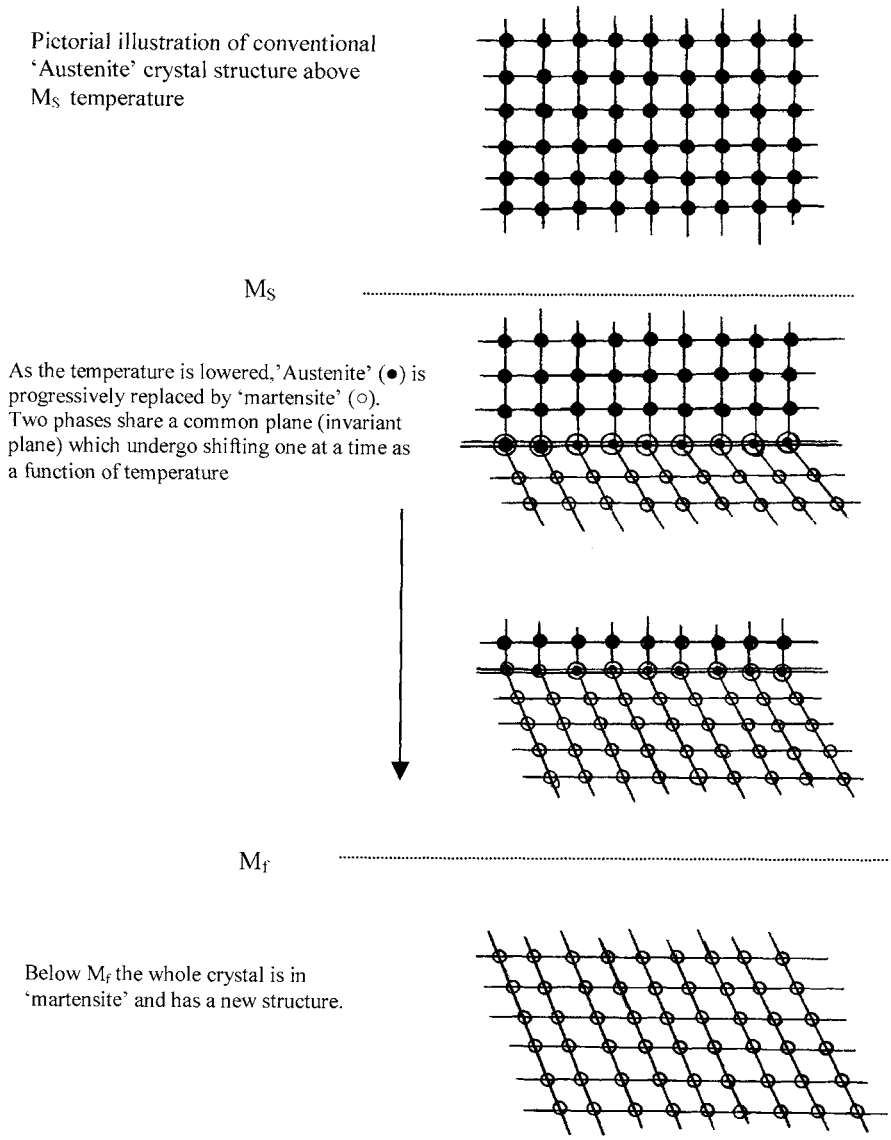

Fig. 4. 2-dimensional pictorial representation of atomic movements in a martensitic transition.

1.2 Absence of Acoustic Emission

The existence of acoustic emission (AE) during the martensitic transition in various systems is well known [7,8,9]. However, in Nitinol the AE is missing as shown in the private communication I had with Dr W.F. Hartman of John Hopkins University as shown in the excerpt below:

THE JOHNS HOPKINS UNIVERSITY · BALTIMORE, MARYLAND 21218

DEPARTMENT OF MECHANICS AND MATERIALS SCIENCE

January 17, 1973

Dr. Frederick E. Wang
U.S. Naval Ordnance Laboratory - White Oak
Silver Spring, Maryland 20900

Dear Dr. Wang:

I enjoyed your presentation at the MIM Meeting last week. Since we are presently engaged in acoustic emission studies, we thought it would be interesting to monitor the emissions from Nitinol during the transitional phenomenon.

Using one of your sample wires, which we stretched under dead load, we heated it (while still under load) and observed the recovery for various amounts of extension. The acoustic emission was monitored during these tests. The result was that the specimen was very quiet throughout the band width of 10MHz-3MHz. This was consistent for a test with another sample.

The results of the above experiments could be very important in supporting your theory of the crystal-structure reversion. I should appreciate it if you would send me copies of your papers on this subject. Also, we would like to perform some additional acoustic-emission tests with our more sophisticated apparatus and we need some 1/2" diameter stock of Nitinol alloys. Please tell me how I can get some.

Best wishes for your continued success in your studies of this interesting material.

Sincerely yours,

William F. Hartman

WFH:rs

William F. Hartman
Assistant Professor

This unique property is actually related with the unique property of 1.1. Because the reason for the AE in martensitic transition is that the transition takes place in steps (as illustrated in Fig. 4) i.e., the whole two-dimensional plane of atoms shifts altogether at a time. This abrupt shift results in audible 'click' sound. On the other hand, Nitinol does not undergo such shift but rather undergo a continuous shearing (as illustrated in Fig. 3) so that there is no audible sound.

1.3. Ultra Small in Size for Nitinol Crystals

As is explained above, single crystals of size within a fraction of a mm (millimeter) are not available in Nitinol alloy (under microscope the grain size was determined to be in 100 micron range). On the other hand, other 'conventional' martensitic transition systems, such as In-Tl, Au-Cd, Al-Cu all have good size of crystals — in the range of 1 ~ 4 cm.

1.4. No Shape Change in Nitinol Transition

One of the well-known properties in the martensitic transition is that it undergoes macroscopic change in shape. This can be visualized by the illustration of Fig. 4. In Nitinol, no macroscopic shape change is observed. This can also be visualized by Fig. 3, in which the atomic shears take place in zigzag fashion. Since the atomic shears are all within interatomic distances macroscopically no shape change is observed.

1.5. Crystallographic Distortion in Nitinol Transition

If there is a crystallographic transformation as shown in Fig. 4, below M_S temperature, a new set of faint diffraction spot will appear in X-ray. These diffraction spots will gain intensities as the temperature is lowered and more martensitic phase appears. Meanwhile the diffraction spots corresponding to 'austenite' observable at M_S will gradually diminish in their intensities and ultimately disappear completely when the temperature reaches M_f. However, this is not what is observed for Nitinol transition. In Nitinol, the diffraction spots begin to form 'streak' at M_S and the 'streaks' becomes longer as the temperature is lowered. The detail of the single crystal X-ray diffraction has been reported[10]. An appropriate terminology for what happens in Nitinol is 'crystallographic distortion' for there is no evidence of crystallographic transformation.

1.6. Second-Order Transition

It is well established that all the known martensitic transitions, before Nitinol, occurs through crystallographic transformation [11]. As described above [10], single crystal X-ray diffraction work shows a crystallographic distortion (rather than transformation) and therefore is a second-order transformation [12]. This conclusion has the support of heat capacity investigation [13] that gave a latent heat of transition $\Delta H >$

4,150 J/mole and also came to the same conclusion that Nitinol transition is of second-order.

But, aside from these unique properties, Nitinol has a number of commonalities with other known martensitic transition systems: (1) it is an athermal transformation, (2) it is diffusionless, (3) it involves displacive or shear-like movement of atoms, (4) the activation energy for the growth of martensite (continuous atomic shear in Nitinol) is effectively zero, i.e., the propagation rate of transformation (transition in Nitinol) is fast and independent of temperature.

It was based on these uniqueness and commonalities, my colleague and I submitted a paper entitled "Crystal Structure and A Unique 'martensitic' Transition of TiNi " to a Journal concerned with metals and alloys for publication in 1965. But, the paper was rejected outright by two anonymous reviewers who could not accept our observation that the Nitinol transition was unique. Obviously the reviews contend that by accepting Nitinol transition being unique, may make all other martensitic transformations 'garden variety.' This may upset the theory of martensitic transition formulated thus far. We then, submitted the paper to the Journal of Applied Physics and was accepted for publication and eventually appeared in print [10]. A few months after the appearance of this article, the editor of the very journal that rejected my paper, asked me to review two papers on Nitinol for the journal. Suddenly, I was an undisputed 'expert' in Nitinol! Up to this point I had not really start to apply covalent-bond concept but devoting more time in collecting experimental data [14,15], which may be important in support or non-support of covalent-bond concept.

2. COVALENT BOND IN NITINOL (TiNi)

In 1967, on April 3 and 4, under the sponsorship of ONR (Office of Naval Research) I organized the first International Conference on Nitinol called '*Symposium on TiNi and Associated Compounds*'. The conference was held at Naval Ordnance Laboratory, the birthplace of Nitinol. As the chairman of the conference I assisted in selecting the papers from this conference that were later published in block form in the Journal of Applied Physics [16]. Despite these efforts the Nitinol transition remained elusive for sometime. In fact, after more than 30 years since the discovery of 'memory effect' and with more than 139 papers have appeared in various journals on this subject, the investigators still do not agree with one another. At the same time more than 4,000 patents worldwide have been filed on the use of the 'memory effect' or 'superelasticity' in Nitinol. Out of all this, the actual application of Nitinol remains only a handful. In sharp contrast other conventional alloys with martensitic transition has no controversy and in fact they are so well understood that a Crystallographic theory of martensitic transformation was formulated [27].

The controversy over Nitinol began with the phase diagram investigation of the Ti-Ni system [17]. The investigation on the phase diagram itself shows principally three different versions [18, 19, 20]. In particular, TiNi compound was reported to decompose into Ti_2Ni and $TiNi_3$ at about 800 °C [21]. This notion was later found to be false as shown by another

work [20], which covered the composition range, 34 – 58 at. % Ni and the temperature range, 0 – 1400°C. Indeed the decomposition of TiNi into Ti_2Ni and $TiNi_3$ claim should be dismissed outright once the TiNi alloy is found to be ductile and malleable. This is because both Ti_2Ni and $TiNi_3$ compound alloy are extremely brittle. Besides, if TiNi indeed undergoes decomposition under equilibrium state it would be a violation of the phase rule!

As to the crystal structure investigation, most metallurgists do not understand the value of single crystal work. They have been trained in powder patterns and polar figures and believe these are sufficient tools. But, the truth is no X-ray crystallographer would regard the "powder pattern" which essentially is a one-dimensional data due to the collapsing of the three-dimensional information as a reliable data particularly when the crystal structure itself is not well established. This fact escapes the attention of many investigators. On the other hand, the people who use electron diffraction or transmission microscopy also do not understand the shortcomings associated with these methods. For, the nature of this tool requires the specimen under investigation not only be limited to a very small area but also have to be very thin. As the result, the orientation of the crystal with respect to the electron beam may not be known with reasonable accuracy. Moreover, because of the smallness, the specimen is susceptible to internal or external stresses that can cause "stress-induced-martensitic-transformation". Since the only single crystal work of Wang et al. [6], suggested a continuous shearing of atoms between M_S and M_f, the electron diffraction study confining to a micron area can have any degree of shear such that ten independent investigations may be reporting ten different crystal structures. This was indeed the case as represented by the work of Marcinkowski et al.[22], Chandra & Purdy [23], Otsuka & Shimizu [24], and Nagasawa [25]. They all did investigate Nitinol transition using electron diffraction and transmission microscopy and they all came up with different crystal structures. Most interesting thing about all this is in the fact that they all duly cite each other's paper but there was no effort made to see how their own work can be reconciled with the results obtained by others particularly when the results are so different. In view of all these confusion, Wang et al. launched yet another investigation of the mechanism of Nitinol transition [15] utilizing both the X-ray and the neutron powder diffraction methods simultaneously as a function of temperature. Through this study, an inference was made for the coexistence of the B2 (CsCl-type) and $P\bar{3}m1$ structures in the TiNi-II phase ('austenite'). In this paper, Wang et al. made a considerable effort to show how their result and conclusion can be reconciled with the result of three independent electron diffraction and transmission microscopy works [22, 23, 24] simultaneously.

Now, as to the Nitinol's composition is concerned, it was made clear based on the work of Mueller & Knott [26], that Ti_2Ni and Ti_4Ni_2O are crystallographically identical to one another including their unit cell dimensions. And it is well known that Ti metal is difficult to purify and be kept pure and it is accepted that some oxygen is always going to be present in the metal as impurity. In fact, Ti sponge is used as a 'getter' to eliminate oxygen from a dry train. Now, the point is that the oxygen impurity at the time of alloying can form Ti_4Ni_2O, a compound that is extremely stable. This means in forming this compound, it extracts 4 Ti atoms for every 2 Ni atoms from the matrix. As the result, the remaining TiNi alloy matrix composition would be Ni-richer than the composition expected from the weight of individual Ti and Ni. How much richer in Ni is going to depend entirely on how much oxygen impurity existed in Ti metal used. Unfortunately, the

degree of alteration of matrix composition cannot be determined by chemical analysis. For, during the chemical analysis, the compound, Ti_4Ni_2O will decompose into Ti and Ni and yield the same composition as expected from the weight of Ti and Ni.

All these things listed above contributed to the non-understanding or miss-understanding of Nitinol transition. Now we shall see how these things can be understood in a logical manner by first trying to understand the cause for the Nitinol transition.

2.1 Atomic d-Orbital Contraction for 3-d Transition Elements

It is well known that among the 3-d transition elements as listed in Fig. 5, the atomic electron orbital energy level of 3-d orbital undergoes 'contraction' in going from K (potassium) to Ni (nickel) i.e., the 3-d > 4-s in K actually changes to 3-d < 4-s in Ni [27]. In fact, this 'd-orbital contraction' is responsible for the magnetic properties exhibited in Mn, Fe, Co, and Ni. The cross-over of the 4-s and the 3-d orbital occurs around Mn and is believed to be responsible for the structural instability observed in Mn [28] (α-Mn, 20~725°C; β-Mn, 725~1095°C; γ-Mn,1095~1134°C; δ-Mn, 1134~1245°C).

The four (4) valence electrons in Ti combined with the ten (10) valence electrons in Ni gives seven (7) valence electrons per atom for Nitinol. This is exactly the number of valence electrons associated with Mn. This fact provides an overt correspondence in the instability observed in Nitinol and in Mn. In the following section we will show in detail how this instability comes about.

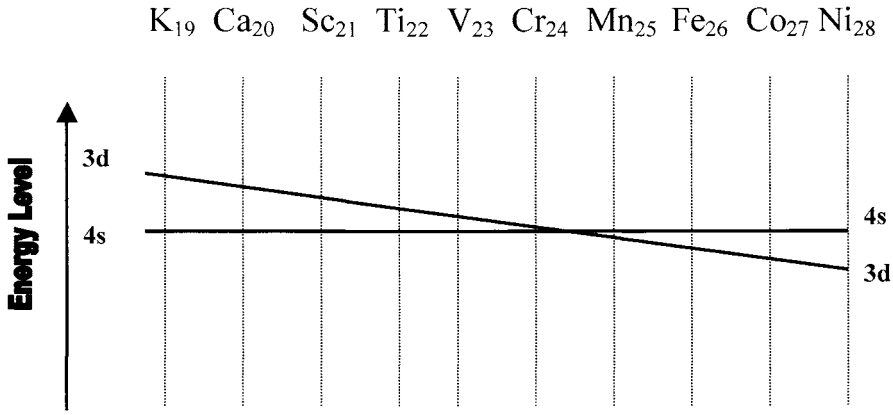

Fig. 5. Pictorial representation of 3-d energy level change with respect to 4-s energy level going from K to Ni in the periodic chart.

2.2 'Covalent' vs. 'metallic' bond in Nitinol

In the absence of hybridization, s-orbital leads to the formation of 'metallic' bond (non-directional) whereas d-orbital leads to the formation of 'covalent' bond (directional). This means the d-orbital of Ti is potentially capable of forming 'covalent' bond with the d-orbital of Ni, providing the energy level of the two d-orbital from Ti and Ni are not too far apart. Now, let us represent this energy level difference as ΔE_d (Ti-Ni). Analogously, there would be ΔE_d (Ti-Co) and ΔE_d (Ti - Fe). From Fig. 5 we see that the order of magnitude for the three ΔE_d's should be

$$\Delta E_d \text{ (Ti-Ni)} > \Delta E_d \text{ (Ti-Co)} > \Delta E_d \text{ (Ti-Fe)}.$$

We shall show that this is indeed the case. All three inter-metallic compounds, TiNi, TiCo and TiFe are known to form CsCl-type crystal structure at high temperatures. Since ΔE_d(Ti-Ni) is the largest among the three systems, one can expect 'covalent' bond formation between Ti and Ni through d-orbital shall be most difficult and even if it did form, its stability should be the least among the three. At this point we shall discuss somewhat on the stability of the atomic orbital in general. That is, atomic orbital can be elevated to a higher energy level at higher temperature. This is illustrated in the example of TiO and NiO; where at room temperature, TiO has a fcc (Fm3m) structure [29] while NiO has a rhombohedral structure [30]. But, above 275 °C, NiO transforms into a fcc (Fm3m) structure identical to that of TiO at room temperature. This is to say that the ΔE_d (Ti-Ni) is not a constant but varies as a function of temperature. In fact, it should be inverse proportional to the temperature, i.e., the higher is the temperature, the smaller the ΔE_d (Ti-Ni) will be. Thus, at about 1200 °C where TiNi is formed, the ΔE_d (Ti-Ni) is small and poses no hindrance to the formation of covalent bond between Ti and Ni. However, as the temperature is lowered, the ΔE_d (Ti-Ni) becomes increasingly large such that the covalent bond already formed between Ti and Ni becomes less and less stable compared to the s-orbital (metallic- bond). At some point, as the temperature continues to decrease, covalent bonds will break-up to form metallic bonds in order to minimize the total energy. Such an electronic orbital change will lead to an interatomic distance change, at which if the temperature is high enough for diffusion, it will lead to a structural change. However, if the temperature was too low for diffusion to occur, the only way to accommodate the interatomic distance change is through a diffusionless transformation (i.e., a martensitic transformation). This, in essence, is the electronic picture of martensitic transformation in Nitinol. We shall now compare this picture against other related observations.

2.3 Nitinol Transition as a Function of $TiNi_{1-x}(M_x)$ Composition

Here M represents Co or Fe, or a combination thereof. For if the argument put forward in 2.2. is correct, transition similar to that occurring in TiNi must also exist in TiCo and TiFe. As was stated earlier during the Nitinol transition one of the most notable phenomenon is the change in the acoustic damping capacity. This change was later confirmed in term of internal friction changes [31] and shown to be more than an order of magnitude change in its acoustic damping capacity. This difference can be detected by ear with ease. Though the exact temperature of transition may be somewhat limited (± 10 °C), this is a convenient way of ascertaining the Nitinol transition. Utilizing this method a whole series of $TiNi_{1-x}(M_x)$ where M is Co or Fe (or a combination thereof) alloys were investigated for their existence and temperature of the transition. The result of this investigation is summarized in the Fig. 6 [10].

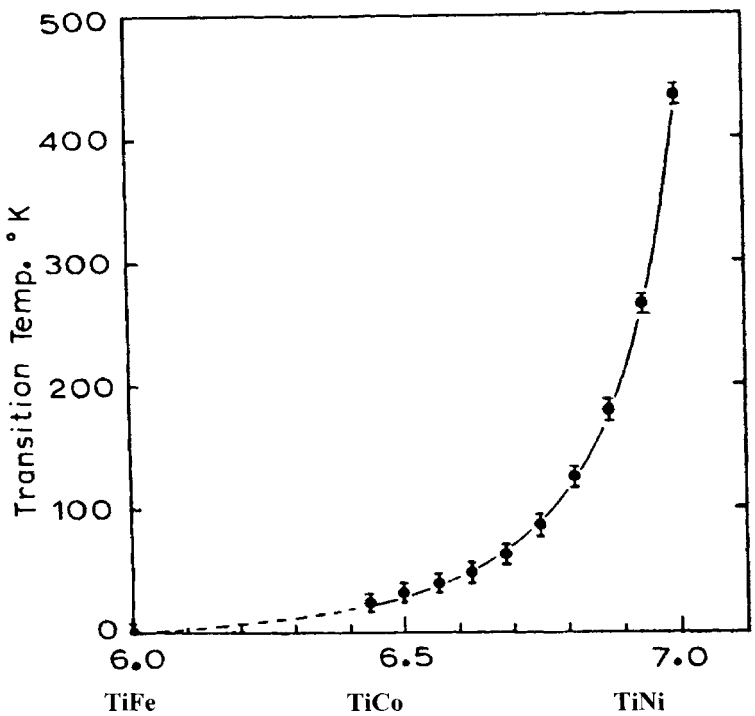

Fig. 6. Nitinol transition temperature vs. $TiNi_{1-x}(M_x)$ composition, where M is Co or Fe.

The result of this experiment shows (a) the covalent bonding assumption is correct, and (b) the order of magnitude for the ΔE_d for Ti-Ni, Ti-Co, and Ti-Fe is also correct.

2.4. 'Free' Electron Concentration N(e) vs. Mechanical Property

Now that we ascertained the existence of Nitinol transition in $TiNi_{1-x}(M_x)$ alloys we may guess and wonder what mechanical property these alloys may have. To do so one must understand first that certain covalent bonds require a certain number of valence electrons and this number cannot be increased or decreased without structural change. This is to say that whatever the number of valence electrons required in forming covalent bond in TiFe, the exact number (no more, no less) of valence electrons will be required in forming the identical covalent bond in TiCo and TiNi. Now, the total valence electrons per atom (as shown in Fig. 6) for TiNi is seven (7), TiCo is six and half (6.5) and TiFe is six (6). If we deduct a constant number of electrons, n, used in forming covalent bonds in the three compounds, we see that the remaining number of 'free'- electrons shall increase from TiFe to TiCo and reaches maximum at TiNi. The prediction of the mechanical properties, limiting to ductility (brittleness) will be very brittle for TiFe, less brittle for TiCo and ductile for TiNi. This is indeed the case is demonstrated in Figs. 7. Concurrently, hardness tests were done on the same group of alloys, using a diamond pyramid indenter in a standard Tukon micro hardness tester at the loads of 500 gm ~ 3,000 gm. The results of these tests are summarized in Fig. 8, which demonstrates a good correspondence between the ductility (brittleness) and softness (hardness) as expected. It is important at this point to recall the fundamental assumption made in laying the bonding theory of metals and alloys in the beginning — that every metal and alloy is composed of both the covalent bond and metallic bond. And the only difference is in the ratio of covalent bond/ metallic bond. While the relationship between the mechanical property and the 'free' electron concentration will be dealt with later in the section of *'MECHANICAL PROPERTIES'*, it is recognized here that more 'free' electrons lead to softer material.

2.5. 'Nitinol Transition' in 4-d and 5d Transition Elements

If the theoretical argument that at Nitinol transition some covalent bond-electrons are broken up and become 'free' electrons and the reason for this breaking up was in the energy difference, ΔE_d, between the d-orbital of Ti and Ni and so forth was valid, the following prediction can be made. An identical transition should exist in the 4-d and 5-d series of corresponding elements. That is the compounds of ZrRu, ZrRh, ZrPd (of 4-d series) and that of HfOs, HfIr, and HfPt (of 5-d series) should all have 'Nitinol Transition'. The investigation of these alloys was hampered by the fact Ru, Rh, Pd, Os, Ir, and Pt metals are all 'exotic' and are expensive so that to prepare them in size large enough for acoustic damping capacity change test, memory effect test, etc was out of the question.

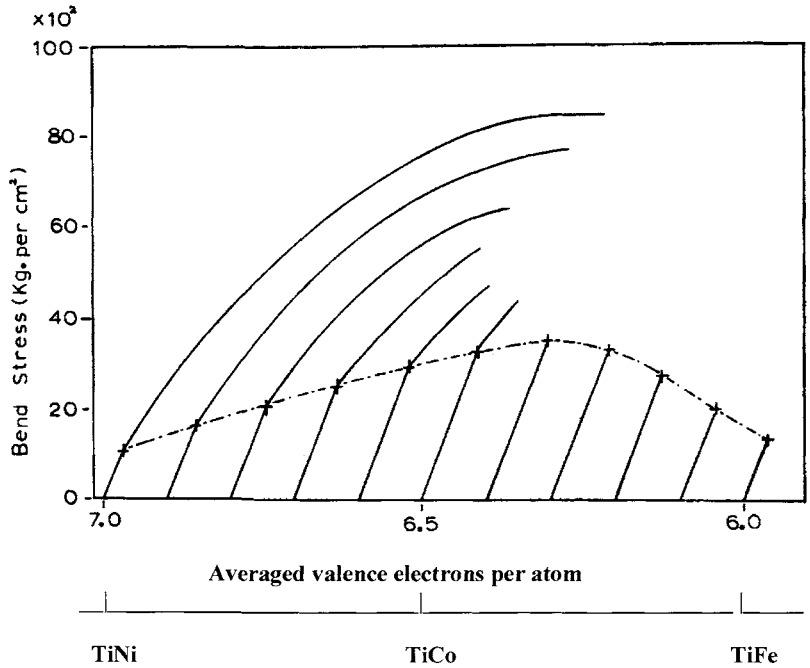

Fig. 7. Bend stress-strain curves of Ti (Ni_xCo_{1-x}) and Ti (Co_xFe_{1-x}) alloys; where x varies from 0 to 1. + indicates the elastic limit in each alloy.

The only way to investigate these alloys was through single crystal X-ray diffraction study. This was particularly worthwhile, because we already have the results of single crystal X-ray diffraction study from Nitinol itself. The results of this investigation are given below.

It should be noted that in a study of CsCl-type equiatomic phases in a binary alloys of transition elements, Dwight [32] has shown through X-ray powder pattern methods that while ZrRu and HfOs are of CsCl-type , the patterns for ZrRh, ZrPd, HfIr and HfPt are extremely complex and their crystal structures could not be identified. This report demonstrates the shortcoming of the X-ray powder pattern method, particularly in light of the single crystal work done on these compounds by my colleague and myself [33,34].

In our work of single crystal X-ray diffraction it was established beyond any doubt that the compounds of ZrRu, ZrRh, ZrPd as well as HfOs, HfIr, and HfPt are all structurally related to CsCl-type. Single crystals of these compounds were grown by the electron-beam zone-refining process and cut into proper sizes by the use of Servo met spark cutting machine. The Laue photographs of these compounds all showed m3m cubic

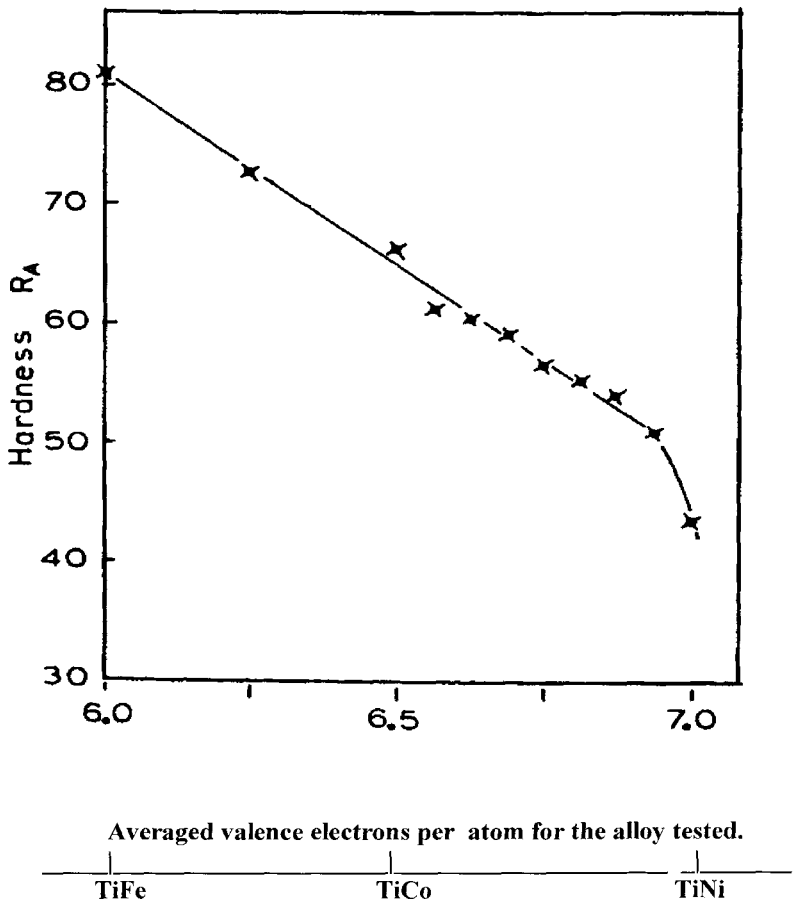

Fig. 8. Result of hardness tests on a series of TiX alloys (where X is a combination of Fe, Co, and Ni). Diamond pyramid indenter in a standard Tukon micro hardness tester was used.

symmetry. However, as shown in Burger precession photos of Fig. 9, the complexity of diffraction spots increase considerably in going from ZrRu to ZrPd and from HfOs to HfPt much in the same manner as TiNi going from R.T. to –50 °C to –190 °C. It should also be noted that there is a one-to-one correspondence between the diffuse streaks appearing in TiNi below its 'M_S' transition temperature and the satellite spots or extra spots appearing in

ZrPd at room temperature. Based on these photographs we shall describe once again the meaning of 'M_S' and 'M_f' temperatures in Nitinol transition.

At 'M_S' temperature; TiNi initiates a uniform (inhomogeneous) distortion of its lattice — through a collective atomic shear movement. The lower the temperature, the greater the magnitude of shear movements. As a result, between M_S and M_f temperature the crystal structure is not definable. In sharp contrast, other known martensitic transformations initiate a nonuniform (heterogeneous) nucleation at M_S and thereafter the growth of martensite is achieved by shifting of a two dimensional plane known as invariant plane [28] at a time. Thus, between M_S and M_f temperature the crystal structure is that of 'austenite' and/or 'martensite'.

At 'M_f' temperature; for TiNi, the magnitude of the shear movements initiated at M_S temperature now reached their maximum. The structure thereby assumes a new crystallographic symmetry that differs from that of the structure above M_S temperature. The theoretical X-ray photographs reflecting these physical changes in TiNi can be described qualitatively in three separate temperature regions: (a) at and above the M_S temperature – discrete spot reflections, (b) between M_S and M_f temperatures – diffuse streaks and spot reflections, where the degree of diffuseness is dependent on temperature, and finally (c) at and below the M_f temperature – new set of discrete spot reflections.

In the investigation of TiNi in the temperature range, – 70 ° through 900 °C, the X-ray evidence corresponding to (a) and (b) were recorded [15]. A close examination of the X-ray photos in Fig. 9 shows that the TiNi above M_S (> 60 °C) temperature is identical to that of ZrRu and HfOs at room temperature. And TiNi at – 50 °C is similar to ZrRh and HfIr at room temperature. Further, TiNi at – 190 °C has a complexity similar to those of ZrPd and HfPt at room temperature. These observations imply that martensitic transition similar to Nitinol transition does exist also in the 4d and 5d transition elements. In order to further prove this contention, ZrRh was heated to high temperature where the existence of the diffuse disappeared and showed a pattern identical to that of ZrRu at room temperature. In heating ZrPd to a high temperature, the M_f temperature was established for this compound at 550 °C. Above this temperature, the spot reflections became diffuse while maintaining m3m diffraction symmetry. This experimental evidence is shown in Fig. 10.

Although in both cases the transition has been confirmed to be reversible, some 50 °~ 80 °C for ZrRh and 70 ° ~ 150 °C for Zr-Pd, thermal hysteresis between heating and cooling cycles have been observed (the temperatures given here are from heating cycles). Based on this investigation the existence of Nitinol transition in TiNi and ZrPd series are plotted and given in Fig. 11 [33,34].

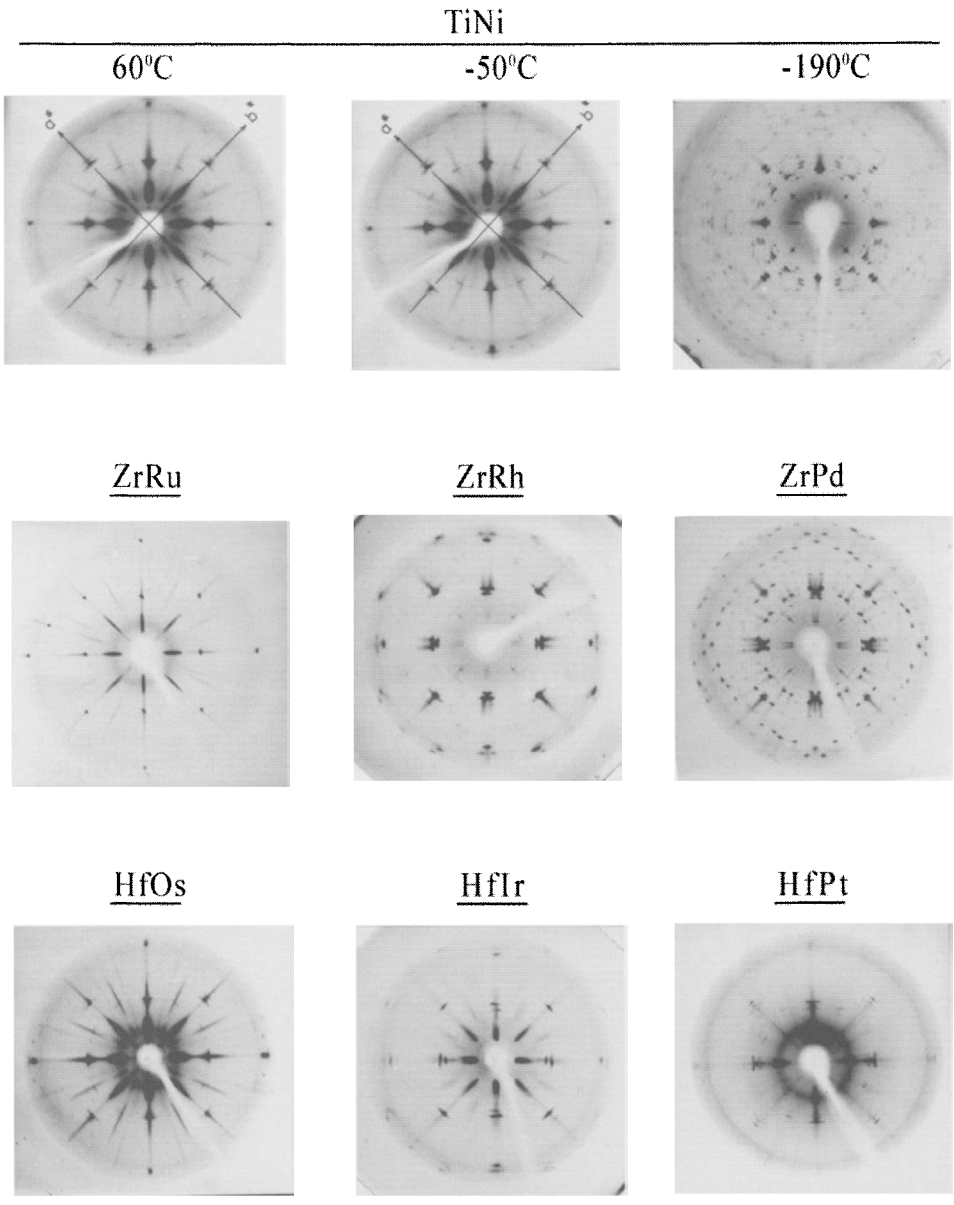

Fig. 9. Single crystal Buerger precession photos of TiNi at 60°, −50°, −190° C and of ZrRu, ZrRh, ZrPd, and of HfOs, HfIr, HfPt at room temperature.

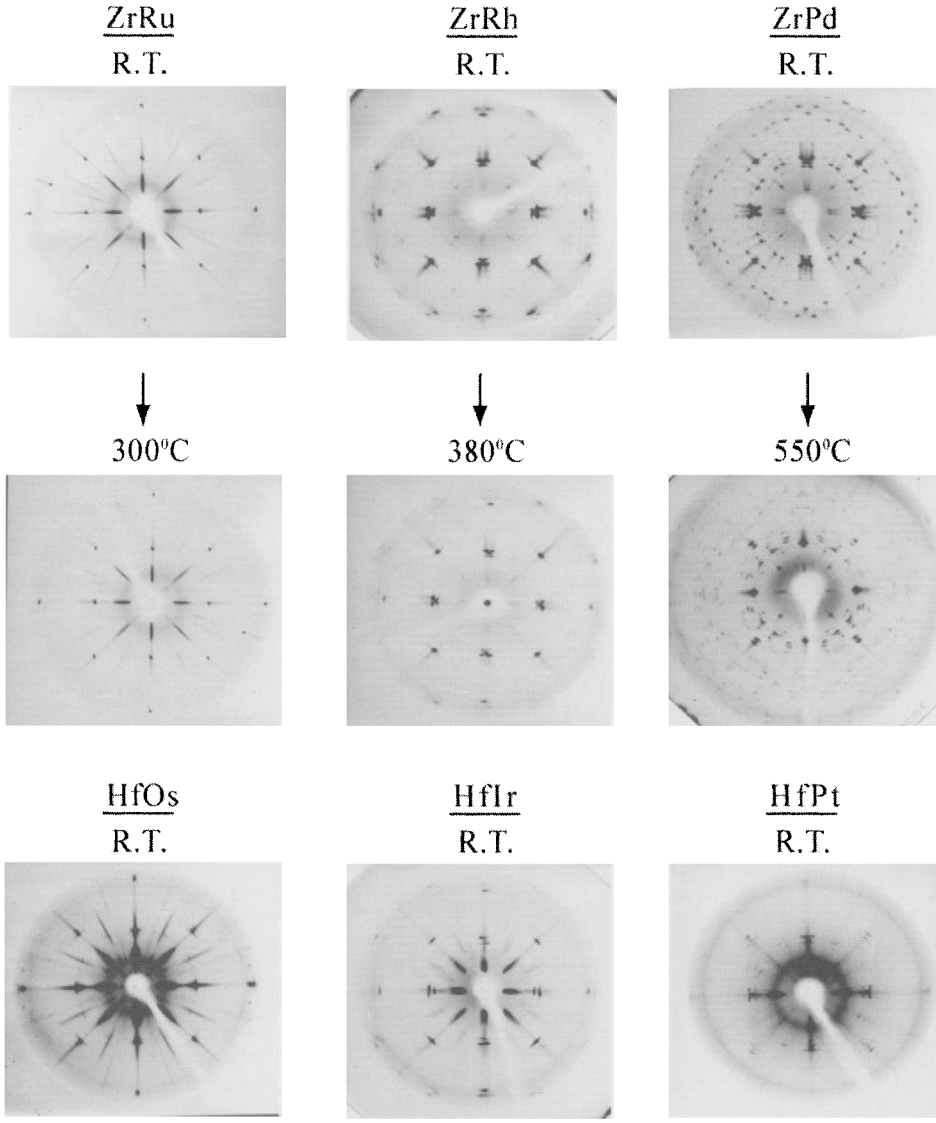

Frg. 10. Single crystal Buerger precession photos of ZrRu, ZrRh, and ZrPd at toom temperature and at high temperature where they undergo the Nitinol transition. Similar photos of HfOs, HfIr and HfPt at room temperature are shown for comparison [34].

The 'transition band' of TiNi (3-d series) bordered by M_S and M_f temperatures are obtained experimentally from a number of Ti (Ni, Co) and Ti (Co, Fe) alloys as shown in Fig. 6. But, the 'transition band' of ZrPd (4-d) series is based on only two X-ray diffraction data and is assumed to be parallel to that of TiNi(3-d) band. It is reasonable, based on these data, to conclude that the crystal structures of the equiatomic compound series of the TiNi, ZrPd, and HfPt are all isotypic and the cause for their diffusionless transition are the same. That is ΔE_d, the d-orbital energy level difference between the two elements change as a function of temperature. It is logical therefore, to conclude that the Nitinol transition is electronic in origin. In order to corroborate this conclusion more data other than crystal structure were obtained as follows.

2.6 Additional Experimental Evidence Associated with the Nitinol Transition

The first set of experiments carried out around the Nitinol transition was the electrical resistivity measurements. The electrical resistivity measured between – 50 °C and 80 °C is shown in Fig. 12(a); arrows indicate the direction of heating or cooling. The M_S, M_S' and A_S are the symbols used by Kaufman and Cohen [35]. It is tempting to interpret the triangular curve, $A_S - M_S - M_S'$ as shown in Fig. 12(a), as the result of a thermal hysteresis effect. However, this notion is proved incorrect by the following experiments. The cooling path, $M_S - M_S'$, and the heating path, $M_S' - A_S$, are irreversible. By this we mean that in a given heating (cooling) cycle, if the heating (cooling) process were halted along these paths and the direction of the cycle process reversed; to cooling from heating or to heating from cooling, the resistivity curve will not retrace its original path. But, rather takes a path whose slope is intermediate between those of $M_S' - A_S$ and $M_S - A_S$, in reversing heating to cooling. In reversing to heating from cooling path, $M_S - M_S'$, the resistivity curve is always coalesce toward point A_S. It is important to point out that the triangular curve form and the irreversible nature of the cycle are totally independent of the rate of heating or cooling.

Experiments show that as long as the thermal cyclings are carried out beyond the temperature range, M_S' to A_S without reversing the thermal cycling direction, the triangular portion of the curve remains unaltered. For convenience, we shall refer to this type of thermal cycling as 'complete' cycles and the other type where thermal cycles are reversed within M_S' and A_S as 'incomplete' cycles. After six such 'incomplete' cycles, the resistivity curve shown in Fig. 12(b) was obtained. A few hundred 'incomplete' cycles yields a resistivity curve with a large peak in the cooling half of cycle, as shown in Fig.

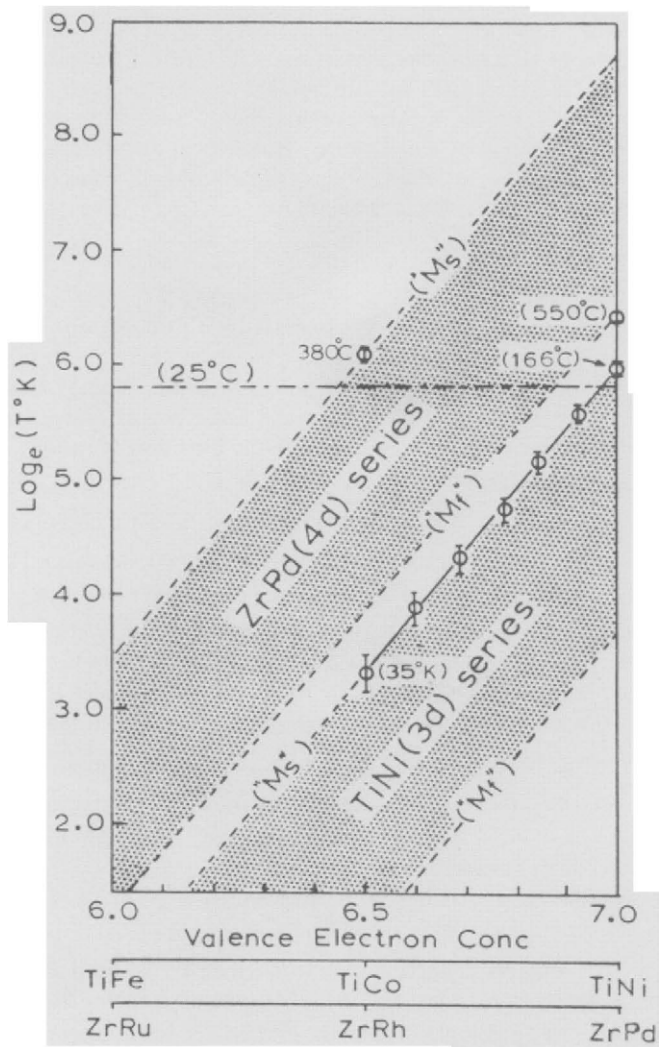

Fig. 11. The logarithmic scale of the M_S transition temperature in °K for TiFe(Co,Ni) compound alloy is plotted against the average number of electrons outside the closed shell per atom. The transition band bordered by M_S and M_f transitions of the TiNi and ZrPd series of alloys based on the X-ray evidence are indicated by dotted lines and shaded areas.

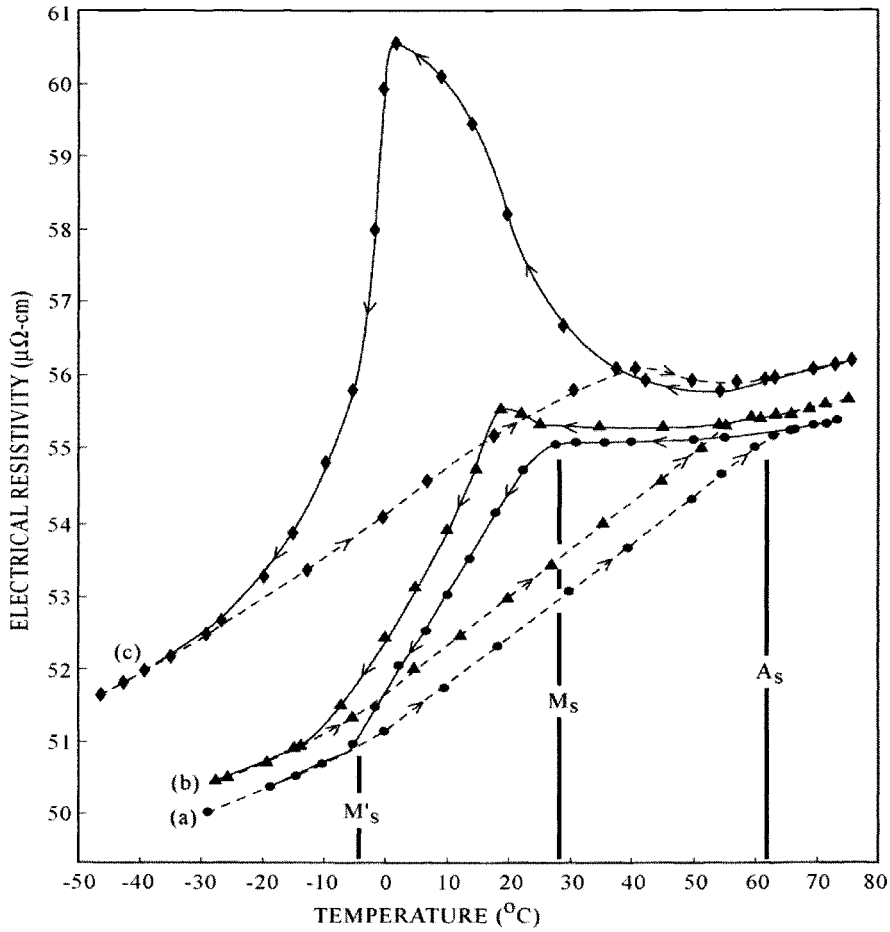

Fig. 12 Electrical resistivity of TiNi (51 at. % Ni) at around the martensitic transition temperature; effect of thermal cycling in (a) no 'incomplete' thermal cycling, (b) after six 'incomplete' thermal cycling, (c) after several hundred 'incomplete' thermal cycling. 'Complete' and 'incomplete' thermal cycling are defined in the text.

12(c), which is what was regarded as the resistivity curve over the Nitinol transition reported earlier [36]. There is a progressive over all increase in the resistivity curve as well as a shift of the triangular portion of the curve to a lower temperature as the number of 'incomplete' cycles is increased. Hence, the resistivity form ranging from that of Fig. 12(a) to that of 12(c) depending on the number of 'incomplete' cycles applied to the alloy.

Further experiments show that the resistivity curve of Fig. 12(c) can be restored to that of Fig. 12(a) only after a prolonged annealing of the alloy at 600 °C or above. The interpretation of the electrical resistivity curve over the Nitinol transition is based on the picture formed through single crystal X-ray diffraction findings: (a) the martensitic transition proceeds through a cooperative shear movement of atoms, and (b) the TiNi(II) structure is a complex of contiguous short-range ordered regions demarcated by antiphase boundaries. The three portions of the resistivity curves, $A_S - M_S$, $M_S - M_S'$ and $M_S' - A_S$ are considered to correspond to three different types of shear movements which differ from one another both in direction and in magnitude. These three shear movements correspond to three Buerger's vectors, $\bar{S}_1$, $\bar{S}_2$, and $\bar{S}_3$. Inasmuch as the resistance at a given temperature is unaltered before and after a 'complete' thermal cycle, the three vectors, $\bar{S}_1$, $\bar{S}_2$, and $\bar{S}_3$ must possess the following property. A given atomic arrangement will remain unaltered after having sequentially undergone the three shear movements represented by $\bar{S}_1$, $\bar{S}_2$ and $\bar{S}_3$. In this context, 'incomplete' thermal cycles are equivalent to a series of incomplete shear movements that can progressively bring the atomic arrangement to a state of 'confusion.' This is responsible for the over-all rise as well as the peak observed in the resistivity curve, after hundreds of 'incomplete' thermal cycles, Fig. 12(c). Additional evidence supporting this model is that a single crystal of TiNi can be transformed into poly-crystals by a few hundred 'incomplete' thermal cycles.

As shown in Fig. 13, the resistivity curve above the A_S temperature is relatively flat to about 125 °C and then turns upward again. The flat portion of the resistivity curve, that is, between A_S and 125 °C is interpreted as the residual resistivity of TiNi(II). The high concentration of antiphase boundaries in TiNi(II) as pointed out above, is presumed to be responsible for this high residual resistivity.

Consequently, the resistivity decrease (increase) within the temperature range, $M_S - M_S'(M_S' - A_S)$, is simply interpreted as the decrease (increase) in the concentration of antiphase boundaries as the cooperative shear movements of atoms take place by way of shear vector, $\bar{S}_2$ ($\bar{S}_3$). This suggests that the total resistivity of TiNi(II) is given by the resistivity curve above 125 °C. Similarly, the resistivity curve below the M_S' temperature is the total resistivity of TiNi(III). By extrapolating the total resistivity of TiNi(II) and TiNi(III) as shown in Fig. 13 (dotted lines), the total resistivity of TiNi(II) is shown to be lower than that of TiNi(III) within the transition temperature range, $M_S' - A_S$. In order to confirm this interpretation, it was logical to obtain other data corresponding to the two extreme resistivity curves, Fig. 12 (a) and (c).

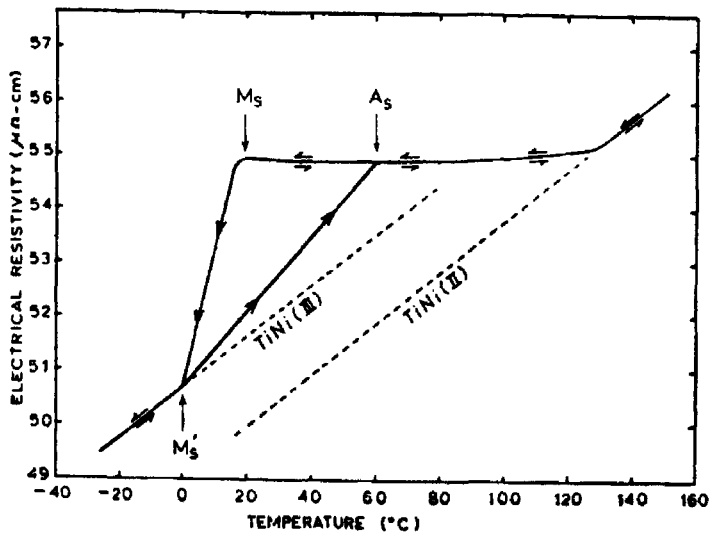

Fig. 13. The electrical resistivity of TiNi (51 at.% Ni) around the Nitinol transition.

The Hall Coefficient: the Hall coefficient showed relatively constant values of 1.8×10^{-4} (cm^3/C) below the M_S' and 0.4×10^{-4} (cm^3/C) above the A_S temperature for both the 'complete' and 'incomplete' cycles as shown in Fig. 14. However, in both cases, within the M_S' and A_S temperature range, the existence of a triangular form whose vertices coincide with the A_S, M_S and M_S' temperatures is definite and significant. Although shifting of the triangular form to a somewhat lower temperature similar to what happened in the resistivity data was noted in 'incomplete' cycles, there is no difference between the two Hall coefficient curves from 'complete' and 'incomplete' cycles. In general, both the electrical resistivity and Hall coefficient can be shown [37] to be the functions of three parameters, m^* (electron effective mass), $\bar{\tau}$ (mean relaxation time) and n (effective number of carriers). However, under certain circumstances these two transport properties become distinctly different; the Hall coefficient becomes a function of a single parameter, n, while the electrical resistivity remains a function of the three parameters.

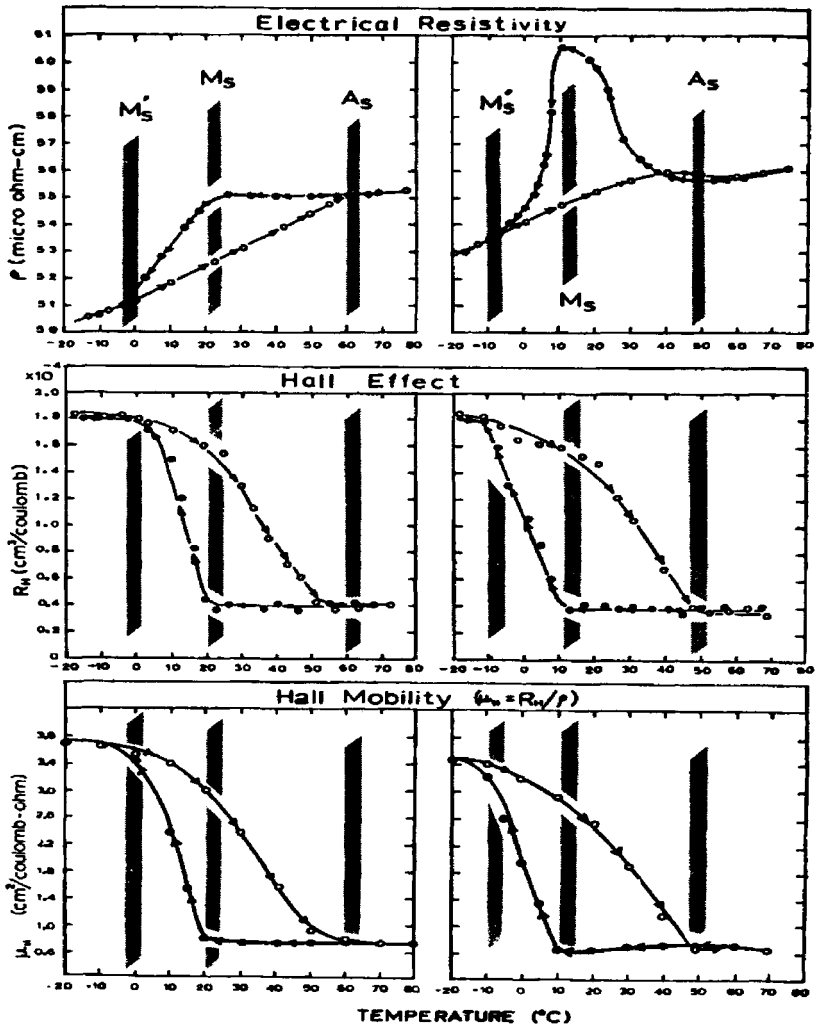

Fig. 14. Electrical resistivity, Hall coefficient and calculated Hall mobility obtained before and after the 'incomplete' thermal cycling; Only 'complete' cycling on the left and after 'incomplete' thermal cycling on the right.

These circumstances are: (a) if the band structure is a single band, or (b) if the band structure is such that one of bands dominates over the rest by virtue of its electron or hole mobility.

Inasmuch as the electrical resistivity peak appeared in the cooling half of the resistivity curve from 'incomplete' cycle was not matched by any such change in the Hall coefficient measurement, the afore mentioned circumstances apply. Consequently, the band structure of TiNi can be regarded as either a simple single band or one positive band dominating over the others in the temperature being considered. This conclusion did have the support of the transport data obtained independently by other investigator [38].

The Hall Mobility: this is calculated from the observed electrical resistivity and Hall coefficient as shown in Fig. 14. As mentioned above the Hall mobility, $\mu_H = c \cdot R_H/\rho$, is again a function of m^*, $\bar{\tau}$, and n. Only in the simplest cases does μ_H become independent of the carrier concentration, n ,

$$\mu_H = c \cdot R_H/\rho = c(1/Nec)(Ne^2 \bar{\tau}/m^*) = e\bar{\tau}/m^* .$$

The resistivity peak observed in the cooling half of an 'incomplete' cycle has a maximum value, $\rho_{max} \approx 61$ ($\mu\Omega$cm) compared to $\rho_{min} \approx 55$ ($\mu\Omega$cm) in the absence of 'incomplete' cycles. On the other hand, the Hall coefficient corresponding to this temperature range is a constant, $R_H = 0.4 \times 10^{-4}$ (cm^3/C). From these data, two respective Hall mobilities, $\mu_H(max) \approx 0.65$ and $\mu_H(min) \approx 0.75$ ($cm^2/C \cdot \Omega$) are obtained. The difference between the two values is less than 4% of the total Hall mobility change observed as shown in Fig. 14. In view of this fact, it is logical to conclude that the overall Hall mobility change could not come from changes in m^* and $\bar{\tau}$ but must be due primarily to a change in the effective number of carriers, n_h. This conclusion is consistent with that derived from Hall coefficient measurements.

These explanations led to the following prediction. Atomic-arrangement-insensitive properties should not show a difference between 'complete' and 'incomplete' cycles, whereas atomic-arrangement-sensitive properties would be expected to behave in much the same way as the electrical resistivity.

Magnetic Susceptibility: of TiNi has been previously observed [39] to be temperature independent and interpreted as due to Pauli spin susceptibility. This categorizes the magnetic property as one that is insensitive to the atomic arrangement. The magnetic susceptibility has the constant values, 2.1×10^{-6} (emu/g) below the M_S and 3.0×10^{-6} (emu/g) above the A_S temperature. Between these two temperatures a plot of the data has a triangular form but as predicted, no difference is observed between those obtained from 'complete' and 'incomplete' cycles.

Sound Velocity Changes: in TiNi, at and around its unique transition temperature has been reported [40]. This report show a considerable difference between the heating and cooling halves of thermal cycles, which is reminiscent of the effect observed in the resistivity curve from 'incomplete' cycles. Acoustic waves traveling through solids are

known to be sensitive to the details of the atomic arrangement [41]. The sound velocity change, being an atomic-arrangement-sensitive property and therefore show the difference. The results also show a dramatic difference for the two cases. Particularly convincing is in the cooling half of the 'incomplete' cycle showing a dramatic difference from that of heating much the same as the resistivity.

Differential Thermal Analysis (DTA): earlier DTA data showed an unusually large heat of transformation: endothermic in heating and exothermic in cooling. Later, through precision calorimetric methods [13], it was determined that the ΔH to be as high as 4,150 (J/mole), and also established the nature of the transition to be second order which is in agreement with our earlier single crystal X-ray diffraction study [6].

Having established a model which comprises three distinct paths, $A_S - M_S$, $M_S - M_S'$ and $M_S' - A_S$ with three independent shear vectors, $\bar{S}_1$, $\bar{S}_2$ and $\bar{S}_3$, it is logical to ask the following question. In what manner is the heat of transition, or more precisely, the anomalous heat capacity change, related with these shear vectors?

The results of DTA, as shown in Fig. 15, indicated that the anomalous heat capacity change is associated with the two irreversible paths, $M_S - M_S'$ on cooling and $M_S' - A_S$ on heating, and that no anomalous heat-capacity change is associated with the reversible path, $A_S - M_S$. Since there was no detectable difference between the DTA curves of 'complete' vs. 'incomplete' cycles, the anomalous heat-capacity change could not have come from change in atomic arrangement. Logically, this leaves electrons as the major cause for the anomalous heat-capacity changes observed.

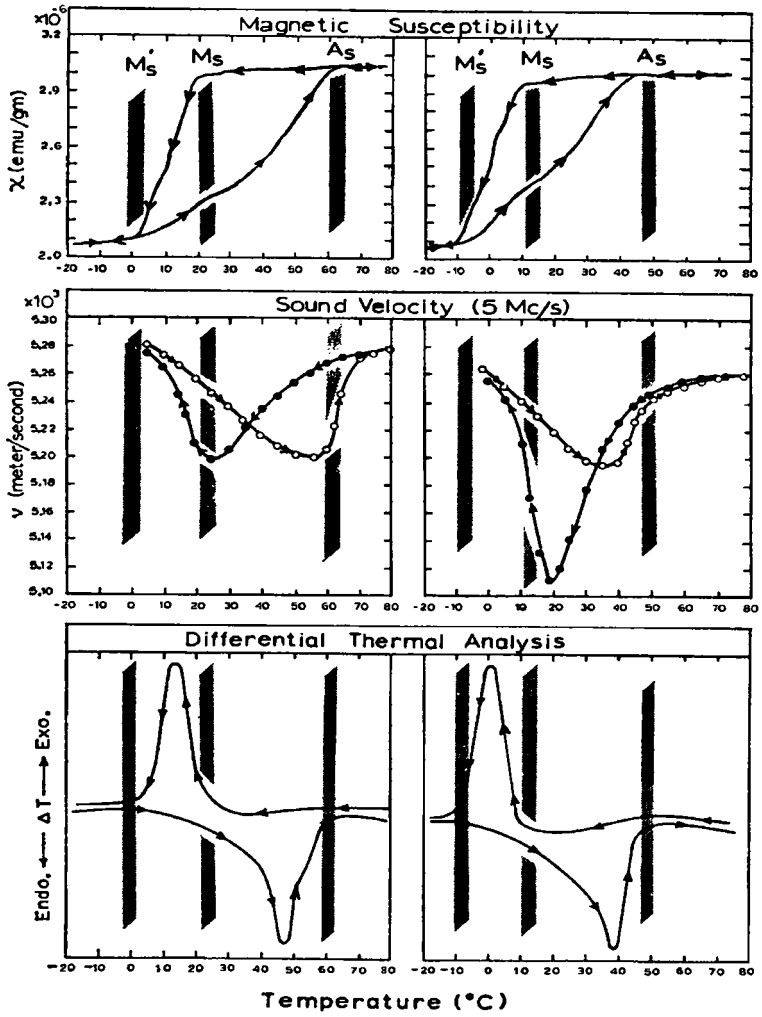

Fig. 15. Magnetic susceptibility, sound-velocity change, and differential thermal analysisobtained corresponding to 'complete' and 'incomplete' thermal cycling at and around Nitinol transition. Three vertically shaded band indicate the corresponding M_S, M_S' and A_S temperatures in Fig. 12. Arrow indicates the direction of temperature change.

3. COVALENT BOND (BOSON) ⇆ METALLIC BAND (FERMION) ELECTRONIC STATE TRANSFORMATION

3.1 Qualitative Agreement

In summary, changes were observed in the following properties:

(a) The ideal resistivity decreased (conductivity increased)

$$\downarrow \Delta\rho_i$$

(b) The positive Hall coefficient decreased

$$\downarrow \Delta R_H(+) \approx 1.4 \times 10^{-4} (cm^3/C)$$

(c) The number of effective hole carriers increased

$$\uparrow \Delta nj \approx 1.1 \times 10^{23} (cm^{-3}) = 18.17 \times 10^{23} (mole^{-1} of\ TiNi)$$

(d) The Pauli paramagnetic susceptibility increased

$$\uparrow \Delta\chi \approx 0.9 \times 10^{-6} (emu/g)$$

(e) Heat is absorbed by the system

$$+\Delta H \approx 4{,}150\ (J/mole) = 24.3 \times 10^{19} (eV/g)$$

The qualitative interpretation of these results in terms of 'conduction' → 'covalent' electronic transformation model is based on the following principles: (1) 'covalent' electrons are localized and therefore are identifiable with a group of ions, whereas 'conduction' ('free') electrons are delocalized and are simultaneously shared by all ions. (2) thus, 'covalent' electrons having no Fermi surface whereas 'conduction' electrons (because of the Pauli exclusion principle) having well defined Fermi surface, and (3) electrons are needed in forming 'covalent' bonds, (i.e., under no circumstances can holes be substituted for electrons in forming bonds); in sharp contrast, holes behave in much the same way as electrons in band structure.

With this understanding, it is clear that in a given 'conduction' ∅ 'covalent' transformation, a decrease or increase in the number of 'conduction' electrons is an essential feature that should be observable in the transport properties. Assuming that the band structure of TiNi consists of a single positive band, a decrease in the number of 'conduction (free)' electrons in the course of $M_S' \rightarrow A_S$ is equivalent to an increase in the number of hole carriers as seen in (c). Consequently, the positive Hall coefficient should decrease and is so observed in (b). Because holes contribute to Pauli paramagnetic susceptibility in precisely the same manner [42] as electrons, the paramagnetic susceptibility, χ, is expected to rise and is so observed in (d). An increase in the hole carrier, N_h, would result in an increase in the conductivity (lowering in the resistivity) as

shown in (a). Finally, due to the difference in electron energy between the 'conduction' and 'covalent' states with $E_{con} < E_{cov}$, an endothermic heat of transformation would be anticipated and is so observed experimentally in (e). It can be argued that, though overwhelming in number, these qualitative agreements are not unique to the 'conduction' → 'covalent' transformation and single positive band assumptions. For, equally good agreement may be obtained by assuming a 'nearly' one-band model in which electrons simply transfer from a positive band of high-mobility to another low-mobility band in the course of the transformation. However, to accept this line of thoughts, one has to ignore other related atomic and macroscopic observations such as: (i) the change in interatomic distances, in TiNi(III) they are 'metallic' radii [6] and (ii) the acoustic damping capacity of TiNi(III) is approximately ten times that of TiNi(II), [31], and (iii) physically TiNi(III) is soft and malleable whereas TiNi(II) is tough and hard. Furthermore, a transfer of electrons from one band to another by itself does not constitute a thermodynamic phase transformation [43], which contradicts a fundamental observation – Nitinol transition is a phase transformation.

The theoretical treatment of a solid-state transition involving 'covalent' (localized) *vs.* 'conduction' (delocalized) electronic transformation was first enunciated by Mott [44]. By considering the Pauli Exclusion Principle and the electron–electron interaction during the transformation, it was shown that such transition will be critically dependent upon the inter-atomic distances. The number of electrons already existing in the 'conduction' state will in turn influence the critical inter-atomic distances and the transition; therefore, it is necessarily a cooperative phenomenon. Later, in a theoretical treatment of the same subject, but based on a different context, Goodenough [45] has shown that the transition is likely to be second-order if the number of electrons per like atom is non-integral. Further, a crystallographic *distortion* is a prominent manifestation of such a transition.

3.2. Quantitative Agreement

Since the number of electrons involved in the Nitinol transition is 1.5 electrons per like atom and as shown above, Δn (hole) $= 18.17 \times 10^{23}$ per mole of TiNi; with density of TiNi = 6.45 (gm/cm^3) , according to theoretical argument [45] the transition should be second-order. This conclusion has the support of anomalous heat-capacity change observed [13] for Nitinol transition. It is therefore necessarily a cooperative phenomenon as suggested by Mott [43]. At this point, the simplified theory of Bragg and Williams [46] on cooperative phenomena in which an order-disorder parameter is involved can be invoked and applied to Nitinol transition. According to Bragg and Williams, if the cooperative anomaly is due to two simple thermodynamic configurations, the energy difference for the whole system for such a transition can be estimated through the equation, $\Delta E = (N \times k \times T_C)/2$ where N = number of units involved in the thermodynamic configuration change, and $k = 1.38 \times 10^{23}$(J/deg) for Boltzman constant and T_C = high temperature limit of the transition. By taking $T_C = 333$°K(60 °C) and $N = \Delta n = 18.17 \times 10^{23}$ per mole of TiNi, the total energy difference per mole of TiNi for the transition.

$$\Delta E = (18.17 \times 10^{23} \times 1.38 \times 10^{-23} \times 333)/2$$

= 4175 (J/mole) --------- theoretical

in excellent agreement with the experimental value [13].

4150 (J/mole) ------ experimental

Previous single crystal X-ray diffraction studies [6, 33, 34] of TiNi transition demonstrated the continuous shear movements of atoms below the transition temperature. It is believed that the critical inter-atomic distance above which the 'conduction' electrons cannot be self-sustaining is somehow related to the continuous variation of inter-atomic distances in the Nitinol transition.

4. ADDITIONAL UNIQUE PROPERTY CHANGES OBSERVED

A number of unique physical property changes such as memory effect and acoustic damping capacity changes etc. associated with Nitinol transition have been known [47,48]. Here are some additional observations that are not well known [49] but show once again the support for the model presented for the Nitinol transition.

4.1. Bending a wrought sheet of TiNi

At a temperature below its TTR (transition temperature range) [14] and when this bending exceeds the elastic limit of the material (see Fig. 16), a considerable amount of heat is generated (+ ΔQ) in the area of inflection. Upon release of the bending force, the heat generation ceases immediately. If the sheet is now unbent in the reverse direction as shown in Fig. 16, not only is heat generation stops but any heat in the bent area is absorbed into metal body. This heat absorption (– ΔQ) manifests itself in the rapid temperature drop in the alloy. The temperature difference between the two extremes is approximately 10 ~ 15 °C.

Thermodynamically, it can be reasoned that the major contribution of heat generation or absorption must have come from source other than the lattice, i.e., such as electrons and changes in their thermodynamic state. Similar phenomena exist in stretching a piece of rubber or other cooperative phenomenon such as the transition between 'ordinary' helium to helium-II.

4.2. Uniaxially stretching a TiNi wire

Somewhat beyond its limit of easy plastic flow (see point A on the stress-elongation curve in Fig. 17). Then applying a localized heat such as a match flame at any point along the wire, the wire will bend abruptly at that point at a fixed angle of 150 °. This heat induced bend will remain unchanged until additional heat is applied. By moving the match flame along the wire, the bent section will travel with the flame until the bent portion is 'chased out' of the wire. This unique bend-and-straighten action is accompanied by a

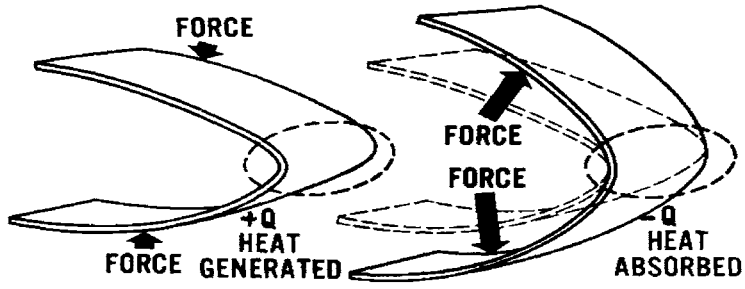

Fig. 16. If a sheet of TiNi is bent beyond its elastic limit, heat is generated at the area of inflection. If the sheet is now unbent in the reverse direction, heat is absorbed into the specimen and becomes cold. – reference [49].

reversion to the stretched wire back to its original strain-free length. If the wire is suspended vertically, the wire will bend to the side of approaching heat.

4.3. An anomalous emf change

During the Nitinol transition is observed. An emf of about 25 mV exists between titanium and TiNi electrodes bathed in a titanium electrolytic solution at temperature above its TTR as shown in Fig. 19. By taking a TiNi wire and coil the wire at temperature below TTR outside the bath and by inserting the coiled TiNi wire into the electrolytic bath (> TTR), the wire will uncoil instantly due to the 'memory' effect. Should the uncoiling TiNi wire touch the TiNi electrode the emf increases instantly to about 500 mV or higher, depending on the degree of initial coiling. This induced emf then decays gradually down to its normal 25 mV within 2 to 3 minutes. A similar effect, but less pronounced, is also observed in a nickel electrolytic solution where the electrodes are nickel vs. TiNi.

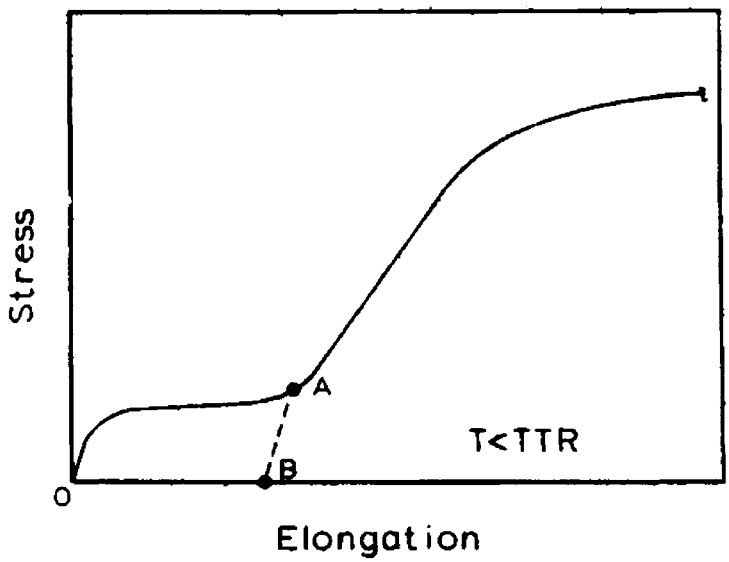

Fig. 17. The stress-elongation curve obtained from Nitinol by applying a uniaxial tensile load at temperature below the TTR. The portion of the curve, 0 – A represents the zone of easy plastic flow. A – B illustrates elastic recovery, and B – 0 is recovery (contraction) possible by heating to above the TTR. – reference [49]

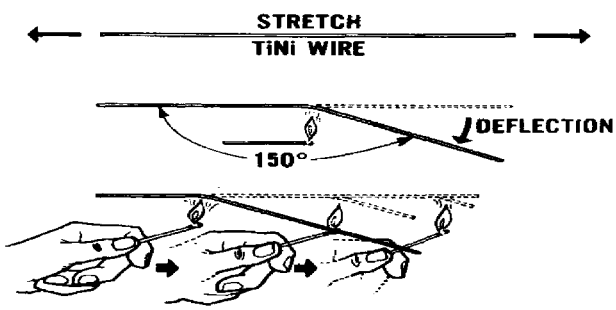

Fig. 18. Upon application of a localized heat to a TiNi wire which has been stretched uniaxially beyond its limit of easy plastic flow, the wire will bend abruptly at the point of heating to the fixed angle of 150 °C. By moving the heat down the wire, the bend will move along the wire with the flame. – reference [49]

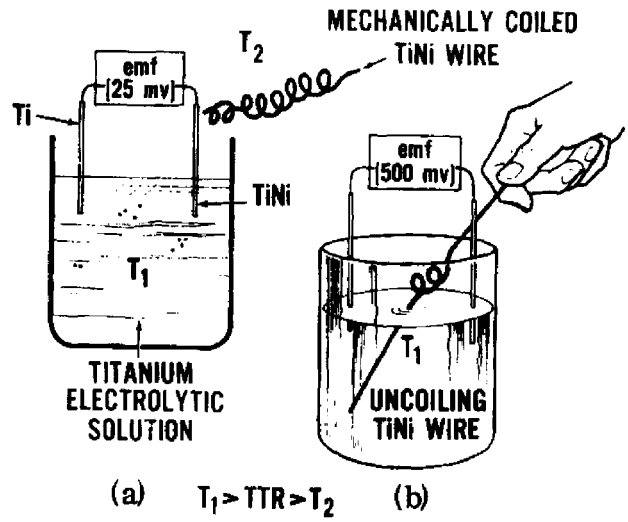

Fig. 19. An emf of about 25 mV exists between titanium and TiNi electrodes at temperatures above TTR. A TiNi wire coiled outside the electrolytic bath below TTR. When this coiled wire is inserted into the bath at temperature above TTR the wire will instantly straighten out due to 'memory' effect. By letting the uncoiling TiNi wire to come in contact with the TiNi electrode, an emf of more than 500 mV is registered.- reference [49].

5. BAND STRUCTURES OF TiNi(II) and TiNi(III)

All the data presented and the interpretation given to this point is to show that Nitinol transition is unique among the whole class of 'martensitic' transformation alloys. Most importantly, it is proposed and argued that the transition is electronic in origin and that a portion of the 'covalent' bonded electrons change its state to 'conduction' electrons during the transition. While some support for this postulate was offered [50], a better understanding of the band structure of TiNi has been limited by the lack of large single crystals [5] and the complexity of the crystal structure [6,15]. It should be pointed out that there have been reports [51,52] of growing TiNi single crystals of size large enough for elastic measurements or structure study through Bridgeman technique or through simple 'strain-anneal' technique. But, my research group at Naval Ordnance Laboratory, the birth place of Nitinol, could not repeat these results, i.e., growing single crystal large enough even for neutron diffraction study. One reason we can offer is that the investigators [51,52] who claim to have grown large single crystals used high frequency induction heater in preparing their TiNi alloy with graphite as container. In our laboratory, this method of alloy preparation always led to carbon contamination.

This is because Ti as an element easily reacts with graphite crucible and lead to a formation of titanium-carbides first before forming TiNi alloy. Whether this is indeed the reason for forming large single crystals has to be investigated. But, it should be pointed out that even between these two groups of investigators a difference was reported: one group admitting a failure to grow single crystals using 'strain-anneal' method [51] while the other group [52] claim to have grown large crystals of TiNi using 'strain-anneal' method. The point is that the first group of investigators [51] made measurement of elastic constants on the large crystal through temperature range between 0° to 80 °C. But, they did not observe any abrupt changes corresponding to the crystallographic change existing in the Nitinol transition as observed in X-ray diffraction work [6,15] or in the internal friction data [31]. The other group [52] simply did not follow through their large single crystals under X-ray or neutron diffraction as a function of temperature and thus there was no independent confirmation of single crystal they had on hand is TiNi with Nitinol transition.

Because of the fact that the average number of valence electrons per atom is seven in TiNi, the general feature of the density of states curve is therefore taken to be similar to that of Mn, also 7 (electrons/atom). Goff [38] also elaborated the similarity between TiNi and Mn. That is to say, the d-band has two maxima enclosing a minimum and the s-band has a broad maximum as depicted in Fig. 20. It is assumed that neither band alters its shape significantly through the Nitinol transition. The basic difference between TiNi(II) and TiNi(III), then is described by a shift of the low-density s-band relative to the high-density d-band as the temperature is lowered (or raised) across the transition temperature range (TTR). It is shown that such an electronic configuration change is consistent with the experimentally observed low-temperature specific heat, magnetic susceptibility, enthalpy, and Hall coefficient changes during the transition.

For detail of these discussion refer to the paper by Mitchell et al.[67]. First, we take as the density of state for TiNi, curves such as those shown in Fig. 20(a) for $T < T_f$ and Fig. 20(b) for $T > T_S$, where T_f (low) and T_S (high). For stoichiometric TiNi, $T_S \sim 120$ °C and $T_f \sim 60$ °C. In both phases the density of states, $N_d(E)$ and $N_S(E)$, chosen are such as to satisfy the following equations:

$$2\int N_d(E)dE = 1 \qquad (1)$$

$$2\int N_S(E)dE = 2 \qquad (2)$$

Eq. (1) is used to find the d-band width (6.5 eV) once the other parameters of the band shape are determined. Similarly, Eq. (2) is used to determine the s-band width (12.9 eV) of a free-electron density of states; symmetric in energy about the middle of the band. The d-band density of states, $N_d(E)$, rises sharply at the lower band edge to about 1.5 states/eV atom then falls off to 0.47 states/eV atom near the middle. With the general shape of $N_d(E)$ and $N_S(E)$ given, the critical magnitude of $N_d(\xi)$, the chemical potential in d-orbital, is determined from the observed linear part of the low-temperature specific heat as follows:

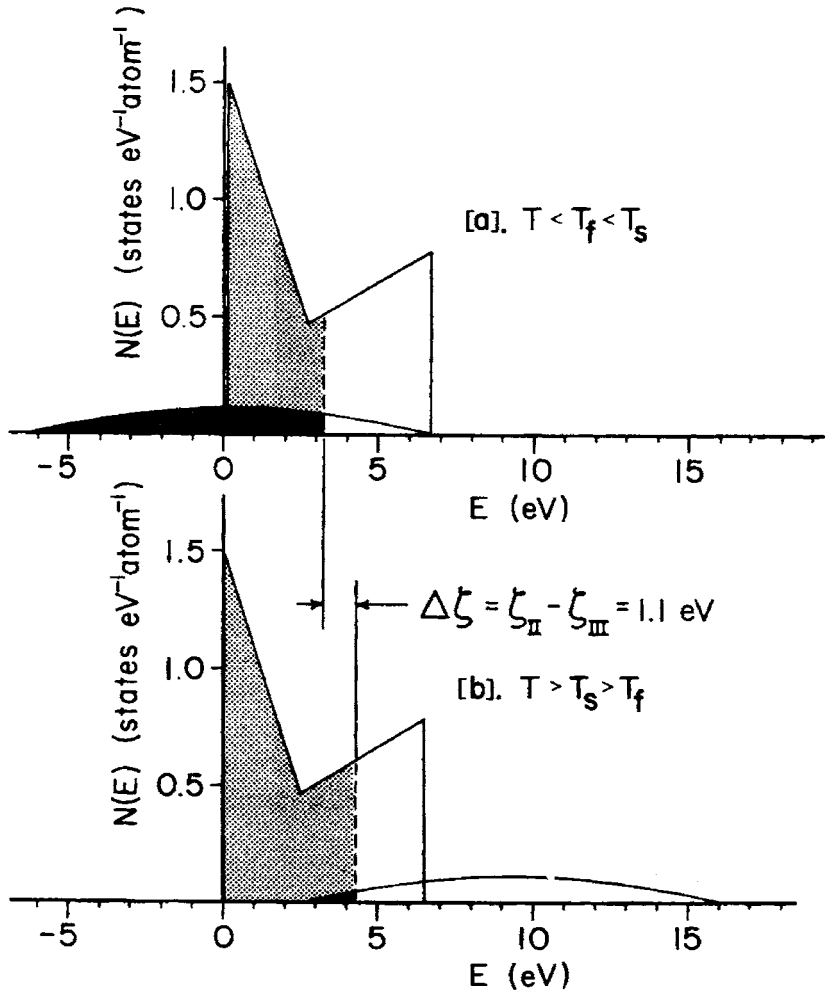

Fig. 20. Density of states of TiNi; T_S and T_F are the upper and lower temperature limits in the TiNi martensitic transition. (a) Density of states below the transition. Note that the llower d-band edge is at 0.17 eV. The s-band contains 1.5 electrons, whereas the d-band Contains 5.5 electrons. (b) Density of states above the transition. The lower d-band edge is at 0 eV. The s-band and d-band contain 0.1 and 6.9 electrons respectively.

The density of states as determined from the specific heat,

$$\gamma(\text{III}) = \tfrac{1}{3}\pi^2 \, K_B^2 \, N(\xi\text{-III})$$

is 0.59 states/eV atom. Only 1/3 of that 1.73 states/eV atom is determined from Pauli-type magnetic susceptibility, $\chi = 2\mu_B^2 N^*(\xi)$ in the low-temperature phase, TiNi(III). Since most of the density of states must have come from the d-band, we take this as evidence of a significant exchange enhancement of the magnetic susceptibility [53]. It is true that the interaction responsible for enhancing magnetic susceptibility, χ , can also lead to an increase in $N(\zeta)$, but it is not expected to be as strong; e.g., in $Ni_{0.7}Rh_{0.3}$ where $N(\zeta)/N^*(\zeta) \approx 1/3$, the effect on γ is only about 20 % larger than it is in pure Rh [54]. That is to say, if we assume that there are no enhancement effects in Rh, γ in $Ni_{0.7}Rh_{0.3}$ is about 20 % larger than its non-interacting value. In fact, this is probably an overestimate. Thus, we take for the 'bare' density of state, $N(\zeta\text{-III}) = 0.59$ states/ eV atom, close to that obtained from the equation given above. Since, γ (II) is not known, $N(\zeta\text{-II})$ is determined from the experimental value of χ (II) and the equation,

$$\chi = 2\mu_B^2 N(\zeta)/[1 - UN(\zeta)] \qquad (3)$$

where U is the interaction energy. In our case, U is assumed to be the same in both phases. Calculating U from the above expression for the experimentally given, χ(III) in the TiNi(III), where $N(\zeta\text{-III})$ is known from the specific heat, we find U is 1.1 eV.

Substituting these values into equation (3), we find in the TiNi(II) phase, a value of $N(\zeta\text{-II}) = 0.661$ states/ eV atom. With $N(\zeta\text{-II})$ and $N(\zeta\text{-III})$ determined, we proceed to specify the parameters of the model as follows.

The shape of the s-band is completely determined: it contains 1 state/atom (2 electrons/ atom) and is symmetric about its half-width point with bandwidth of 12.9 eV. The values of 0.5 and 2.1 holes/atom below and above the TTR are known from the Hall coefficient data. It is reasonable therefore to assume that most of the hole contribution comes from the high-mobility s-band, and thus the chemical potential in the s-band above and below the TTR can be fixed by using

$$n_S = 2\int_0^{\zeta} N(E)\, dE \qquad (4)$$

with $n_S \approx 1.5$ and 0.1 electrons/atom below and above the TTR.

The s-band density of states is small and contributes little to the susceptibility and specific heat. Nonetheless, we subtracted $N_S(\zeta\text{-II})$ and $N_S(\zeta\text{-III})$ from $N(\zeta\text{-II})$ and $N(\zeta\text{-III})$ respectively, to obtain the parameters in the d-band density of states, $N_d(\zeta\text{-II}) = 0.51$ and

$N_d(\zeta\text{-III}) = 0.61$ states/ eV atom. The size of the initial peak in N_d was chosen to be 1.5 states/ eV atom, which is the height of the lowest peak in the calculated density of states for Mn [54]. The parameters to be determined are therefore E_m (the energy at which the slope of N_d changes its sign, $N_m = N_d(E_m)$, and ζ (II) and ζ (III) – the Fermi levels below and above the TTR respectively. These parameters are determined as follows:

The negative-slope portion of the N_d curve contains five electrons,

$$2\int_0^{E_m} N_d(E)\,dE = 5 \ .$$

Also, $N_d\,2\int_0^{\zeta} N_d(E)\,dE$, where $N_d = 5.5$ ($\zeta = \zeta$-II) and $N_d = 6.9$ ($\zeta = \zeta$-III) below and above the TTR. Finally, the requirement that the slope of N_d be the same in the two phases leads to the equation,

$$\frac{\zeta_{II} - E_m}{N_{II} - N_m} = \frac{\zeta_{III} - E_m}{N_{III} - N_m} \qquad (5)$$

The results are $\zeta_{II} = 4.30$ eV and $\zeta_{III} = 3.05$ eV, $E_m = 2.54$ eV (from the bottom of the d-band) and $N_d(E_m) = 0.47$ states/ eV atom. The d-band width calculated from equation (1) is 6.54 eV.

The s and d bands were adjusted relative to one another by matching their chemical potentials. Finally, the s- and d-band configurations above and below the TTR were adjusted relative to one another by setting the average electron energy difference between the high- and low-temperature configurations equal to the observed enthalpy change [13] through the TTR,

$$H_{III} - H_{II} = 4.15 \text{ (J/mole)} = 6.1 \text{ meV/ electron},$$

where $H = \left[2\int E\,N(E)\,dE\right]\left[2\int N(E)\,dE\right]^{-1}$. The limits of integration extend from the bottom of the lowest band to the chemical potential. Shown in Fig. 20, is the resulting density of states below and above the TTR. Below TTR, the average electron energy is 0.65 eV for the s-band and 1.08 eV for the d-band; above the TTR, the average electron energy is 0.054 eV for the s-band and 1.68 eV for the d-band. The chemical potential difference between the high- and low-temperature states is found to be 1.1 eV, which is a measurable work-function change in going through the transition.

While the model presented herein is crude and there is no certainty that the free energy is minimized with the choices of parameters, the model accounts well for the properties which depend most directly on the magnitude of the density of states, i.e., low-temperature electronic specific heat, magnetic susceptibility, enthalpy, and Hall coefficient changes observed through the TTR. Since the band-structure model is limited to the den-

sity of states, therefore, is insufficiently formulated for discussion of the bulk modulus and transport property changes other than the Hall coefficient. The 'metallic' → 'covalent' change embodied in the s-band shift relative to the d-band through the TTR is qualitatively consistent with the unusual acoustic damping capacity change [31,48]. It is reasonable to expect that the 'covalent' nature of TiNi above the TTR leads to a strengthening of inter-atomic forces with a consequent increase in elastic modulus. The assumption that the shape of the s- and d-bands remaining more or less invariant is justified from the fact that the 'lattice' (with regard only to the atomic sites, but not the type of atom occupying the site) remains the same in both the TiNi (II) and TiNi(III) phases [15]. Transition similar to that existing in TiNi has been shown to exist [10,33,34] in the TiX (where X = Ni, Co, Fe, or a combination thereof), ZrY (where Y = Ru, Rh, Pd), and HfZ (where Z = Os, Ir, Pt) series. It is apparent that the transition has a close relationship with the elements of d-atomic orbital series. As argued in the "Origin of Nitinol Transition" the motivation force in the transition is the d-atomic orbital contraction.

6. CONCLUSION & DISCUSSION

It should be obvious by now that my presentation of Nitinol transition has been focused on the nature of the transition rather than on the mechanism of the transition. This is because the Nitinol transition provides the basis for proving once again the role of 'covalent' bond in metals and alloys. Starting with the atomic d-orbital contraction, the cause of the Nitinol transition was viewed as due to the breaking and forming of 'covalent' bond between titanium (Ti) and nickel (Ni). This led to the prediction and confirmation of similar transition not only in the 3-d series Ti–Fe (Co,Ni) but also in the 4-d series, ZrRu (Rh, Pd) as well as in the 5-d series, HfOs (Ir, Pt) of alloys. In this context, the Nitinol transition is inferred as a transition involving 'covalent' ∅ 'conduction' electronic state transformation. This inference is supported by a series of experimental evidence starting with (a) acoustic damping capacity change, to (b) electrical resistivity change, to (c) Hall coefficient change, to (d) magnetic susceptibility change, to (e) sound velocity change to (f) anomalous heat capacity change and finally (g) a band-structure calculation that showed the electronic change between s- and d-band. However, most impressive supporting evidence is the fact, once the number of electrons involved in the transition of 'covalent' to 'conduction' is known, the heat of transformation then was calculated using the Bragg-Williams formula for the second-order transformation. The agreement between the calculated vs. experimental value for the heat of transition is simply spectacular (4175 J/mole-cal. *vs.* 4150 J/mole-exp.). Having started with single crystal X-ray diffraction work that showed the transition to be a crystallographic 'distortion' rather than of 'transformation' and therefore is a second-order transformation which is unique among the class of alloys with martensitic transformation. This thesis is supported in a roundabout way by the electronic state transformation, which must be a second-order as well. The conclusion is that the Nitinol transition is electronic in origin. And it involves 'covalent' ⇆ 'conduction' electronic state change and thermodynamically a second-order transformation. Within the TTR, the atomic shear takes place continually and results in an indeterminate crystal structure. Indeed, this feature misled so many investigators to report of so many different crystal structures for TiNi-II and TiNi-III. In fact, not only people

were reporting different crystal structures, they were announcing the 'pre-martensitic' phase or 'R-phase' etc. to justify their irreconcilable observations. But, all these investigation and observations ultimately failed to show the way toward the understanding of the Nitinol transition. Unfortunately, the metallurgists as a whole have seen the class of alloys with martensitic transformation in the past that behaves in the same way. These notions lead to the formulation of the "Crystallographic Theory of Martensitic Transformation' based on the existence of an invariant plane [56] and other crystallographic attributes. To admit that Nitinol transition is martensitic (diffusionless) in nature but is **unique** among the class of martensitic transition alloys (also admitted by Mercier [50] to be unique based on their elastic constant study) is tantamount to refute the Crystallographic theory so painstakingly formulated through the years past. I fully understand the pain to do so. To avoid such consequence the efforts, in my view, were made to create 'R-phase' or 'pre-martensitic phase' to cover the inconsistencies observed experimentally. In some case, an effort was made to show the existence of 'habit' (invariant) plane [57] in TiNi but without the rigorous proof of reversibility. These authors used an alloy that is Ti –rich with – Ni (49.5 at %) that has been shown to be much less sensitive to the martensitic transition [6]. And they also used 'carbon' crucible as a container for melting the alloy. There is no question that titanium as element reacts vigorously with carbon to form titanium-carbide and can cause a contamination in the TiNi alloy. These authors also chose to ignore the 600 °C order-disorder transition between A2 (body-centered) and B2(CsCl-type) structure and no care was taken to properly anneal the alloy at this temperature.

The mechanics of the TiNi transition is, as shown by the X-ray, quite complex particularly when it comes to formation of 'twin' or 'antiphase' boundary. Although, personally I consider them as secondary importance toward the understanding of Nitinol transition itself, perhaps they should be mentioned to complete the picture. It has been known that the martensite (low-temperature phase) always has a crystal structure with lower symmetry than the austenite (high-temperature phase). In order to lower the 'free-

Transformation Twinning of *B*2(CsCl)-Type Structure Based on an Inhomogeneous Shear Model

Frederick E. Wang
U.S. Naval Ordnance Laboratory, Silver Spring, Maryland 20910
(Received 31 August 1970; in final form 7 June 1971)

It is shown that in addition to the heretofore accepted homogeneous (simple) shear model, there is yet another mechanism that is inhomogeneous which can bring about mechanical twins in an *A*2(bcc) structure. In martensitic transformations where the cause for transformation is primarily internal, inhomogeneous-but-cooperative shear may take place in preference to homogeneous shear. Application of the inhomogeneous-but-cooperative shear model to a *B*2(CsCl)-type structure leads to a triclinic structure. In the course of this structural transformation, two modes of transformation twinning and one mode of trilling are possible.

Fig. 21. The first paper of Wang published in 1971, in which an inhomogeneous shear modelproposed as the mechanism leading to a 'twining' of B2-type structure. J. Appl. Phys. Vol. 43, p.92 (1972).

energy' in the lower-symmetry phase, the crystals invariably form 'twinning' to achieve a pseudo higher symmetry. Antiphase boundary is formed fundamentally for the same purpose except that there is a phase changes across the twin boundary. In 1970, anticipating the twinning in Nitinol transition I wrote a paper [58] proposing an 'inhomogeneous' shear mechanism as a possible means for the formation of 'twining' in the B2 (CsCl-type) structure (Fig. 21).

It is well known that a homogenous shear applied to an A2 (bcc) structure can lead to a twin [60]. However, neither homogeneous nor inhomogeneous shear applied to B2(CsCl-type) structure can lead to a twin. Therefore, mechanical twinning involving no structure change of a B2 structure must be explained by a different mechanism or possibly by an inhomogeneous shear with 'shuffles.' The 'inhomogeneous' shear proposed [58] was based on the following characteristics:

a) The magnitude of shear is smaller than the interatomic distances and it is cooperative (at least in one dimension).
b) The shear vector, $1/6\langle 111\rangle$ is the smallest possible shear vector that gives rise to the twinned state in an A2 structure [61]. Therefore, it is expected to be operative in structures with an A2 lattice.
c) The long-range net strain resulting from inhomogeneous shear is small.

The 'inhomogeneous' shear as proposed was then applied to the Nitinol transition [59] as shown in Fig. 22. In this paper it was demonstrated that: (1) How the inhomogeneous shear mechanism proposed [58] earlier to explain the X-ray and neutron diffraction data [15] observed during the Nitinol transition can also serve to derive 'twining' and 'antiphase' boundary formation in TiNi as observed [61], and subsequently, (2) How the anomalous electrical resistiviy (due to incomplete thermal cycling) observed [14] in the Nitinol transition can be reconciled in terms of the density of twin formation, and finally (3) How the relationship between the electrical resistivity anomaly and the sensitivity of the 'memory' effect observed [63] can all be logically tied together through twin formation.

Now, after more than ten years passed from the year (1973) Wang's paper (published in the J.Appl. Phys.) on the subject of 'twin' in TiNi, Goo et al. [64] published a paper in 1985 (Fig. 23), dealing with the same subject, TiNi ($Ti_{49}Ni_{51}$ is not different from TiNi) and the same mechanism. But, in this paper the authors claim themselves as the first ones to observe the twining in TiNi! There were no remark or reference made (either good or bad) in their paper to the Wang's work published more than 10 years earlier on the same subject. Were these people unaware of the earlier work? Should we consider this as an innocent careless oversight? Don't they know the first thing to do in writing a paper is to do literature search? In this high-tech information age, it would seem without much effort, a computer-search should find who did what on the subject in the past decade or century. Or these authors intentionally chose to ignore any previous works on the subject so they can take the credit of being the first to do this? This is but one example to show how much 'noise' was created in the open literature on the subject of Nitinol transition.

Twin and antiphase boundary formations in TiNi through inhomogeneous shear mechanism

Frederick E. Wang

Naval Ordnance Laboratory, Silver Spring, Maryland 20910
(Received 9 February 1973; in final form 26 March 1973)

The atomic mechanism, based on the previously proposed "inhomogeneous" shear, leading to the formation of twinning and antiphase boundaries in TiNi with the CsCl-type structure is described. The twinning mechanism described herein explains the electrical resistivity anomaly due to "incomplete" thermal cyclings observed previously in TiNi. This explanation is in keeping, in a qualitative manner, with the "memory" effects observed in relation to the electrical resistivity anomaly.

Fig. 22. Showing how the 'inhomogeneous' shear proposed (Fig. 21) in 1972 to apply in TiNi in the formation of 'twin' and 'antiphase boundaries. This paper was published in 1973, more than 10 years before Goo et al claimed to have observed for the first time 'twining' in B2 structure of TiNi (see Fig. 23). J.Appl.Phys. vol 44, p.3013 (1973).

MECHANICAL TWINNING IN $Ti_{50}Ni_{47}Fe_3$ AND $Ti_{49}Ni_{51}$ ALLOYS

E. GOO[1], T. DUERIG[2], K. MELTON[2] and R. SINCLAIR[1]

[1]Department of Materials Science and Engineering, Stanford University, Stanford, CA 94305 and [2]Raychem Corp., 300 Constitution Drive, Menlo Park, CA 94025, U.S.A.

(*Received* 24 *November* 1984)

Abstract—Pseudo-twinning and mechanical twinning have been observed in a transmission electron microscopy study of $Ti_{50}Ni_{47}Fe_3$ and $Ti_{49}Ni_{51}$ alloys which have the B2(CsCl) structure. Observation of twinning in ordered alloys is rare and this is the first observation of twinning reported in a B2 structure. The twin planes are the {112} and {114} planes. For {112} pseudo-twins, the composition plane is not the twin plane and the pseudo-twin does not have the B2 structure. For {114} mechanical twins, the composition plane is the twin plane and the twin does have the B2 structure. It is shown that a shear on the {114} plane plus a shuffle of the atoms results in the ordered B2 structure in the twinned region.

Fig. 23. Published in 1985 (12 years after Wang's paper on the same subject). Yet, no mention whatsoever (or reference made on Wang's paper-Figs. 21,22). These authors claim that they are the first discoverer of 'twining' in B2 structure in TiNi; Acta Met. Vol. 33. page 1725.

People publish their own data without making efforts to see who else did what and how. And when they did find the earlier works, they simply list them as another reference. Only in a few cases efforts are made by the authors to see how their data can be reconciled with the data published by others — on the same subject and utilizing same technique. For example, there are no less than 15 papers published on Nitinol transitions utilizing the electron transmission or diffraction technique – these papers are collectively referenced in [65]. A number of different structures were reported but resulted in no agreement. As stated in the beginning of this chapter, Nitinol is indeed elusive to characterize. In fact, as mentioned earlier some minor change in the process of alloying can results in a drastically different properties. This is the very reason no one can agree with anything. I can recall back in 1962 when Nitinol phenomenon was beginning to be known, a professor from University of Illinois visited our laboratory and was shown the Nitinol 'memory' effect. He was very impressed and said that as soon as he returned to the University he will make the alloy. A few weeks later he called me to say that they could not make an alloy that show the same effect. This is the very reason, after all these years to this date with all that promising properties; the big industries are simply not in it. Some years back there was a concerted effort made by a group of metallurgists to assemble a 'Data Base' for Nitinol much in the same manner they did for many other metals and alloys. Unfortunately, to this date no 'Data Base' for Nitinol has made its appearance, as far as I am aware of.

These, therefore, are the reason I have avoided a full discussion of the mechanics of the Nitinol transition. For as long as the atomic shear is known to be continuous during the TTR, some one is bound to find a structure at a particular point within the TTR corresponding to his or her experimentation. In view of this dilemma, writing a review article on the subject of Nitinol transition based on one-sided view [66] should be avoided. By this I mean writing a review article on the mechanism of Nitinol transition must be written with a great care or should not be written at all.

REFERENCES

[1] A. Martens, VDI – Zeitschrift 22(1878)205.
[2] L. Guttman, J.Met.Trans., AIME 188(1950)1472.
[3] P.R. Swann and H. Warlimont, Act.Met., 11(1963)511.
[4] L.C. Chang and T.A. Read, Trans. AIME 189(1951)47.
[5] F.E. Wang, A.M. Syeles, W.I. Clark and W.J. Buehler, J.Appl.Phys., 35(1964)3620.
[6] F.E. Wang, W.J. Buehler and S.J. Pickart, J.Appl.Phys., 36(1965)3232.
[7] R.G. Liptai, H.L. Dunegan and C.A. Tatro, Inter.J.Non-Dest.Testing, 1(1969)213.
[8] H.I. Dunegan and C.A. Tatro, Technique of Metals Research , volume V, part 2, Wiley Interscience, New York, (1971).
[9] A.G. Beattie (Ed.), Ultrasonics Symposium Proc., IEEE, New York (1972).
[10] F.E. Wang, Proc.The First Inter.Conf. on Fracture, Sendai, Japan 2(1965)899.
[11] C.M. Wayman, Inrod.to Crystallography of Martensitic Transformation, Mcmillan, New York (1964).
[12] L.D. Landau and E.M. Lifshitz, Statistical Physics, Pergamon Press, London (1959).
[13] H.A. Berman, E.D. West and A.G. Rozner, J.Appl.Phys., 38(1967)4473.
[14] F.E. Wang, B.F. DeSavage, W.J. Buehler and W.R. Hosler, J.Appl.Phys., 39(1968)2166.
[15] F.E. Wang, S.J. Pickart and H.A. Alperin, J.Appl.Phys., 43(1972)97.
[16] 'Selected Papers From the Symposium on TiNi and Associated Compounds,' J.Appl.Phys., 39(1968)2165.
[17] M. Hansen (1938); R.P. Elliot, 1st Supplement (1965); F.A. Shunk, 2nd Supplement (1969), Constitution of Binary Alloys, Mcgraw-Hill Book Co., New York.
[18] H. Magolin, E. Ence and J.P. Nelson, Trans. AIME, 197(1953)243.
[19] D.M. Poole and Hume-Rothery, J.Inst.Met. , 83(1954)473.
[20] G.R. Purdy and J.G. Parr, Trans. AIME 221(1961)636.
[21] P. Duwez and J.L. Taylor, Trans. AIME 188(1950)1773.
[22] M.J. Marcinkowski, A.A. Sastri and D. Koskimaki, Phil.Mag., 18(1968)945.
[23] K. Chandra and G.R. Purdy, J.Appl.Phys., 39(1968)2195.
[24] K.Otsuka, T. Sawamura and K. Shimizu, Phys.Stat.Sol. a-5(1971)457.
[25] A. Nagasawa, J.Phys.Soc.Jap, 31(1979)136.
[26] M.H. Mueller and H.W. Knott, Trans. AIME, 227(1963)674.
[27] M. Bonn, Atomic Physics, Dover Pub.Inc., New York (1989).
[28] W.B. Pearson, Handbook of Lattice Spacings and Structure of Metals, Pergamon Press (1958).
[29] P. Ehrlich, ZAnorg.Chem., 1(1949)259.
[30] H.P. Rookeby, Acta.Cryst., 1(1948)259.
[31] R. Hasiguti and K. Iwasaki, JAppl.Phys., 39(1968)2182.
[32] A.E/ Dwight , Trans.Met.Soc., AIME, 215(1959)283.
[33] F.E. Wang, J.Appl.Phys., 38(1967)822.
[34] F.E. Wang and D.W. Ernst, J.Appl.Phys., 39(1968)2192.
[35] L. Kaufman and M. Cohen, Prog. In Metal Physics, Pergamon Press, New York (1958).
[36] D.P. Dautovich amd G.R. Purdy, Can.Met.Quart., 4(1959)129.
[37] J.M. Ziman, Electrons and Phonons, The Clarendon Press, Oxford (1963); Principles of the Theory of Solids, Cambridge Univ.Press, Cambridge, England (1964).

[38] J.F. Goff, J.Appl.Phys., 35(1964)2919.
[39] B.F. DeSavage and J.F. Goff, J.Appl.Phys., 38(1967)1337.
[40] D.Bradley, J.Acoust.Soc.Amer., 37(1965)700.
[41] W.P. Mason, Physical Acoustic and the Properties of Solids, van Nostrand Co., Inc. Princeton, N.J. (1958).
[42] A.H. Morrish, The Physical Principle of Magnetism, John Wiley & Sons, Inc. New York (1965)
[43] N.F. Mott and H. Jones, The Theory of the Properties of Metals Alloys, Dover Pub.Inc., New York (1958).
[44] N.F. Mott, Can.J.Phys., 34(1956)1356.
[45] J.B. Goodenough, Conference on the Characterization of Materials, Penn Stat.Univ.(1966).
[46] W.J. Bragg and E.J. Williams, Proc.Roy.Soc. A145(1934)669, ibid. A151(1935)540.
[47] W.J. Buehler and R.C. Wiley, Trans.Quart. ASM, 35(1962)269.
[48] W.J. Buehler and F.E. Wang, Ocean Eng., 1(1968)105.
[49] F.E. Wang and W.J. Buehler, Appl.Phys.Lett., 3(1972)105.
[50] N.G. Pace and G.A. Saunders, Phil.Mag., 22(1970)73.
[51] O. Mercier, K.N. Melton, G. Gramaud and J. Hagi, J.Appl.Phys., 51(1980)18.
[52] Y. Kudoh, M. Tokomari, S. Miyazaki and K. Otsuka, Acta Met., 33(1985)2049.
[53] J.R. Schrieffer, J.Appl.Phys., 39(1968)642.
[54] E. Bucher, W.F. Brinkman, J.P. Maoita and H.J. Williams, Phys.Rev., 18(1967)1125.
[55] E.C. Snow and J.T. Weber, Acta Met., 17(1969)623.
[56] C.M. Wayman, Introd. to the Crystallography of Martensitic Tramsformations, MaCmillan Series in Meterial Science, New York (1964).
[57] S. Miyazaki, S. Kimura, K. Otsuka and Y. Suzuki, Scripta Met., 18(1984)883.
[58] F.E. Wang, J.Appl.Phys., 43(1972)92.
[59] F.E. Wang, J.Appl.Phys., 44(1973)3013.
[60] M.V. Klassen-Neklyudova, Mechanical Twinning of Crystals, Consultant Bureau, New York (1964)
[61] M.A. Jaswon and D.B. Dove, Acta Cryst., 10(1957)14.
[62] K. Iwasaki and R.R. Hasiguti, Third Bolton Landing Conf., Lake George, New York (1969).
[63] W.B. Cross, A.H. Kariotis and F.J. Stimler, NASA Report No Cr-1433 (1969).
[64] E. Goo, T. Duerig, K. Melton and R. Sinclair, Acta Met, 33(1985)1725.
[65] M.J. Marcinkowski et.al., Phil.Mag., 18(1968)945; Chandra et al., J.Appl.Phys., 39(1968)2195; Otsuka et al., 62nd Ann.Meet.Jap.Inst.Met.,(1968), Phys.Stat.Sol., a-5(1971)457; Nagasawa, J.Phys.Soc.Jap., 26(1969)1560, ibid. 29(1970)1386, ibid. 30(1971)1505, idid., 31(1971)1683, ibid., 31(1971)136.
[66] S. Miyazaki and K. Otsuka, Development of Shape Memory Alloys, ISIJ, International 29(1989)353.
[67] M.A. Mitchell, F.E. Wang and J.R. Cullen, J.Appl.Phys., 45(1974)3337.

VI. Mechanical Properties

1. BACKGROUND

Physicists regard metals and alloys as a periodic array of ionic cores held together by the 'free' conduction electrons. This concept has already been disputed by the existence of Miscibility Gap in the liquid state as described earlier in chapter I. Furthermore, it can be argued that if the concept is correct, the crystal structures of metals will be solely a matter of packing problem. Thus, the crystal structures of metals at low temperature should all be close-packed such as face-centered cubic or hexagonal close-packed and at high temperature should become less close packed structure such as body-centered cubic. But, the experimental evidence does not follow this trend. For example, lithium (Li) metal has a hexagonal structure at low temperature (inter-atomic distance of 3.11 A) but has a body-centered cubic structure at high temperature (inter-atomic distance of 3.02 A). Further, the concept is placed in a serious doubt by the fact, the melting temperature of element metal, can vary from one metal to another by as much as thousand times (e.g. Hg at –38 °C vs. W at 3410 °C). For, if free electrons are the only contribution to the cohesive energy of metals, the melting temperature of metals cannot vary by this magnitude. This much difference cannot be reconciled in term of the 'free'- electron density, which differ from one metal to another only within an order of magnitude.

In fact, there are no other physical parameters, (such as electro-negativity, atomic radius, atomic number, dielectric constants, electrical conductivity, specific heat etc), differ by this much. If the structure of metals were indeed a collection of periodically aligned ionic cores in a sea of free electrons, the treatment of metals can be done with the *kinetic theory of gases* instead of the *many body problems.* This is to say that the motion of each ion is not independent but rather depends on that of every other ion linked to it by the network of 'bonds'. This brings about the mode of atomic vibration in terms of 'phonon' vibration [1]. Because the phonon vibration was needed to explain how conduction electrons are scattered by the 'phonon' vibration and subsequently the temperature dependence of electrical conductivity. In fact, phonon dispersion curves, whether by the Einstein model or the Debye's model [2], are utilized in the theoretical calculation of heat capacity. But, throughout the treatment of solid-state physics, there are no other mention of the potential relationship between the mechanical properties (such as the tensile strength, Young's or shear modulus, fracture toughness, or hardness etc.) and the free electron model they proposed for the same material.

In sharp contrast, metallurgists are very interested in the mechanical properties of metals and alloys. Once they discovered the dislocation, which they can actually see and measure, the Dislocation Theory was quickly formulated — unfortunately without electrons. However, in spite of this shortcoming, the Dislocation theory served to explain nearly everything from plasticity to hardness to the melting temperature of metal [3]. Since it explains everything, the result is that it predicts nothing — or predicts wrong. For example, a huge discrepancy exists between the theoretical calculation and the observed shear strength of a material. The theoretical strength based on the Dislocation theory for Aluminum with a modulus of about 3×10^{11} dynes/cm^2 is in the order of 10^{11} dynes/cm^2. And yet, single crystals of aluminum can be deformed at stresses as low as 3×10^6

dynes/cm^2, a discrepancy from the theoretical model in the order of $\approx 10^5$! According to Weertmans [4], this discrepancy was simply mentioned as "A discrepancy of 10^5 or so between what we think should happen and what actually happen will always stimulate the curiosity of men." The basic problem is that it deals only with atoms and completely ignores the electrons. The situation of the Dislocation theory is much similar to the days when chemists were describing chemical bonds with 'hands' instead of electrons. It was not till the chemists began to deal with electrons in terms of covalent bonds that they have the success of not only explaining what is observed but also predicting the thing to come.

Let us see if we can illustrate the problem in terms of two-car collision. One day, two cars collided at an intersection. The police department was duly notified and officers were dispatched to investigate the collision. Officers measured the skid marks and noted the direction of the skid marks and their lengths. Based on these data police department did come to a conclusion that the car A and the car B were coming together at such speed and in such direction. From these data they were able to determine which car was traveling at excessive speed and which driver was at fault etc. However, the most important factors, as far as to prevent further occurrence of such event, could not be obtained from these physical measurements. For example, the reason for the collision may be: a) driver A was drunk; b) driver B may be color-blind so he did not see the red-stop light. c) Driver B fell asleep on the wheel, d) driver A had a stroke and lost the control, e) driver B was committing a suicide etc. All these reasons cannot be obtained from the physical measurement of tracks (or dislocations?). This is to say that the physical observation of skid-marks (dislocations) alone is not enough. Only by incorporating the electrons the basis for the mechanical properties can be known. The fact that an aggregate of carbon atoms can assume the form of diamond, graphite and charcoal or fullerenes is entirely due to their electronic configuration and certainly not because of their atomic arrangement.

On the other hand, chemists were only interested in chemical reactions, which do not involve moving free electrons or atomic arrangements in terms of dislocations. Their sole interests were limited to corrosion of metals and alloys understood in terms of oxidation and reduction processes. These studies were useful in predicting what metal might be suited for building batteries or how to prevent corrosions. Metallic corrosion involves the loss of electrons by a metal with the electrons absorbed usually by some chemical. Most metals were assigned a chemical- potential, which is equated to the corrosion reactivity. Again, there was no effort made to understand the relationship between these chemical reactivity and the mechanical properties of the metal. The chemists' view of metallic bonds are based on alternating covalent bonds or multi-centered covalent bonding much as what is happening in benzene ring, H_3^+, or boron-hydrides where three boron nuclei sharing one covalent bond.

2. GENERAL MECHANICAL PROPERTIES

For metallic material, the mechanical property can be illustrated in a stress-strain curve typified by that of iron as shown in Fig. 1-(a). The curve is a plot of stress in pounds per square inch versus strain, usually measured in inches per inch along the x-axis. The portion of the curve, starting with zero stress up to yield stress, is elastic in that upon the release of stress the strain will revert to zero and of is known as the Young's modulus of elasticity. Further increase in stress beyond the yield stress will result in non-recoverable strain. The stress in this portion is known as tensile strength and the region is known as plastic region. Further increase in stress may result in a "necking-down" of the material and ultimately lead to fracture. This is known as ultimate tensile strength. The reason for the lower stress at breaking point is because the contraction of the material prior to breaking is not taken into computation for the stress. Thus it is not a true stress.

Fig. 1-(b) shows a stress-strain curve for a brittle material such as non-metallic material, (the material that does not conduct electric current), or an intermetallic compound, such as TiFe for which failure occurs before any appreciable plastic deformation. Thus, there is no yield stress or plastic deformation. The fracture strength is essentially at the elastic limit or the yield stress.

Toughness or Impact Strength is a measure of the amount of energy a material is capable of absorbing without breaking. In general, in order to absorb a fair amount of energy in impact, a material must either be highly elastic or ductile. Concurrently, the ultimate strength of the material must be high. A combination of these two properties makes an extremely tough material. Thus analytically the toughness of a material can be estimated from the total area covered under the stress-strain curve, the wider the area the tougher is the material. For example, brittle material as shown in Fig. 1-(b) would have a very small area, therefore has no toughness or impact strength. The units of toughness are given as foot-pounds of energy absorbed by a given size of specimen.

Hardness is the resistance to plastic deformation. This property is usually related to the resistance to wear and abrasion. Experimentally, it is observed that for a given material, the hardness is roughly proportional to its tensile strength.

3. MECHANICAL PROPERTIES IN TERMS OF COVALENT BOND AND FREE ELECTRON BAND

It is essential at this point to recall some of the fundamental bonding theory laid out for metals and alloys in the very beginning that:

(1) Covalent bond and free electron band coexist in metals and alloys.
(2) The ratio of covalent bond / free electron band is a fixed value for a given metal or alloy for a given crystal structure. This ratio may be upset momentarily but the nature of bonding is to restore this ratio as soon as possible.

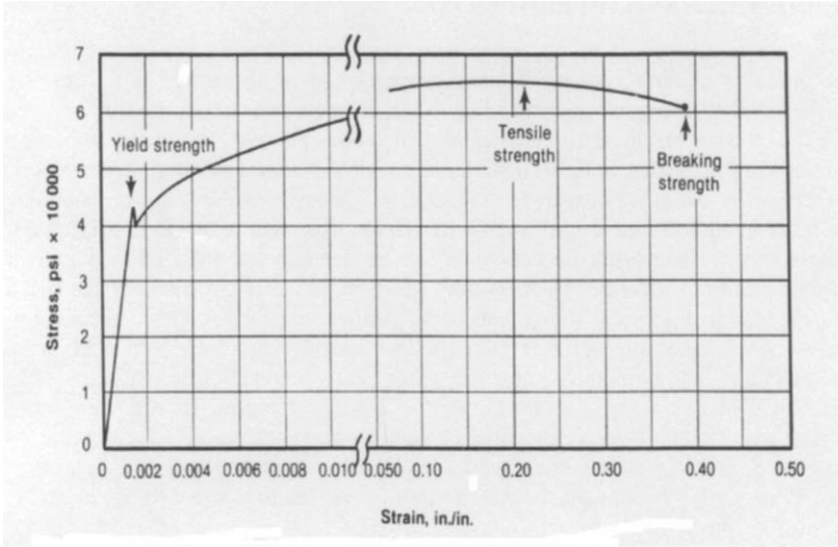

(a)

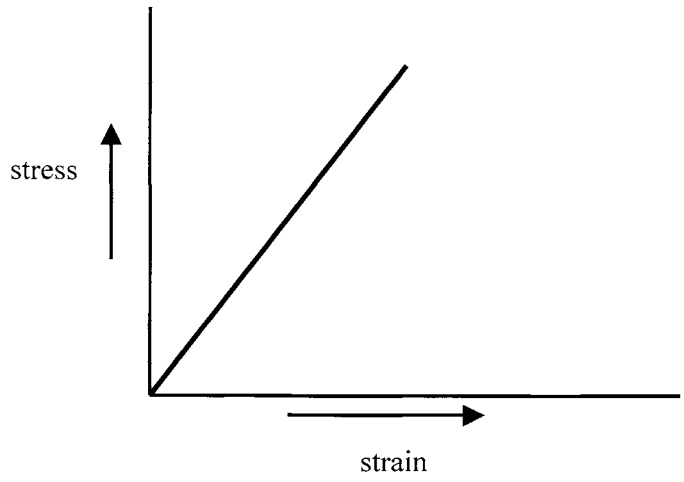

(b)

Fig. 1-(a). Stress-Strain curve of iron (Fe) containing 0.15 wt. % carbon (C) at room temperature; 1-(b). Representing material without conduction band; no plastic region, and is brittle.

(3) Covalent bonded electrons are bosons and a large number of bonded electrons can occupy the same energy level. Free electron band, on other hand, consists of fermions and therefore according to Pauli Exclusion Principle no two electrons can occupy the same energy level. This is the reason they exists in a band

Now, we shall define an energy gap between covalent bond and free electron band as ΔE. All metals and alloys with covalent bond and free electron band shall have its ΔE, the magnitude of which shall depend on the degree of separation between its covalent bond and its free electron band. The free electron band energy is usually obtainable through its band structure calculation. The Brillouin zone boundaries forming a cage are dictated by the crystal structure in terms of $\bar{a}, \bar{b}, \bar{c}$ vectors. Our interest here, however, is not in the detailed calculation of energy bands but rather in establishing a general relationship between the electron energies and the mechanical properties. In our theory, the mechanical property as a whole can be related to the three electronic energy parameters:

a) The energy gap, ΔE between covalent bond and free electron band (as illustrated in Fig 2) and
b) The energy needed to break covalent bond, ΔE and finally,
c) The shape of covalent bond energy potential (Fig. 3).

We shall see how these three electronic energy factors can be related to the mechanical properties.

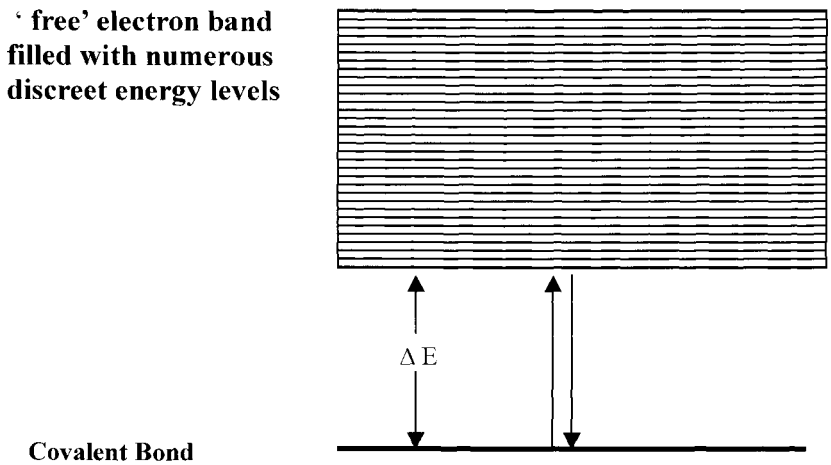

Fig. 2. Pictorial illustration of an electron pair transfer from covalent bond to free electron band and back to covalent bond

3.1. Elasticity (Young's, Shear, and Bulk Modulus)

This part of mechanical property has nothing to do with the free electron band itself. This property has to do only with the shape of the covalent bond energy curve up to the shaded area (Fig. 3) where the potential energy curve is symmetric from the equilibrium interatomic distance, R_0. As stress is applied to the material and atoms are forced to move away from its equilibrium position the potential energy of the bond will be elevated upward. As long as the energy level does not exceed the shaded area, on releasing the stress the potential energy will drop back to the equilibrium state and the material will restore to the equilibrium position. This characteristic therefore represents the relationship between elastic modulus and the shape of the covalent bond energy curve. This interpretation is possible only if we agree that covalent bonds exist in metals and alloys. To demonstrate that this relationship is correct, we invoke the following example.

The modulus of a material being dependent on the shape of its energy potential-well, two curves corresponding to two different types of covalent bonds are shown in Fig. 4. The #1 potential well is shallow and wide whereas #2 has a deep and narrow potential well. Consequently, the elastic constant and modulus for the two cases will be different and so will be their moduli. Because covalent bond can vary in so many ways – from saturated to unsaturated bond or multi-bond with or without conjugation or hybridization etc [5], the strength of covalent bond particularly in a metal cannot be estimated or easily calculated [6,7]. Another fact to bear in mind is that the covalent bond is sensitive to temperature change. Thus, elastic moduli for metals invariably undergo changes as a function of temperature. In fact, Young's modulus is observed to decrease with increasing temperature. This s not surprising in that the covalent bond potential will change its shape to a shallower potential well with increase in temperature. This results in a continuous decrease in Young's modulus as a function of temperature as shown in Fig.5. In an extreme case one set of covalent bond may change to another set such that an abrupt change in modulus may result due to the crystal structure change. This is observed in Fe(iron) shown in Fig. 5 when iron(Fe) with bcc structure transforms into a fcc structure. The fact that covalent bonds are anisotropic and strongly dependent on the crystal structure, the modulus is expected to be anisotropic as well according to the structure — and is so observed experimentally (Table 1).

Further experimental support of this view comes from the following reasoning and experimental evidence. The depth of the symmetrical potential energy curve shown in Fig. 3 will be deeper if the covalent bond is stronger, i.e., the interatomic distance is shorter. The deeper energy potential means higher modulus. With this line of reasoning, we conclude that the shorter lattice constants can be equated to the shorter interatomic distance for the same crystal structure. Figure 6 is a plot of Young's modulus against the inverse of lattice constants for eight metallic elements with fcc crystal structure showing support for the theory.

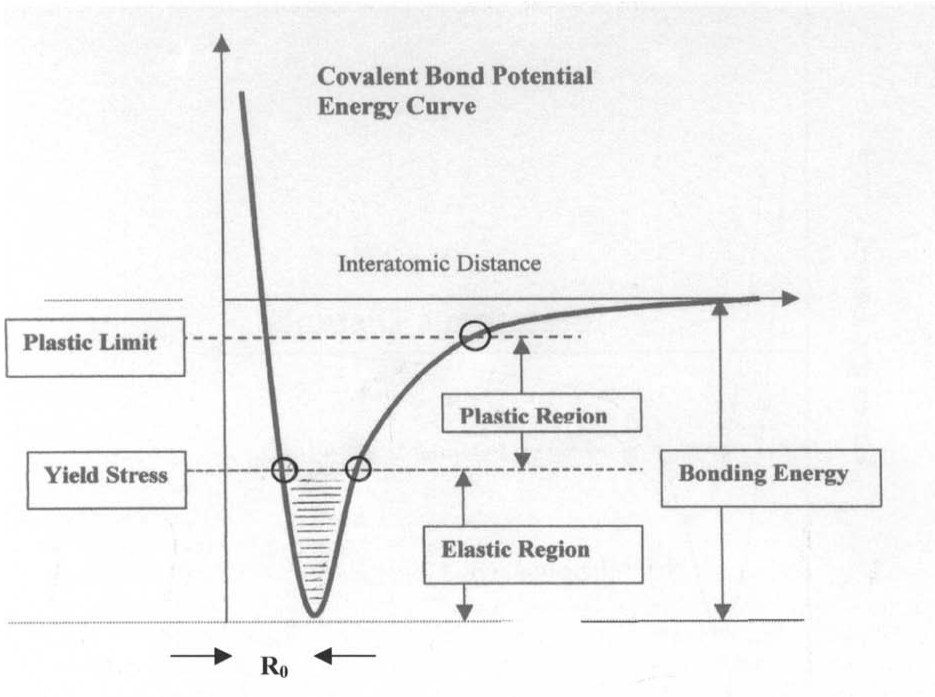

Fig. 3. Two-dimensional representation of Covalent bond potential energy curve.; Subdivided into three regions: Elastic region where the curve is symmetric with respect to R_0, Plastic region where the curve is asymmetric and affect only on the side of R greater than the yield stress. Beyond plastic limit the atoms physically breaks away

3.2. Yield Stress

By definition, yield stress demarcates the point beyond which the material looses its ability to elastically return as shown in Fig.1(a). Thus, beyond this point the material is plastically deformed. From the electronic bonding point of view, this demarcation correspond to the upper limit of the energy potential well where the energy curve begins to deviate from symmetric shape (see Fig. 3). It must be emphasized that it is not the mechanical strength required to break the covalent bond completely but rather the stress required to move beyond the symmetric portion of the potential curve.

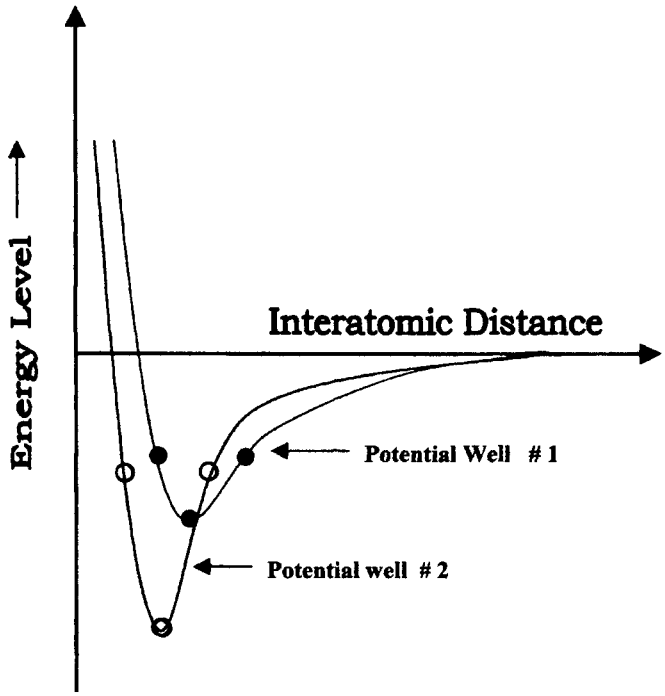

Fig. 4. Two examples of covalent bond potential well: # 1 being shallow well whereas # 2 being deep well. ○ and ● Circles indicate the approximate elastic limit.

3.3. Plasticity (Ductility)

This region of mechanical property corresponds to the potential energy in the region beyond yield strength where the potential energy curve becomes asymmetric on the left and on the right of the position R_o. Once, the potential energy is raised into this region, it is not recoverable to R_0 position. The covalent bond pushed to this region can best be described as in an 'excited' state. In my opinion, this is equivalent to the 'free radical' in covalent bonded compounds [7]. Sometime this state is referred to as 'free valence' [8]. For example, at high temperature, ethane can thermally decompose by *homolytic* bond fission.

$$\mathbf{CH_3{:}CH_3} \rightarrow \mathbf{2}\,\mathrm{CH_3^{\bullet}}$$

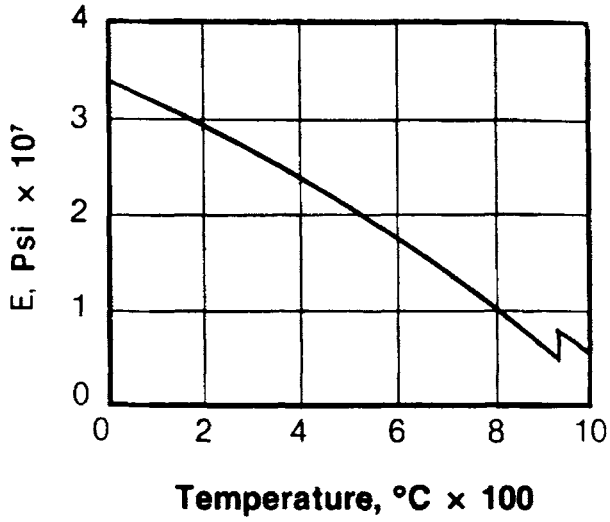

Fig. 5. Young's modulus versus temperature in iron. Notice the continuous decrease as a function of temperature. The abrupt change in modulus when bcc iron transforms to fcc.

Table 1
Anisotropic Young's Moduli in Metals (ksi)

Metal	<111>	<100>
Aluminum (fcc)	11	9
Copper (fcc)	28	10
Gold (fcc)	16	6
Iron (bcc)	41	19
Lead (fcc)	4	1
Tungsten (bcc)	57	57

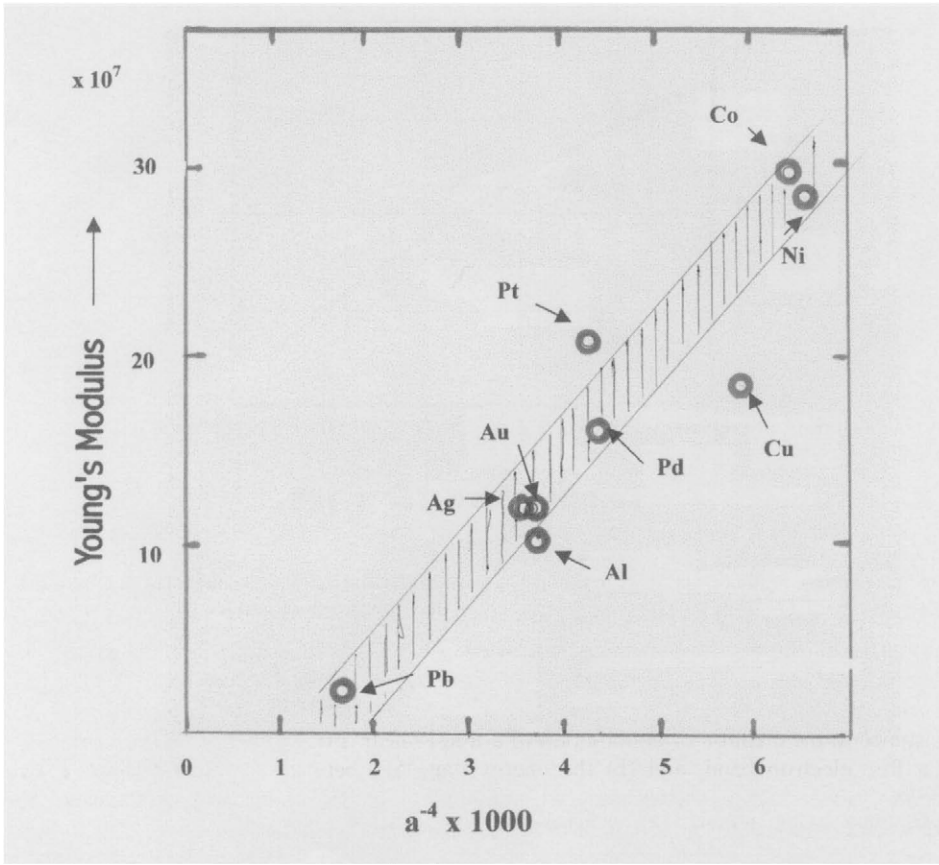

Fig. 6. Relationship existing between Young's modulus and their lattice constants for elements with fcc crystal structure.

A fragment such as $CH_3^{\bullet}$ carrying an odd electron is known as *free radical.* Similarly, we can consider covalent bond in metal brought to the 'excited state' as 'free radical' that gave_up one electron to the free electron band (see Fig. 7). Thus, the formation of free radical in a material under stress is possible only if there is a conduction band to absorb the extra electron. This will result in an upsetting of the electron ratio (between covalent bond and free electron band) due to such electron transfer. However, this may be remedied by another 'free radical' somewhere in the crystal to restore to a non-free radical state by absorbing an electron from the conduction band. Since free radicals are created by externally applied stress, it is to be expected that the greater is the stress the more in number of free radicals are created. The free radicals are expected to be concentrated along

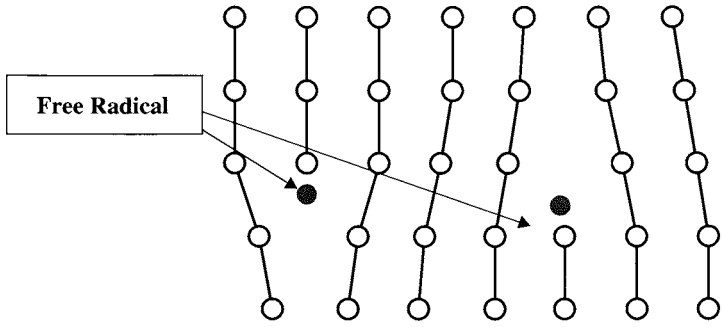

Fig. 7. Pictorial representation of 'free radical's in a metal matrix. • represent single electron radical.

the area of high internal stress; such as micro-crack, impurity concentration, twin-boundary, antiphase boundary, grain boundary etc.

In general, one can make the observation that the greater is the number of free electrons the wider will be the free electron band width (due to Pauli Exclusion Principle). Subsequently, the wider is the band the smaller is the ΔE. A large percentage of free electrons also mean a small percentage of covalent bond electrons and will results in a weaker covalent bonding. Thus, it is easier to form free radicals. As shown in Fig. 2, the resistance to the creation or annihilation of a free radical is dependent on: (a) the existence of a free electron band, and (b) the energy gap, ΔE, between covalent bond and free electron band. Since the creation or annihilation of free radicals is equated to the mechanical plastic deformation, following conclusion can be made.

3.3.1. **For a material without free electron band there would be no ductility**, i.e., the material shall have no plasticity and fracture at the yield stress. This type of material includes all organic, inorganic, ceramic material that do not have electronic conduction band. This results in no possibility for creation or annihilation of free radicals.

3.3.2. **For material with small amount of free electron and subsequently a narrow conduction band, the plastic region will be very small,** i.e., the material will be brittle and weak in impact strength or toughness. This type of material includes intermetallic compounds or n-type semiconductors.

3.3.3. **For material with good conductivity (i.e. with wide free electron band) shall be very ductile.** This is due to their small ΔE and less resistance to plastic flow. These materials include high conductivity material such as: Ag, Cu, Au, Fe, and alkali metals.

A rough estimate of the number of free electrons in a metal can be made based on its electrical conductivity. In general, high conductivity means having more free electrons (i.e., smaller ΔE) and less electrons for covalent bond (i.e., easier to form free radicals) and results in the material being softer and more malleable. Conversely, a material with low conductivity means having less free electrons and therefore having stronger covalent bond (less likely to form free radicals) and will be less malleable and more brittle.

Experimentally, an intermetallic compound, A_xB_y, formed between A and B takes up more electrons for covalent bonding, and results in the stronger ΔE. At the same time there will be less free electrons and the band will be narrower and the ΔE will be larger as well. The result is an intermetallic compound of A_xB_y will most likely be more brittle and less malleable than the element A and/or B. This is observed experimentally. Another example is seen in the mechanical properties of the series of $TiNi_x$ (Co_{1-x}) and $TiCo_x$ (Fe_{1-x}) alloys (where $x = 0 \sim 1$) as shown in the previous chapter (Fig. 8). The idea is that starting with TiFe certain numbers of electrons, Nc, are covalent bonded. But, with the total number of valence electrons, Nv, being equal to N_c (covalent bonded electrons) plus N_f (free electrons). And Nc shall remain constant, because covalent bond can only take a

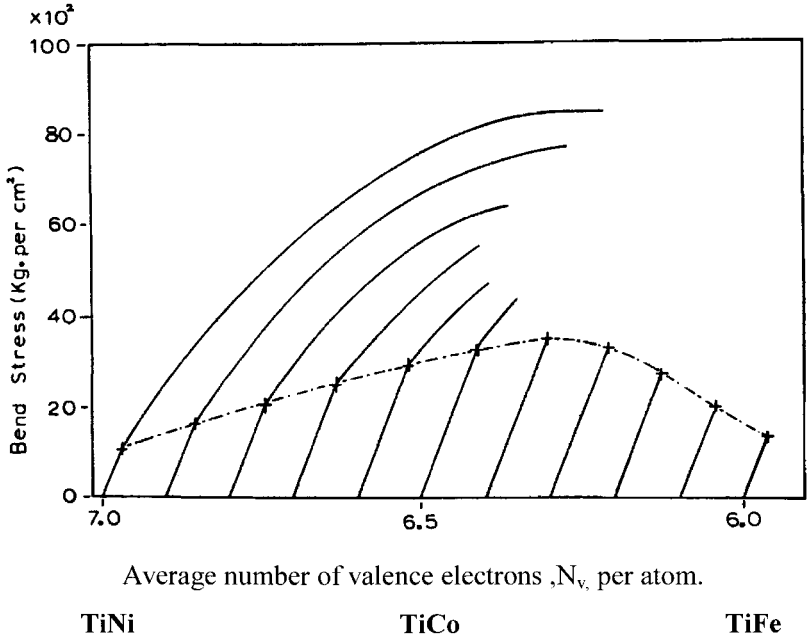

Fig. 8. Demonstrate the change from ductile TiNi to semi-ductile TiCo to totally brittle TiFe and the alloys in-between.

constant number of electrons, the increase in N_v due to the substitution of Co for Fe can only lead to an increase in, N_f (free electrons). This trend continues when Co is replaced with Ni. The result is a continuous increase in the number of free electrons, N_f, which is reflected in a continuous increase in the ductility of the alloy as shown in Fig. 8 (reproduced from Chapter V- NITINOL). It should be pointed out that the crystal structure of TiFe, TiCo, and TiNi are all identical, being CsCl-type or bcc (in disordered state) with unit cell dimensions practically the same [7]. Therefore, mechanical properties of alloys and their free electrons can be compared directly with validity.

As stress is increased, there would be more free radicals created. But, then comes a saturation point at which further creation of free radicals is no longer possible. This is the point of plastic limit. Any increase in stress beyond this point then lead to material fracture. Ability to convert covalent bonds into free radicals by giving up one electron, which is deposited in the free electron band, is in essence the basis for plasticity, ductility or malleability. Within this understanding, the degree of ductility shall be dependent on ΔE (as shown in Fig. 2) and the shape of the potential energy curve, particularly in the region where the energy curve is asymmetric. Still, it should be emphasized that at this point free electron energy band is only indirectly involved in the mechanical property. Concentration of free radicals can be reduced substantially through 'annealing.' Annealing is a process of heating a metal to an elevated temperature and hold the metal at that temperature for a length of time. In our view, this process allows free radicals to restore to normal covalent bonding by having two radicals to come together or by abstracting one electron from the free electron band. Thus mechanically the metal would be soft again and restore the malleability.

3.4. Ultimate Tensile Strength

This refers to the stress at which material breaks in a stress-strain curve. From electronic point of view this is equivalent to the stress that leads to a complete breaking of covalent bond (Fig. 9) such that physically covalent bond cannot be restored. When a cylindrical piece of metal is stressed uniaxially in a testing machine, it stretches elastically at first until the yield stress is reached. As shown in Fig. 9 this energy is designated as ΔE_1. Further stress, in our theory, creates internally free radicals of covalent bonds and externally exhibiting plastic deformation of the metal, usually by necking down, which leads to a moderate decrease in the cross-sectional area. We shall term this energy between 'yield strength' and 'free radical' as ΔE_2. Further increase in stress is accompanied by continuous increase in free radicals. At some point the concentration of free radicals reaches a maximum and further increase in stress causes certain 'free radicals' to break off completely. This, in turn brings about an abrupt increase in stress that causes further breakage of free radical – creating a 'domino effect' and results in a catastrophic fracture of the metal. This energy difference between 'free radical' and 'breaking of bonding' shall be ΔE_3. Since the energy level of free radical is already very close to the upper limit of the energy curve, the tensile strength is usually close to fracture tensile strength.

3.5. Melting Temperature

In considering melting temperature of a metallic element, it was discussed in detail in chapter III that it is the point at which liquid and solid state coexist in equilibrium. This implies, the thermal energy is sufficient at this point to break covalent bond energy, ΔE. But how large is ΔE ? From Fig. 3 one can say that generally speaking there is a one to one relationship between the covalent bond energy and the modulus of the material. And if this was true and our conjecture is correct, there should be a direct relationship between the melting temperature and the modulus of the material. This relationship is shown in Fig. 10, where the melting temperature is shown to be directly proportional to the modulus (again, limiting to the same structure type).

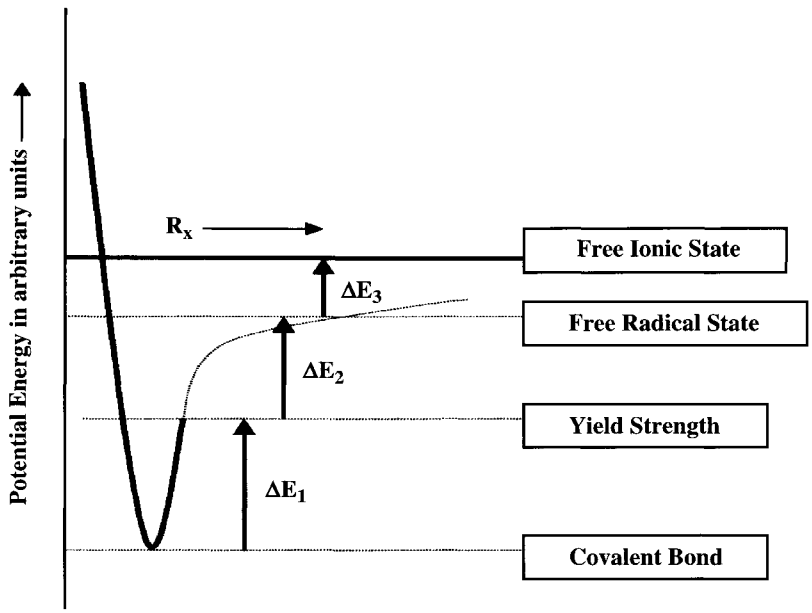

Fig. 9. Revised potential energy curve reflecting the energy jump beyond the yield strength. ΔE_1 is the energy difference between Covalent bond and Yield Strength (elastic region) ; ΔE_2 is the energy difference between Yield Strength and Free Radical State (plastic region) ; ΔE_3 is the energy difference between Free Radical State and Free Ionic State (complete breaking of bonding). Therefore, $\Delta E_1 + \Delta E_2 + \Delta E_3$ = Bonding Energy.

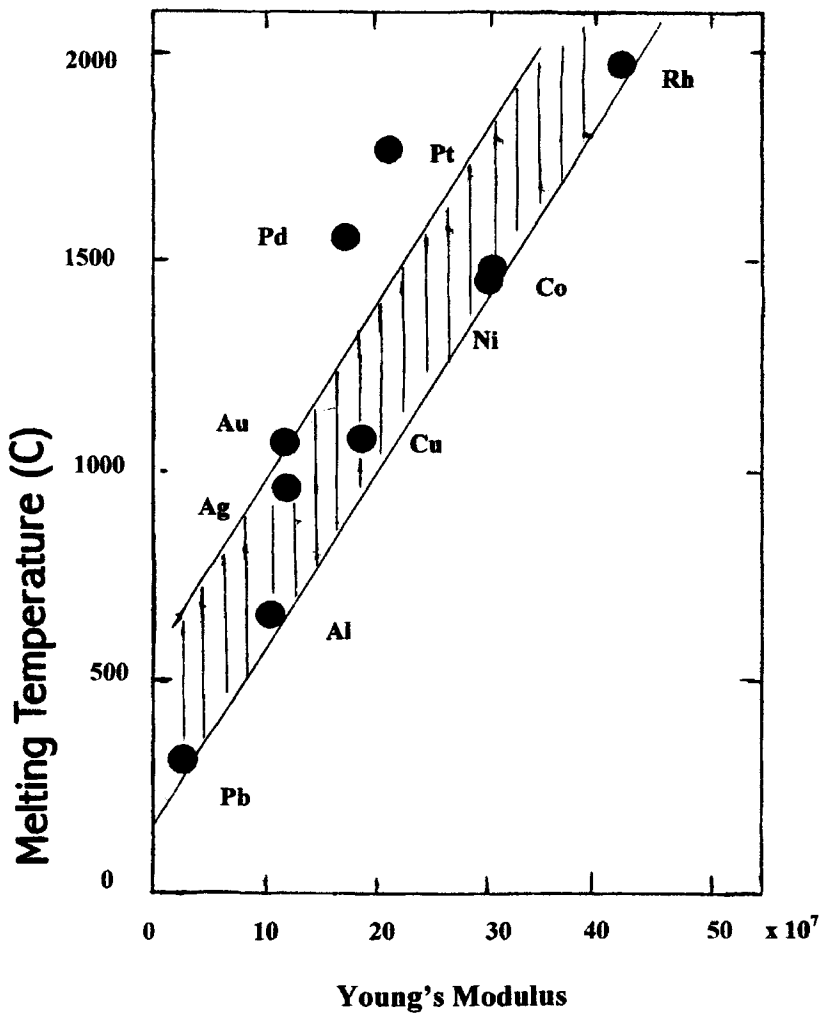

Fig. 10. Plot of melting temperatures of metal elements against their Young' s moduli.

3.6. Boiling Temperature

If covalent bonds are broken at melting point the liquid metal above this point will be truly held together by the 'glue' called free electrons. Thus, beyond melting point up to boiling point, the material's cohesive energy will be totally dependent on the free electron concentration. At the boiling point the kinetic energy of the ions essentially overcome the cohesive energy of the free electrons and boils off into vapor. Within this picture, the ΔT, the temperature difference between the melting point (T_m) and the boiling point (T_b), must be proportional to ne, the number of free electron per unit volume. To ascertain this prediction, the ne is obtained through the measurement of Hall coefficients. With the inverse of Hall coefficients being directly proportional to the ne, number of free electrons per unit volume can be known from published Hall coefficient data. Thus, ΔT ($T_b - T_m$) can be plotted against ne. Such a plot for 14 metals is given in Fig. 11.

Considering the fact that: (1) the Hall coefficients were obtained from bulk material and that (2) the Hall mobility was assumed to be the same for different bands, the rough agreements as shown in Fig. 11 is rather impressive. Obviously we do not know how to treat the metals showing a positive Hall coefficient without a detailed knowledge of the band structure involved. Therefore, the metals with positive Hall coefficients are not included in the statistical tabulation.

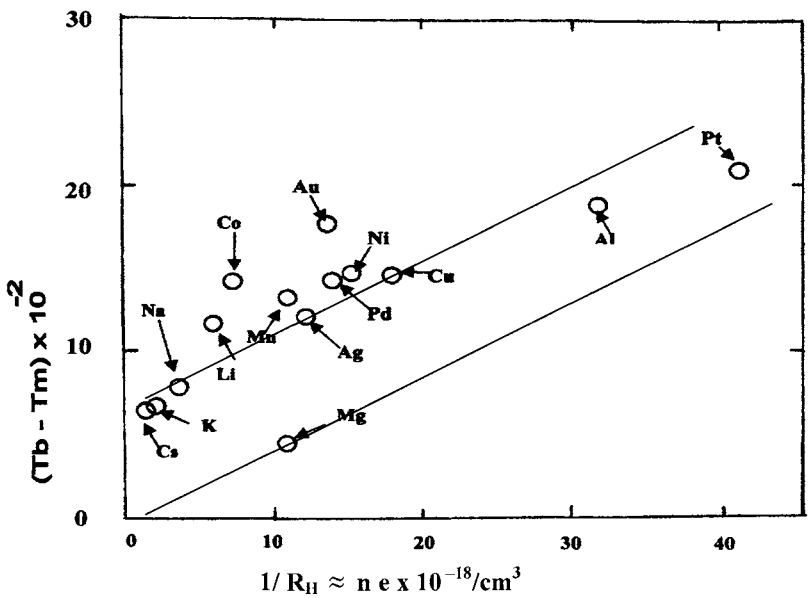

Fig. 11. Tb – boiling point; T_m – melting point R_H – Hall coefficient; ne – number of free electrons per unit volume.

4. LIQUID METAL EMBRITTLEMENT (LME)

There is a phenomenon, known as 'Liquid Metal Embrittlement' (LME) in which a metal or an alloy becomes brittle, with or without stress, when it is coated (wetted) with a liquid metal. This phenomenon has been known for more than fifty years. Although the phenomenon may not have been known widely, it attracted many investigators. The most recent overview of experimental evidence and theories proposed for LME are summarized in the Applied Physics of the European Physical Journal [12]. According to this review article, " a qualitative_explanation of LME has not yet emerged and its prediction is still missing despite decades of research." We shall show how, in the context of the covalent bond plus free electron band view, this phenomenon can be understood, at least, qualitatively. To begin, we shall list the experimental facts observed and agreed on by most investigators on LME phenomenon.

4.1 Principal Observations in LME

4.1.1. One of the most striking characteristics of LME is a very high crack propagation rate compared with the rate in air or vacuum. The rate may vary from one system to another, but they all fall in the range of a few centimeters to several meters per second [13,14].

4.1.2. In every LME system, strain to rupture is drastically reduced compared to that in air or in vacuum. This loss of ductility appears to be limited to a particular temperature range known as "ductility trough". An example of this phenomenon is shown in Fig. 12 [15]. The lower limit of this 'tough' is close to the freezing temperature of liquid metal (Hg) and the upper limit is at about 160° C. Above 160° C the ductility appear to restore to the value that is similar to that in air or vacuum.

4.1.3. Below yield strength of the metal, coating of liquid metal has no effect whatsoever on the mechanical properties of the metal.

4.1.4. Should there be intermeallic compound formation between the solid metal and the liquid metal, no embrittlement is observed.

4.1.5. If the contact between the metal and the liquid metal is intervened by the presence of an oxide film or similar material, or by removal of the liquid metal after preliminary contact, LME does not take place. In short, 'wetting' is a necessary condition for LME to occur.

4.1.6. The composition change in a binary liquid metal often asserts significant change in LME. The results can be either a decrease or an increase of the embrittlement. In sharp contrast, the change in the composition of solid metal leads to little or no effect on the embrittlement. The effect due to composition change in solid metal is often found around grain-boundaries [16].

4.1.7. LME is enhanced by an increase in grain size. At the same time the brittle to ductile transition temperature is increased by an increase in grain size.

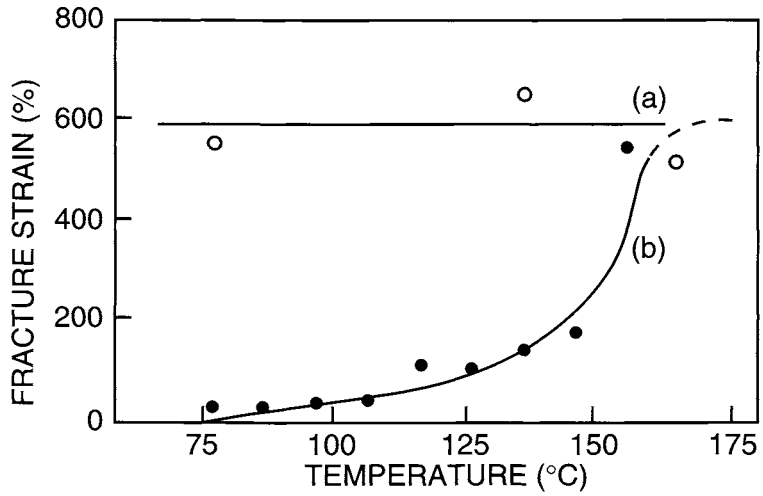

Fig. 12. Dependence of zinc single-crystal fracture strain on temperature and environment: (a) air,(b) mercury (after Rozhanskii et al. – ref. 15)

4.2 Theory vs. Observation

As the name implies, the phenomenon is based on coating a solid metal with a liquid metal. In our theory, liquid metal (being above its melting temperature) has no covalent bonds and the free electrons essentially provide the cohesive energy. It can be recalled that this was the basis for obtaining the correlation (Fig. 11). Thus, by coating **a** metal that has a distinct ratio of covalent bond over free electron band with a liquid metal that has only free electrons (no covalent bond) can have no effect whatsoever in the ΔE_1 (for these notations refer to Fig. 9) which has to do only with covalent bond. This is the observation of 4.1.3.

The fact that LME can take place only when there is a good contact between the metal and the liquid metal – observation.4.1.5 – means free electrons must be free to move from solid metal to liquid metal and vice versa. This logically means the phenomenon of LME is due to the change in the free electron density in the solid metal under the influence of the free-electron density in liquid metal. Our task is to characterize: a) the type of change, b) the type of mechanical effects (based on the theory proposed here) that can come from such a change and c) comparison between these theoretical intuitions against the experimental evidence to see how they fit together.

First, we can state with reasonable certainty that the density of free electrons in liquid metal, $N(e)_L$, must be higher than the density of free electron in solid metal, $N(e)_S$. That is, $N(e)_L > N(e)_S$. With the coating of liquid metal on solid metal, free electrons are now free to roam in the new system composed of liquid metal on the surface and solid metals in the bulk. This leads to a new electron density, $N(e)_N$, which shall be lower than $N(e)_L$ but will be higher than $N(e)_S$. This is pictorially illustrated in Fig. 13. Consequently, the Ratio (covalent bond / free electron band) for the solid metal is upset with more free electrons than that dictated by the ratio. This makes it difficult (and even impossible depending on the magnitude of increase in free electron density) for covalent bonds to transform into free radicals, which as stated above is the essential factor for creating ductility. This is because the covalent bond → free radical process requires release of free electrons whereas the free electrons in solid metal is already increased to $N(e)_N$ through the introduction of free electrons from the liquid metal. Therefore, further increase of free electrons by any other processes is rather difficult. This situation is similar to solid metal (without liquid metal coating) with its ductile elongation stretched to near its limit, i.e., with the concentration of both the free radicals and free electrons are near its limit and further stretch will only results in a fracture.

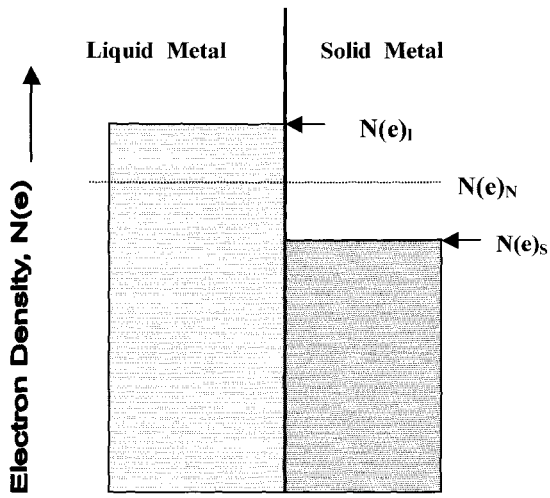

Fig. 13. Electron density, N(e), in arbitrary units of liquid metal and solid metal before contact (shaded) and after contact (the level is shown with dotted line) is pictorially shown.

Within this understanding, it is easy to see why LME phenomenon does not take place if and when inter-metallic compounds are formed between liquid metal and solid metal (observation 4.1.4.). For, there would be no direct free electron flow between liquid metal and solid metal and subsequently there would be no upsetting of the fundamental Ratio (covalent bond / free electron band) and therefore no LME phenomenon.

The 'ductility trough' observed in 4.1.2. is bordered by the freezing temperature of liquid metal at lower end and a certain high temperature end (somewhere below the melting temperature of solid metal). The low-end-limit where liquid metal freezes into solid is easy to understand with the same logic as that of forming an intermetallic compound. For at this point, abundance of free electrons disappears upon solidification of liquid metal. And the density of free electrons in solid, $N(e)_S$ is no longer affected. The high temperature limit of 'ductility trough' I believe should correspond to a decrease in the elastic modulus of the solid metal. It should be recalled that the decrease of elastic modulus with increase in temperature is typical for metals as shown in Fig. 5. It is my belief that at about 160° C, where the ductility of Zn in LME system is shown to be the same as that in air, the elastic modulus of Zn becomes near zero. Essentially, the decrease of elastic modulus is equivalent to a decrease in ΔE_2 such that at the temperature where elastic modulus becomes near zero, the ΔE_2 also become negligible. Under this circumstance LME effect disappears. This essentially is the theoretical picture of the 'ductility trough' in LME.

Another important observation lies in the change of liquid metal composition through doping with another liquid metal– 4.1.6. This appears to have a significant consequence in the phenomenon of LME by either increasing or decreasing the degree of embrittlement. In the context of present theory, this observation is easity understood. For by changing the composition of liquid metal, the free electron density in liquid metal is altered. This in turn shall influence the equilibrated electron density, $N(e)_N$, of the solid metal and leads to an increase or decrease in the degree of embrittlement. Checking the electron density in liquid metal before and after the doping can easily test the validity of this logic. The prediction is that the brittleness should be directly proportional to the value of free electron concentration. At the same time the limited effect of solid metal composition in LME can also be understood – because it does not influence the ratio of covalent bond to free electron band.

Finally there is the observation of grain-size effect – observation 4.1.7. It should be pointed out that the free electrons may not be shared by all grains due to lack of good contact at the grain boundary. As a result, the smaller are the grain size the probability of grains being isolated from the bulk increases. Because of this isolation, the grains that are isolated from conduction band are not affected by change in the ratio (covalent bond over free electron band) brought about by liquid metal and therefore not embrittled. This is, therefore, a statistical matter and shall be based on the average grain size.

In summary, LME in my view is due to the upsetting of the Ratio of covalent bond to metallic band and resulting in an increased difficulty in the creation of free radicals. This takes away the ductility and results in brittleness. In this context, one can venture to predict that if solid metal is coated with a 'liquid metal' whose electron density is less than that in solid metal, solid metal may become free electrondeficient and may actually facilitate the creation of free radicals. In this case an enductilement may result in lieu of embrittlement.

5. SUPERPLASTICITY

An unusually high ductility was first observed in (α + β) brass by Bengough in 1912 [17]. Subsequently, Jenkins [18] reported more than 300 % elongation in the eutectics of the Cd-Zn and Pb-Sn systems. Superplasticity of 1950 % was obtained [19] in 1934 on a Sn-Bi eutectic alloy. From that time on to this date, a series of alloys have been found to possess this property [20] as shown in Table 2 [21]. Thus far all the materials of binary systems that exhibit superplasticity are experimentally found to be falling into two categories: a) their alloy composition falls either at eutectic or eutectoid and b) an intermetallic compounds such as Ni_3Si [22] and Ni_3Al [23] that are formed peritectically. In a recent review article by Chokshi et.al [24] some ceramics were also mentioned as another category of material that exhibit superplasticity. Since the theory being presented in this book is about metal and alloys therefore I would not extend my discussion on this category of material. However, it should be mentioned that the authors [24] agree based on their own criteria that the basic mechanisms operating in ceramics are different from those in metallic systems. Thus, whether these materials fall in the definition of superplasticity is also open to question. Further, the ceramic systems that exhibit degrees of superplasticity were tested at 1923°K temperature. Are not all material become 'superplastic' to certain extent if the temperature is high enough?

Naturally, a number of phenomenological theories have been proposed to explain the phenomenon [25]. However, as admitted in this Review Article that "....none of the theories proposed is entirely consistent with all experimental observations." This is despite the well-established observations such as:

1) Almost all superplastic materials have a fine equiaxed grain size < 10 μm. The grains grew only slightly during superplastic deformation, but remained essentially equiaxed. This is to say the grain elongation was considerably less than the macroscopic specimen elongation
2) Superplasticity was exhibited only on deformation at above approximately half the melting point and over a specific range of strain rate, 10^{-2} to 10^{-4} sec^{-1}.
3) There was a sigmoidal relationship between the logarithms of stress and strain rate.
4) The fracture processes frequently included cavitations.
5) Considerable grain boundary sliding (GBS) was observed during the process.
6) There were weak stable textures components present after large superplastic strains.
7) Transmission electron microscopy evidence shows little or no dislocations in super-plastically deformed material.

Many of the theories proposed to explain the phenomenon are all mechanical in origin and based on Grain Boundary Sliding (GBS), Diffusion Controlled Flow Rate or

Dislocation Motion Accommodation Rate etc. But, none of the theories was considered satisfactory in that they did not explain all the experimental evidence intrinsic defects in the theories have been pointed out in length in the literature [26].

My own criticism on the theories proposed for superplasticity can be summarized in one word, 'electrons', or more accurately the lack of electronic consideration. This is similar to the theoretical consideration brought forward in the study of LME (liquid metal embrittlement) described in the previous chapter – no electronic consideration. As shown in Table 2, all superplastic alloys of binary system are found either at eutectic or eutectoid compositions. This is illustrated in Fig.14 in which a few binary phase diagram involving superplastic alloys are shown. However, the people who made efforts in the formulation of theories did not consider this well-known fact important enough to incorporate into their theory formulation [24]. In fact, this observation is so consistent one should ask the question of the special attributes associated with eutectic or eutectoid composition. Or the fact that the intermetallic compounds with superelastic property are all of the peritectic type. It must be emphasized that to this date there is no report of finding superplasticity in congruently-melting compounds.

Table 2

List of alloys showed superplasticity; composition at which superplasticity occurs; percent of elongation observed; literature reference.

Material	Elongation (pct)	Reference
Al – 33 wt/o Cu (eutectic)	1300	[21-1]
Bi – 44 wt/o Sn (eutectic)	1950	[21-2]
Mg –33 wt/o Al (eutectic)	2100	[21-3]
Pb – 18 wt/o Cd (eutectic)	1500	[21-4]
Pb – 62 wt/o Sn (eutectic)	4850	[21-5]
Zn – 22 wt/o Al (eutectoid)	2900	[21-6]

5.1. Superplasticity in Terms of the Phase Diagram

In order to understand the attributes of the 'eutectic or eutectoid' one must understand the meaning of phase equilibrium diagrams as described in the theoretical treatment of PHASE DIAGRAM in the earlier chapter.

5.1.1. **Eutectic and Eutectoid Alloys**; The liquidus curves in a given phase diagram are essentially the probability curve for the formation of the compound. At its maximum point the probability is the highest for the formation of the compound (for congruently-melting compounds). And the atomic configuration in the liquid is practically identical to the configuration in the solid state. But as the composition is moved away from compound composition, the liquidus (probability) curve for the formation of the compound decrease. Generally, the amount of decrease is proportional to the deviation from compound composition. Let us assume a compound (element) A at one end of a phase diagram and at the other end of the phase diagram a compound (element) B. The liquidus (probability) curves of both A and B shall decrease as the composition deviates from their respective compound composition toward one another. At some composition between compounds (elements) A and B these two liquidus (probability) curves will meet and cross one another. This is the point known as eutectic point and is represented by the Sn-Bi and Sn-Pb systems in Fig. 14. If the liquidus (probability) curves were to be replaced by solidus (probability) curve the point is known as eutectoid as represented by the Al-Zn system in the same figure. At these points the probability for the formation of A or of B is identical and places the stability of A as well as B in jeopardy. This is to say the continuous existence of the probability curve will bring about the nucleation of A and B but since they are unstable they cannot grow to a large size grains. In essence, the alloy containing both A and B compounds (elements) are unstable due to the electronic effect and reflected in their grain size being small, < 10 μm.

5.1.2. **Incongruent-Melting (Peritectic) Compounds**; these compounds unlike congruent-melting compounds, are inherently unstable. The reason is, as described in the earlier chapter on PHASE EQUILIBRIUM DIAGRAMS, the atomic configuration in the liquid state and the atomic configuration in the solid state are considerably different. The crystal structure for these compounds does not have the feature of 'A surrounded by B and B in turn surrounded by A'. Instead the structure is consisted of A-chain or A-island surrounded by B's. or vice versa. Good example is found in Nb_3Al in which the Nb-chains are surrounded by Al. This makes the compounds inherently metastable. The peritectic nature of the compounds, Ni_3Al and Ni_3Si are shown in Fig.15. The metastable nature of these compounds is again electronic in nature, as that exists in the eutectic and eutectoid alloys. However, the degree of instability should be much more sensitive to the thermal history of the formation of the compounds. This is demonstrated by the fact the super-plasticity of these compound alloys amount only to little over 600 %. Small compared to

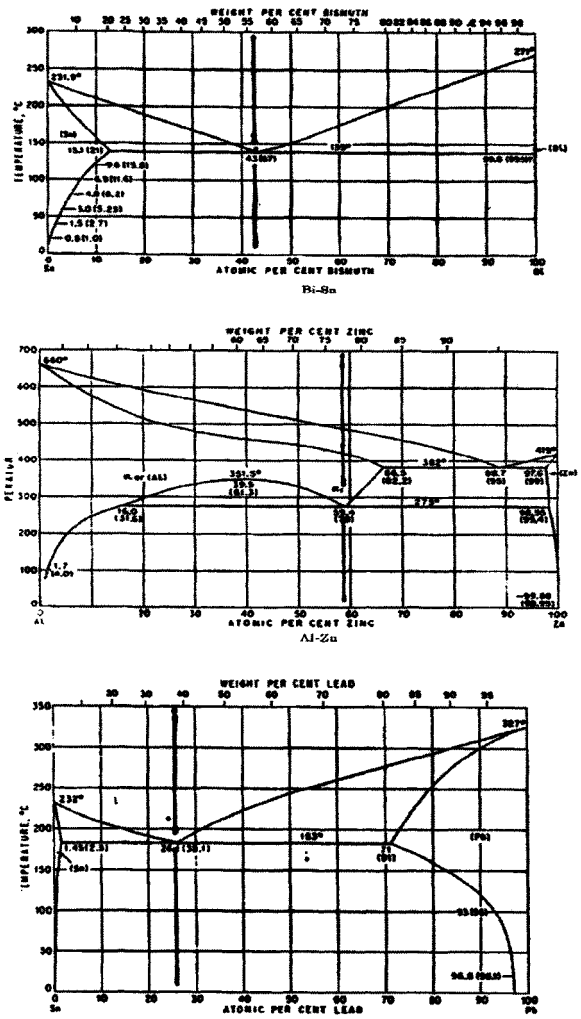

Fig. 14. Phase diagrams, in which the 'superplastic ' alloys are found, show the alloys texclusively located at compositions corresponding to 'eutectic' or 'eutectoid' points.These compositions are marked by a vertical line

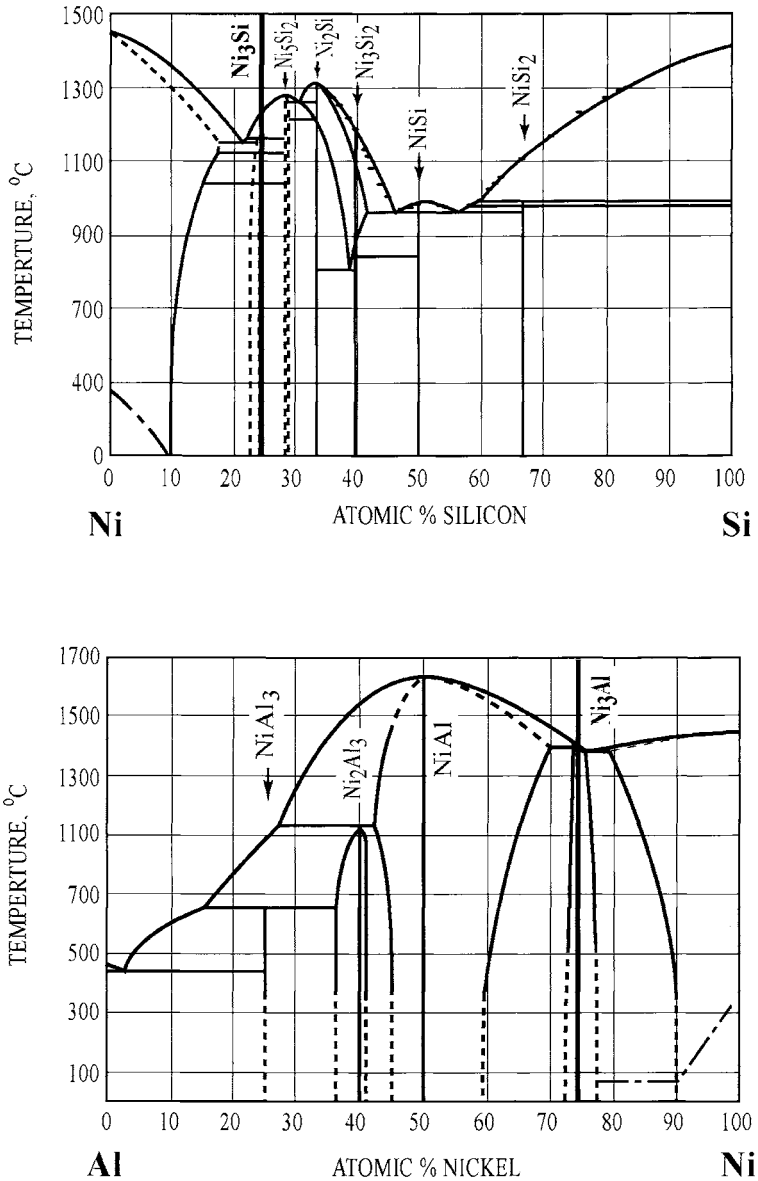

Fig. 15. The peritectic nature of Ni_3Si and Ni_3Al are shown in their respective phase diagrams.

eutectic or eutectoid alloys (more than 1000% - see Table I). As the result the temperature range in which the superplastic deformation is possible is quite limited, 1000 ~ 1100 °C [27, 28] and also very high temperature. In sharp contrast, it should be noted the eutectic or eutectoid alloys are superplastic at 100 to 200°C. However, similar to eutectic and eutectoid alloys these compound alloys also show small grain sizes because of their instability.

At this point it would be worthwhile to discuss in little more detail the unique nature of eutectic and eutectoid alloy composition as follows:

5.1.3. On the Eutectic Composition; A eutectic system is best represented by the Ag-Cu phase diagram as shown in Fig 16. As explained earlier, the eutectic point is the point at which two liquidus curves meet. And the horizontal line intersecting the eutectic point is known as eutectic line. Normally, the eutectic composition of 28.1 at. % Cu below eutectic line is left open [29] as shown in Fig. 16-(a). However in a strict sense this is not correct and in my view as well as in the view of a few other scientists [30], the eutectic composition should be indicated with a straight vertical solid or dotted line as shown in Fig.16-(b). We shall now examine in detail the reason for the correctness of such view i.e., indicating the eutectic composition by a solid or dotted vertical line as shown in Fig. 16-(b).

Let us take a composition of 20 at.% Cu and at temperature 900°C. As the temperature is lowered slowly it will intersect the liquidus line The crystals of α will begin to form and change the composition of liquid. Further lowering of temperature will bring more α crystals out of the liquid and continue to change the composition of liquid. This process will continue till the temperature ultimately reaches the eutectic line. According to the phase diagram in Fig. 16-(a) below eutectic line temperature, assuming at 700° C solid state will consist two phases α and β whose proportionality will follow the lever rule that is, ab/ac = β/α.

Now if we choose the same starting point in Fig. 16-(b) and begin to lower the temperature, everything will happen the same way as in Fig. 16-(a) up until the eutectic line. However, once the eutectic temperature is crossed and the temperature reaches 700° C , the composition distribution should be α + *eutectic composition* instead of α + β . One may argue that the *eutectic composition* is essentially made up of α and β and therefore it is immaterial whether using Fig. 16-(a) or Fig. 16-(b) and there is no need to stress the *eutectic composition* as though it is a compound. But, there is a distinct need for such nomenclature as well as the designation. This is because electronically as well as mechanically the eutectic composition is distinct from a simple mixture of α and β. In fact, it is so important to the metallurgist that they assign the name of "*Constituent*" for the eutectic composition [30]. And compositions located to the right of constituent is known as "*hyper-eutectic*" whereas to the left of constituent is known as "*hypo-eutectic*". The microstructure shown in Fig. 17 is from the alloy of 20 at. % Cu in a eutectic Ag-Cu system. The alloy has been cooled slowly from the liquid phase. At low magnification the eutectic composition shows up as a uniform grayish phase with white region of α phase (Fig.17-(a)). At higher magnification, Fig. 17-(b) the grayish area is seen clearly consists of α and β phase at the ratio governed by the eutectic composition. Cold-working and annealing this alloy will not change the phase ratio of α to β as appeared in the microstructure. The eutectic composition remains constant whether an alloy is cooled from

hyper-eutectic or hypo-eutectic composition. The observation is not limited to the eutectic composition but also on the eutectoid composition. Good example is found in the phase equilibrium diagram of Fe-C system in which 'austenite' is converted directly into '*pearlite*' at 0.77 % of Carbon (eutectoid composition). I find in the literature a number of mentions about '*bainite*' whose characteristics are quite similar to that of pearlite (such as a combination of ferrite and cementite). Although no detailed investigation appear to exist on bainite, I wonder whether bainite may be the eutectic composition (the constituent) at 4.32 % carbon. As is seen here the importance of eutectic and/or eutectoid composition in *SUPERPLASTICITY* is obvious. This is the reason it is desirable to draw a dashed line at the eutectic or eutectoid composition as is done in Fig. 16-(b). It is clear that these inherent instability is also the reason for the easy formation of 'amorphous' (non-crystalline) material through quenching for these materials. It should be made clear that there is no sharp distinction between 'amorphous' and 'crystalline' materials. This is because crystalline material would have wide range of crystallinity, in terms of grain sizes. The amorphous material can also require its range of amorphicity. For example, the amorphous silicon can be viewed as not really 'amorphous' because the short-range tetrahedral clustered units of silicon still exists. It's just they do not have the long-range crystalline arrangement. Or in some cases one can find a material that is part amorphous and part crystalline. Because of their small grain size the superplastic material may be regarded as partly crystalline and partly void. This is to say that the void among the grains would be rather large in volume. These voids definitely would contribute to their super-plasticity. In surveying through the literature I did not find any data on the porosity (or density) of the alloy before and after the superplastic deformation. Thus, no comparison can be made to see whether the idea is valid. On the other hand, there are many reports on the observation of 'grain boundary sliding', 'grain rotation' or shift in grain-orientation etc. during tensile pull. The results in these aspects are abundant and regarded as the reason for superplasticity

In summary, my view is that the fundamental cause for superplasticity is electronic in origin which has to do with the probability curves for the formation of compounds. This in turn creates the instability of the compounds and results in the ultra small grain size. Then, on the application of tensile stress, the plastic deformation is purely mechanical and has nothing to do with electrons. This is completely different from that observed in the normal plasticity as described above. The cause and mechanism for super-plasticity and normal plasticity are therefore fundamentally different. The phenomenon of superplasticity therefore can be viewed stepwise as follows:

Instability of the compound formation brought about through electronic consideration – whether it be eutectic, eutectoid or peritectic compound is the cause for the inherent instability. Subsequently, this inherent instability is the reason for grain size being small, < 10 μm. That is, while the nucleation is possible but grain growth is prevented by the instability.

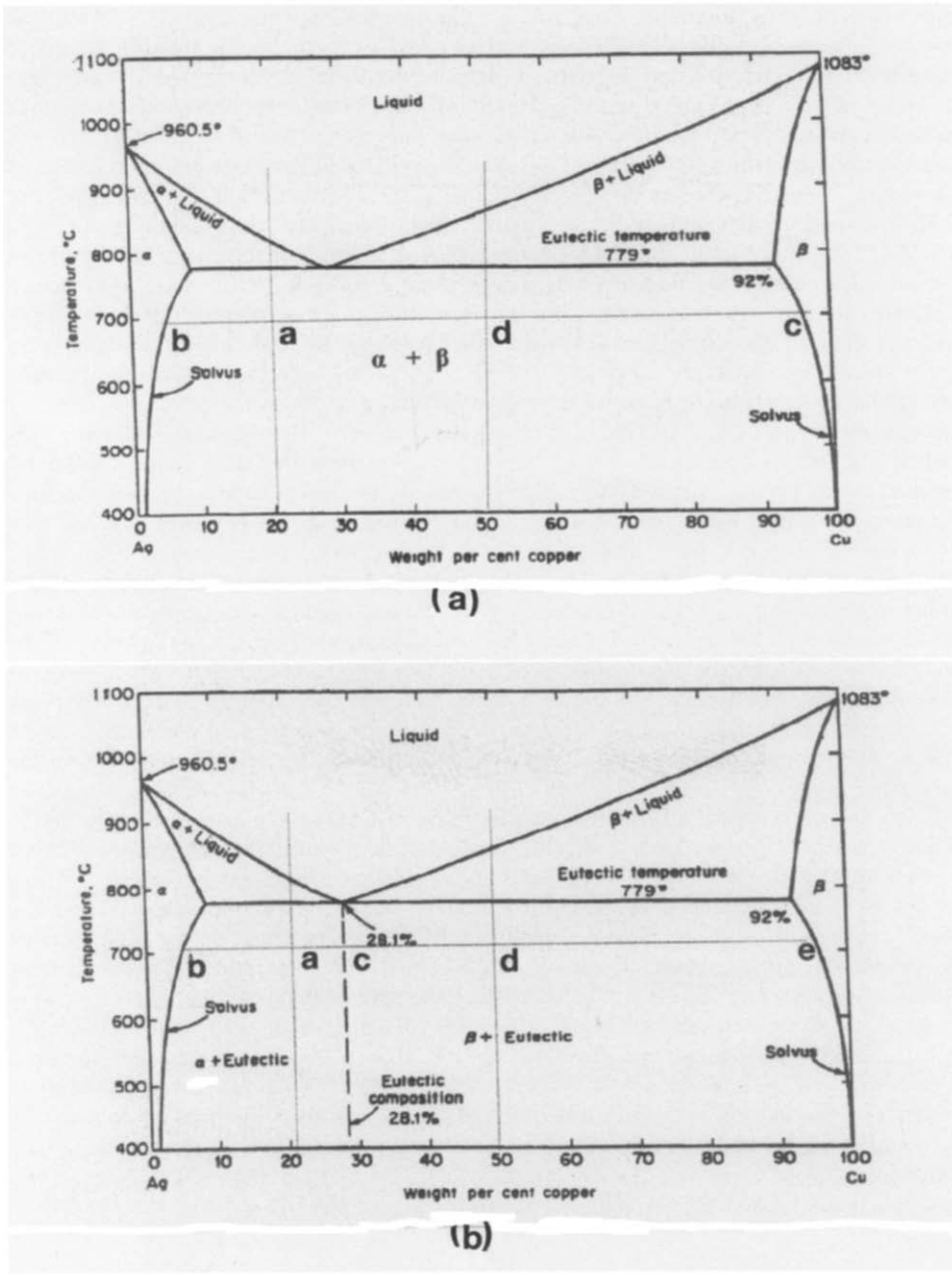

Fig. 16-(a). (b); Showing the difference in a eutectic system in which the eutectic composition not indicated vs. eutectic composition indicated.

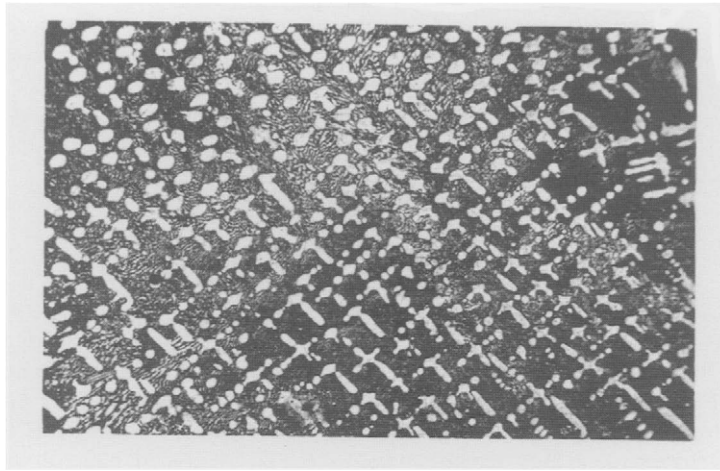

(a)

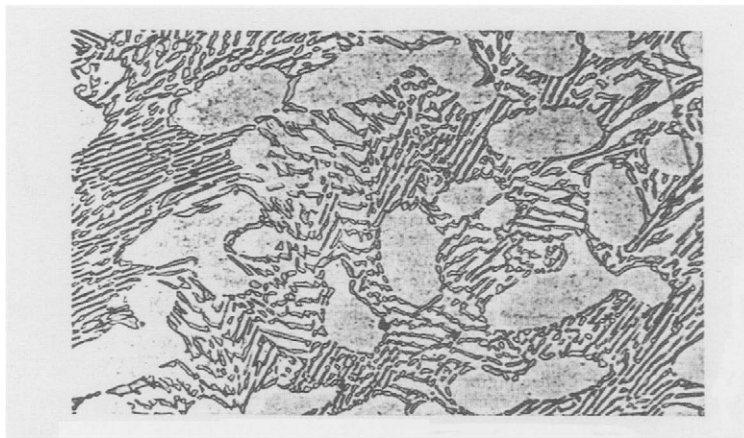

(b)

Fig. 17-(a); Photograph of 20 at. % Cu indicating two distinct regions, namely α phase and the constituent (eutectic composition). –(b) shows at higher magnification the constituent actually consists of α and β composition ratio equivalent to the eutectic composition.

a) The inherent instability not only prevents the small grains from growing into larger grains at elevated temperature but also keeps grain equiaxed under tensile deformation.
b) Mechanically, the small grain size brings out the grain boundary sliding, grain rotation and/or shifting in their orientation which all contribute to the superplasticity.
c) Because of the small grain size, the void (cavity) volume percentage will be extraordinary large and contributes greatly to the superplasticity by increasing the cavity volume or facilitating the mechanisms listed in d).

Since the small grain size is a pre-requisite to superplasticity, in some cases the grain size may be made small artificially through addition of some second and third elements. In the case of aluminum alloy (IN90211) mechanical addition of 4.4% Cu and 2% Mg the investigator [29] were able to bring about the grain size of ~ 0.5 μm and achieved some 500% elongation at a high temperature of 475° C (where Al melts at about 660° C). However superplasticity achieved in this manner suffers not only from the percentage of elongation being small but also the temperature of superplastic deformation is near the melting point such that the definition of superplasticity is brought into question for these alloys. Because the small grain size is brought about artificially the small size tend to coalesce into larger size with temperature rise.

6. CORROSION RESISTANCE

It is well known through our experience that material with conduction electrons suffer from the phenomenon called 'corrosion' i.e., metals turning into metallic oxides in time in air. On the other hand, the materials without conduction electrons do not suffer from corrosion. Technically, the presence of conduction electrons implies the existence of 'free electrons' and conduction band. As pointed out in the mechanical property section these two distinct properties exhibit themselves also in term of 'plasticity'. That is, the existence of free electron band allows plastic deformation whereas in the absence of free electron band the 'plasticity' is nonexistent. It is recalled that the theory we are proposing for metals and alloys requires not only the coexistence of covalent bond and free electron band but also that the ratio of the number of these two type of electrons be maintained at a constant value for a given **metal**. Within such understanding, we now construct corrosion process in steps:

(1) Oxygen molecules (O_2) in air come to rest on the surface of a metal.
(2) Chemically these O_2 molecules have a strong tendency to become $2O^{=}$. that is, $O_2 + 4e^{-} \leftrightarrows 2O^{=}$
(3) The second step requires as much as 4 electrons per molecule of O_2. This supply of free electrons is available only if the material, on which the oxygen molecule come to rest, has free electron band. Thus, organic or inorganic material such as diamond, plastic etc. which do not have free electron band do

not suffer corrosion. All metals and alloys that have free electron conduc-tion band are able to contribute to the second process will therefore corrode in time.

(4) The process of $O_2 + 4e^- \rightarrow 2O^=$, abstract free electrons from the free electron band and results in upsetting the ratio of $R = N_f / N_c$ (number of free electrons over number of covalent bonded electrons). In order to restore this ratio, some covalent bond (particularly those near the surface) will have to give up their covalent bonding to become positive ions. In this process free electrons are created:

$$M \rightarrow M^{+(n)} + n(e)$$

This makes it possible to restore the fundamental ratio.

(5) In the mean time $O^=$ 'sees' $M^{+(n)}$ and will bond together to form M_xO_y compound which is an extremely stable compound and stay permanently as oxides.

Through these five steps oxidation process (corrosion) of a metal or alloy is accomplished. Within this mechanism, it is clear, in order to prevent corrosion (oxidation) the following processing come to mind.

(a) Prevent direct contact of O_2 molecule to the bare surface of metal. This can prevent the (2) process from taking place and in time O_2 will fly away into air. This is accomplished in the real world by painting the surface of a metal or coating the surface of metal with oil. Sometime nature takes care of itself by forming a tight-bond oxide layer to prevent further oxidation such as seen in aluminum metal.

(b) Destroy or prevent formation of all covalent bonds such as to eliminate the R ratio entirely. In this manner, if O_2 absorbs free electrons and become $2O^=$, it would not result in upsetting no ratio. In the real world this is hard to achieve except in truly 'amorphous' metal where no short range structure exist. Since no perfect amorphous metal exists, corrosion cannot be eliminated completely. However, even in an incomplete destruction of covalent bond the 'amorphous' material is shown to have a considerable higher resistance to corrosion [10].

(c) This method is based on preventing a formation of positively charged metallic ions, $M^{n(+)}$. As is stated above, the reason for the formation of metallic ions is to restore the ratio of $R = \mathbf{N_f / N_c}$. Thus, if there is a mean of supplying free electrons to the system in lieu of forming metallic ions to restore the ratio, corrosion resistance will improve. In the real world this is seen in 'stainless steel' where the iron metal is doped with elements such as Cr, Mn, and Mo. It is noted these elements are all chemically known as multi-valence elements. That is to say, these elements have an ability based on their atomic orbital to exist in various oxidized states.

Cr : +2, +3, and +6

Mn: +1, +2, +3, +4, +6 and +7

Mo: +2, +3, and +6

Wherever these elements are located in the matrix (solid) they respond to the call for more free electrons by yielding electrons and changing their valency to a higher state. In doing so they yield free electrons to the system and restore the constancy of the ratio required. In this manner, covalent bonded iron atoms need not breaking their covalent bond to become positive ions. Without the presence of $Fe^{+(n)}$ ions the $O^{=}$ has no possibility of forming stable chemicals and in time would fly away into air as O_2 molecule. At this point, free electrons will be returned to the system and in turn the dopant will lower their oxidation state to again, maintain the ratio. In another words, the dopant, Mn, Cr and Mo serve as the buffer to either give up or take up electrons to maintain the RATIO. Thus, the 'stainless steel' is born. Following this line of reasoning, it is important to note the effecttiveness of anti-corrosion in Fe requires a maximum of about 12 wt. % of Cr doping [11]. Obviously, further increase in the percentage of Cr would not continue to enhance its ability to inhibit corrosion. For once a buffer is saturated further increase in the buffering capacity would not serve the purpose.

7. FURTHER DISCUSSION

It is well recognized that among the materials; wood, mineral, plastic, ceramic and metal etc., the strongest material is metal. This is principally due to the unique properties associated with metal, such as malleability, fracture toughness, tensile strength and extraordinary high modulus. In trying to formulate the coexistence of covalent bond and free electrons in metal, I came upon the strongest structural material constructed by man known as 'steel concrete'. My thought is that these two materials, 'metal' on one hand and 'steel concrete' on the other have something in common if covalent bond is accepted to exist in metal. The common feature is the existence of a rigid structure that is composed of a network of 'Covalent bond' (in metal) and 'steel rod' (in steel concrete) that are directional in nature and are bonded all together. An isotropic media called 'free electrons' in metal and 'cement' in steel concrete in turn wraps around this anisotropic skeleton structure. These configurations are pictorially shown in Fig. 18. In this manner the 'metal' created by God and the 'steel concrete' created by man turns out to be the strongest material in nature and the strongest synthetic structural material. Man, created by God in His image, turns out to be not that dumb after all. The fundamental importance of maintaining the Ratio in metal and alloys can also be illustrated by the experimental facts that: (a) it is impossible to force additional electrons into a piece of metal. It is, nevertheless possible to build up electron charges on the surface. (b) Electron conduction through metal can be viewed as a phenomenon in which electrons can be drawn away from one end as long as same number of electrons is supplemented from the other end – to maintain the Ratio.

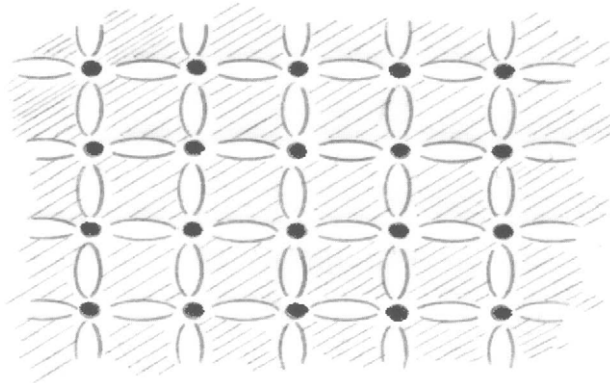

(a)

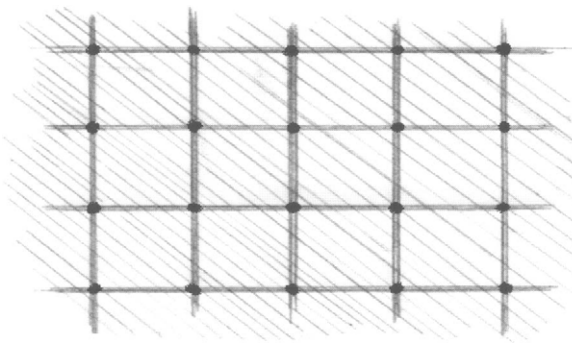

(b)

Fig. 14. (a) Pictorial representation of 2-dimensional metal depicting the coexistence of **COVALENT** bond , () and isotropic free electrons (shaded).. (b) Pictorial representation of 2-dimensional steel concrete showing the coexistence of steel rod (straight lines) surrounded by isotropic concrete (shaded).

REFERENCES

[1] J.M. Ziman, Electrons and Phonons, The Clarendon Press, Oxford (1960).
[2] M. Bonn and K. Huang, Dynamical Theory of Crystal Lattices, The Clarendon Press, Oxford (1954).
[3] Dislocation in Solids, vol. 1-8, North-Holland, Amsterdam (1979-1989).
[4] J. Weertman and Julia Weertman,, Elementary Dislocation Theory, Oxford Univ. Press, New York (1992).
[5] H.B. Gray, Chemical Bonds, Benjamin/Cummings, Pub.Co. (1973).
[6] R. McWeeny, Coulson's Valence, Oxford Univ.Press (1979).
[7] Y.N. Chiu, P. Palting, S.T. Lai, M..Z. Fu and F.E. Wang, J.Sol.Stat.Chem. 129(1997)174.
[8] A/E/ Remick, Electronic Interpretations of Organic Chemistry, John Wiley & Sons Inc. (1949).
[9] W.B. Pearson, Lattice Spacings and Structure of Metals & Alloys, Pergamon Press, New York (1956).
[10] Metallic Glasses, Material Science Seminar, ASM, Metals Park, Ohio (1976).
[11] Metals Handbook, ASM, Metals Park, Ohio, 7th Printing (1972).
[12] B. Joseph, M. Picat and F. Barbier, Euro.Phys. J.AP., 5(1999)19.
[13] M.H. Kandar, Treatise on Material Science to Technology, Acad.Press, 25(1983)36.
[14] N. Rhines, J.A. Alexander, W.F. Barclay, Trans.Amer.Soc.Met., 55(1952)22.
[15] V.N. Rozhanskii, N.V. Perstov, E.D. Chchukin and P.A. Rebinden, Sov.Phys.Dokl, 2(1957)460.
[16] E.E. Glickman, Yu. V. Goryumov et al. , Izv.Vyssh.Uchebn.Zaved., Fiz, 5(1976)7.
[17] G.D. Bengough, J.Inst.Metals, 7(1912)123.
[18] H.M. Jenkins, J.Inst.Metals, 40(1928)21.
[19] C.E. Pearson, J.Inst.Metals, 54(1934)111.
[20] T.G. Langdon, Metall.Trans. 13A(1982)689.
[21] -1 G. Rai and N.J. Grant, Met.Trans., 6A(1975)385.
-2 C.E. Pearson, J.Inst.Met., 54(1934)111
-3 D. Lee, Act.Met., 17(1969)1957.
-4 P. Chaudhari and S. Mader, High Speed Testing, Interscience, N.Y. VII(1969)1.
-5 M.M.I. Ahmed and T.G. Langdon, Metall.Trans., 8A(1977)1832.
-6 H. Ishikawa, F.A. Mchamed and T.G. Langdon, Phil.Mag., 32(1975)1269.
[22] T.G. Nieh and W.C. Oliver, Scripta.Metall., 23(1989)851.
[23] C.T. Liu and C.C. Koch, NBS- IR-83-2679-2, National Bureau of Standards, Wash.D.C. (1983)
[24] A.H. Chokshi, A.K. Mukherjee and T.G. Langdon, Mater.Sci. & Eng., R-10(1993)237.
[25] J.W. Edington, Metall.Trans., 13A(1982)703.
[26] J.W. Edington, K.N. Melton and C.P. Cutler, Prog.Mat.Sci., 21(1976)61; A.K. Mukherjee, Amer.Rev.Mat.Sci.,9(1979)191;R.C.Gifkins,J.Mat.Sci.,13(1978)1926;W.Beere,Tans.Roy. Soc., London, 228(1978)177; R.C. Gifkins and T.G. Langdon, Mat.Sci.Eng.36(1978)27.
[27] A. Chudhury, V.K. Sikka and A.K. Mukherjee, J.Mat.Sci., 25(1990)3142.
[28] S.L. Stoner, W.C. Oliver and A.K. Mukherjee, Mat.Sci.Eng. A153(1992)465.
[29] T.R. Bieler, T.G. Nieh, J. Wadsworth and A.K. Mukherjee, Script.Metall, 22(1988)81; K. Higashi, T.Okada, T. Mukai and S. Tamura, Script.Metall., 25(1991)1052.
[30] R.E. Read-Hill and R. Abbaschian, Physical Metallurgy Principles, PWS Pub.Co., Boston, (1994).

VII. Summary of the Bonding Theory

1. BASIC ASSUMPTION

Metals and alloys all have three types of electrons: (1) the inner core electrons which do not normally participate in the bonding but at times can provide a strong magnetic moment through its unpaired electron spin and (2) the covalently bonded electrons providing strong bonds between ions; anisotropic in nature and thus dictate the crystal structure, and finally, (3) the 'free electrons' which permeate throughout the whole crystal, provide long range bonding force and are the source for metallic luster, electronic conduction etc. and most importantly provide a mechanism for metals and alloys to be ductile and malleable.

The only difference from one metal to another metal or one alloy to another alloy lies in the percentage (or the ratio) of each type of electrons. Particularly important is in the ratio of covalent bonded electrons over 'free' electrons. Oftentimes we hear the remarks of — such elements are metallic elements and such elements are non-metallic. I believe this is an erroneous statement and a misnomer. For an element can only be identified by its atomic number and atomic weight. Whether an element becomes a metal or non-metal has something to do only after the elements come together and form an aggregate and turn into a solid mass. Therefore, as an element it cannot be labeled as 'metallic' or 'non-metallic'. This brings up an interesting question — in bringing atoms together to form a metallic solid, does covalent bond forms first or 'free' electrons forms first? This question can be answered if we are able truly to carry out the basic calculation from the first principle. But, since we do not know how to carry out this calculation, we shall take the following philosophical argument to shed some light on this question.

When atoms are brought together all the electrons are in atomic orbitals that are quantized by a series of quantum numbers [1] according to the following rules:

(a) Each electron is represented by a wave function Ψ, such that Ψ^2 is the density of the charge cloud for this electron.
(b) Each atomic orbital is designated in terms of a set of *quantum numbers*. Beginning with the principal quantum number, 1,2,3,...., which determines the 'shell' the atomic orbital is in. Followed by the geometrical shape given by the quantum number, s, p, d...etc. with appropriate suffix as in p_x, p_y, p_z to show which degenerate state the electron is in.
(c) Following the Pauli Exclusion Principle each atomic orbital can be occupied by two electrons and two electrons only, provided the two electrons have opposing spin.

These restrictions embody what is known as the '*aufbau*' approach to the description of atomic orbitals. Thus hydrogen is represented in its ground state by (1s), helium by $(1s)^2$, lithium by $(1s)^2(2s)$ etc. The similarity between the atomic orbital and covalent bonding lies in the "two electrons and only two electrons" per orbital or per bonding.

This is the reason covalent bonding is referred sometimes as the product of LCAO (Linear Combination of Atomic Orbital). Since each covalent bond uses two and only two electrons, any excess (more than the number of electrons required for covalent bond) valence electrons will automatically become 'free' electrons. This is because their atomic

orbitals are already so close to one another such that overlapping of the remaining orbitals will occur and yield the 'free' electrons. Logically we do not see problems in this line of reasoning. The second case is the assumption that the formation of 'free' electrons comes first and then the covalent bonding. In this case there exists a formidable difficulty of finding a mechanism of first transforming electrons in atomic orbitals to 'free' electrons (fermions), then another mechanism to transform free electrons (fermion) into covalent bond (boson). This essentially involves a 'boson condensation', which is a formidable task even for theoretical physicists. This mental exercise in logic appears to favor the formation of covalent bond first, then 'free' electrons second. Or even a simultaneous formation of both the covalent bond and 'free' electrons. But, for 'free' electron formation to come first before the formation of covalent bonds appear to be an almost impossible task. Within this understanding it is easy to see that in the material world there can be a material that involves only covalent bond (such as diamond) where the valence electrons are just enough to satisfy the covalent bonding and no electrons leftover for 'free' electron formation. Or a material that has more than enough electrons for covalent bonding and ends up with covalent bond plus 'free' electrons such as in metals and alloys. But, certainly one would not expect a material with only 'free' electrons, which may exist only in the liquid state.

2. CONSTANCY OF THE RATIO, R.

Thus far, in every aspect of the phenomenon of metals and alloys we have discussed, it was attributed one way or the other to the constancy of the ratio, R, covalent bond / free electron band. Under the theory we stress that there is an inherent tendency to maintain the ratio constant for a given metal and/or alloy. Here we must add a condition, i.e. for a given crystal structure. This is because in many instances a metal or an alloy of specific composition can change its crystal structure as a function of temperature. It is logical to assume that for a given metal or alloy the ratio will be different for different crystal structure. This is because different crystal structure would assume different type of covalent bonding and thus takes up different number of valence electrons for covalent bonding – and subsequently a different ratio. It is important to point out that organic or inorganic compounds often assume different crystal structures at same temperature. This is because the molecules within the crystals are separated by Van der Waals distances such that the free energy of one type of packing differs very little from that of another type. In sharp contrast, in metals and alloys, atoms or molecules are not separated by Van der Waals' distances within the crystals such that for a given composition and given temperature there can be only one type of crystal structure. In a rare occasion two crystal structures may appear to coexist on the left and right of a given compound composition as seen in $TiCo_2$ (Fig. 1) but in the final analysis the two crystal structures do not share the same composition [2].

It was pointed out before, covalent bond is rather sensitive to temperature changes and as a result may change its potential energy curve as attested in the change of Young's modulus in the previous section of *Mechanical Properties*. The question that needs answer-

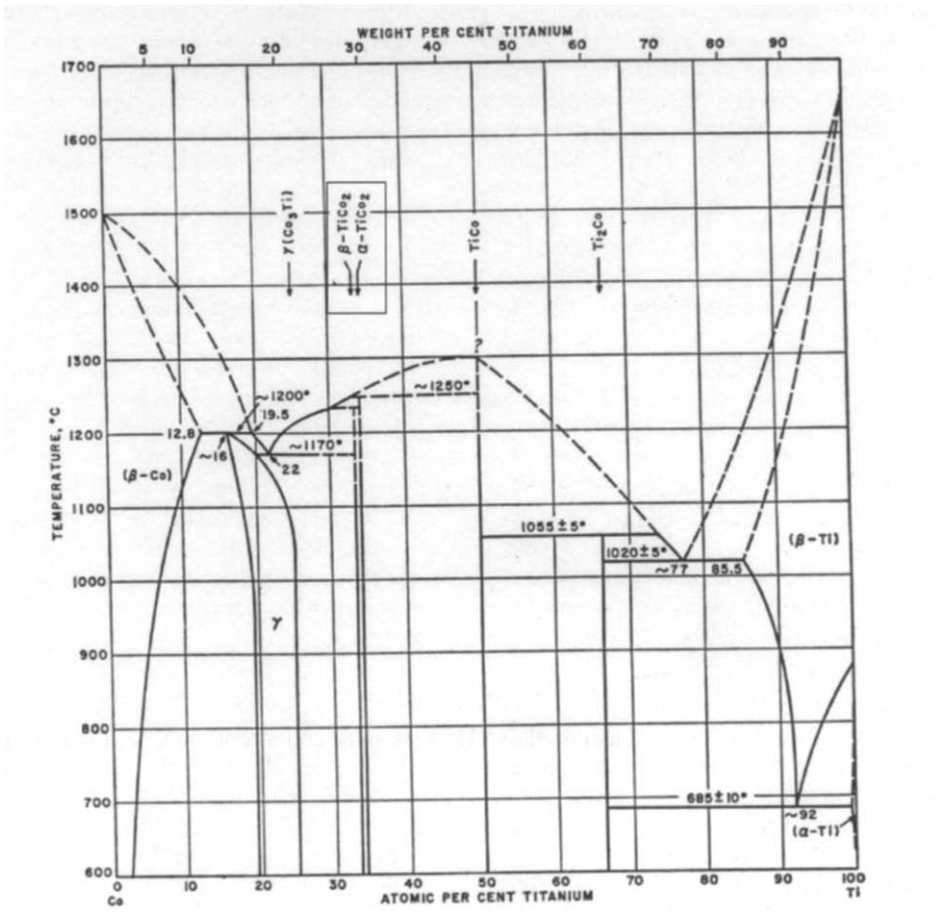

Co-Ti System

Fig. 1. The phase diagram of Co-Ti in the range of 600°C thrugh 1700°C. Particular attention shuld be paid on the side by side coexistence of α- and β- $TiCo_2$ compound.

ing is – how the change in potential energy curve affects the ratio? To answer this question, we should refer back to the Fig. 9 of Mechanical Properties Section, where the potential energy curve as a whole is divided into E_1, E_2, and E_3. My own view is that for a given crystal structure the temperature variation would affect only the E_1 and leaves E_2 and E_3 intact. Therefore, the fundamental ratio, **R**, shall remain constant. Inasmuch as the potential energy curve becomes shallower with temperature rise, the E_1 is expected to become smaller. Consequently, it would be easier to reach E_2 and the ductility should increase. But, if at certain high temperature, the crystal structure transforms to another

crystal structure, the ratio, R, should change and all three factors, E_1, E_2 and E_3 should all change. In essence, the ratio, R, is expected to remain constant for a specific composition and for a specific temperature range in which the crystal structure remains the same. There is no question that this ratio can be upset to a certain degree and for a certain period of time – as a metastable state. Further investigation are required to know the factors involved and to what degree and under what circumstances such metastable state can be allowed to exist.

3. THE 'FREE' ELECTRON BAND

We have shown how the 'free' electron band is unique to metals and alloys and how it served to help in creating the 'free radicals' and in turn the ductility. As was pointed out before, this is also the reason for the existence of corrosion. In other aspects, the 'free' electron band is also the reason for the metallic 'luster' and color that is unique to metals and alloys, e.g., gold metal is yellowish, and silver metal white bluish etc. Sometime in undergoing diffusionless martensitic transformation a compound can exhibit a variety of colors – reddish to yellowish and to silver white [3]. In the discussion of ductility we invoked the mechanism of creating (or eliminating) free-radicals by giving up (or absorbing) electrons to (and from) 'free' electron band within the metals and alloys. However, in the world of 'organic synthesis', this mechanism also comes into play in the form of catalysis. In organic synthesis, it is often found that the yield for a given reaction can be increased several fold in the presence of catalytic agent [4]. It is well known that the catalytic agents do not directly participate in the reaction but rather standing by as 'cheer-leaders' in helping the reaction to go forward. Can you guess what makes a good catalytic agent? You are right – almost all the known catalytic agents are METALS! They range from Mg, Al, Pd, and Ni to a mixture of metals. Our theoretical reasoning is that being a metal, they have the 'free' electron band that can serve as a temporary reservoir for intermediate free radicals to deposit electrons and absorbing them back after they readjust the molecular structure. In this manner the catalytic agents facilitate the chemical reaction and results in high yield.

According to solid-state physicists whether a material is a metal or non-metal is based on the band structure and the number of valence electrons per atom available to fill the band structure. The skeleton of band structure is formed based on the 'Brillouin' zone boundaries. These boundaries are erected solely based on the crystal structure (periodic atomic arrangement), which then create the zones in which the valence electrons can fill from the 1^{st} zone to the 2^{nd} and so forth. In the free electron theory each zone is separated from another zone by an energy gap such that if the valence electrons are just enough to fill the zones and leaving no more electrons, the material will be an insulator. On the other hand should there be partially filled zones, the material will be a conductor. There are problems, however, in this line of approach. There is no doubt that there exists 'Brillouin' zone and zone boundaries [5]. For these boundaries and zones come from the crystal structure. The problem is in the accounting of the total number of (valence) electrons to be used in filling these zones. The assumption is that all the valence electrons are 'free' electrons. The whole idea being exhorted in the theory given here is that there exists covalent And if this is true, for the 'Brillouin' zone theory to work, covalent bonded electrons (bosons) must be subtracted from the total number of valence electrons first then

fill the zones with the remaining valence electrons (fermion). This means one must know the number of electrons used in the covalent bonding. In this manner the prediction based on the zone theory and experimental fact may come to agree. Also in many cases in the discussion of these concepts with theoretical physicists, they would try to convince us that there are narrow bands in their band structure calculation such that the electrons in these bands have a very low mobility — and these are therefore essentially the covalent bond I am talking about. Such suggestion I find to be extremely naive and very far from the truth. The fact is no matter how narrow the band is and how low the mobility might be, the electrons in these bands are fermion and distinct from covalent bonded electrons – boson. And boson can all exist at one energy level and subsequently cannot be used to fill zones or bands like fermion can. This is similar to the argument that because molecules in a gaseous state happen to have higher density and lower kinetic energy than the same molecules in the liquid state, therefore they should be considered as in liquid state. The truth is there are other factors that differentiate liquid state from gaseous state.

It should also be noted that when a physicist decides to calculate a band structure of a metal, he first asks for the crystallographic data for that metal. Then, he starts his calculation based on the data given including symmetries and lattice constant etc. This is to say that he does not start his calculation from the first principle but rather based on experimental evidence — the crystal structure. Thus, the calculation is semi-empirical at best. The Bloch wave function is based on the idea that the eigen-functions of the traveling wave in a periodic potential are in the form of the product of a plane wave exp (ik • r) times a function of potentials, uk(r) with the periodicity of the crystal lattice. The solutions for this function are composed of traveling waves that can propagate freely through the periodic potential field of the ion cores. From these waves the energy gap are calculated at the zone boundaries. However, the traveling free electron waves may not be completely free if there exists high electron density area of covalent bonds between ionic cores. The free electrons would have to dodge these areas particularly because the covalent bonded electrons are boson and the free electrons are fermion. The band structure constructed by considering both the ions and covalent bond simultaneously may be different from that constructed by considering ions alone. We do not expect the band structure thus calculated to be fundamentally different from that calculated with ionic cores alone. However in some cases where covalent bond is strong, there may be significant difference in the details. And in some cases these minor details may be critical in understanding a metal.

4. THE FORMATION OF Li_5B_4 COMPOUND ALLOY

In admitting the existence of covalent bond in metals and alloys brought forth an interesting possibility that an alloy or more specifically an intermetallic compound may be formed only at certain high temperature. This belief is based on the fact some covalent bond may not form except at high temperature. For example, the 'inert-gas' elements of He which is known to be inert but under high temperature and high pressure, one of its 1s electrons can be promoted to 2s and results in a formation of compounds with other elements [9], e.g. Pt_3He, PdHe, BiHe, etc. Let us say that at temperature, T_1 (see Fig. 2

below) in a binary A-B system, an alloy of A(x)B(y) composition may exist as a liquid metal-alloy above the liquidus line. Since the liquid metal-alloy is in liquid state it is logical to assume that there is no covalent bond exists between A and B. Conventionally in the free electron model there is no consideration for covalent bond in compounds and thus there is no necessity for carrying out experiments above the T_1 temperature. However, if we know and expect a formation of covalent bond between elements A and B at a higher temperature, our experimentation may have to be carried out to a higher temperature. Thus, we shall and may find an A_xB_y intermetallic compound formation at T_2. I found just such an example in the Li-B binary system [6].

Up until my experiments [6] in 1978 no work on the Li-B was carried out. This was understandable in a way because lithium has a melting point of 182° C whereas boron melts at 2300° C. To melt them together is equivalent to put fire and water together. Another possible reason for not investigating the Li-B system might be the fact boron has never shown any tendency to form metallic compound with any other elements. Furthermore the boron-hydrides (B-H) are rather unstable and at times explosively react in air. Therefore there is concern that lithium being chemically identical to hydrogen formation of boron-lithium may also be explosive. Undaunted by these historical facts and considerations, I decided to investigate the Li-B system. The motivation for this investigation was in the performance of beryllium as metal which is one of the lightest of all metals, and has one of highest melting point (1280° C) of the metals. Its modulus of elasticity is about one third greater than that of steel etc. I believed lithium (Li) and boron (B) sandwiching beryllium (Be) in the atomic chart can come together to form an alloy similar to beryllium and hopefully it would possess even better properties than beryllium itself. I discovered to my own pleasant surprise that boron easily dissolved into liquid lithium at around 300° C, almost in the same way sugar or salt dissolve in water, and form liquid metallic solution of Li and B. In order to assure a complete dissolving of boron, temperature was raised higher. However, by heating this liquid metallic solution to a higher temperature to around 500°C the liquid metal freezes into a solid state. Raising temperature further to about 550°C the formation of an intermetallic compound Li_5B_4 takes place [7,8] with a vigorous exothermic reaction (Fig. 3). The amount of heat release at the formation of the compound is measured to be 2.2 (ķ 0.3) kcal per gram of B. The compound alloy thus formed is totally metallic, malleable, extrudable and machinable (Fig. 4) with silver color metallic luster, and stable from room temperature up to 1000°C (pictorially illustrated in Fig. 4). Above 1000°C, the compound-alloy sublimes with a vaporization of Li metal leaving a blackish substance mostly boron.

The formation of Li_5B_4 compound alloy is overtly similar to two well-known phenomena in alloy physics. These are: (a) amalgamation involving alloying of liquid Hg with various metals e.g., Sn, Cd, Ag, and (b) 'retrograde' melting e.g., Ag-Bi [11], Ag-Pb [12], or 'inverse-peritectic' melting, Li-Sr [13] which involves within a narrow composition and temperature range, a mixture of solid and liquid at low temperature solid-

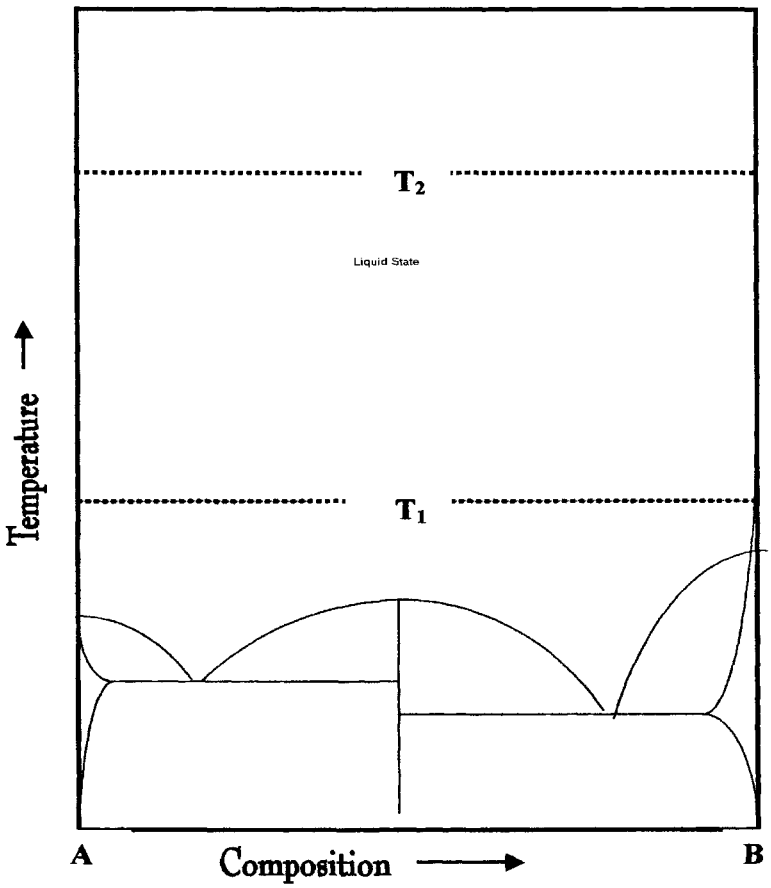

Fig. 2. An imaginary phase diagram between elements A and B. Showing the possibility of forming intermetallic compounds at temperature higher than liquid state temperature.

ifying upon heating to a higher temperature. The only way to melt amalgams is to heat them to a higher temperature. And upon cooling the liquid will revert back to a solid-liquid mixture. These phenomena are completely understandable in terms of their phase diagrams. In contrast, Li_5B_4 formation involves no solid-liquid mixture and unlike amalgamation, the liquid metal solution remains in the liquid state independent of annealing time. Furthermore the compound alloy thus formed will not revert to liquid state upon cooling. The most outstanding and unique feature is the exothermic formation of Li_5B_4 at about 550° C. Alloys in the composition range, 5 ~ 50 at.% B all have metallic luster of silver-white color and are all chemically reactive in air. The electro-chemical

potential of the Li-rich compound alloy is shown to be quite close to that of Li metal — approximately 3.3 V *vs.* chlorine electrode. The 5 at. % B alloys has a ductility that is similar to that of Li metal. At about 40 at.% B, the alloy is still rather ductile having a Young's modulus of 3.45 GN/m^2 (0.5 Mpsi) with 8~9 percent elongation as determined by a stress-strain measurement.

The electrical conductivity of these alloys is metallic i.e., inverse proportional to the temperature between 4 to 300° K and is about 7 x 10^6 $(\Omega m)^{-1}$ at room temperature. The crystal structure determination [7] shows the B atomic arrangement to consist of coplanar 4B clusters (isolated from one another) with three B atoms at the vertices and one B at the center of a triangle as shown in Fig. 5. This isolated 4B atomic arrangement has no precedent either in metal-borides [14] or boron hydrides [15].

Through the formation of Li_5B_4 we see the possibility of forming intermetallic compounds at a higher temperature beyond their liquid state. We are not advocating that in every binary or tertiary intermetallic system this phenomenon will take place. We are suggesting that with a proper matching of atomic orbitals between the elements, in their excited state at high temperature certain type of covalent bond may take place and results in formation of an intermetallic compound whose existence cannot be detected in the low temperature investigation. This line of thought opens up a possibility that a number, if not all, of the Binary Alloy Phase Diagram [10] investigation may not be complete. And in a number of systems further investigation may be warranted. Thus far, all the phase diagram investigations [10] are halted within 50 ~100° C above the highest temperature of the liquidus line. The assumption is that nothing could possibly take place beyond these temperatures (beyond liquid state). This is rather unfortunate in that the 'other half of the story' i.e., the story of high temperature side is yet to be told.

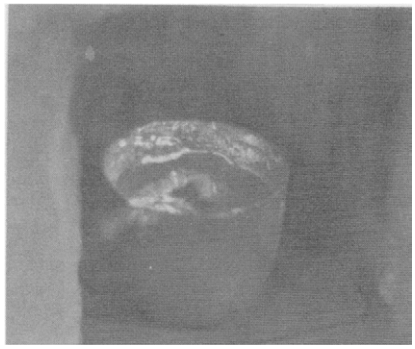

(a)

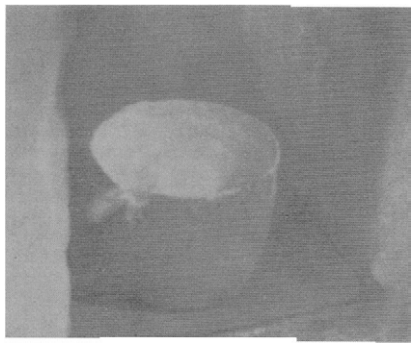

(b)

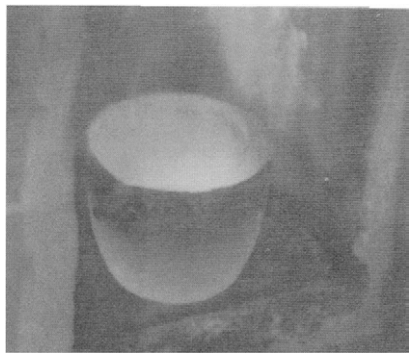

(c)

Fig. 3. Visual observation of th formation of Li_5B_4 (inside the dry box) at various temperatures.

(a) Homogeneous liquid solution of Li and B around 400° C., (b) Just prior to the 550° C exothermic reaction where metallic luster disappear and (c) At the 550° C exothermic reaction with the formation of Li_5B_4.

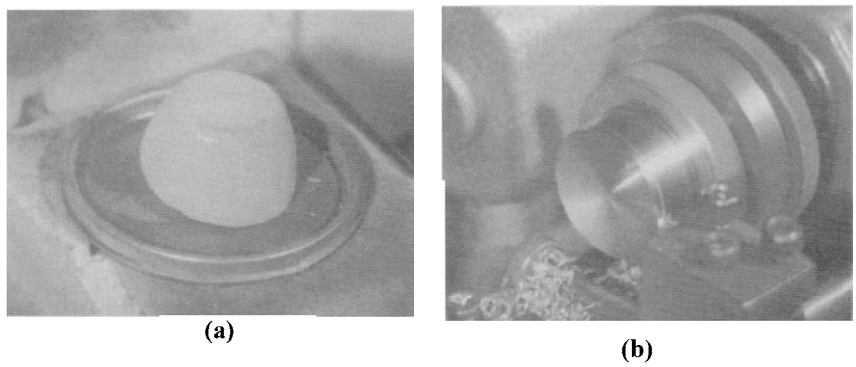

Fig. 4. (a) The Li_5B_4 compound alloy tapped out of the crucible, (b) Demonstration of the compound alloy being metallic (with luster) and easily machined despite the high content of boron.

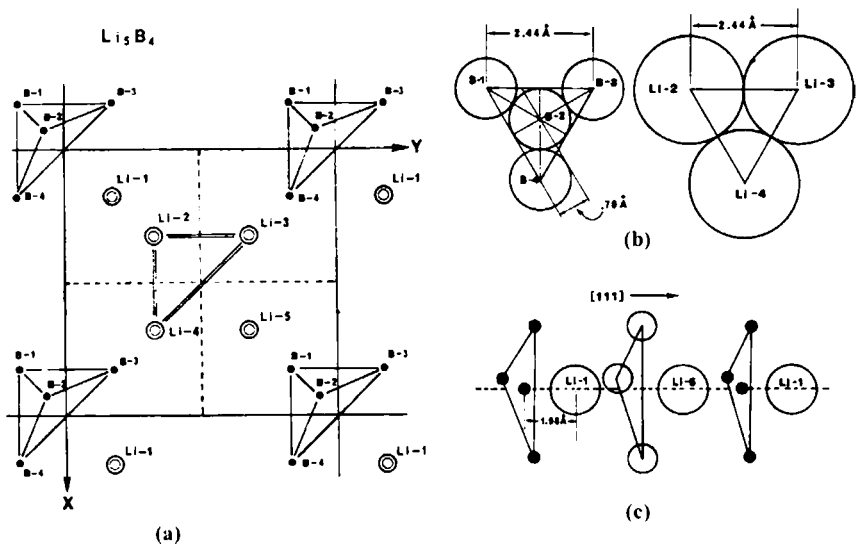

Fig. 5. (a) The short range R3m (rhombohedral) structure of Li_5B_4 (projected onto the x-y plane, (b) Trigangular cluster of four B atoms and similar cluster of three Li atoms., (c) Sequence of the Li and B clusters interleaved with Li atoms along the cubic [111] direction.

5. CURRENT SCIENTIFIC JOURNAL REVIEW SYSTEM

You may wonder what the Current Scientific Journal Review System has to do with the Bonding Theory in Metals and Alloys being proposed. My answer to this question is that there is no direct relation. However, there is a strong indirect relation between them. For example it is nearly impossible to have a paper that criticizes or repudiates a Nobel-prize- wining theory on superconductivity, accepted for publication. Therefore you have to 'tiptoe' around if you wish to have your paper, falling into this category, published through the current reviewing system. Two examples of the 'tiptoeing' are shown below as inserts.

phys. stat. sol. (b) 156, 583 (1989)

Subject classification: 74.20

Materials Research Laboratory, Pennsylvania State University[1])

New Approach to the Theory of High-Temperature Superconductivity

By

M. FUKUHARA[2]) and G. W. SMITH II

A new approach to the theory of high-T_c superconductivity in cuprate oxides is proposed, based on the possibility of superelectrons derived from inner closed shells in shrunken atoms induced by a strong screened attractive interaction between an electron and an ion. An electrostatic fluctuation connected with an electronic polarizability halts the breaking-up of the pre-existing pairs of electrons with antiparallel spins in the shells. The transport of superelectrons can be explained by the virtual tunneling.

Theor Chim Acta (1995) 90: 205–224

Theoretica Chimica Acta

Vibronic pairwise charge transfer in copper-oxide sheets: A possible approach to high temperature superconductivity theory

Ying-Nan Chiu[1], Samuel H. Brown[2], Neal Sondergaard[2], Frederick E. Wang[3]

[1] Center for Molecular Dynamics and Energy Transfer, Department of Chemistry, The Catholic University of America, Washington, DC 20064 USA

[2] Naval Surface Warfare Center, Carderock Division, Annapolis, MD 21402 USA

[3] Innovative Technology International Inc. 10747-3 Tucker Street, Beltsville, MD 20705 USA

Received 22 April 1993/Accepted August 16, 1994

Summary. To accommodate the number of holes and fractional number of atoms

Both these papers has one thing in common – title of the paper – stating "New approach to high temperature superconductivity theory." You see, they never mentioned the Nobel Prize winning theory of superconductivity. Instead they suggest that the theory they are proposing is for the 'high temperature superconductivity' as though there are two types of superconductivity, a) low temperature superconductivity governed by the BCS theory and b) high temperature superconductivity for which the theory is being proposed. Since these authors are not criticizing the BCS theory therefore it is 'safe' from rejection. It should be noted that these two papers were not published in "Physical Review" where the BCS theory was published originally. Have these authors tried to publish in the Physical Review'? Isn't Physical Review the most appropriate journal for these articles? There is no chance for these papers to be accepted by Physical Review. One paper is published in Phys.Sol.Stat. and the other one in Theor. Chem. Acta. This is exactly what I mean by 'tiptoeing' around. How dare you, a totally unknown factor be criticizing the 'bible'? Such attitude prompted a frustrated physicist to state "Since we already have a beautiful theory on 'superconductivity' all we need is a theory of 'superconductors.' My own friend from Harvard days used to tell me after our long discussion session that " I see you have a point but since the BCS theory has already received Nobel prize it must be good, — maybe what you are talking about is a special case of the BCS theory." In fact, in recent years with the discovery of high temperature superconductors in cuprate-oxides the origin of paired electron states is moving away from "Cooper Pair" concept. Instead the pair state is attributed to the atomic nature [16] but again these authors are tiptoeing around the BCS theory. Recalling what I described in the 'Nitinol' section. My first paper on the subject of Nitinol was titled "Crystal Structure and a Unique Martensitic Transition of TiNi.' The referee summarily turned it down because I used the word, "unique" in the title. The referee's comment was "What do you mean 'unique'? — Are all other martensitic transitions, a garden variety?" This is despite the fact I took pain in describing and explaining why the Nitinol transition was experimentally observed to be unique in the paper. Obviously the referee did not even bother to read the paper. For had he read the paper his critique would not be centered on the term 'unique.' The central reason for the referee to be upset was because there already exists a 'Crystallographic Theory on Martensitic Transition' [17] that relies on the common observation on this class of transition. Therefore, to have one transition that is unique from the rest is very upsetting to the theory that has been formulated. But as a scientist I had to report what I observed. My interpretation of the observation may be challenged but the observation itself must be viewed with great care despite the unfavorable situation.

On one occasion I was asked to review a paper written by a well known scientist who happens to be one of the advisory Board members for that journal. In due course I sent my comments to the Editor advising him that the paper as it was, in my view, should not be published unless the points I raised are answered or revised. For the points I raised, as they were, in my opinion, would mislead many readers. A few days later the Editor advised me on the fact that the paper had already been sent to the publication editor and there was no way to change them at that point. However, the editor asserted that he had the assurance from the author that he would submit a follow-up short note to correct his own paper with respect to the points I raised. The question is why did the editor send the paper that was still under review to the publication editor? The thinking of the editor, I believe, was that the author is a renowned scientist and the referees would accept as is. Therefore no

question was anticipated. So you see there are problems in the existing review system. In summary, the review system as it stands now hinders more than aiding scientists from telling their story to their colleagues. As the result they were denied the opportunity to receive the criticism or triggered further research on these subjects to advance the understanding of metals and alloys. My proposal for the remedy of the review system is as follows.

Almost all scientific journals are owned and supported by the society. The journals are established as a means of communication among the society members. Most articles published in the journal are therefore considered as new information whether it is the data, idea or theory. Since the things published are something new, the society under which the journal is published always has a disclaimer which states, "The acceptance and publication of an article in this journal does not imply that the editor, the reviewer, the society as a whole do accept approve, or endorse the data, opinion and conclusion of the authors." Having stated so clearly the disclaimer, the editors, the anonymous reviewers still can and does exercise the "God-given" right to control the publication of a given paper under the present system. This fact I find to be paradoxical. Through my own experience I would say that in the majority of cases I have benefited considerably from the comments I have received from the reviewers. These comments resulted in a better presentation of my paper or an improvement in the substance of the presentation. Therefore I am not advocating or urging the abolishment of the review system but only to point out the system's weakness and fallacy with the hope that with some remedy the system will function better for every member of the scientific community.

To begin, I question the validity for the reviewers to remain anonymous. This is presently justified by: (1) the reviewers would feel more freely in expressing their comments and results in a better review, and (2) If the reviewers cannot remain anonymous high number of potential reviewers would recline to review. To rebut the justification (1), it must be remembered the articles submitted for publication are something NEW! Therefore, the paper may contain 'radical' idea or concept that may not win the approval of the reviewer with the conventional thought and thus it may be 'rejected outright' for publication. However, this is tantamount to denying the author's 'right' to communicate with his or her fellow society member – the very purpose for which the journal was created in the first place. In my opinion, if the author after reading the anonymous reviewer's comments and still insists on publishing his manuscript I would say he or she must be allowed to do so under certain conditions to be described below. For after all, the Journal is protected by its disclaimer anyway. My own experience shows that it is possible for an anonymous reviewer to reject a paper out-right and yet stealing a part of the idea expressed and quickly published in a short communication as his own idea. To prevent such occurrence I suggest that the author of the paper rejected outright be given an option to have its paper published under certain format. Concerning point (2) the rebuttal is even easier. The history of science has always been with full of controversies. Anyone who would rather avoid controversy, in my opinion should not be in this 'kitchen' or the society.

Scientific technical books are usually written not on his (her) own new idea or concepts but rather a collection of ideas and concepts written by others. Therefore, books unlike scientific paper are not expressing something new. And yet the book reviews are done by the people who do not hide behind the cloak of anonymity. If the book review can

be done without anonymity, there is no reason a paper review cannot be done in the same way. In my view there is no room for anonymity for the reviewer in this case particularly because papers are describing something new.

Another concern I have has to do with the papers that are judged by the reviewer to be totally unacceptable as such they must be forbidden from publication. For the reviewer to be convinced so strongly that the paper submitted must be rejected outright I would say he or she must be prepared to defend his or her position and/or reasoning publicly. In my own experience as the reviewer I had to reject outright the paper under my review only once, because the author was not aware of the identical work done before in the literature. In fact, I did not have to reject the paper – the author chose to withdraw the paper once he knew the fact. In many cases the reason for the outright rejection may not be this trivial and straight forward. It is this group that I wish to address and explore a format for improvement. In fact, the current review system creates a fallacy that because the papers had to go through some kind of the 'review' system, the papers printed must be somehow correct. This false idea must have prompted the old saying, "Do not trust everything that in print".

The format I am proposing as a remedy for these weakness and shortcomings can be summarized in the following manner.

(A) The reviewers can remain anonymous as long as the paper being reviewed does not fall in the category of "outright rejection". Once a paper is judged to be in the outright rejection category, the reviewer must know that the anonymity is off and he or she must be prepared to defend its position in the open.

(B) The journal creates a section called "outright rejected papers" at the end of the journal. It is in this section the author of the outright rejected paper can publish his or her paper under the following condition.

(1) The author or the author's institution must agree beforehand to pay for the total (not partial) printing cost.

(2) On the other hand the reviewer must know that his or her name as well as the logic used to reject the paper will appear side by side on the paper. This is so that the public can pass its own judgment on the paper as well as on the reviewer's comments. Thus anonymity has no place in this case. .

(3) The rebuttal by the author(s) to the comments of the reviewer(s) will also appear.

Under this format it may be criticized as opening up a possibility for creating a lots of "junk." My answer is there already exists lots of junky stuff anyway. And if both the author and the reviewer know that their positions may ultimately be open for public scrutiny they will state things with greater care and results in less junky stuff. If the institute behind the author is willing to pay for all the cost of printing and willing to take the risk of becoming the laughing stock of the whole society I would say no big harm is

done. Just maybe through this format not only the very basic principle of the Journal being the forum for communication for the whole society can be restored but also some very important breakthrough based on a revolutionary idea or approach in science may be saved.

According to the legend, upon completing his book, "*ORIGIN OF SPECIES*" Charles Darwin showed it to his professor. After reading the book the professor laughed so much his stomach ached – because he thought it was so 'funny and comical.'

REFERENCES

[1] L. Pauling and E.B. Wilson Jr., Introduction to Quantum Mechanics, McGraw-Hill Book Co. New York (1935).
[2] R.W. Fountain and W.D. Forgeng, Trans. AIME, 215(1959)998; A.E. Dwight, Trans.ASM, 50(1958)617.
[3] F.E. Wang and W.J. Buehler, J.Appl.Phys., 42(1971)4515.
[4] E.E. Royals, Advanced Organic Chemistry, Prentice-Hall, Inc., New York (1954).
[5] H. Jones, The Theory of Brillouin Zones and Electronic States in Crystals, North Holland Pub.Co. Amsterdam, (1960).
[6] F.E. Wang, Met.Trans., 10A(1979)343.
[7] F.E. Wang, M.A. Mitchell, R.A. Sutula, J.R. Holden and L.H. Bennett, J.Less-Common Met., 61(1978)237.
[8] J. Letelier, Y.N. Chiu and F.E. Wang, J.Less-Common Met., 67(1979)179.
[9] T. Moeller, Inorganic Chemistry, John Wiley and Sons, London, (1954).
[10] Constitution of Binary Alloys, Hansen, Elliot and Shunk; Metallurgy and Metallurgical Engineering Series, McGraw-Hill Book Co., (1958,1965, 1969).
[11] C.T. Heycock and F.H. Neville, Philos. Trans.Roy.Soc., London A189(1897)67.
[12] K. Friedrich, Metallurgie, 3(1906)396; G.I. Petrenko, Z.Anorg.Chem., 53(1907)201.
[13] F.E. Wang, F.A. Kanda and A.J. King, J.Phys.Chem., 66(1962)2138.
[14] J.Less-Common Metals, v. 47 (1976).
[15] W.N. Lipscomb, Boron Hydrides, W.A. Benjamin, Inc., (1963).
[16] M. Fukuhara, Phys.Stat.Sol., b-213(1999)415.
[17] C.M. Wayman, Introduction to the Crystallography of Martensitic Transformations, McMillan Series in Material Science, New York, (1964).

PARTING THOUGHT

By recognizing the existence of covalent bonded electrons in metals and alloys I have shown how it is possible to explain and understand simultaneously a variety of physical phenomena observed, ranging from Phase Diagrams to Superconductivity to Mechanical Properties to Martensitic Transition in Nitinol. In this aspect I personally derived a tremendous gratification. It is my fervent hope that the material presented here will touch the hearts of the reader in some small way and will make them pause to think the importance of electrons, particularly the covalent bonded electrons, in the world of metals and alloys.

If the answer to the question of "What binds atoms together in forming materials?' is "Electrons!" then, we have no choice but to think and interpret the phenomena come out of these materials in terms of electrons. Admittedly, as of now we have no mathematical tools to precisely calculate more than three particles system let alone sea of electrons. Nonetheless, this should not hinder us from thinking that way. For by not thinking in terms of electrons we may be misled to think in terms of atoms that may provide an ad hoc explanation for an isolated phenomenon. The danger is that such an ad hoc explanation may in time turn into an ad hoc theory and be taught to the students year after year as a fundamental truth even though the explanation or theory shall never lead us to a true understanding of metals and alloys. Such is the case in Dislocation Theory that has to do only with atoms and ignores electrons completely (as though they do not exist). The statistical Thermodynamic is often invoked to explain or even calculate the Phase Diagrams. Such an approach is not recognizing the fact that the statistical Thermodynamic as we know has to do only with ensemble of atoms and therefore has its limitations. Electron interactions or nucleus process (such as $E = mC^2$) are not governed by the statistical Thermodynamic as we defined it. For example, the absolute Kelvin temperature scale at $T = 0$ is defined to be where atomic vibration is zero. But, at this temperature motion of electrons are not defined. This shows the Thermodynamic as we know does not deal with electrons. Thus to invoke the thermodynamic to deal with the world of metals and alloys that contains sea of electrons and electronic interaction is not justified and will not lead to a fruitful result. This is the very reason we have to use the terms "ideal" or "non-ideal" to circumvent the shortcoming of $PV = nRT$ law of the Statistical Thermodynamics.

The ultimate goal of understanding metals and alloys is the ability to design specific alloys to meet specific needs whether it is magnetic, electronic or mechanical or a combination thereof. The alloys in use today are all come from 'trial and error' or accidental discovery or even from our intuition but not from our fundamental understanding. By incorporating covalent bonded electrons in metals and alloys I am hoping that one-day we will reach the goal.

To me, the most important thing to remember is,

"**THINK!**" and never say, "**THAT'S HOW I LEARNED.**"

SUBJECT INDEX